

Aus dem Institut für Medizinische Mikrobiologie und Krankenhaushygiene
der Medizinischen Fakultät
der Otto-von-Guericke-Universität Magdeburg

**Insights into the mechanisms of mitochondria-regulated airway
epithelial cell dysfunction upon cigarette smoke extract exposure and
pneumococcal infection**

D i s s e r t a t i o n

zur Erlangung des Doktorgrades

Dr. rer. medic.

(doctor rerum medicarum)

an der Medizinischen Fakultät

der Otto-von-Guericke Universität Magdeburg

vorgelegt von D. V. M. Mahyar Aghapour Ask

aus Amol, Iran

Magdeburg 2022

From the Institute of Medical Microbiology and Hospital Hygiene
of Otto von Guericke University Magdeburg

**Insights into the mechanisms of mitochondria-regulated airway
epithelial cell dysfunction upon cigarette smoke extract exposure and
pneumococcal infection**

D i s s e r t a t i o n

for the attainment of the doctoral degree

Dr. rer. medic.

(doctor rerum medicarum)

At the Faculty of Medicine
of Otto von Guericke University Magdeburg

Submitted by D. V. M. Mahyar Aghapour Ask

From Amol, Iran

Magdeburg 2022

Preamble

Text used in sections 1.7, 1.8, 1.9, 1.10, 1.11, 1.12 and 1.13 was partly taken from the published reviews that were written by the first author:

Aghapour, M., Raei, P., Moghaddam, S. J., Hiemstra, P. S., & Heijink, I. H. (2018). Airway epithelial barrier dysfunction in chronic obstructive pulmonary disease: Role of cigarette smoke exposure. *Am J Respir Cell Mol Biol*, 58(2), 157–169.

Aghapour, M., Remels, A. H. V., Pouwels, S. D., Bruder, D., Hiemstra, P. S., Cloonan, S. M., & Heijink, I. H. (2020). Mitochondria: At the crossroads of regulating lung epithelial cell function in chronic obstructive pulmonary disease. *Am J Physiol Lung Cell Mol Physiol*, 318(1), L149–L164.

Results of this thesis has been published in *Cells*:

Aghapour, M.; Tulen, C. B. M.; Abdi Sarabi, M., Weinert, S.; Müsken, M.; Relja, B.; van Schooten, F. J.; Jeron, A.; Braun-Dullaeus, B.; Remels, A. H.; and Bruder, D. (2022). Cigarette smoke extract disturbs mitochondria-regulated airway epithelial cell responses to pneumococci. *Cells*, May 28, 11(11), 1771.

Text sections and graphs from the above-mentioned manuscript were used in sections 5 and 6.

Bibliographical description

Aghapour Ask, Mahyar; Insights into the mechanisms of mitochondria-regulated airway epithelial cell dysfunction upon cigarette smoke extract exposure and pneumococcal infection. – 2022. – 132 pages, 46 figures, 15 tables.

Abstracts

Cigarette smoking is considered as one of the major risk factors for development of airway diseases, inducing airway epithelial dysfunction, sustained inflammation as well as a decline in lung function. Bacterial and viral infections may aggravate smoke-induced airway diseases by inducing further airway inflammation. *Streptococcus pneumoniae* (*Sp*) is one of the most commonly isolated bacteria from the airways during airway diseases that may escalate condition by eliciting further oxidative stress and inflammation. Mitochondria as the central regulator of ROS production were also recently identified to be involved in innate immune responses to the pathogens. Mitochondrial function is impaired in airway epithelial cells of smokers. However, the mechanistic pathways linking mitochondrial dysfunction to airway epithelial innate immune responses and airway epithelial barrier function is still lacking. We found that mitochondrial dysfunction induced by cigarette smoke extract may link to dampen innate immune responses and disrupted epithelial barriers upon *Sp* infection in the airway epithelium. Mitochondrial dysfunction was reversible by using mitochondrial targeted compounds, which may provide a promising therapeutic strategy to overcome bacterial-induced airway epithelial cell dysfunction.

Keywords

Cigarette smoke, Lung epithelial cells, Pneumococci, Mitochondrial dysfunction, Innate immune responses

Table of Contents

List of Abbreviations	VI
List of Figures	XIII
List of Tables	XV
List of Publications	XVI
Conference Contributions	XVII
1. Introduction	1
1.1. CS components and airway damage.....	1
1.2. <i>Sp</i> and airway damage	2
1.2.1. <i>Sp</i> structure and airway epithelial colonization	3
1.2.2. <i>Sp</i> airway epithelial colonization and host immune response	6
1.3. Airway epithelium in health	8
1.3.1. Structure of healthy airway epithelium.....	8
1.3.2. Airway epithelial barriers (chemical barriers and cell junctions).....	8
1.4. Airway epithelial disruption in smokers.....	10
1.4.1. Mechanisms of CS-induced disruption of cell-cell contacts	11
1.4.2. CS-induced pro-inflammatory responses and cell-cell contact disruption	13
1.5. Mitochondrial function in AECs	17
1.5.1. Mitochondrial oxidative respiration in health.....	17
1.5.2. Mitochondrial dynamic processes in health	19
1.5.3. Mitophagy machinery in AECs in health	21
1.6. Mitochondrial abnormalities in AECs exposed to CS.....	26
1.6.1. Mitochondrial morphological abnormalities	26
1.6.2. Mitochondrial functional damages	26
1.6.3. Mitochondrial quality control processes.....	27
1.7. Innate immune responses in airway mucosa; potential links to mitochondria	30
1.8. Mitochondrial dysfunction and airway epithelial barrier function upon CS exposure	34
2. Aim of the study	35
3. Materials	37

3.1. Consumables.....	37
3.2. Technical devices	39
3.3. Antibodies- immunostaining	40
3.4. Buffer and media composition	41
4. Methods	44
4.1. Cell culture	44
4.2. <i>Streptococcus pneumoniae</i> culture	44
4.3. CSE preparation.....	44
4.4. Proliferation assays (based on metabolic activity)	45
4.4.1. MTT assay	45
4.4.2. RealTime-Glo MT assay	45
4.5. Oxidative stress assays	46
4.5.1. Intracellular ROS levels.....	46
4.5.2. FACS staining for MitoSOX	46
4.6. Mitochondrial membrane potential analysis.....	46
4.7. Gene expression array	47
4.7.1. RNA isolation.....	47
4.7.2. DNA removal by DNase.....	47
4.7.3. Microarray analysis	48
4.8. Sample preparation for immunoblotting.....	48
4.8.1. Total cell lysate.....	48
4.8.2. Mitochondrial fractionation	48
4.9. Immunoblotting	49
4.10. Immunocytochemistry	50
4.11. Mitochondrial ultrastructure analysis	50
4.12. Epithelial antibacterial response test	51
4.13. Statistical analysis	51
5. Results.....	52
5.1. AEC proliferation upon CSE exposure	52

5.2. Total and mitochondrial oxidative stress upon CSE exposure	53
5.3. Mitochondrial membrane potential upon CSE exposure.....	55
5.4. Mitochondrial complex protein levels upon CSE exposure	56
5.5. Mitochondrial-specific autophagy (mitophagy) upon CSE exposure.....	58
5.6. Involvement of AMPK and ULK1 in CSE-induced alterations in mitophagy	60
5.7. Mitochondrial fission and fusion levels upon CSE exposure	60
5.8. Mitochondrial biogenesis upon CSE exposure.....	62
5.9. CSE-induced epithelial barrier dysfunction rescued with mitochondrial compounds	64
5.10. Effect of CSE on <i>Sp</i> growth	65
5.11. Mitochondrial oxidative stress upon CSE and <i>Sp</i> co-stimulation	66
5.12. Mitochondrial membrane potential upon CSE followed by <i>Sp</i> infection.....	68
5.13. Mitochondrial complex protein expression upon CSE followed by <i>Sp</i> infection.....	69
5.14. Mitochondrial biogenesis levels upon CSE followed by <i>Sp</i> infection	71
5.15. Mitophagy levels upon CSE followed by <i>Sp</i> infection.....	72
5.16. Mitochondrial fission and fusion upon CSE followed by <i>Sp</i> infection	74
5.17. Gene expression analysis upon CSE followed by <i>Sp</i> infection	75
5.17.1. Results of GSEA.....	77
5.17.2. K-mean clustering.....	85
5.18. Mitochondrial morphology upon CSE followed by <i>Sp</i> infection	91
5.19. Effect of CSE-induced mitochondrial dysfunction on innate immune responses to <i>Sp</i> infection	92
5.20. Effects of CSE on epithelial <i>Sp</i> colonization/clearance	93
6. Discussion	95
7. Summary	105
8. References	107
9. Acknowledgment	130
10. Appendix	131
10.1. Ehrenerklärung	131
10.2. Curriculum vitae	132

List of Abbreviations

% (v/v)	Volume percent
%	Percent
α	Alpha
Adr	Attenuator of drug resistance
AEC	Airway epithelial cells
AIM2	Absent in melanoma 2
AJs	Adherens junctions
AKAP-9	A-kinase anchor protein 9
ALI	Air-liquid interface
AMPK	adenosine monophosphate-activated protein kinase
ATGs	Autophagy-related genes
ATP	Adenosine triphosphate
ATP5A	ATP synthase subunit alpha
β	Beta
BAL	Bronchoalveolar lavage
BgaA	Beta-galactosidase
BNIP3	BCL2-Interacting protein 3
BNIP3L	BCL2 interacting protein 3-Like
BSA	Bovine serum albumin
CaCl ₂	Calcium chloride
cAMP	Cyclic adenosine monophosphate
CBPs	Choline-binding proteins
CC10	Club cell secretory protein-10
Cdc42	Cell division cycle 42
CDK1	Cyclin-dependent kinase 1
CDK1NA	Cyclin dependent kinase inhibitor 1A
CFU	Colony formation unit
ChoP	Phosphorylcholine
CLDN	Claudin(s)
CO ₂	Carbon dioxide
COX	Cytochrome c oxidase
CSE	Cigarette smoke extract
CuZnSOD	Copper zinc superoxide dismutase
CXCL	Chemokine (C-X-C motif) ligand
Cyto	Cytoplasmic

DAI	DNA-dependent activator of IFN-regulatory factors
DAPI	4',6-diamidino-2-phenylindole
DCFDA	Dichlorofluorescein diacetate
DMSO	Dimethyl sulfoxide
DNA	Deoxyribonucleic acid
DRP1	Dynamin-related protein 1
ECL	Enhanced chemiluminescence
ECSOD	Extracellular SOD
EDTA	Ethylenediaminetetraacetic acid
e.g.,	<i>Latin</i> : “exempli gratia”
EGFR	Epidermal growth factor receptor (EGFR)
EMT	Epithelial mesenchymal transition
Eno	Enolase
ER	Endoplasmic reticulum
ERK	Extracellular signal-regulated kinase
ERR α	Estrogen-related receptor α
ETC	Electron transport chain
FACS	Fluorescence-activated cell sorting
FAD	Flavin adenine dinucleotide
FAM13A	Family with sequence similarity 13 member A
FC	Fold change
FCCP	Carbonyl cyanide-p-trifluoromethoxyphenylhydrazone
FCS	Fetal calf serum
FDR	False discovery rate
FEV1	Forced expiratory volume 1
FIS1	Fission protein 1
FITC	Fluorescein isothiocyanate
FUNDC1	Fun14 domain-containing protein 1
FVC	Forced vital capacity
g	Gram(s)
γ	Gamma
GABARAPL1	Gamma-aminobutyric acid receptor-associated protein-like 1
GAPDH	Glyceraldehyde-3-phosphate dehydrogenase
gDNA	Genomic DNA
GO	Gene Ontology
GPX	Glutathione peroxidase
GSEA	Gene set enrichment analysis

GSH	Glutathione
GSR	Glutathione reductase
GTPases	Guanosine triphosphatase
h	Hour(s)
H ₂ O ₂	Hydrogen peroxide
HER2	Human epidermal growth factor 2
HEPES	N-2-hydroxyethylpiperazine-N'-2-ethanesulfonic acid
HIF-1 α	Hypoxia-inducible factor 1 α
HKII	Hexokinase II
HLA-DMA	HLA class II histocompatibility antigen DM alpha chain
HRP	Horseradish peroxidase
i.e.,	<i>Latin</i> : "id est"
IFN	Interferon
IFNAR	Interferon-alpha/beta receptor
IgA1	Immunoglobulin A1
IKBE	IKB kinase epsilon
IL	Interleukin
IMM	Inner mitochondrial membrane
<i>In vitro</i>	<i>Latin</i> : "in the glass"
<i>In vivo</i>	<i>Latin</i> : "within the living"
IRFs	Interferon regulatory factors
ISGs	Interferon stimulated genes
JAK	Janus-associated kinase
JAM	Junctional adhesion molecule
JNK	C-Jun N-terminal kinase
kDa	Kilodalton (atomic mass)
LC3B	Microtubule-associated protein 1A/1B-light chain 3B
LDHA	Lactate dehydrogenase A
LPS	Lipopolysaccharide
LytA	Pneumococcal autolysin lytic amidase
M	Molar mass
mM	Millimolar
μ M	Micromolar
MAPK	Mitogen-activated protein kinase
MAVS	Mitochondrial antiviral signaling
MDA5	Melanoma differentiation-associated protein 5
Med	Medium

MEM	Minimal essential medium
MgCl ₂	Magnesium chloride
MFF	Mitochondrial fission factor
MFI	Mean fluorescence intensity
MFN2	Mitofusion 2
μg	Microgram
MHCII	Major histocompatibility complex II
MID49	Mitochondrial dynamic protein 49
MilliQ	Purified, deionized water
Min	Minute(s)
Mito	Mitochondrial
ml	Milliliter
μl	Microliter
MnSOD2	Manganese superoxide dismutase 2
MOI	Multiplicity of infection
MOTS-c	Mitochondrial ORF of the 12S rRNA type-c
mPTP	Mitochondrial permeability transition pore
mtDAMPs	Mitochondrial danger-associated molecular patterns
mtDNA	Mitochondrial DNA
mTOR	Mammalian target of rapamycin
mtROS	Mitochondrial reactive oxygen species
MTT	3-(4,5-Dimethyl-2-thiazolyl)-2,5-diphenyl-2H-tetrazoliumbromid
Muc5AC	Mucin 5AC
NaCl	Sodium chloride
NADPH	Nicotinamide-adenine dinucleotide phosphate
NanA	Neuraminidase
n. d.	Not detectable
NFκB	Nuclear factor kappa-light-chain-enhancer of activated B cells
NLRP3	Nucleotide-binding domain and leucine-rich repeat-containing family, pyrin domain-containing 3
NLRX1	Nucleotide-binding domain and leucine-rich repeat-containing protein X1
NOX	NADPH oxidase
NRF1	Nuclear respiratory factor 1
Nrf2	nuclear factor erythroid 2-related factor 2
NRG-1	Neuregulin
n. s.	Not significant
OCLN	Occludin
OH	Hydroxyl radical
OMM	Outer mitochondrial membrane

OPA1	Optic atrophy 1
OXPHOS	Oxidative phosphorylation
P	Phosphorylated
PAFR	Platelet-activating factor receptor
PAH	Polyaromatic hydrocarbons
PAMPs	Pathogen-associated molecular patterns
PavA	Pneumococcal adherence and virulence factor A
PBS	Phosphate-buffered saline
PepO	Pneumococcal endopeptidase O
PGC-1 α	Peroxisome proliferator-activated receptor-gamma coactivator-1alpha
PgdA	Peptidoglycan N-acetylglucosamine deacetylase
pH	Potential of hydrogen
PI3K	Phosphatidylinositol 3-kinase
PIGR	Polymeric immunoglobulin receptor
PINK-I	Phosphatase and tensin homolog (PTEN)-induced kinase-I
PKA	Protein kinase A
PKC	Protein kinase C
PLK1	Polo-like kinase 1
PLY	Pneumolysin
PM	Particulate matter
PMT	Photomultiplier tube
PpmA	Putative proteinase maturation protein A
PRRs	Pattern recognition receptors
PrsA	Parvulin-type peptidyl-prolyl isomerase
PspA	Pneumococcal surface protein A
PVDF	Polyvinylidene difluoride
Rac1	Ras-related C3 botulinum toxin substrate 1
RAGE	Receptor for advanced glycation end-products
RIG-I	Retinoic acid-inducible gene I
RIPA	Radio-immunoprecipitation assay
RLRs	Retinoic acid-inducible gene-I-like receptor
RLU	Relative light unit
RNA	Ribonucleic acid
Rock	Rho kinase
ROS	Reactive oxygen species
rpm	Rounds per minute
RTK	Receptor tyrosine kinase
SDHB	Succinate dehydrogenase subunit B
SDS	Sodium dodecyl sulfate

SDS-PAGE	Sodium dodecyl sulfate-polyacrylamide gel electrophoresis
Sec	Second(s)
SEM	Standard error of the mean
SIs	Signal intensities
SIRT1	Sirtuin 1
SOD	Superoxide dismutase
<i>Sp</i>	<i>Streptococcus pneumoniae</i>
SQSTM1	Sequestosome 1
StarD7	Steroidogenic acute regulatory protein D7
STAT1	Signal transducer and activator of transcription 1
STING	Stimulator of interferon genes
StrH	Surface exoglycosidase beta-N-acetylhexosaminidase
tBHP	tert-butyl hydroperoxide
TBK1	TANK-binding kinase 1
TBST	Tween20 Tris-buffered saline
TCA cycle	Tricarboxylic acid cycle
TEER	Trans-epithelial electrical resistance
TEM	Transmission electron microscopy
TEMED	Tetramethylethylenediamine
TFAM	Transcription factor A
Th	T helper
THY	Todd Hewitt broth supplemented with bacto yeast extract
TJs	Tight junctions
TLR	Toll-like receptor
TNF- α	Tumor-necrosis-factor alpha
TNFAIP2	Tumor-necrosis-factor alpha-induced protein 2
TOMM20	Translocase of outer mitochondrial membrane20
TRAF6	TNF receptor associated factor 6
Tris	Tris(hydroxymethyl)aminomethane
TUFM	Tu mitochondrial translation elongation factor
UCP2	Uncoupling protein 2
ULK1	Unc-51-like kinase 1
UPR	Unfolded protein response
UQCRC2	Ubiquinol-cytochrome c reductase core protein 2
URT	Upper Respiratory tract
VDAC1	Voltage-dependent anion channel 1

vs.	versus
ZBR	ZO-1-binding tyrosine residue
ZO-1	Zonula occludens-1

Note: Standard SI units and abbreviations of chemical elements were used.

List of Figures

Figure 1: <i>Sp</i> structure and virulence factors	4
Figure 2: Molecular mechanisms of <i>Sp</i> colonization into the respiratory epithelium.....	6
Figure 3: Recognition of <i>Sp</i> by host cell's pattern recognition receptors	8
Figure 4: Schematic illustration of airway epithelial cell junctions	10
Figure 5: Molecular mechanisms underlying CS-induced airway epithelial barrier dysfunction	13
Figure 6: Airway epithelial barrier dysfunction induced by CS-induced changes in pro-inflammatory responses	16
Figure 7: Mitochondrial genome structure.....	18
Figure 8: Schematic illustration of oxidative phosphorylation and electron transport chain in mitochondrion	19
Figure 9: Mitochondrial fusion and fission processes.....	20
Figure 10: Phosphorylation of DRP1 and fission processes	21
Figure 11: Three different types of autophagy	22
Figure 12: Schematic illustration of mitophagy machinery	23
Figure 13: Balance between mitophagy, mitochondrial dynamic processes and mitochondrial biogenesis	24
Figure 14: Signaling pathways involved in mitophagy.....	26
Figure 15: Schematic figure illustrating processes involved in CS-induced mitochondrial dysfunction in AECs	29
Figure 16: Links between CS-induced mitochondrial dysfunction and altered innate immune responses in airway epithelium.....	31
Figure 17: Mitochondrial effectors regulate innate immune responses to pathogens	33
Figure 18: Schematic illustration of three aims of the study.....	36
Figure 19: Logarithmic phase of <i>Sp</i> growth.....	44
Figure 20: Optimization of CSE-induced epithelial dysfunction model by measurement of cell proliferation in 16HBE cells	52
Figure 21: Cellular oxidative stress levels upon stimulation of 16HBE cells with CSE.....	54
Figure 22: Mitochondrial membrane potential upon stimulation with various concentrations of CSE	55
Figure 23: Abundance of mitochondrial complex components as well as constituents of OMM upon CSE15 % stimulation in 16HBE cells.....	57
Figure 24: Abundance of key regulators involved in mitophagy in 16HBE cells upon stimulation with CSE15 %	59
Figure 25: Mitophagy factors regulatory protein levels upon stimulation of 16HBE cells with CSE15 %	60

Figure 26: Mitochondrial fission and fusion levels upon stimulation of 16HBE cells with CSE15 %	62
Figure 27: Mitochondrial biogenesis upon stimulation of 16HBE cells with CSE15 %	63
Figure 28: Post-treatment with mitochondrial-targeted compounds reverses CSE-induced airway epithelial barrier disruption	65
Figure 29: Growth curve of <i>Sp</i> upon CSE stimulation	66
Figure 30: CSE15 % pre-exposure followed by <i>Sp</i> infection induced an increase in mitochondrial oxidative stress	68
Figure 31: CSE15 % followed by <i>Sp</i> infection alters mitochondrial membrane potential	69
Figure 32: Mitochondrial OXPHOS and OMM protein expression upon stimulation with CSE15 % and <i>Sp</i>	70
Figure 33: CSE15 % followed by <i>Sp</i> infection altered mitochondrial biogenesis in 16HBE cells	71
Figure 34: Mitophagy protein expression upon stimulation with CSE15 % and <i>Sp</i>	73
Figure 35: Mitochondrial fission and fusion upon stimulation with <i>Sp</i> and CSE15 %	74
Figure 36: Gene expression volcano plots upon CSE15 % stimulation and <i>Sp</i> infection	76
Figure 37: CSE15 % increases ROS hallmark genes and decreases apical junction gene hallmarks in 16HBE cells	80
Figure 38: CSE15 % and <i>Sp</i> affect enrichment of mitochondrial hallmark genes in 16HBE cells	82
Figure 39: CSE15 % promotes enrichment of autophagy hallmark genes in 16HBE cells	83
Figure 40: CSE15 % impairs innate immune responses to <i>Sp</i> in 16HBE cells	84
Figure 41: Microarray analysis of gene expression upon CSE15 % stimulation and <i>Sp</i> infection	91
Figure 42: CSE15 % followed by <i>Sp</i> infection induced ultrastructural alterations in mitochondria in 16HBE cells	91
Figure 43: CSE15 %-induced impairment innate immune responses may associate with NLRX1	92
Figure 44: CSE15 % pre-stimulation reduced the number of <i>Sp</i> in the supernatant of 16HBE cells	93
Figure 45: Schematic figure summarizing key findings of the thesis	94
Figure 46: Summary of proposed mechanisms linking CS-induced mitochondrial alterations to airway epithelial responses	104

List of Tables

Table 1: Chemicals	37
Table 2: Kits	38
Table 3: Technical devices	39
Table 4: Antibodies used for immunoblotting.....	40
Table 5: Antibodies used for immunofluorescence.....	41
Table 6: <i>Sp</i> culture media	41
Table 7: MEM complete.....	41
Table 8: FACS buffer	42
Table 9: 1X sample buffer for immunoblotting.....	42
Table 10: 1X SDS-PAGE running buffer.....	42
Table 11: 1X transfer buffer	42
Table 12: TBST buffer (<i>i</i>) for immunoblotting	42
Table 13: TBST buffer (<i>ii</i>) for immunoblotting	42
Table 14: Fixative buffer for TEM.....	43
Table 15: 0.1 M EM-HEPES buffer for TEM.....	43

List of Publications

Original Publication

Aghapour, M., Tulen, C. B. M., Abdi Sarabi, M., Weinert, S., Müsken, M., Relja, B., van Schooten, F. J., Jeron, A., Braun-Dullaeus, R., Remels, A. H., Bruder, D. (2022). Cigarette smoke extract disturbs mitochondria-regulated airway epithelial cell responses to pneumococci. *Cells*, 11, 17771. doi: 10.3390/cells11111771.

Impact factor (2022): 6.6

Others

Aghapour, M., Surender, S., Bruder, D. (2022). Beware the intruder: Gasodermin A as molecular guardian preventing systemic dissemination of group A streptococci following local skin infection. *Cell Mol Immunol*, online ahead of print. doi: 10.1038/s41423-022-00863-4. Research Highlight.

Impact factor (2022): 11.53

Aghapour, M., Ubags, N., Bruder, D., Hiemstra, P. S., Sidhaye, V., Rezaee, F., Heijink, I. H. (2022). Role of air pollutants in airway epithelial barrier dysfunction in asthma and COPD. *Eur Respir Rev*, 31, 210112. doi: 10.1183/16000617.0112-2021. Review.

Impact factor (2022): 8.8

Aghapour, M., Remels, A., Pouwels, S. D, Bruder, D., Cloonan, S., Hiemstra, P. S., Heijink, I. H. (2020). Mitochondria: at the crossroad of regulating lung epithelial cell function in chronic obstructive pulmonary disease. *Am J Physiol Lung Cellr Mol Physiol* 318, L149–L164. doi: 10.1152/ajplung.00329.2019. Review.

Impact factor (2020): 4.65

Linfield, D. T., Raduka, A., **Aghapour, M.**, Rezaee, F. (2021). Airway tight junctions as targets of viral infections: Tight junctions and viral Infections. *Tissue Barriers*, 9(2). doi: 10.1080/21688370.2021.1883965. Review.

Impact factor (2021): 4.12

Ogger, P. P., Silva, J. D., **Aghapour, M.**, Persson, I. M., Tulen, C., Jurkowska, R., Ubags, N. D. (2020). Early career members at the ERS lung science conference 2020: Metabolic alterations in lung ageing and disease. *Breathe*, 16(3),1–8. doi: 10.1183/20734735.0063-2020. Conference Highlight.

Impact factor (2020): 1.16

Aghapour, M., Raee, P., Moghaddam, S. J., Hiemstra, P. S., Heijink, I. H. (2018). Airway epithelial barrier dysfunction in chronic obstructive pulmonary disease: Role of cigarette smoke exposure. *Am J Respir Cell Mol Biol*, 58(2),157–169. doi: 10.1165/rcmb.2017-0200TR. Review.

Impact factor (2018): 4.34

Conference Contributions

Mahyar Aghapour. *Effects of environmental exposures in lung pathology and the underlying mechanisms (Thematic Poster session coordinator).* ERS International Congress, Madrid, Sep 28th – Oct 2nd 2019.

Mahyar Aghapour, Andreas Jeron, Dunja Bruder. *Streptococcus pneumoniae induces broad alterations in mitochondrial functions in human airway epithelial cells (Poster presentation).* ERS Lung Science Conference, Estoril, Portugal. March 4th – 9th 2020

Mahyar Aghapour, Andreas Jeron, Dunja Bruder. *Streptococcus pneumoniae induces broad alterations in mitochondrial functions in human airway epithelial cells (Poster presentation).* ERS International Congress, Online, Sep 6th – 9th 2020

1. Introduction

1.1. CS components and airway damage

CS as the major risk factor for the development of airway diseases is a complex mixture composed of more than 5000 toxic components and carcinogens including but not limited to nicotine, aldehydes, benzene and heavy metals. Different products of smoke i.e., cigarettes, cigar and water pipe contain different proportion of these hazardous components, imposing a large population using these products to considerable health risk. With cigarette smoking during puffing, the mainstream smoke come from the butt end of the cigarettes (filter end), while sidestream smoke originates from burning of coal part in the front. Different patterns of burning in these two types of smokes cause changes in the chemical compositions. For instance, mainstream smoke contains more cyanide, catechol and hydroquinone and less nicotine, ammonia and phenols than sidestream smoke. In addition, CS contains gas phase components together with particles with various sizes but mainly ultrafine and fine particles (ultrafine PM, $\leq 1 \mu\text{m}$ or PM₁ and fine particles ≤ 2.5 or PM_{2.5}). Gas phase smoke that are dissolved in the lung fluids contains various known gases already present as air pollutants e.g., CO₂, methane, ammonia, acrolein and nitrosamine. On the other hand, solid phase includes phenols, nicotine and PAH, which are deposited in the lung. These classifications help researchers to optimally generate an appropriate disease model based on the research questions via mainstream or sidestream smoke or gas phase and solid phase materials (Centers for Disease Control and Prevention (US), 2010).

Enhanced oxidative stress in the lung is one of the main features of smoking-induced airway diseases (Barnes, 2020). Many components of CS either in gas form or particles induce oxidative stress in the lung either via free radical activity of the components or by activating endogenous ROS activators such as NOX and xanthine oxidase e.g. myeloperoxidase released by neutrophils, leading to lipid peroxidation via increased levels of hydroxyl, H₂O₂ and nitrite radicals (Thimmulappa et al., 2019). However, certain components have been reported to be more involved in oxidative stress. Of note, semiquinones, hydrogen cyanide, nitrogen oxide and cadmium has been shown to exert more oxidative stress in the lung (Wooten et al., 2006). ROS-induced lipid peroxidation may lead to increased protein carbonylation in the lung (Negre-Salvayre et al., 2008) as observed in smokers, which associated with severity of airway diseases (Kirkham et al., 2011). Increased carbonylation of proteins may lead to protein modifications and cellular dysfunction (Barnes, 2020).

Although ROS may play a beneficial role in elimination of pathogens by immune cells such as macrophages, uncontrolled ROS levels may impair the physiological functions of the cells (Bhattacharyya et al., 2014). Enhanced oxidative burden have been observed in the lung and blood smokers (Rahman & Adcock, 2006), which may lead to several consequences in the structural cells of the lung including increased inflammation, resistance to treatments, DNA damage, mucociliary dysfunction, increased autophagy and apoptosis, all of which play detrimental roles in the pathogenesis of airway diseases (Bailey et al., 2018; Domej et al., 2014; Korfei et al., 2020; Van Eeden & Sin, 2013)

The cells are normally protected against increased levels of ROS induced by CS through several mechanisms including antioxidant responses, leading to alleviated oxidative damage (Domej et al., 2014). However, long-term exposure to CS may change the antioxidant capacity of the airways, which may lead to more oxidative burden (Aghapour et al., 2018; Bezerra et al., 2011). Many enzymes are involved in the antioxidant system that include GPX and GSR, catalase and SOD (Cantin, 2010). Of note, GSH, an antioxidant enzyme, which is highly found in the lung fluids has been shown to be decreased in the smokers. Furthermore, patients with airway disease have defective Nrf2 responses, which is one of the main transcription factors involved in regulation of cellular antioxidant response (Cantin, 2010). SOD levels and particularly CuZnSOD or cytosolic SOD1 which is downstream target of Nrf2, have been shown to protect against CS-induced emphysema by reducing apoptosis (Foronjy et al., 2006; Petrache et al., 2008). Mitochondrial MnSOD or SOD2 and ECSOD also known as SOD3 have also been reported to play protective roles against lung injuries (Ilizarov et al., 2001; Nagata et al., 2007; H. Yao et al., 2010).

1.2. *Sp* and airway damage

In addition to CS, bacterial pathogens may induce airway damage by triggering pro-inflammatory responses. Bacterial pathogens are widely reported to be associated with respiratory infections such as pneumonia, of which infection with different serotypes of *Sp* placed at third most frequently bacterial infection during airway disease (Sethi & Murphy, 2008). Experimentally, it was reported that repetitive exposure to *Sp* in combination with CS exposure exacerbate lung inflammation in mice by increasing bacterial load, airway inflammation and a decline in lung function (Gou et al., 2019). *Sp* is a gram-positive encapsulated bacterium that is predominantly colonized in the mucosal layers of the URT (Weiser et al., 2018). The colonization of *Sp* in the URT may not necessarily induce pathogenic symptoms, as they comprise a normal flora in healthy individuals. However, in certain condition such as in immunosuppressed patients they

may disseminate to the lower conducting airways, where they colonize and exert their pathogenic effects (Brooks & Mias, 2018). This colonization stimulates mucosal immune responses and enhances recruitment of neutrophils to the mucosal surfaces to engulf bacteria and eliminate infection.

1.2.1. *Sp* structure and airway epithelial colonization

Similar to all gram-positive bacteria, *Sp* composed of structures which support its survival, colonization and pathogenicity. *Sp* composed of three layers which include surface polysaccharide capsules, cell wall and cell membrane (Kadioglu et al., 2008). The negative charge of polysaccharide in the *Sp* capsule enables it to escape from host immune responses by evading mucosal trap and opsonization/phagocytosis, thus contributing to increased viability, colonization, and virulence of *Sp* (Hyams et al., 2010; Kadioglu et al., 2008). There are non-encapsulated strains of *Sp* that have greater colonization capacity compared to other colonizing serotypes that showed resistant to antibiotics and in interaction with capsular serotypes can acquire capsules during systemic infections, which leads to more survival and increased pathogenicity (Bradshaw et al., 2020; Kadioglu et al., 2008). The cell wall is composed of a peptidoglycan teichoic acid (wall teichoic acid and lipoteichoic acid) and a phospholipid bilayer. The peptidoglycan in the cell wall has phosphorylation residues that is used by surface proteins known CBPs such as PspA and LytA as binding anchor (Vollmer et al., 2019). These CBPs are served as virulence factors that are either responsible for evasion from opsonization by complement factors as PspA or cause a degradation of cell wall and capsule leading to autolysis of *Sp* and release of bacterial virulence factors as LytA (Mitchell & Mitchell, 2010). Another component of cell walls is an adhesin called ChoP, which facilitates colonization of *Sp* in the URT (Kadioglu et al., 2008). ChoP attaches to the receptor for platelet-activating factor which is widely expressed on the epithelial surfaces of host URT and activates host cell responses. CbpA (also known as PspC) is another cell adhesion molecule that bind to ChoP and facilitate colonization to the host epithelial cell surfaces (Weiser et al., 2018). In addition to CBPs, there are other cell surface proteins such as metalloproteins (e.g. PsaA), cell wall bound protein with LPXTG motif (e.g. Neuraminidase) as well as non-classical cell surface proteins (e.g. PavA), all of which contribute to bacterial colonization to the host epithelium (Brooks & Mias, 2018).

Apart from cell surface proteins, *Sp* secretes several polypeptides upon colonization, including PLY, H₂O₂ and Immunoglobulin A1 that increases their invasiveness and leads to more pathogenicity (Brooks & Mias, 2018). IgA1 impedes host response by cleaving IgA1 produced by host cells, increasing *Sp* viability (Janoff et al., 2014). PLY is a toxin produced by *Sp*, which binds to the cholesterol-rich part of the host cell membrane and disrupt the cell membrane by

forming pores (Nishimoto et al., 2020). Upon release, PLY is recognized by host's TLR4 and stimulates host cell pro-inflammatory responses via activation of p38 mitogen-activated protein kinase and host complement and impairing phagocytic activity (Henriques-Normark & Tuomanen, 2013; C. T. Nguyen et al., 2015). Furthermore, PLY induces DNA damage potentially by enhancing ROS production via increased calcium influx into the cytoplasm through formation of ion channels in the cells (Rai et al., 2016). Unlike PLY which almost produced by all serotypes of *Sp*, H₂O₂ only released by serotypes that have pyruvate oxidase activity. H₂O₂ has bactericidal activity and stimulate host pro-inflammatory responses potentially via increasing reactive hydroxyl (as a ROS) in the host cells (Brooks & Mias, 2018). Similar to PLY, H₂O₂ also induces DNA double strand breaks but by forming hydroxyl free radicals (OH molecules), leading to cell death (Rai et al., 2015). *Sp* cell structure as well as virulence factors have been illustrated in **Figure 1**.

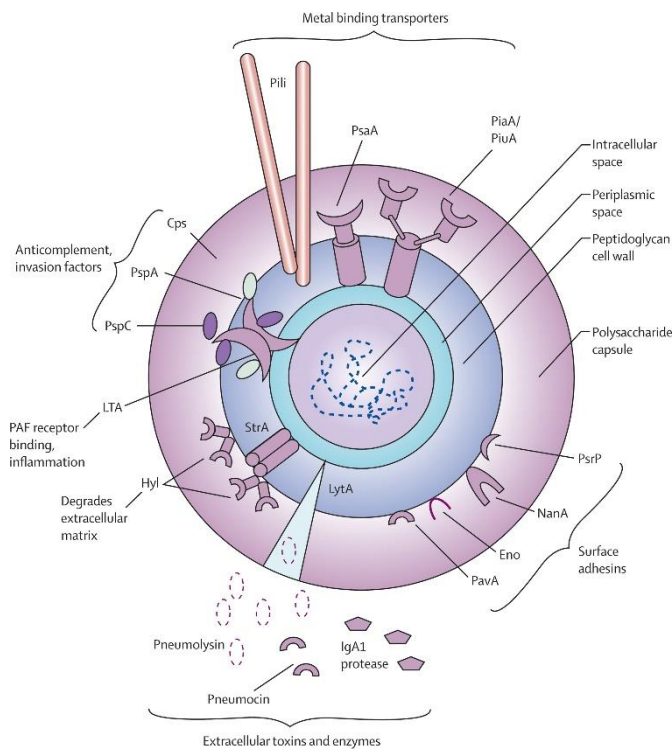


Figure 1: *Sp* structure and virulence factors. *Sp* cell surface composed of a polysaccharide capsule, peptidoglycan cell wall and cell membrane. *Sp* benefits from several surface components includes adhesins, glycosidases and anticomplement factors all of which enhance virulence in the infected cells. *Sp* also releases proteases such as IgA1 protease and pneumolysin to evade host immune responses. The figure was adopted from a cited reference (van der Poll & Opal, 2009).

Sp are categorized based on their capsular types to different strains that can further be divided based on their pathogenicity into colonizing serotypes such as 19F, 23F and 14 and invasive strains such as serotypes 1 and 4 (Henriques-Normark & Tuomanen, 2013). Certain serotypes are more isolated from the sputum of patients undergoing airway complications of which 19F

and 9V serotypes were amongst the frequently isolated serotypes (Domenech et al., 2013; Mantero et al., 2017). These encapsulated serotypes which commonly colonizing in the respiratory epithelium are also more resistant than other serotypes to antibiotic therapy. Surprisingly, the death caused by common colonizer serotypes was more than invasive serotypes, highlighting the importance of these strains in the pathogenesis of lung diseases (Henriques-Normark & Tuomanen, 2013). However, the capacity of these serotypes in colonization of the mucosal surface is different. It was shown that *Sp* 19F is lowly colonized into the 16HBE cells as compared to serotype 2 and 4 (Surabhi et al., 2021).

Colonization of *Sp* to the mucosal surface is vital for its long-term survival and pathogenicity. *Sp* uses several strategies to evade immune responses and persistent adhesion to the mucosa (**Figure 2**). Of note, *Sp* expresses certain enzymes including PgdA and Adr to modify their peptidoglycan which protects *Sp* against lytic degradation by the host responses. Surface components of *Sp* including capsule, PspA, CbpA, Eno and PepO also provide protection by evading recognition by host complement. CbpE component of *Sp*'s cell wall also promotes attachment by disrupting PAFR on the cell surface, inhibiting neutrophil recruitment. Moreover, *Sp* utilizes mechanisms to circumvent mucociliary entrapment by host cells. *Sp* not only binds to the glycans in the mucus (e.g., by glycosidases such as StrH, NanA and BgaA), which is a gel-like glycoprotein secreted by mucosal cells, but also repel the polysaccharide components of the mucus by its negatively charged capsule. Avoiding host immune responses enable *Sp* to attach to the host mucosal surface which is mediated by *Sp*'s surface components. For example, *Sp* uses adhesive components to attach to fibronectin and plasminogen in the host cell surface such as surface located PavA, PavB and Eno. Moreover, ChoP in the cell wall of *Sp* binds to the PAFR, while CbpA binds to the PIGR as well as factor H protein, facilitating attachment to the cell surface. Other *Sp* adhesion molecules include peptidyl-prolyl isomerase and surface-exposed lipoproteins foldase protein (PrsA or PpmA) (Weiser et al., 2018).

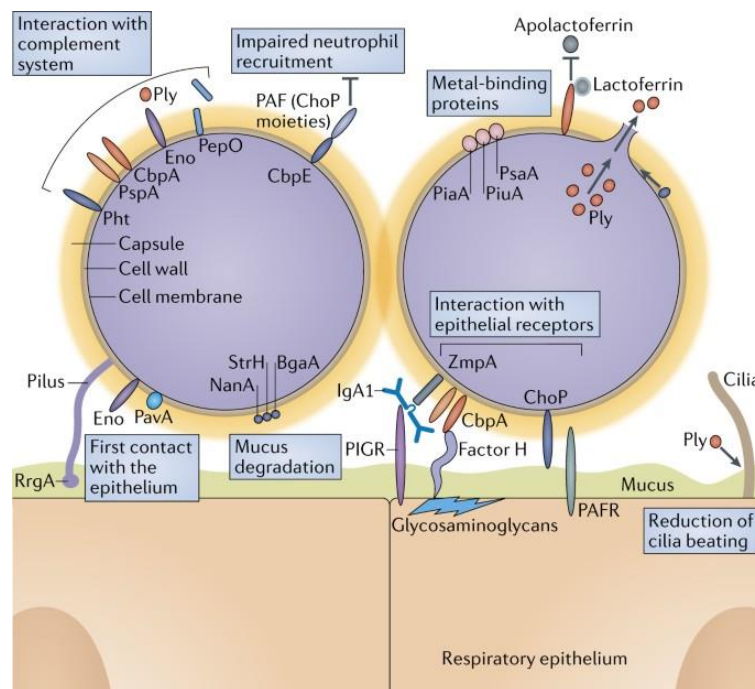


Figure 2: Molecular mechanisms of *Sp* colonization into the respiratory epithelium. Certain virulence factors in *Sp* facilitate attachment to the cell surfaces. First, *Sp* attaches to the host respiratory mucosa using cell surface proteins such as Eno and PavA. CbpA binds to *Sp*'s factor H which establishes *Sp* attachment to mucosal glycosaminoglycans. Moreover, CbpA binds to the PIGR in the host cell surface. Another surface virulence factor, ChoP, binds to the PAFR in the respiratory mucosal surface, inducing host inflammatory responses. *Sp* evades host defense responses by inhibiting mucociliary machinery and evading complement responses. Several glycosidases in *Sp* structure are responsible for degradation of mucus including NanA, β -N-acetylglucosaminidase StrH and BgaA. Certain cell surface factors in *Sp* interact with host complement factor that decrease *Sp* opsonization including PspA, CbpA, Eno and PepO. The figure was adopted from a cited reference (Weiser et al., 2018).

1.2.2. *Sp* airway epithelial colonization and host immune response

Colonization of *Sp* into the respiratory epithelium further accompanied by host immune recognition by pattern recognition receptors including TLRs and NLRs, which leads to the activation of pro-inflammatory responses (**Figure 3**). Of note, colonization of *Sp* 19F serotype in lung epithelium of mice lead to increased pro-inflammatory responses and particularly cytokine production including TNF- α , IL-17, IL-23 and IL-10 and increased number of Neutrophils in BAL 4 h after infection (Wilson et al., 2015), which is potentially triggered via virulence factors like PLY (I.-H. Yoo et al., 2010). Cell surface proteins as well as PLY are recognized by PRRs on the mucosal surfaces of the host such as TLRs and NLRs, triggering an inflammatory response. Of note, PLY and cell wall components of *Sp* (e.g. lipoteichoic acid) are recognized with TLR4 and TLR2/6 in turn, which leads to activation of NLRP3 inflammasome and AIM2 and subsequent inflammatory responses by release of IL-1 β , TNF- α and IL-6 (Koppe et al., 2012). MDP, a cell wall component of *Sp*, is recognized via a cytoplasmic PRR NOD2, which leads to RIP2-mediated activation of NF κ B and thus pro-inflammatory responses (Wiese

et al., 2017). However, studies revealed that *Sp* capsule impairs the recognition by specific TLRs and NLRs, therefore mucosal sensing receptor may not recognize the capsular serotypes (de Vos et al., 2015; Hommes et al., 2015). PLY may induce pro-inflammatory responses in the cells by forming pores in the cell membrane, which leads to the transfer of *Sp* circular CpG-containing DNA into the cytoplasm (Parker et al., 2011). Growing *Sp* usually undergo autolysis that leads to the release of *Sp* DNA and subsequent transmembrane acquisition into cytoplasm. The released DNA could be recognized with endosomal receptors such as TLR9 and DAI. TLR9 activation by *Sp* DNA leads to MyD88-mediated activation of NFκB (Koppe et al., 2012). Sensing of cytoplasmic *Sp* DNA by endosomal sensors such as DAI have been shown to trigger inflammatory responses in the lung of mice by inducing type I interferon responses, which contributes to the clearance of *Sp* (Parker et al., 2011). This protective type I interferon responses which is mediated by STING (Koppe et al., 2012) could be dampened during acute lung injuries by promoting barrier dysfunction and cell death (Maier et al., 2016). Type I interferons act on IFNAR and induces pro-inflammatory responses via phosphorylation of JAK-STAT1 that in turn lead to IRF9-dependent and independent expression of several ISGs (Makris et al., 2017). In addition to *Sp* DNA and PLY, it has been shown that *Sp*-derived H₂O₂ trans-diffuses the cellular membrane and induces a pro-inflammatory response by activating NLRP3 inflammasome in AECs leading to the release of IL-1β and subsequent protective cell death by activated caspase-1 (known as pyroptosis) (Surabhi et al., 2021). Therefore, *Sp* infection triggers protective pro-inflammatory responses in respiratory epithelium that may mitigate further damage.

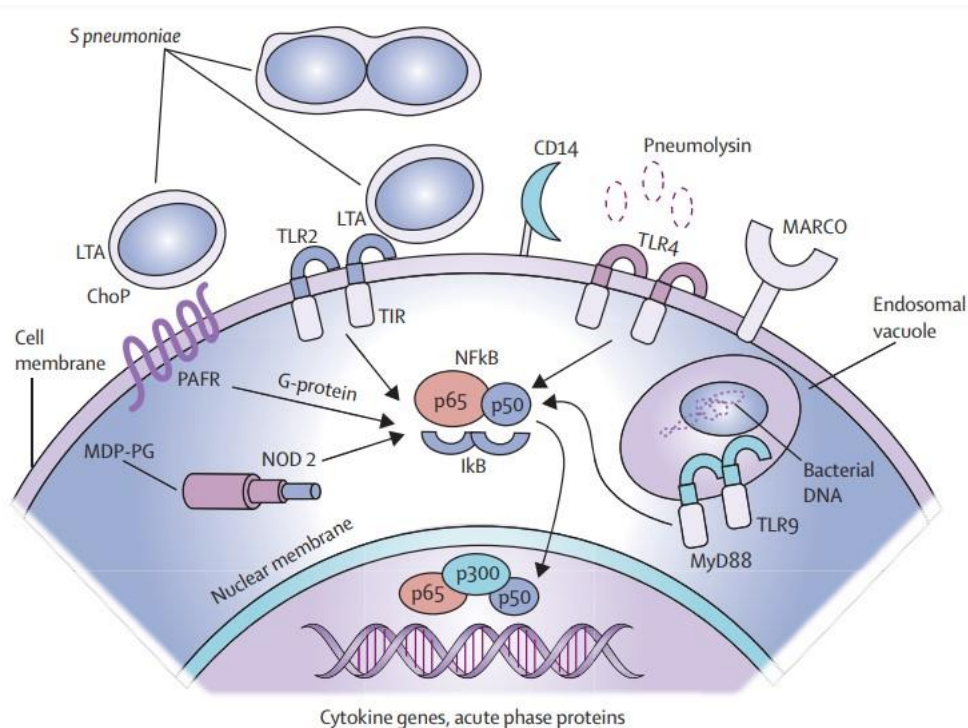


Figure 3: Recognition of *Sp* by host cell's pattern recognition receptors. Components of *Sp* are recognized by several host receptors including toll-like receptors such as TLR2, TLR4 and TLR9 or by PAFR-mediated activation of NOD2 and NLRs such as NLRP3, all of which leads to activation of NFκB pathway and subsequent pro-inflammatory response. The figure was adopted from a cited reference (van der Poll & Opal, 2009).

1.3. Airway epithelium in health

1.3.1. Structure of healthy airway epithelium

Airway epithelium of the respiratory tract is the first line of the physical defense barrier against inhaled noxious particles and gases in the inhaled air, thus understanding the normal architecture and function of airway epithelium is relevant in the pathogenesis of respiratory diseases (Aghapour et al., 2018). The epithelium of the human small airways is lined with a multilayer epithelium known as ciliated pseudo-stratified epithelium, which is composed of several subsets of cells, i.e., ciliated cells, secretory goblet cells, tuft cells, neuroendocrine cells, ionocyte, club and basal cells, of which the latter two have stem cell properties, acting as progenitor cells for other subset of the cells (Alysandratos et al., 2021). Maintaining this progenitor activity together with correct differentiation play a major role in re-epithelialization and repair of the airway epithelium upon damage i.e. with CS (Hewitt & Lloyd, 2021).

1.3.2. Airway epithelial barriers (chemical barriers and cell junctions)

In addition to providing a physical barrier, airway epithelial layer provides another means of defense by mechanochemical action known as mucociliary clearance by the is provided by ciliated cells and goblet cells, which are mostly found in larger airways and almost absent in the smaller airways (Ganesan et al., 2013). In human, mucous is produced by both goblet cells and submucosal glands (Bals & Hiemstra, 2004), providing a gel layer on the epithelial surface of the respiratory tract that traps pathogens and inhaled particles (Aghapour et al., 2018). Trapped pathogens and particles are removed by the concerted actions of cilia and by cough reflexes controlled by central nervous system (Aghapour et al., 2018). Moreover, the mucociliary function neutralize the toxicants in the inhaled air before introducing damage to the airway epithelium and sub-epithelial layers (Tilley et al., 2015).

Physical barrier function of the airway epithelium is maintained by the formation of epithelial junctions (Aghapour et al., 2018). Epithelial junctions act to functionally segregate the basal from the apical compartment to allow epithelial polarization, and may thus be critical for differentiation of basal epithelial cells into mucociliary epithelium (Cereijido et al., 1998). Additionally, apical junctional complexes between airway epithelial cells are an integral part of the mucosal immune system, regulating the protection against pathogens (Aghapour et al., 2018).

Barrier function restricts transepithelial crossing of such inhaled pathogens, and the importance of this function in airway diseases is illustrated by this fact that viral and bacterial infections are implicated in nearly half of patients experiencing exacerbations of airway complications (Sethi & Murphy, 2008). The junctional complex consists of TJs and AJs (Aghapour et al., 2018). TJs are located in the apical part of the mucosal surface, limiting permeability of the epithelium (Heijink et al., 2014), and are composed of the transmembrane proteins CLDN, TJ-associated MARVEL proteins such as OCLN, Tricellulin and MarvelD3 and JAMs (Ebnet et al., 2004; Krause et al., 2008; McCarthy et al., 1996; Schulzke & Fromm, 2009). In addition, several other cytoplasmic molecules such as ZO-1, ZO-2, ZO-3, cingulin, Par-3, Par-6 and afadin have been implicated in the formation of TJs. Such molecules act as a scaffold by binding to the transmembrane proteins and linking them with actin microfilament and other cytoplasmic proteins which preserve the stability of TJs (Anderson, 2001) (**Figure 4**).

AJs reside at the basolateral side of the more apically located TJs, connecting neighboring cells and initiating the formation of cell-cell contacts through homotypic, calcium-dependent adhesions by E-cadherin, a type I cadherin transmembrane glycoprotein (Niessen & Gottardi, 2008). The cytoplasmic domain of E-cadherin is stabilized in the membrane when bound to the anchor proteins p120 catenin, β -catenin and α -catenin, linking the complex to the cytoskeleton (Hartsock & Nelson, 2008) (**Figure 4**). Many signaling pathways regulating TJs formation and function, of which PKA, PKC, AMPK, MAPK and PI3K-Akt are well-known pathways (González-Mariscal et al., 2008).

It has been shown that α -catenin alone does not have the ability to join the E-cadherin/ β -catenin complex to the actin skeleton and cooperates with other proteins, such as epithelial protein lost in the neoplasm (EPLIN), vinculin and metformin (Dufour et al., 2013). Binding of the p120-catenin to the transmembrane domain of E-cadherin has been shown to be critical for the stability of E-cadherin in AJs (Hartsock & Nelson, 2008). E-cadherin is thought to provide the architecture required to form TJs, since the lack of proper E-cadherin expression in the epidermis, results in delocalization of TJ proteins ZO-1, OCLN and CLDN (Tunggal et al., 2005). In addition, genetic deletion of E-cadherin resulted in decreased ZO-1 expression in association with reduced epithelial resistance in airway epithelial monolayers (Heijink, Brandenburg, et al., 2010). Several studies proposed that kinase families of epidermal growth factor receptor (EGFR), Src and tyrosine phosphatases can be localized on the surface of AJs and cause interactions in the cytoplasmic domain of cadherin, β -catenin and p120-catenin (Hoschuetzky et al., 1994; Niessen & Gottardi, 2008).

Airway lumen

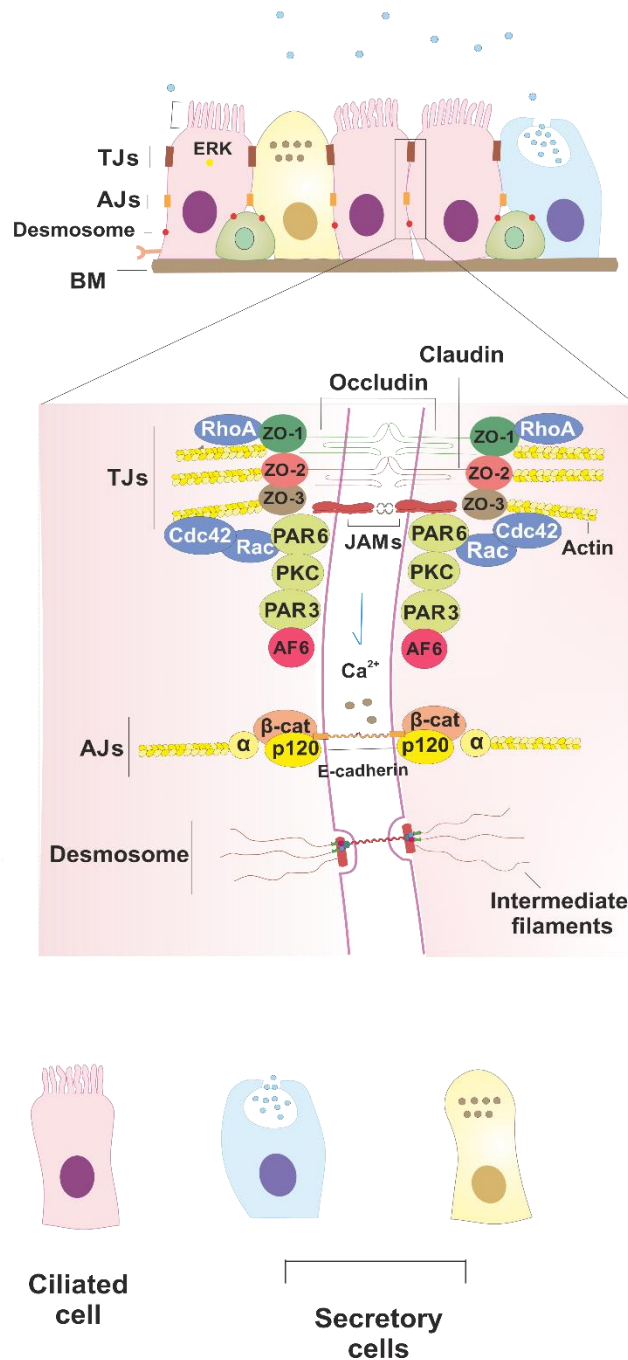


Figure 4: Schematic illustration of airway epithelial cell junctions. Apical junctions are composed of AJs and TJs regulating paracellular permeability of the cells. As the basolateral side of epithelial cells desmosomes maintain cellular integrity in the airways. The figure was adopted from a cited reference (Aghapour et al., 2018).

1.4. Airway epithelial disruption in smokers

Smoking has been reported to reduce known apical junction genes in the airway epithelium (Shaykhiev et al., 2011). It was reported that TJ protein expression is disrupted in lung tissue of patients with airway diseases as well as in air-liquid interface differentiated epithelial cells from these patients compared to controls (Heijink et al., 2014). This may have important consequences

for the pathogenesis of airway diseases, as outlined below. Therefore, it is of interest to gain insight into the mechanisms responsible for airway epithelial barrier dysfunction and the impaired ability to re-differentiate into intact epithelium upon smoking.

In addition to cell-cell contacts, cigarette smoking alters the airway epithelial layer, leading to goblet cell hyperplasia (Schamberger et al., 2014) and affecting cilia length as well as cilia turnover by a selective autophagy, named ciliophagy (Cloonan & Choi, 2016). In addition, cigarette smoking impacts on epithelial barrier function. Early *in vivo* smoke-exposed models have shown that CS induces permeability of the airway mucosa (Hogg, 1982). Moreover, several studies have reported that CS also transiently impairs epithelial barrier function *in vitro*, disrupting TJs such as OCLN and ZO-1 as well as JAM3 and CLDN11 and CLDN18 (Amatngalim et al., 2015; Gindele et al., 2020; Heijink et al., 2012; Petecchia et al., 2009; Schamberger et al., 2014). In line, it was demonstrated that CSE, which only preserved gas properties of CS, reduces expression of E-cadherin and ZO-1 *in vitro* in primary AECs from patients with airway disease but not control smokers, an effect that may be caused by ROS-dependent decrease in cAMP (Milara et al., 2013).

1.4.1. Mechanisms of CS-induced disruption of cell-cell contacts

Several mechanisms have been implicated in the cigarette smoke-induced barrier dysfunction, which are summarized in **Figure 5**. Of note, CS exposure induces disruption of E-cadherin-mediated barrier function in airway epithelial cells *in vitro* by downregulation of A-Kinase anchoring protein expression (AKAP)-9 (Oldenburger et al., 2014). AKAP-9 regulates sublocalization of PKA, which was shown to be involved in localization of E-cadherin to the basolateral membrane (Oldenburger et al., 2014). As PKA is a downstream effector of cAMP, these findings may help to explain why decreased cAMP levels lead to disrupted expression of E-cadherin (Milara et al., 2013). Of note, a decrease in E-cadherin protein expression was observed in lung tissue of patients with airway complications compared to controls matched for smoking history (Oldenburger et al., 2014). Activation of EGFR and downstream ERK upon the generation of ROS has been observed upon CS exposure in AECs (Heijink, van Oosterhout, et al., 2010; Petecchia et al., 2009). CS exposure and subsequent ROS production have also been shown to induce EGFR phosphorylation at Tyr-845, leading to Src kinase phosphorylation and inhibiting EGFR degradation (Khan et al., 2008). Additionally, CS has been shown to induce EGFR activation through Rac1 and Cdc42 and p120-catenin-dependent mechanism (L. Zhang et al., 2012, 2013). CSE-induced decrease in trans-epithelial resistance and cleavage junctional delocalization of scaffolding proteins ZO-1 and OCLN in airway epithelial cells *in vitro* was

shown to be EFGR-dependent (Heijink et al., 2012). In addition, CSE-induced downregulation of junctional-related genes and reduction of trans-epithelial resistance in basal airway epithelial cells has also been shown to be mediated by EGFR activation (Shaykhiev et al., 2013; Zuo et al., 2017). Another mechanism was reported for CS-induced airway epithelial barrier dysfunction, in which HER2-dependent EGFR activation followed by MAPK-mediated IL-6 release decreases trans-epithelial resistance through an unknown IL-6 dependent mechanism (R. Mishra et al., 2016). CS has been demonstrated to activate ROCK and phosphorylate ZBR in OCLN in AECs, thereby dissociating these two proteins and consequently disrupting epithelial integrity (Olivera et al., 2010). Finally, it has been shown that ROS present in CS induces fragmentation of hyaluronan in AECs *in vitro*, impairing barrier integrity by binding to its epithelial surface receptor layilin and mediating RhoA/ROCK-dependent decrease in E-cadherin expression, both at the gene and protein level (Forteza et al., 2012). Importantly, it has previously been shown that SOD3, a susceptibility gene for airway diseases (Siedlinski et al., 2009), abrogates hyaluronan fragmentation (F. Gao et al., 2008). Increased fragmentation of hyaluronan as a result of lower SOD3 expression may thus induce disruption of epithelial junctions and increase permeability of the airway epithelium in smokers (Aghapour et al., 2018). In line, higher levels of low molecular hyaluronan have been observed in lung tissue of patients with severe airway complications (Dentener et al., 2005). Furthermore, in smokers with airway disease, a polymorphism in the antioxidant genes SOD3 as well as glutathione S-transferase isoenzyme was associated with reduced lung function compared to asymptomatic smokers (Aghapour et al., 2018; S. L. Cheng et al., 2004; Dahl et al., 2008; Sørheim et al., 2010).

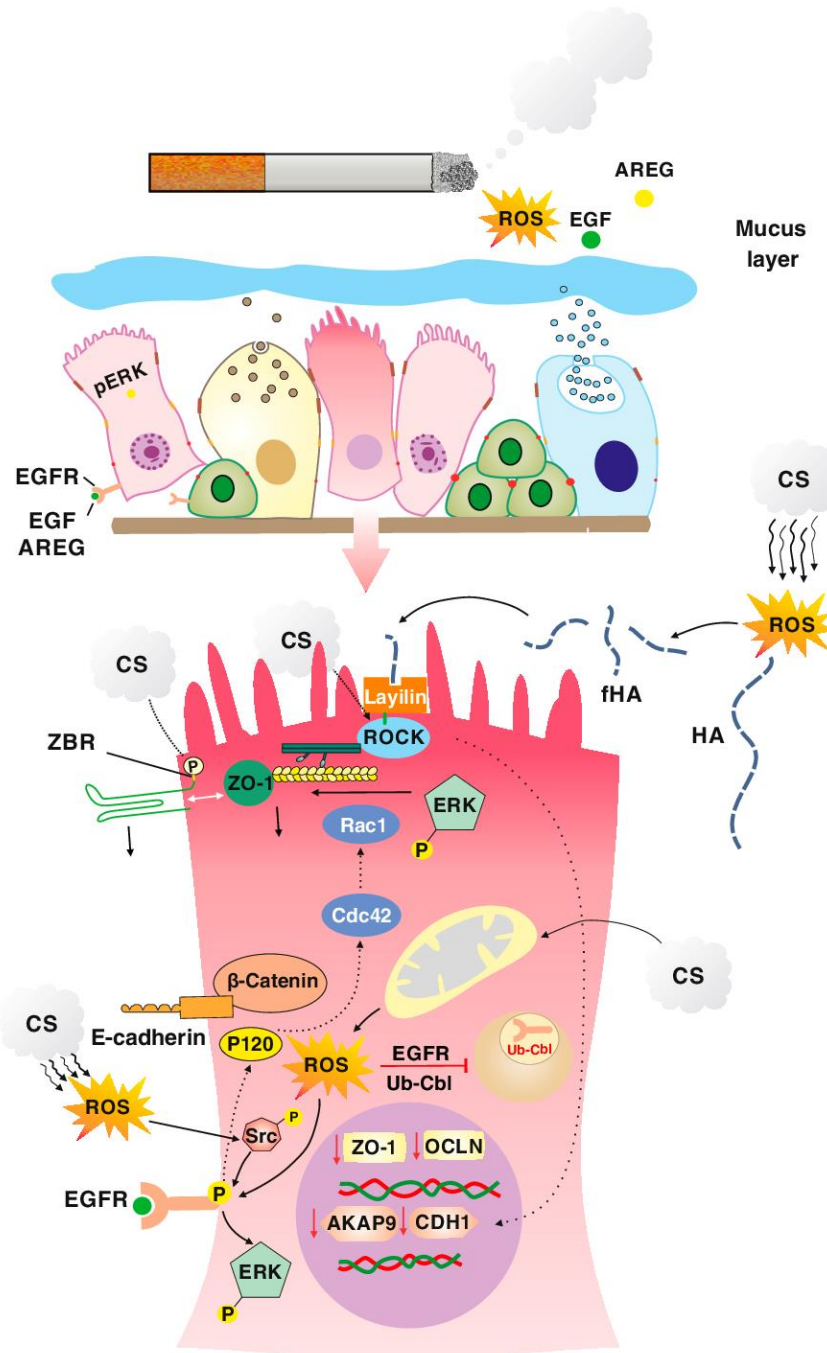


Figure 5: Molecular mechanisms underlying CS-induced airway epithelial barrier dysfunction. CS-induced increase in ROS either directly or indirectly disrupts airway epithelial barriers. ROS-regulated activation of EGFR and ERK are involved in disruption of apical junctions. The figure was adopted from a cited reference (Aghapour et al., 2018).

1.4.2. CS-induced pro-inflammatory responses and cell-cell contact disruption

Moreover, CS induces changes in pro-inflammatory responses that may induce airway epithelial barrier disruption (Aghapour et al., 2018). Many mediators of innate and adaptive immunity are known to regulate the physical barrier function of the airway epithelium, including cytokines, chemokines, antimicrobial peptides and lipophilic factors (Aghapour et al., 2018). Among cytokines, especially Th2 and 17 cytokines have been proposed as key disruptive factors for

epithelial integrity. Higher levels of the Th2 cytokines IL-4 and IL-13 have been observed in the airway epithelium of smokers with chronic bronchitis versus healthy smokers (Ramezanzpour et al., 2016; Saatian et al., 2013). Though higher IL-4 levels have been reported in the bronchoalveolar fluids of patients with airway disease, reduced IL-4 expression has been observed in lung tissue of these patients compared to controls and this was shown to be associated with the severity of disease (Barceló et al., 2006; Perotin et al., 2014). On the other hand, results of a gene expression analysis have shown an elevation in IL-13 expression in lung tissue of severe airway disease as compared controls (Alevy et al., 2012). The direct exposure of AECs to IL-4 and IL-13 *in vitro* was shown to induce enhanced permeability of the epithelium through the activation of JAK (Saatian et al., 2013). Nevertheless, to the best of our knowledge, there is no evidence of association between Th2 cytokine levels and increased permeability in smoke-exposed airway epithelium (Aghapour et al., 2018). IL-17 is mainly released from Th17 cells, but its expression has also been observed in the AECs (Di Stefano et al., 2009; Shen et al., 2011). The number of Th17 cells has been reported to elevate in blood samples and airway of patients with airway disease compared to controls (Vargas-Rojas et al., 2011; J. Zhang et al., 2013). Furthermore, increased expression of IL-17 has been observed in the airway epithelium of stable as well as patients with severe airway disease which was accompanied with a decline in lung function (Doe et al., 2010; Roos et al., 2015). This elevated expression of IL-17 seems to activate Th17 cells and promote airway neutrophilic inflammation. An *in vivo* study has unraveled that CS-induced over-secretion of IL-17 may induce secretion of IL-6 and IL-8 in the airway epithelium which was associated with the severity of airway complications (Shen et al., 2011). It was shown that Th17 cytokines are the predominant inducers of AJs disruption in a rhinosinusitis animal model (Ramezanzpour et al., 2016), whereas no significant change observed with either Th1 or Th2 cytokines, which is in contrast with earlier findings indicated that IL-17 is not responsible for epithelial barrier dysfunction, while IL-4 and IFN- γ disrupted epithelial integrity in primary cultures of human sinonasal epithelial cells resected from rhinosinusitis patients. In addition, higher levels of Th1 cytokines IFN- γ have been observed in the lung tissue, bronchoalveolar lavage and sputum samples of patients with airway disease (Soyka et al., 2012). Although earlier studies showed increased level of pro-inflammatory mediator TNF- α both in sputum and bronchoalveolar lavage of patients with airway disease (Aaron et al., 2001; Hodge et al., 2007), lower level of TNF- α has been observed in sputum samples of these patients compared to the control (Moermans et al., 2011). Pre-treatment with IFN- γ or TNF- α has been described to induce EGFR-mediated airway junctional disintegration and their co-treatment induces PKC-dependent dissociation of AJs in AECs (Coyne et al., 2002; Petecchia et al., 2012).

Moreover, recent evidence shows that TNF- α mediated loss of E-cadherin is in Src-dependent fashion (Hardyman et al., 2013). Another pro-inflammatory cytokine that may participate in airway junctional dysfunction is IL-1 β (Aghapour et al., 2018). A marked elevation in IL-1 β levels has been observed in AECs of smokers with airway disease and asymptomatic smokers exposed to mainstream CS compared to non-smokers (Rusznak et al., 2000). In line, the protein levels of IL-1 β were shown to be increased in sputum samples of both stable and exacerbated airway disease (Damera et al., 2016; Pauwels et al., 2011). Recent investigations have reported that upon *in vitro* exposure of AECs to exogenous IL-1 β , HER2 is activated through a disintegrin and metalloproteinase 17-dependent release of NRG-1 ligand, dissociating intercellular β -catenin-E-cadherin adhesion complex and reduce barrier function (Finigan et al., 2011). In addition, IL-6 as a cytokine extensively described for its implication in pathogenesis of airway disease (Rincon & Irvin, 2012), has been demonstrated to disrupt airway epithelial integrity (R. Mishra et al., 2016). Of note, CS-induced EGFR-dependent activation of HER2 has also been shown to increase airway epithelial permeability through overproduction of IL-6 (Aghapour et al., 2018; R. Mishra et al., 2016). These mediators and their mechanisms for induction of airway epithelial barrier disruption have been summarized in **Figure 6**.

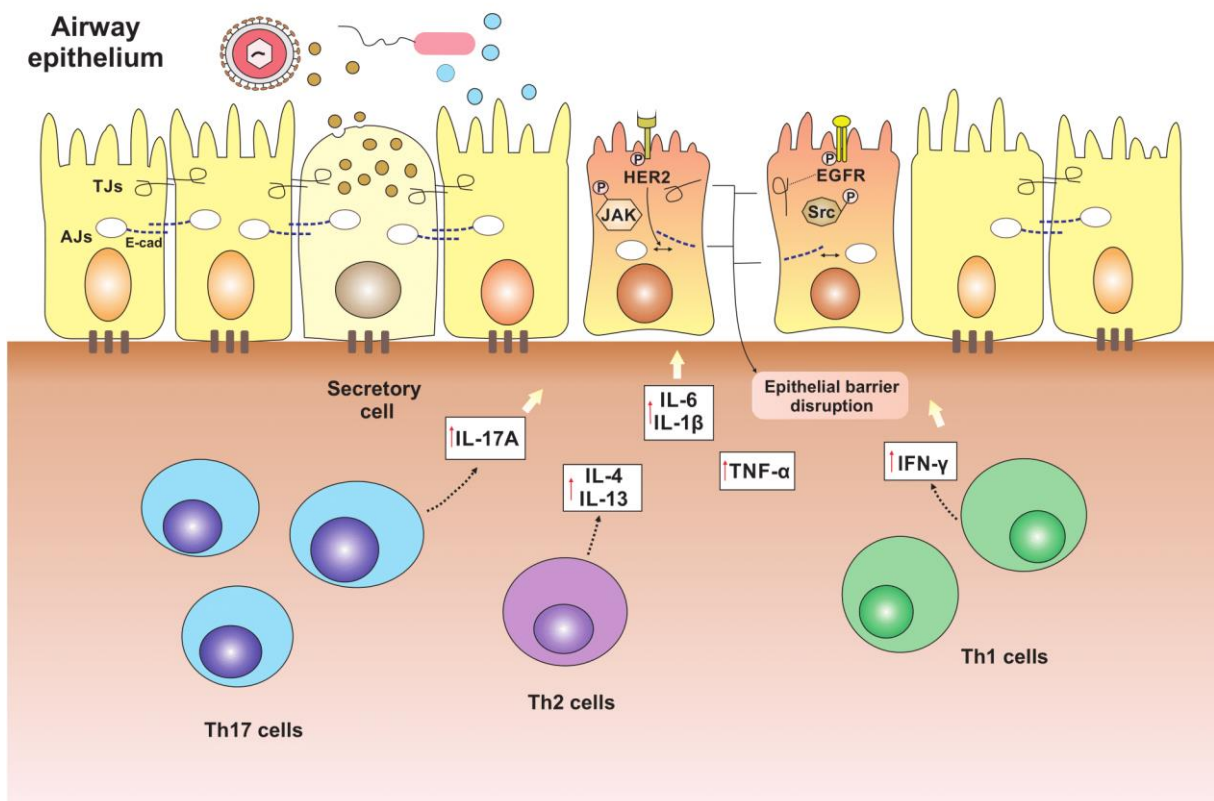


Figure 6: Airway epithelial barrier dysfunction induced by CS-induced changes in pro-inflammatory responses. Three known pathways of JAK and EGFR are affected by pro-inflammatory mediators induced by CS that leads to epithelial barrier disruption. The figure was adopted from a cited reference (Aghapour et al., 2018).

There are also barrier protective mediators released by AECs that their levels may alter in response to CS (Garmendia et al., 2012). CC10 acts as an essential barrier protective factor for airway epithelium (Hiemstra & Bourdin, 2014). Down-regulation of CC10 has been observed in lung tissue of patients with airway disease and CS-exposed animals and may indirectly contribute to the leaky manifestation of airway epithelium (Hiemstra & Bourdin, 2014; Laucho-Contreras et al., 2015; Zhu et al., 2015). Moreover, the elevated expression of RNase 7, an epithelial antimicrobial peptide, have been associated with EGFR-dependent disintegrated airway epithelium induced by CS, implying a compensatory protective role in maintaining epithelial integrity for RNase 7 (Aghapour et al., 2018; Amatngalim et al., 2015). Cathelicidin LL-37 is another known antimicrobial peptide that has shown epithelial barrier protective effects. Of note, treatment of AECs with LL-37 reduced *Pseudomonas aeruginosa*-induced permeability (Byfield et al., 2011). More recently, it was shown that 2 h stimulation of AECs with LL-37 inhibits CS-induced decrease in TEER until 48 h post CSE and restored CS-induced decrease in ZO-1 and OCLDN, suggesting a barrier protective effect for LL-37 upon CS (Tatsuta et al., 2019).

Loss of barrier function may also lead to alterations in the production of immune modulators by the airway epithelium in a feedback loop manner (Aghapour et al., 2018). Previously published findings indicated that airway epithelial disruption induced by genetic deletion of E-cadherin promotes the release of pro-inflammatory cytokines by activation of EGFR and downstream signaling pathways (Heijink et al., 2007). Furthermore, it has been reported that damaging stimuli can increase cytokine pro-inflammatory response in ALI airway epithelial cultures (Hackett et al., 2011). These observations reinforce the importance of immune mediators in the regulation of airway barrier function (Aghapour et al., 2018).

As a structure with high functionality, the airway epithelium is a highly energy-dependent structure that might be affected by bioenergetic imbalances that is observed in airway disease (Aghapour et al., 2020). Furthermore, the airway epithelium actively responds to the inhaled toxicants e.g., CS by production of antimicrobial peptides, pro-inflammatory cytokines and signaling pathways affecting physical barrier junctions that either stimulated by changes in these two earlier factors or other factors that regulating these signaling pathways. These mechanisms will be further elaborated in the next chapter.

1.5. Mitochondrial function in AECs

1.5.1. Mitochondrial oxidative respiration in health

Mitochondria are double-membrane organelles with prokaryotic ancestors that are thought to have been incorporated into the eukaryotic cell cytoplasm during evolution (Zimorski et al., 2014). Despite this evolutionary adaptation, mitochondria have preserved their own specific structures such as CpG-rich DNA, membrane lipids (e.g., cardiolipin), N-formylated peptides and bioenergetic pathways, while functioning as a part of an integrated intracellular system, mostly regulated by genomic DNA. MtDNA encodes 37 genes (**Figure 7**), most of which regulate OXPHOS, a process on the inner mitochondrial membrane in which transfer of electrons through a chain of enzymatic complexes (I-IV) leads to the production of ATP in the last electron recipient ATP synthase (complex V) (Cloonan & Choi, 2016) (**Figure 8**). Generation of ATP, as the most important function of the mitochondrion, provides the energy required for a wide variety of cellular processes. Interestingly, different subtypes of lung epithelial cells, including ciliated cells, secretory goblet and club cells, and progenitor basal cells, each responsible for a specific task, contain a distinct number of mitochondria with different intra-cellular organization to best facilitate energy demand and cellular function (Aghapour et al., 2020). For instance, in ciliated AECs mitochondria with highly folded cristae and a dense matrix are mostly concentrated in the apical side (Xu et al., 2014), while in airway goblet cells mitochondria reside around the nucleus (Bueno et al., 2015; Bustamante-Marin & Ostrowski, 2017). In basal and club cells of the airway epithelium, mitochondria spread throughout the cytoplasm (De Proost et al., 2008; Rokicki et al., 2016). This cell-specific distribution of mitochondria affects ATP levels that are subsequently used for specific functions of these different cell types (ciliary beating or mucus secretion in differentiated AECs). In addition, different epithelial cell subsets display a range of sensitivity in response to mitochondrial damage. For example, mitochondria in club cells were shown to be most susceptible to metabolic changes compared to other cell types within the airway epithelium (Kuroda et al., 2017). Recent data from single-cell transcriptome sequencing verifies that human club cells are metabolically active with extensive number of functional mitochondria, rendering them highly sensitive to oxidative damage (Aghapour et al., 2020; Zuo et al., 2018).

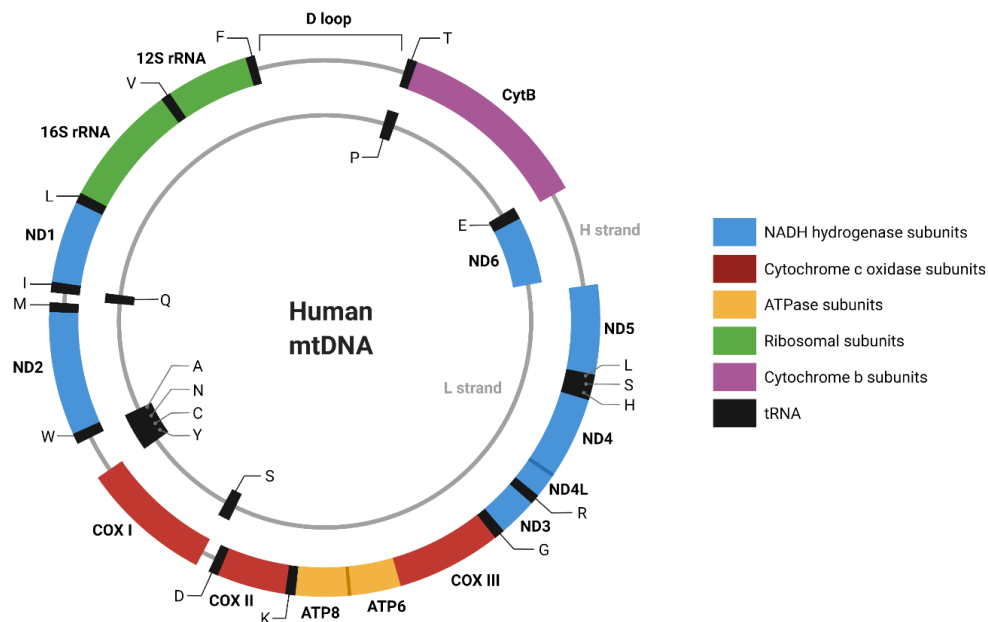


Figure 7: Mitochondrial genome structure. MtDNA encodes 36 genes mostly regulating OXPHOS in the cells. The schematic figure was modified by a template image from BioRender.com.

Disturbances in production of ROS in mitochondria can also contribute to cellular injury. Under normal physiological condition, ROS released from the mitochondria act as second messenger to maintain cellular homeostasis (Aghapour et al., 2020). Several mitochondrial proteins, in particular those in the ETC, can contribute to ROS formation including complex I and III of the

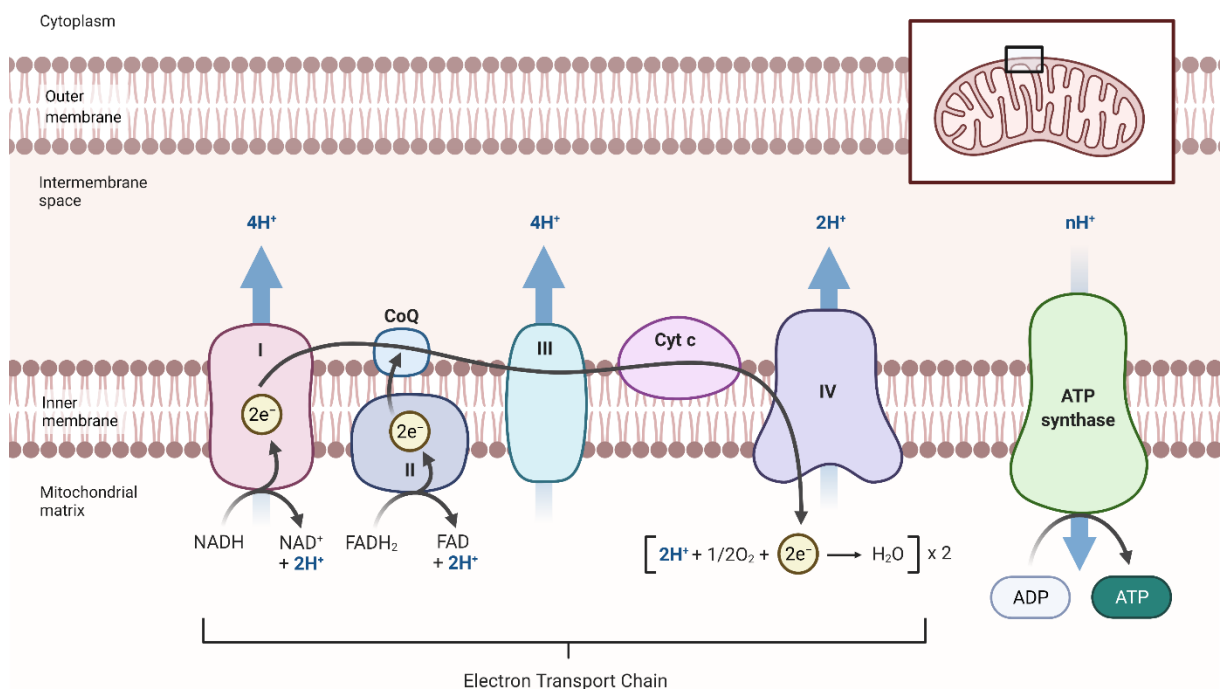


Figure 8: Schematic illustration of oxidative phosphorylation and electron transport chain in mitochondrion. Oxidative phosphorylation, a process that ATP generates as a result of proton gradients, occurs in the inner membrane of mitochondria. The process of transfer of electron through four mitochondrial complexes (I, II, III and IV) known as electron transport chain causes enzymatic oxidation of nutrients. Mammalian cells harbors energy from nutrients in form of NADH (entering at complex I) or succinate (generated at complex II) mainly originating from Krebs cycle taking place in complex II. NADH and FADH₂ provide the electron for the initiation of process which leads to electron transport and proton pumping. The generated proton gradient is received by complex V, where ADP is phosphorylated to form ATP. The figure modified by a template image from BioRender.com.

ETC, UQCRC2 (Aguilera-Aguirre et al., 2009) and UCP2 (Mailloux & Harper, 2011). ROS however are excessively generated in damaged mitochondria. Besides being the main endogenous producers of ROS, mitochondria are also the main targets of ROS, resulting in oxidative damage to the mtDNA or mitochondrial proteins. Indeed, prolonged exposure to oxidative stress can lead to mtDNA damage and mutations with excessive electron leakage, inflicting further oxidative stress in a vicious cycle (Aghapour et al., 2020).

1.5.2. Mitochondrial dynamic processes in health

The mitochondrial network is highly dynamic allowing adaptation to changes in homeostatic conditions and cellular responses to damage. Processes involved in remodeling of the mitochondrial network include fusion and fission events, e.g., to exchange mtDNA during repair processes, biogenesis of new organelles and mitochondrial clearance by mitophagy (Ni et al., 2015). The biogenesis of mitochondria is largely regulated by PGC-1 α and PGC-1 β , with TFAM and NRF1/2 acting as key downstream regulators (Ploumi et al., 2017). Activation of several kinases can contribute to mitochondrial biogenesis via regulation of PGC-1 α . Among these, PKC, MAPK and AMPK, an upstream regulator of mechanistic mTOR (Herzig & Shaw, 2018), are of interest because of their role in CS-induced epithelial cell dysfunction (Antico Arciuch et al., 2012). Although increased biogenesis seems to be beneficial for cellular functions, increased ROS as a result of an increase in the number or activity of mitochondria may potentially render the cells more vulnerable to deleterious processes such as irreversible growth arrest or senescence (Aghapour et al., 2020; Hara et al., 2018).

Mitochondrial fusion and fission events are primarily regulated by specialized proteins in the OMM and IMM. These proteins belong to GTPases family of dynamin proteins, which are chiefly regulated by the proteolytic machinery (R. Mishra et al., 2016). During fission the OMM is segregated by DRP1 upon recognition by the OMM receptors, FIS1, MFF, MID49 and MID51, resulting in a fragmented mitochondrial network (Aghapour et al., 2020; P. Mishra & Chan, 2014) (**Figure 9**). Phosphorylation of DRP1 play a key role in activity of DRP1. Phosphorylation of DRP1 at Serine 616 leads to translocation of DRP1 from cytosol to outer mitochondrial membrane, while phosphorylation at Serine 637 deactivates DRP1. DRP1 is phosphorylated by

many kinases including AMPK (Ducommun et al., 2015), MAPK (Kashatus et al., 2015) and CDK1 (Taguchi et al., 2007) (**Figure 10**). During fusion, the OMM proteins MFN1 and MFN2 as well as the IMM protein OPA1 tether mitochondrial membranes, encouraging fusion, allowing neighboring mitochondria to exchange genetic material, as well as promoting OXPHOS capacity (R. Mishra et al., 2016). Silencing fusion factors OPA1 and MFNs lead to mitochondrial fragmentation and subsequent irreversible cell growth arrest in AECs, while inhibition of FIS1 and DRP1 does not impact cell growth (Hara et al., 2013), suggesting an essential role of mitochondrial fusion and not fission in regulation of cell growth (Aghapour et al., 2020) (**Figure 9**).

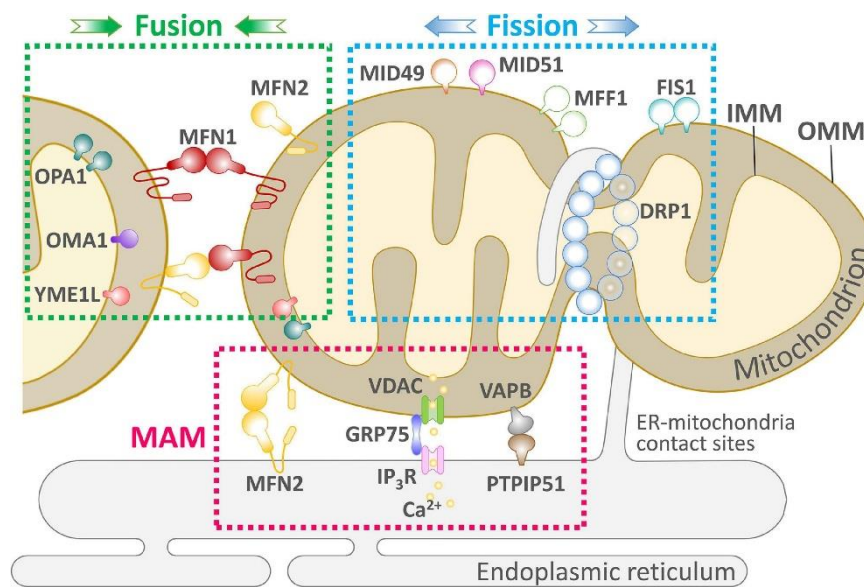


Figure 9: Mitochondrial fusion and fission processes. The main regulators of mitochondrial fusion are mitofusion proteins (MFN1 and MFN2), which mediate fusion of mitochondria at outer mitochondrial membrane. Mitochondrial fission is mainly regulated by DRP1, which is oligomerized upon phosphorylation and attachment to mitochondrial fission regulators MID49 and FIS1. The figure was adopted from a cited reference (Chiu et al., 2021).

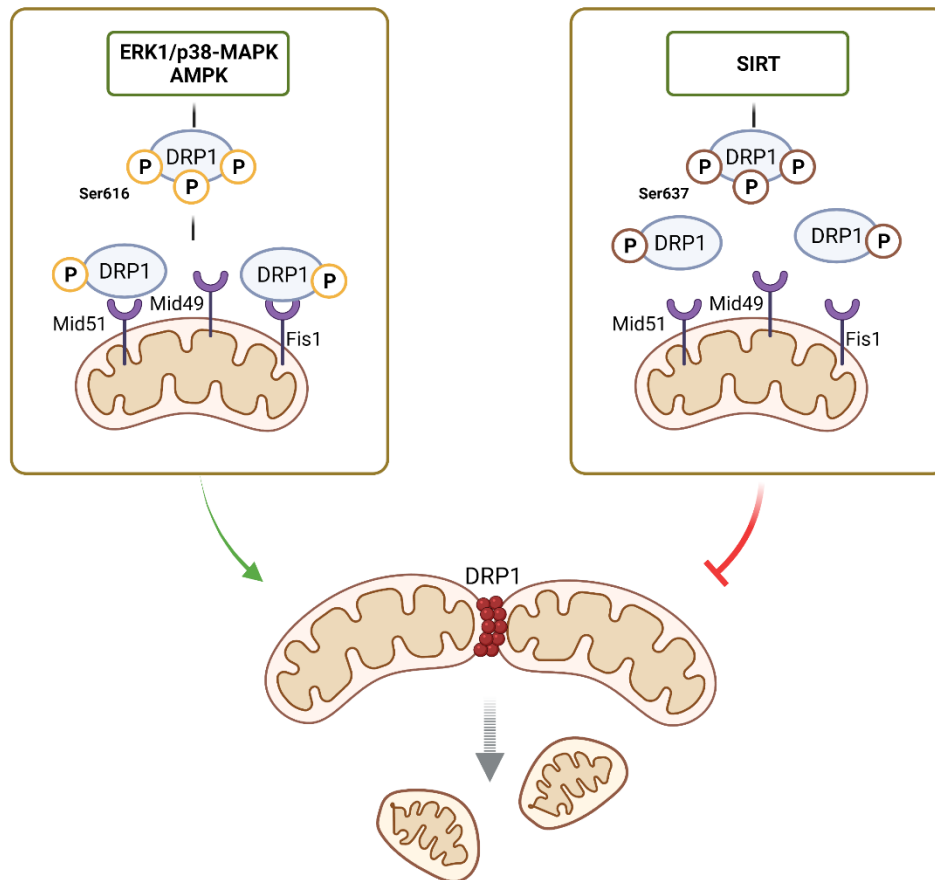


Figure 10: Phosphorylation of DRP1 and fission processes. Phosphorylation of DRP1 at Serine 616, which is triggered by activation of ERK or AMPK signaling pathways, leads to subsequent attachment of p-DRP1 to mitochondrial fission regulators MID49 and FIS1 and oligomerization of p-DRP1 on OMM, leading to degradation of OMM. In presence of SIRT activation, DRP1 phosphorylates at Serine 637 which inhibits attachment of DRP1 to cell surface adaptor proteins and leading to inhibition of mitochondrial fission. SIRT1 not only activate mitochondrial biogenesis via PGC1 α but also prevent degradation of mitochondria by inhibiting mitochondrial fission via phosphorylating DRP1 at Ser637. The figure is a modified version of the figure used in a cited reference (Ren et al., 2020) and is created with BioRender.com.

1.5.3. Mitophagy machinery in AECs in health

Autophagy is a cellular process that promotes physiological turnover of cells and intracellular organelles, leading to cell survival (Das et al., 2012). There are three major types of autophagy: 1) Macroautophagy, 2) Microautophagy, and 3) Chaperon-mediated autophagy. Macroautophagy is a process mediated by formation of membranous cytosolic structure namely autophagosome that is fused to lysosome to sequester the cargo. Unlike macroautophagy, chaperone-mediated autophagy is independent of autophagosome formation during which specific unfolded proteins are transported across the lysosomal membrane. During microautophagy, the cargo directly invaginate into the lysosome for degradation. All different types of autophagy eventually culminate in degradation of the organelles in the lysosome

(Parzych & Klionsky, 2014) (**Figure 11**). Mitophagy is a term used for specific type of macroautophagy that leads to degradation of damaged mitochondria (Onishi et al., 2021). Under conditions of mitochondrial injury, damaged or dysfunctional mitochondria are removed by mitophagy (Ni et al., 2015). PINK1, a master regulator of mitophagy (Hara et al., 2018) undergoes proteasomal degradation in healthy cells via recruitment of E3 ligase PARK2-encoded Parkin upon translocation to the IMM (Youle & Narendra, 2011). Under stressful conditions (e.g., oxidative damage) this proteasomal degradation is impaired, leading to accumulation of PINK1 in the OMM and subsequent recruitment of Parkin. Parkin then ubiquitinates several proteins in the OMM, acting as tagging signal for engulfment of stressed mitochondrion in an autophagosome (T. N. Nguyen et al., 2016). Autophagosomal degradation of mitochondria is mediated by several adaptor proteins including ATGs, Beclin-1, LCB3 and p62 or SQSTM1 and GABARAPL1 (Ryter & Choi, 2010). Additionally, there is a receptor-mediated mitophagy that is triggered via PINK1-independent dephosphorylation of the OMM receptor FUNDC1, and PINK1-dependent phosphorylation of BNIP3 and BNP3L or Nix proteins, facilitates the formation of the autophagosome (Aghapour et al., 2020; S.-M. Yoo & Jung, 2018) (**Figure 12**).

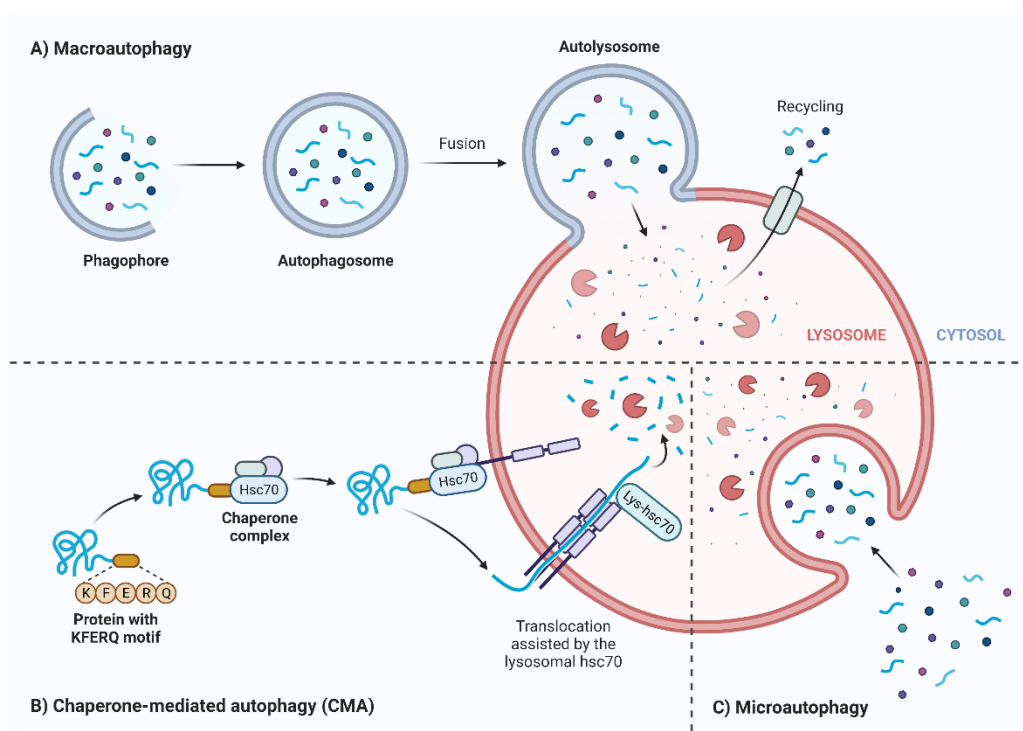


Figure 11: Three different types of autophagy. **A)** Macroautophagy process is initiated via formation of double membrane phagophore and autophagosome which is fused to lysosomal membrane to generate autolysosome. **B)** Chaperone-mediated autophagy directly transfer unfolded proteins containing KFERQ motif across lysosome. **C)** Microautophagy is triggered via direct transfer of cargo by engulfment into lysosome. The figure was modified by a template image from BioRender.com.

Mitophagy process, mitochondrial dynamic processes (fission and fusion) and mitochondrial biogenesis are in a balanced situation in physiologic state in the cells (**Figure 13**). Increased mitochondrial fission may lead to either more mitochondrial degradation via mitophagy or may cause formation of new mitochondria (Ma et al., 2020). This balance may be altered which may cause perturbation in mitochondrial function.

CS may induce disruption of mitochondrial morphology and function as well as imbalances in mitophagy, mitochondrial fission and fusion and mitochondrial biogenesis in lung epithelial cells, causing mitochondrial dysfunction, thereby depleting cellular energy and altering various homeostatic cellular functions. This may include those regulating epithelial barrier function, innate immunity, cell growth and differentiation, ultimately contributing to development and progression of airway disease (Aghapour et al., 2020).

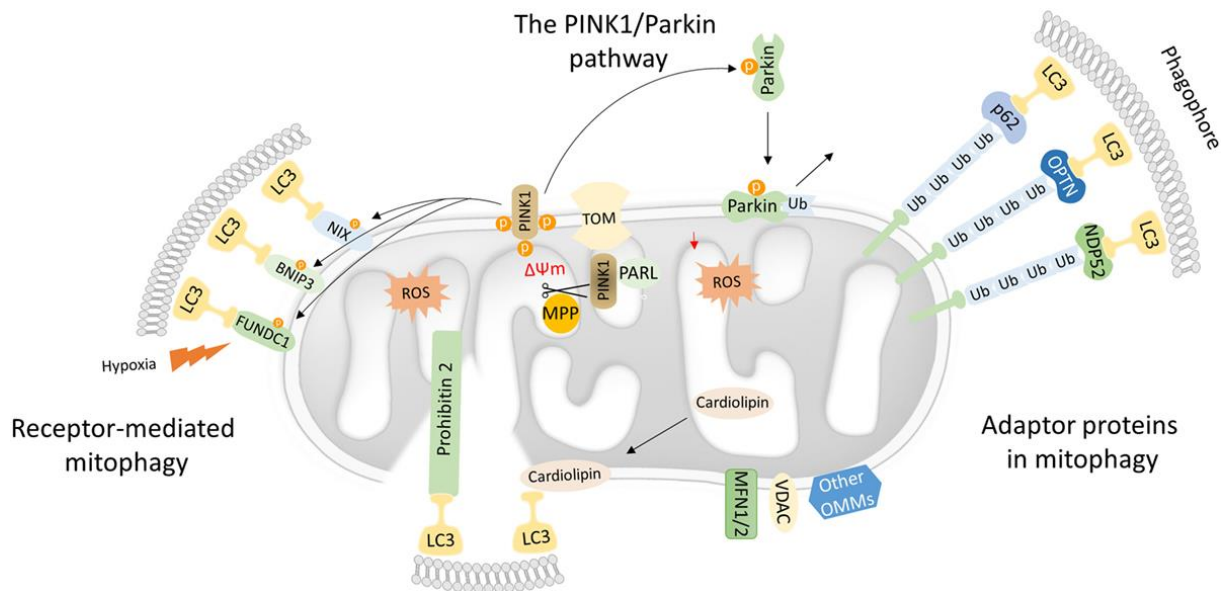


Figure 12: Schematic illustration of mitophagy machinery. There are two types of mitophagy: 1) Ubiquitin-mediated mitophagy that is mediated by proteasomal degradation of PINK1 via a E3 ligase Parkin and 2) receptor-mediated mitophagy that is mediated by certain receptors such as FUNDC1, BNIP3 and BNIP3L (Nix) all of which interact with LC3 to promote formation of autophagosome. The figure was adopted from a cited reference (Gkikas et al., 2018).

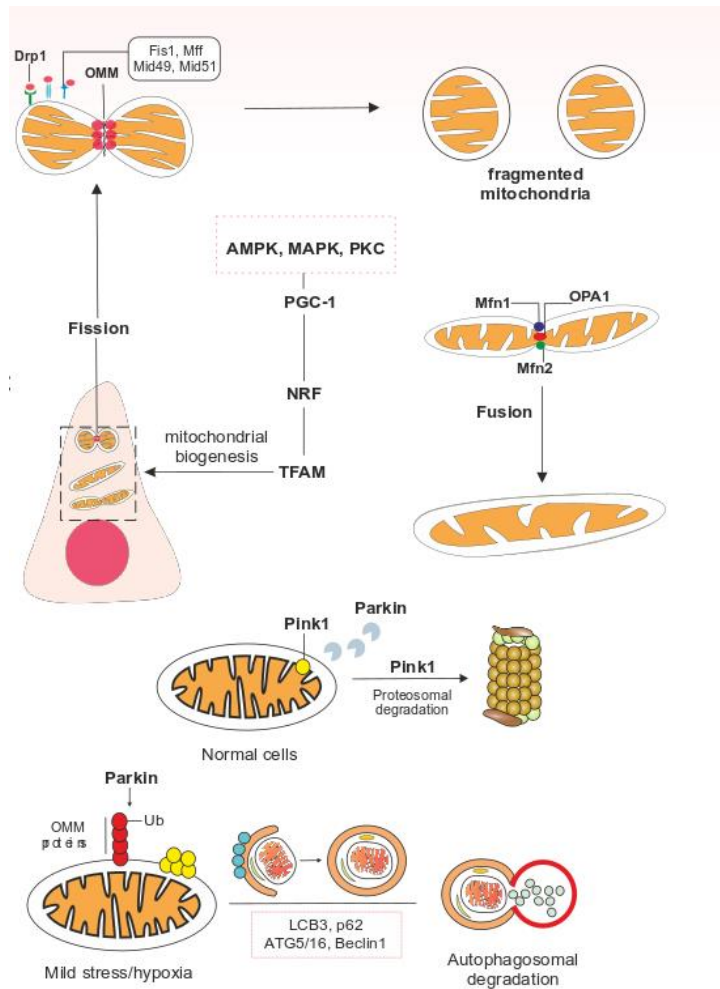


Figure 13: Balance between mitophagy, mitochondrial dynamic processes and mitochondrial biogenesis. Mitophagy is regulated by several proteins including PINK-1 and Parkin. In homeostatic condition, translocation of PINK-1 to the inner membrane triggers recruitment of E3 ligase Parkin, which leads to proteasomal degradation of PINK-1. However, upon mild stress some mitochondria undergo complete degradation by mitophagy, in which accumulation of PINK-1 in the outer membrane and subsequent ubiquitination of several proteins by Parkin leads to engulfment of the damaged mitochondrion by autophagy compartments. Formation of new mitochondria can also be triggered by activation of PGC-1 α and downstream signals, NRF1/2 and mitochondrial TFAM. Activation of several proteins, including AMPK, MAPK and PKC may activate PGC-1 α signaling pathway and in turn lead to synthesis of mitochondria. The figure is a modified version from a cited reference (Aghapour et al., 2020).

Many cellular signaling pathways can regulate mitophagy in the cells including mTOR and AMPK pathways (Aghapour et al., 2020). These pathways contribute to mitophagy by either directly affecting mitophagy regulators or by promoting autophagosome formation. Activation of mTOR pathway and in specific mOTRC1 which is triggered by oxidative stress (J.-H. Kim et al., 2018), not only contributes to cell survival, but also inhibits mitophagy process by phosphorylating ULK1 at Ser757, leading to segregated interaction between mTOR and AMPK (J. Kim et al., 2011). Phosphorylation of ULK1 leads to increased mitophagy with phosphorylation of BNIP3, promoting its interaction with LC3 (Poole et al., 2021). In contrast, while deficiency in cellular energy activates the energy sensor, i.e. AMPK by phosphorylation at Ser555, it inhibits mTOR leading to activation of mitophagy process (Tian et al., 2015). Activation of PI3K/Akt by e.g. cytokines or growth factors, acts as upstream regulator of mTORC1 leads to activation of mTOR and decreased autophagosome formation via phosphorylation of ULK1 at Ser757 (S. Wang et al., 2020). Furthermore, mitophagy process is dependent on activation of MAPK was shown to regulate mitophagy by regulating Parkin/PINK1 (Hirota et al., 2015). ROS-mediated activation of ERK1/2 and JNK was also shown to inhibit Parkin E3 ligase activity leading to accumulation of PINK1 in mitochondria and increased mitophagy (Park et al., 2017) (**Figure 14**).

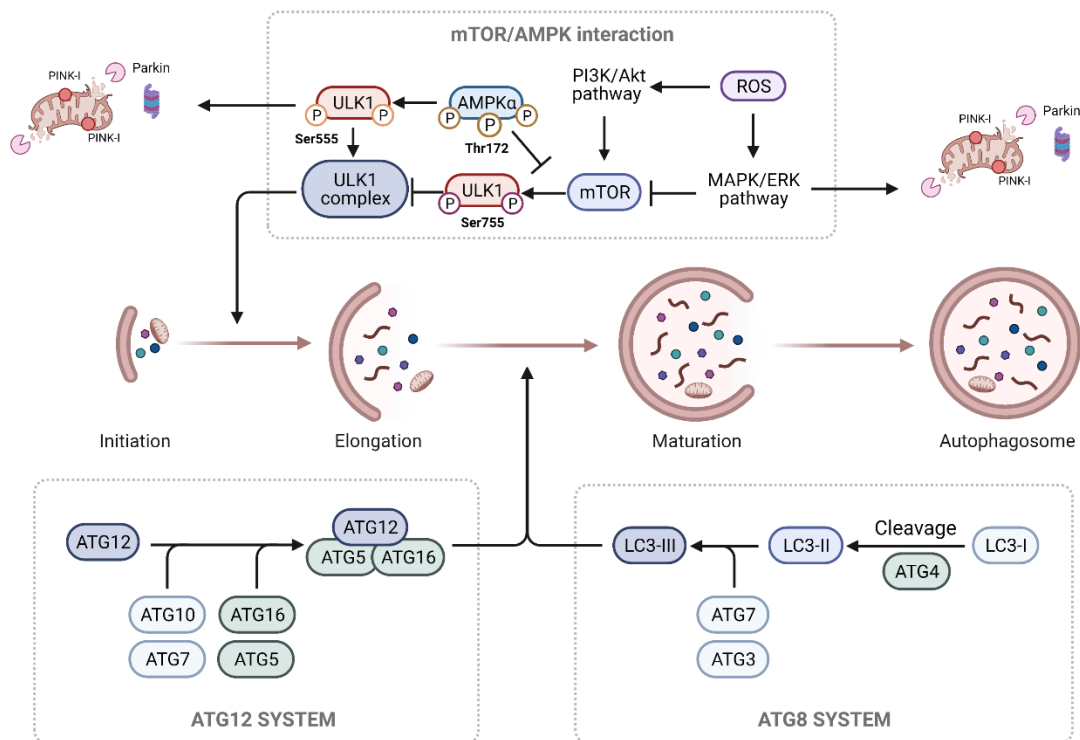


Figure 14: Signaling pathways involved in mitophagy. Inhibition of mTOR signaling via PI3K/Akt or via ROS-mediated MAPK/ERK activation leads to formation of ULK1 complex, which subsequently contributes to initiation of autophagosome formation. Moreover, phosphorylation of AMPK α at threonine 172 leads to phosphorylation of ULK1 at serine 555 which further triggers the initial phase in mitophagy. ULK1 and MAPK activation also directly leads to increased proteasomal mitophagy via PINK-1. Other ATGs such as ATG8 and ATG12 promote maturation of later phase autophagosome. The figure was modified by a template image from BioRender.com.

1.6. Mitochondrial abnormalities in AECs exposed to CS

1.6.1. Mitochondrial morphological abnormalities

Several studies have provided evidence for mitochondrial abnormalities in AECs of subjects with airway disease. These studies reported loss of cristae, abnormally branched, swollen and fragmented organelles (Hara et al., 2013; Hoffmann et al., 2013; Mizumura et al., 2014). In support of a causative role of CS exposure in mediating these morphological abnormalities, long-term exposure of human as well as murine AECs to CSE recapitulates observations made in airway disease, with CSE inducing similar abnormalities in mitochondrial morphology (Cloonan & Choi, 2016; Hara et al., 2013; Hoffmann et al., 2013). Since both of these studies that investigated CS-induced alterations in mitochondrial morphology in AECs isolated from human lung tissues used submerged cultures instead of cells differentiated in an ALI, the main cell type investigated in these studies is likely predominantly basal-like undifferentiated cells. It is still unknown exposure of differentiated cultures of AECs containing ciliated cells and goblet cells to CS *in vitro* results in similar changes in mitochondrial morphology (Aghapour et al., 2020).

1.6.2. Mitochondrial functional damages

In line with the above-mentioned *in vitro* studies, three months *in vivo* exposure of mice to CS also resulted in mitochondrial damage in both the airway and alveolar compartment (Mizumura et al., 2014). Suggestive of a potential link between these morphological changes and impairments in mitochondrial function as well as aberrations in cellular functionality in response to CS exposure, abnormalities in mitochondrial morphology were associated with a lower mtDNA content, decreased oxygen consumption rates, reduced ATP levels, decreased activity of the ETC, loss of mitochondrial membrane potential, increased levels of mtROS and loss of ciliary function (Agarwal et al., 2014; Hara et al., 2013; Hoffmann et al., 2013; Kosmider et al., 2019; Malinska et al., 2018; Mizumura et al., 2014; Valdivieso et al., 2018; van der Toorn et al., 2009). Taken together, these studies convincingly demonstrated that CS exposure results in aberrations in mitochondrial morphology and function in AECs. Interestingly, in apparent contrast to these studies, hyperfusion of mitochondria and increased metabolic activity were reported in primary mouse type II alveolar epithelial cells in response to CSE (Ballweg et al., 2014), suggestive of mitochondrial adaptation. In line with this, 8 weeks exposure of mice to CS increased expression of genes involved in metabolism, ETC and mitochondrial transport and dynamics in lung tissue

(Agarwal et al., 2012). The increased expression of components of the ETC was also reported in primary human AECs exposed to CSE for three months and may serve as a compensatory mechanism (Hoffmann et al., 2013). The above conflicting results in the effect of CSE on mitochondrial function are most likely attributed to the different concentrations of CSE used and possibly relate to an initial dose-response phase (hormesis) of increased activity followed by a decline in functional and irreversible cell death (Aghapour et al., 2020).

In addition to deteriorative effects of CS on mitochondrial morphology and function in AECs, studies have also reported similar detrimental effects of CS in other cells of the airways, including human airway smooth muscle cells and lung fibroblasts, indicating that detrimental effects of CS components on mitochondrial function likely extend beyond the epithelium (Ahmad et al., 2015; Aravamudan et al., 2014). Collectively, these studies indicate that CS alters mitochondrial structure and function in various cells of the airway walls and lung parenchyma (Aghapour et al., 2020).

1.6.3. Mitochondrial quality control processes

Given that mitochondrial function and mitochondrial content (i.e., mtDNA copy number) in AECs are significantly impacted by exposure of these cells to CS, it is not surprising that the pathways controlling mitochondrial turnover such as mitochondrial biogenesis, mitochondrial fission and fusion and mitophagy are also affected in these cell types in response to CS and in the airways of patients with airway disease (Aghapour et al., 2020). Indeed, PGC-1 α protein levels were higher in peripheral lung tissue from moderate airway disease compared to controls with levels progressively decreasing with increasing disease severity (Li et al., 2010). In addition, significantly higher transcript levels of PGC-1 α were reported in primary AECs from patients with advanced airway disease compared to those from control subjects (Hoffmann et al., 2013). Suggestive for a role of CS exposure, 24 h exposure of primary human AECs to CSE increased PGC-1 α transcript levels (Vanella et al., 2017). As PGC-1 is also known to control expression of genes involved in mitochondrial fusion, the observation that hyperfusion of mitochondria in primary mouse type II alveolar epithelial cells exposed to CSE was associated with increased expression of the mitochondrial fusion protein MFN1 is also in line with this (Ballweg et al., 2014). In this context, increased levels of PGC-1 α may reflect an adaptive cellular mechanism in response to reductions in mitochondrial content and function, while decreased levels in more advanced disease stages or in response to longer exposure or higher dose of CS may reflect an inability to compensate for these changes in a chronic setting. (Aghapour et al., 2020). In line with this notion, in rats exposed to CS for one month pulmonary PGC-1 α protein levels were

significantly reduced, suggesting the long-term deteriorative effects of CS on mitochondrial biogenesis (X.-L. Wang et al., 2017).

As for the mitophagy, it was shown that PINK1 protein levels were significantly higher in whole lung homogenates of patients with airway disease compared to controls (Mizumura et al., 2014). In line with this, increased levels of PINK1 mRNA were observed in primary AECs of patients with airway disease compared to controls (Hoffmann et al., 2013). In addition, higher PINK1 protein levels in lung tissue of patients with airway disease were associated with increased abundance of the activated form of the fission protein DRP1 (Mizumura et al., 2014). This likely resulted from exposure of AECs to CS components as in the same study CSE exposure of BEAS-2B cells resulted in significant increases in both PINK1 as well as phosphorylated DRP1 protein abundance and smoke exposure (3 weeks) of mice increased the abundance of phosphorylated DRP1 protein in the lung (Mizumura et al., 2014). These changes were associated with CS-induced activation of mitophagy evidenced by enhanced mitochondrial clearance. Other studies confirmed this by demonstrating increases in PINK1 protein levels, increased abundance of activated fission proteins and decreased mRNA levels of fusion genes in response to CS *in vitro* and *in vivo* (Mizumura et al., 2014). In addition to increased mRNA and protein abundance of PINK1, decreased protein levels of PARK2 have been reported in lung tissue of patients with airway disease (Ito et al., 2015). Moreover, PARK2-deficient mice demonstrated enhanced airway wall thickening with aggravated emphysematous changes following CS exposure in comparison to wild-type mice (Araya et al., 2019). These results collectively suggest that disturbances in the PINK/PARK2 pathway may play a pivotal role in pathogenesis of airway disease by regulating mitophagy and suggest that PARK2 induction could mitigate the progression of airway complications. The lower levels of PARK2 observed in airway disease could lead to the accumulation of damaged mitochondria. Nevertheless, whether mitophagy in the context of airway disease and smoking, is mainly protective or contributes to epithelial injury remains controversial. This controversy is illustrated, for example, by the observations that blocking mitophagy prevented CS-induced airspace enlargement and inhibition of ciliary function in mice, whereas activation of mitophagy prevented smoke-induced cellular senescence of small AECs. Further studies assessing the cell-specific function of mitophagy and mitochondrial fission/fusion in the pathogenesis and progression of airway disease will help shed light on these outstanding questions (Aghapour et al., 2020). CS-induced abnormalities in mitochondrial function in AECs have been summarized in **Figure 15**.

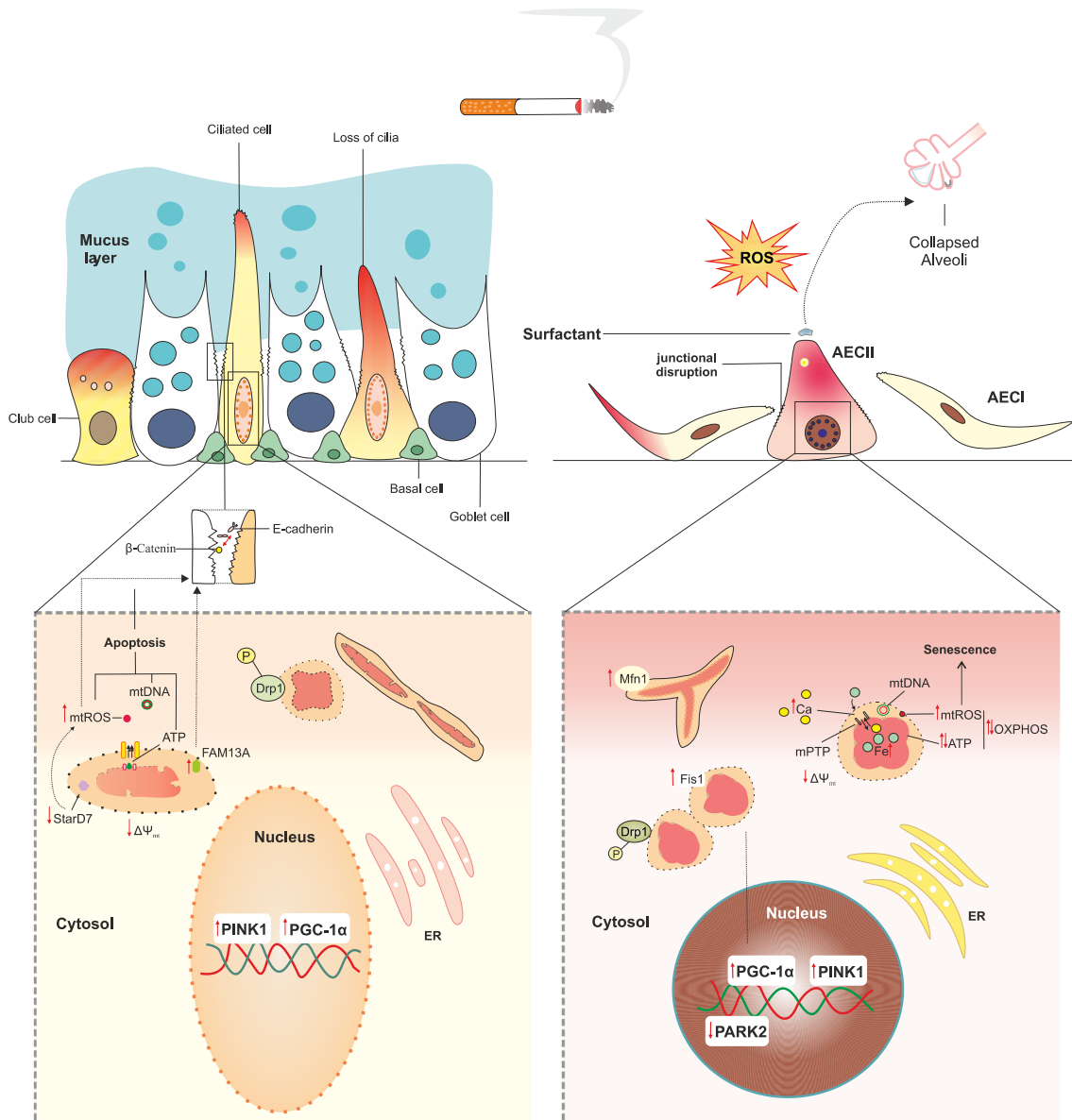


Figure 15: Schematic figure illustrating processes involved in CS-induced mitochondrial dysfunction in AECs. CS induces swollen and branched mitochondria with condensed matrix in AECs. Moreover, CS induces functional alteration in mitochondria including altered OXPHOS with higher ROS production and lower ATP generation, depolarization of mitochondrial membrane, all of which cause subsequent changes at cellular level. These changes include loss of ciliary function, increase in mucus production in the airway epithelium. CS also increases permeability of mitochondrial membrane and opens ion channels such as mPTP in the inner membrane, leading to overload of iron in mitochondria and cytoplasmic accumulation of mtDAMPs including calcium, ATP, mtROS, mtDNA, cardiolipin and formyl peptides, further inducing oxidative damage and cell death. CS-induced mitochondrial dysfunction may also contribute to leaky manifestation of the airway epithelium by increase in mtROS and weakening cellular junctions. Short-term CS exposure may enhance mitochondrial biogenesis via increase in PGC-1 α transcript levels, while longer exposure times suppress this process. In addition, CS induces imbalance in fusion/fission process by more trends to fission, leading to fragmentation of mitochondria in AECs. The figure was adopted from a cited reference (Aghapour et al., 2020).

1.7. Innate immune responses in airway mucosa; potential links to mitochondria

AECs not only provide a physical barrier against environmental insults, but also release antimicrobial peptides, antioxidants and pro-inflammatory mediators, which are able to attract and activate cells of both the innate and adaptive immune systems (Hiemstra et al., 2015). Lung epithelial cells express a wide array of pro-inflammatory PRRs, including TLRs, NLRs, RLRs, and RAGE, which can be activated by PAMPs and DAMPs, including mtDAMPs. Next to mtDAMPs, it has been shown that mtROS are able to induce a pro-inflammatory response by directly activating NF- κ B pathway and HIF-1 α (Banoth & Cassel, 2018). Unlike other PRRs, the NLRs reside in the cytoplasm and specific members of the NLR receptor family are able to form inflammasomes (Kanneganti, 2015). The best studied NLR inflammasome is NLRP3, which has a strong link to mitochondrial dysfunction. NLRP3 can be activated by various mtDAMPs, either indirectly by extracellular ATP which activates the P2X7 receptor or directly by mtDNA and cardiolipin (Iyer et al., 2013; Shimada et al., 2012). Furthermore, activated NLRP3 inflammasomes co-localize with mitochondria, which may act as a scaffold for NLRP3 assembly and activation (Elliott et al., 2018; Zhou et al., 2011). Activation of NLRP3 inflammasomes has been reported in airway epithelium of patients with airway disease undergoing an exacerbation (Faner et al., 2016). Several studies have shown that the NLRP3 inflammasome anchors at the mitochondria via MAVS, while also cardiolipin and the anti-apoptotic c-FLIP protein have been suggested as mitochondrial anchors (Banoth & Cassel, 2018b; Faiz et al., 2018; Subramanian et al., 2013; Y.-H. Wu et al., 2014). Activation of NLRP3 induces mitochondrial damage and the subsequent release of mtROS and *vice versa* (Murakami et al., 2012; Zhou et al., 2011). In line, dysfunctional mitophagy augments the activation of NLRP3 (Lupfer et al., 2013). The correlation between mitochondrial dysfunction and NLRP3 activation may be caused by high cytosolic calcium levels, which are needed for NLRP3 activation and which may induce damage to the mitochondria (Aghapour et al., 2020; Banoth & Cassel, 2018). The molecular mechanisms linking mitochondrial dysfunction to immune responses upon CS have been illustrated in **Figure 16**.

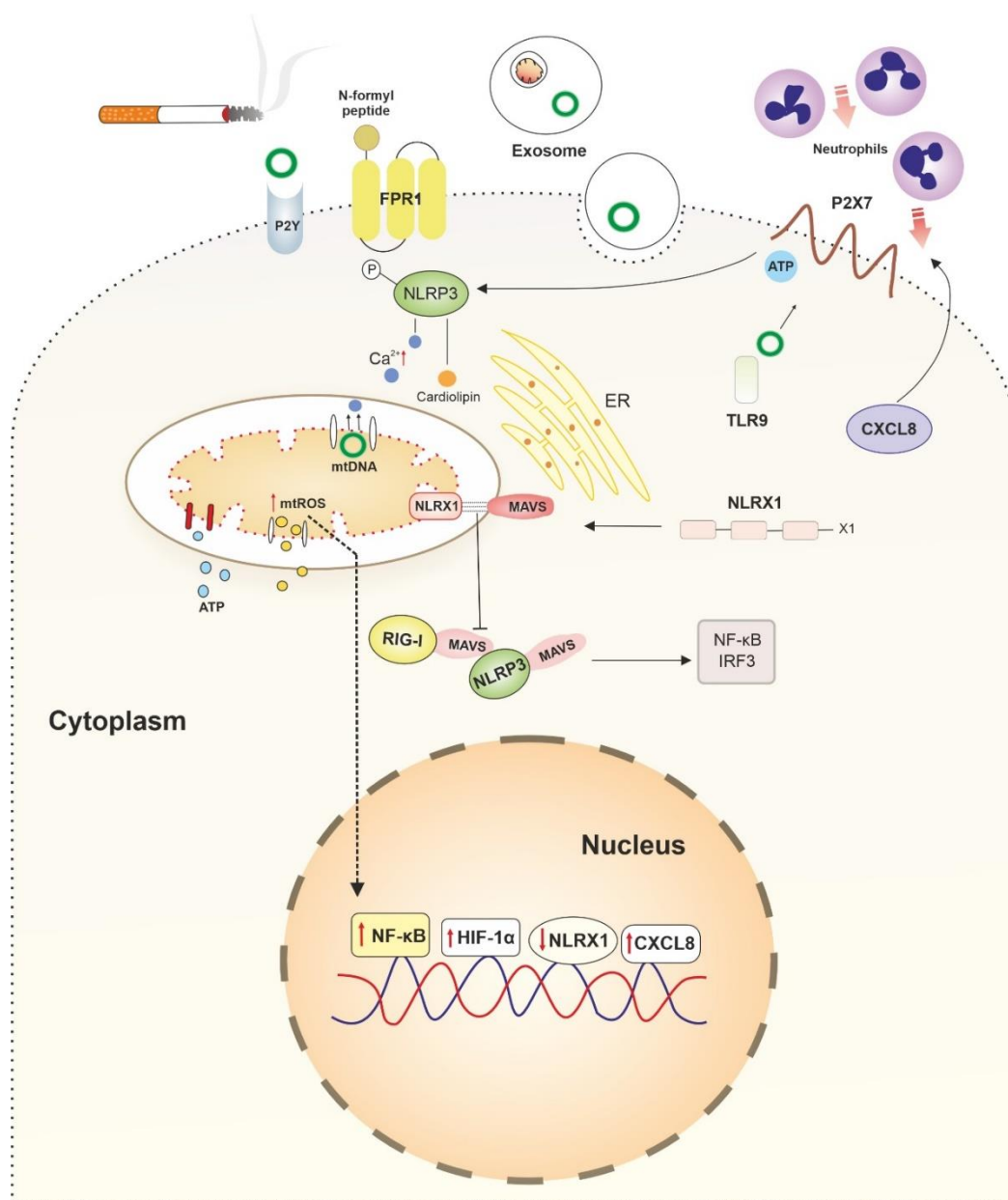


Figure 16: Links between CS-induced mitochondrial dysfunction and altered innate immune responses in airway epithelium. Damaged mitochondria as a result of CS exposure release its compartments and products to cytoplasm, acting as DAMPs for innate immune responses. Cytoplasmic level of mtDAMPs including mtROS, mtDNA, ATP, cardiolipin and Ca increases upon CS exposure in AECs. Enhanced levels of cytoplasmic mtDNA, mtROS, Ca and cardiolipin activate innate immune responses by stimulation of intracellular PRRs, in particular NLRP3 inflammasome. mtDNA acts as a ligand for other intracellular PRRs TLR9 and P2X7 receptor, further activates NLRP3. Extracellular ATP also activates NLRP3 via purinergic receptors P2X7 and P2Y. Activated NLRP3 localized into mitochondria, which subsequently induces more damage by enhancing mtROS production. This increase in mtROS levels directly induces pro-inflammatory responses by overexpressing NF- κ B and HIF-1 α mRNAs. Furthermore, mtDAMPs elicit pro-inflammatory responses by inducing strong CXCL8 responses in airway epithelial cells, recruiting neutrophils to the site of damage. Another PRR, NLRX1, is also localized to mitochondria and interacts with MAVS, exerting anti-inflammatory responses by precluding interaction of NLRX1 with NLRP3 and RIG-I and subsequent activation of NF- κ B and IRF3. CS reduces the expression of NLRX1 in the lung both at gene and post-transcriptional levels, perpetuating inflammation. The figure was adopted from a cited reference (Aghapour et al., 2020).

The above-mentioned observations clearly link dysfunctional mitochondria to inflammation. In addition, mitochondrial dysfunction may contribute to increased susceptibility to infection by changing the energy balance in affected cells as well as through direct involvement of mitochondria in antimicrobial activity of cells (Aghapour et al., 2020). Mitochondria have been shown to contribute to antibacterial activity through various mechanisms, including the regulation of innate immune responses but also through direction of mitochondria toward the phagolysosome and subsequent delivery of mtROS, which in concert with phagosomal NADPH-oxidase-derived ROS contribute to bacterial killing within the phagolysosome (Pinegin et al., 2018). Such studies help to explain the observed link between mitochondrial dysfunction and decreased antibacterial activity of macrophages in airway disease. In addition, mitochondria contribute to antiviral responses in cells by facilitating RLR signaling, including that of the mitochondria-associated MAVS, thus regulating the production of antiviral type I and type III interferons and pro-inflammatory cytokines following viral infection (S.-J. Kim et al., 2018; Pourcelot & Arnoult, 2014). This was first shown in studies demonstrating that mitochondrial fragmentation and loss of mitochondrial membrane potential, as observed in cells exposed to CS, result in a marked impairment of MAVS-mediated antiviral immunity (Hara et al., 2013; Hoffmann et al., 2013). Viruses exploit this mechanism by inducing mitochondrial dysfunction (e.g., by increasing mitophagy), thus escaping efficient antiviral host defense. These observations may help to explain how exposure of cultured AECs to CS increases infection by, e.g., rhinoviruses (Eddleston et al., 2011; Proud et al., 2012), as well as the observed antiviral immunity in, e.g., patients with frequent exacerbations (Singanayagam et al., 2019). Collectively, these studies show that mitochondrial dysfunction as observed in smokers with and without airway disease may contribute to their increased susceptibility to respiratory infections. Conversely, these findings suggest that such infections may contribute to the observed mitochondrial dysfunction (Aghapour et al., 2020).

Another NLR family member, NLRX1 also co-localizes with mitochondria by binding to MAVS (Moore et al., 2008). Thereby, NLRX1 acts as an anti-inflammatory decoy-receptor, limiting the binding and activation of NLRP3 and RIG-I, which subsequently results in decreased NF- κ B and interferon IRF3 activation (Y.-H. Wu et al., 2014) (**Figure 17**). However, recently it was shown that NLRX1 may also have pro-inflammatory functions under specific conditions e.g., viral infections (Feng et al., 2017), suggesting that NLRX1 may have pro- as well as anti-inflammatory function and is thus important for the modulation of inflammatory responses (Aghapour et al., 2020). NLRX1 expression is lower in CS-exposed mice for three months as well as in severe stages of airway disease compared to healthy controls both at gene and protein levels (Kang et

al., 2015). Interestingly, it was shown that loss of NLRX1 levels induces mtROS-mediated oxidative stress in ischemia-reperfusion injury model in renal epithelial cells by interacting with the subunit of mitochondrial complex III UQCRC2 (Stokman et al., 2017), thus, acting as a mediator between innate immune compartments and mitochondrial ETC (Aghapour et al., 2020). Therefore, dysfunctional mitochondria may potentially affect innate immune responses by the release of both mtDAMPs and mtROS and by anchoring and modulating the pro-inflammatory inflammasomes in AECs (Aghapour et al., 2020).

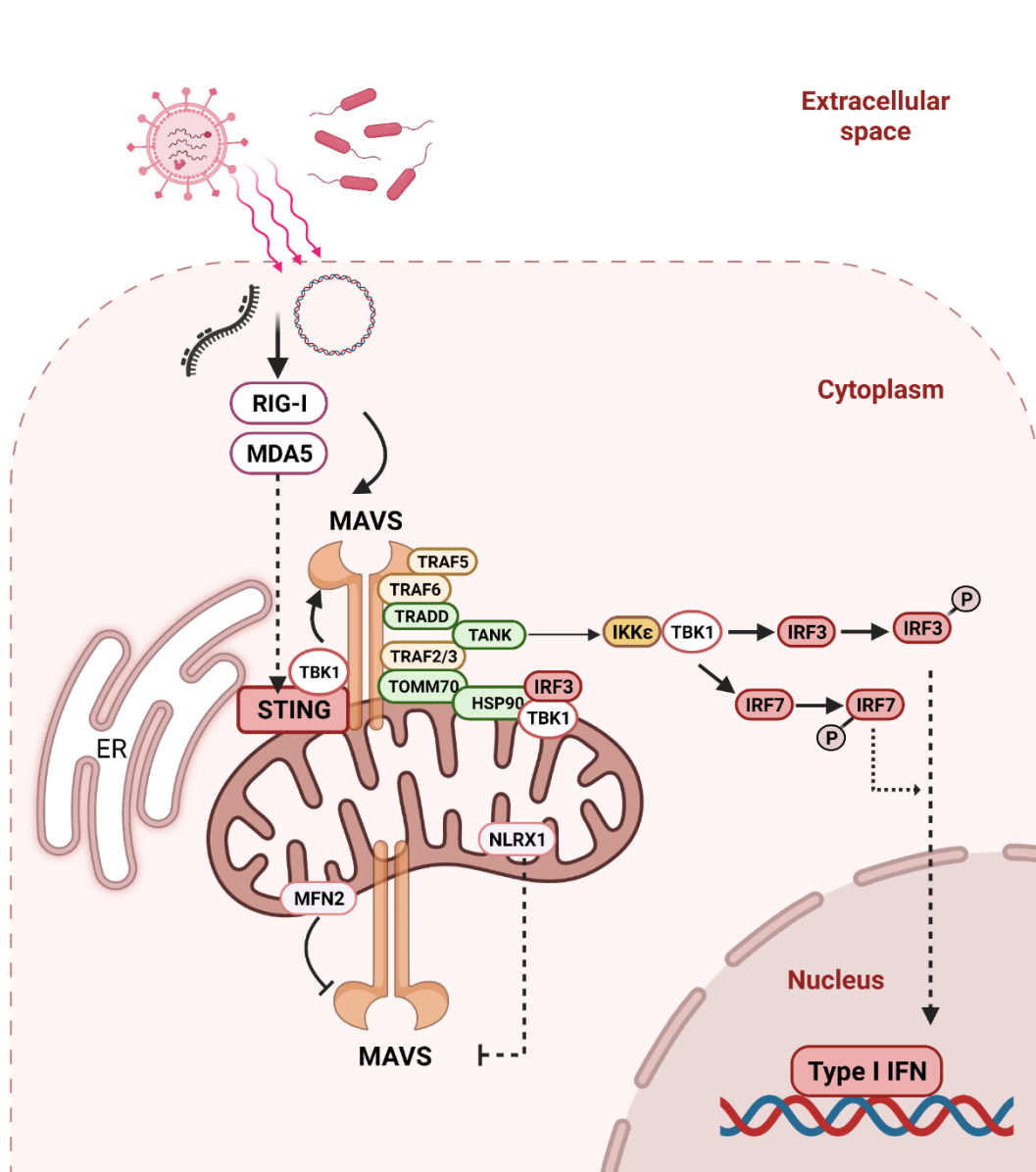


Figure 17: Mitochondrial effectors regulate innate immune responses to pathogens. Viral RNA or bacterial DNA are recognized in the host cells either by RIG-I or MDA5. Upon recognition, innate immune system responds by activation of MAVS which may activate host pro-inflammatory responses by recruitment of several signaling molecules and further activation of interferon responses by phosphorylation of IRF3 and IRF7. Certain molecules negatively regulate MAVS activation, of which NLRX1 and MFN2 are mitochondrially localized proteins. The figure is a modified version of the figure used in the reference (West et al., 2011) that is created by a template image from BioRender.com.

1.8. Mitochondrial dysfunction and airway epithelial barrier function upon CS exposure

In the airways, epithelial cell contacts, such as tight junctions and adherens junctions as well as the trapping function of the mucociliary system constitute a robust physical barrier against pathogens and inhaled toxicants such as CS (Aghapour et al., 2018). Mitochondrial function not only meets cellular metabolic demands, but also modulates epithelial integrity in various organs through regulation of ATP, calcium and mtROS homeostasis (Crakes et al., 2019; Hu, Ren, Li, et al., 2018; Hu, Ren, Ren, et al., 2018; Saxena et al., 2017; Unger et al., 2014; A. Wang et al., 2014; Yang et al., 2017). Indeed, it was already shown that ATP-deprived cells as well as high levels of mtROS and mitochondrial calcium overload cause disruption of epithelial tight junctions (Canfield et al., 1991; Sebag et al., 2018; Unger et al., 2014). Although there is no evidence for direct link between smoking and mitochondrial dysfunction-induced airway epithelial barrier disruption, studies in intestinal epithelium highlight the concept that mitochondrial dysfunction may contribute to breakdown of the epithelial barrier in a mtROS-dependent mechanism (Hu, Ren, Li, et al., 2018; Sebag et al., 2018; A. Wang et al., 2014). CS was shown to disrupt apical and basal junctions between AECs through various mechanisms. The excessive oxidative burden is considered as one of the underlying mechanisms of epithelial barrier disruption (Aghapour et al., 2018). Mitochondrial dysfunction also induces exaggerated oxidative stress by overproduction of mtROS, which increases permeability of the epithelial barrier (A. Wang et al., 2014). Indeed, increased mtROS was shown to disrupt airway epithelial barrier integrity in response to the viral mimic poly (I:C) (Unger et al., 2014). In agreement, loss of StarD7, a lipid transfer protein, was shown to disrupt airway epithelial tight and adherens junctions by enhancing mtROS and subsequent mtDNA damage *in vitro* and *in vivo* (Yang et al., 2017). MtDNA damage, ATP depletion and oxidative stress enhance apoptosis (X. Liu & Chen, 2017), which may eventually lead to epithelial barrier disruption (Aghapour et al., 2020). Of note, this barrier-disruptive effect was reversible by mitochondrial-targeted antioxidant therapy, acknowledging the role of mitochondrial dysfunction-derived oxidative stress in epithelial barrier integrity (Aghapour et al., 2020). Moreover, several studies showed that restoring PGC1 α in AECs recover airway epithelial barrier disruption, potentially via improving OXPHOS/glycolysis or a redox activity of PGC1 α (Maurice et al., 2019; Michi et al., 2021; Saito et al., 2021). FAM13A, a reported susceptibility gene for airway disease (Morrow et al., 2017), mediates ROS-producing fatty acid β -oxidation in stressed mitochondria of AECs (Hawkins & Mora, 2017; Mora et al., 2017). Of relevance, it was shown that FAM13A interacts with the adherens junction-associated protein β -catenin, promoting its degradation in alveolar epithelial

cells (Jiang et al., 2016). β -catenin is crucial for stabilization and membrane localization of the adherens junction protein E-cadherin in the AECs (Aghapour et al., 2018). Thus, regulation of FAM13A may have implications for epithelial barrier disruption in airway disease, in part by the ability of FAM13A to regulate E-cadherin function through its effect in β -catenin stability in AECs. Together, these studies suggest that mitochondrial dysfunction induces oxidative damage that may in turn disrupt cell-cell contacts in AECs. Epithelial damage may not only lead to increased susceptibility to environmental factors such as smoke and pathogens but is thought to contribute to pro-inflammatory and remodeling processes as well (Aghapour et al., 2018). Furthermore, the epithelial barrier is thought to be important for polarization and differentiation and could thus impact ciliary and secretory cell differentiation (Rowart et al., 2018). Indeed, it was shown that CS-induced increase in mtROS mediates autophagy-dependent overexpression of *MUC5AC* in AECs, suggesting the contribution of mitochondria to mucociliary differentiation (Aghapour et al., 2020; J.-S. Zhou et al., 2016).

2. Aim of the study

Cigarette smoking is largely associated with development and progression of airway complications by inducing mitochondrial dysfunction in the AECs, however the impact of CS on mitochondrial function in AECs during *Sp*-induced infection is unclear. First, to optimize the model, the impact of CSE on mitochondrial function in AECs was assessed. Mitochondrial fission process which is believed to be involved in regulation of mitophagy and innate immune responses was investigated at phosphorylated levels in CS-stimulated AECs. Next, to decipher the impact of CS pre-exposure on mitochondrial function in *Sp*-stimulated human AECs, a model of post-CSE *Sp* infection was generated. Mitochondrial function was investigated by measuring mitochondrial oxidative stress, mitochondrial membrane potential and quantifying the key proteins involved in mitochondrial-specific autophagy and mitochondrial fission and fusion as well as mitochondrial biogenesis processes in the *in vitro* model. Mitochondrial dysfunction was confirmed in CSE pre-exposed *Sp* infection condition via measuring the levels of mitochondrial oxidative stress in AECs. It was also unclear whether CSE-induced mitochondrial dysfunction affect innate immune responses prior to infection with *Sp* in AECs. To investigate this, the mRNA levels of innate immune response genes was measured in the *in vitro* model. Given the role of AMPK α as the metabolic regulator that is decreased upon smoke exposure, and its regulatory role in innate immune responses and barrier function as well as autophagy, we hypothesized that mitochondrial dysfunction may in part control the innate immune response and

airway epithelial barrier function through AMPK α signaling in the used *in vitro* model. We thus explored association between mitochondrial function and innate immune responses by investigating phosphorylation of AMPK α . Furthermore, pharmacological treatment for improvement of OXPHOS was utilized to evaluate the role of mitochondrial oxidant improvement on CS-induced mitochondrial dysfunction and airway epithelial barrier dysfunction. The three core aims of the current thesis have been depicted in the **Figure 18**. The current study further clarifies the mechanisms involved in AEC dysfunction in post-CSE pneumococcal infection and provides a basis for development of therapeutics that could be applied in clinical interventions.

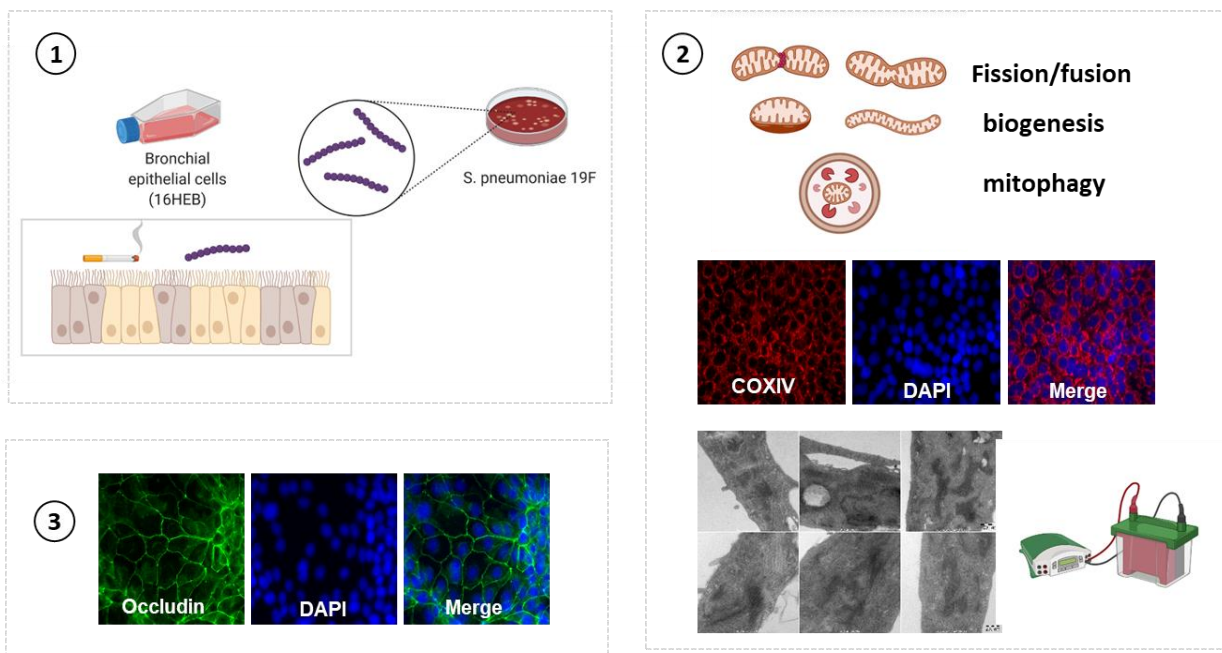


Figure 18: Schematic illustration of three aims of the study. In frame of this thesis, we aimed to expand the current knowledge on the contribution of mitochondrial function to pathogenesis of *Sp*-induced exacerbation. First, we optimized the model by pre-exposing 16HBE cells to CSE followed by *Sp* infection. Furthermore, the impact of CSE pre-exposure on mitochondrial function in 16HBE cells upon *Sp* infection was investigated by assessing various functional and morphological studies. To assess the effect of mitochondrial OXPHOS treatments on the improvement of airway epithelial barrier integrity, immunofluorescence staining of the cell junctions was used in 16HBE cells stimulated with CSE with and without post-treatments. The figure was created with BioRender.com.

3. Materials

3.1. Consumables

All reagents and kits that have been used in this study have been listed in the tables below.

Table 1: Chemicals

Products	Cat Number	Manufacturer
Ammonium persulfate	A3678-100G	Sigma-Aldrich
β -Mercaptoethanol	1610710	BioRad
Bacto™ Yeast extract	212750	BD Bioscience
BD FACS™ Clean	340345	BD Bioscience
BD FACS™ Flow	342003	BD Bioscience
BD FACS™ Rinse	340346	BD Bioscience
BSA fraction V	K45-001	GE-healthcare
Columbia blood agar	254005	BD Bioscience
cComplete™, Ultra Mini, EDTA-free protease inhibitor cocktail	4693159001	Roche
EDTA	E6758-500G	Sigma-Aldrich
DAPI	MBD0015	Sigma-Aldrich
DMSO	A9941	Carl Roth
Ethanol, absolute	2246.1000	CHEMOSOLUTE®
Ethanol, 100 %	8025	Baker
FCS	P4047500	PAB Biotech
FCCP	C2920-10MG	Sigma-Aldrich
Fixable Viability dye eFlour™ 780	2290919	Invitrogen
Glycine	3908.2	Carl Roth
L-Glutamine (200 mM)	25030081	Gibco
Methanol	67-56-1	Baker
MEM (+L-Glutamine)	2242351	Gibco
MEM, no phenol red	51200038	Gibco
MilliQ water	-	-
MitoTEMPO	SML0737-5MG	Sigma-Aldrich
MOTS-c	AS-65587	Eurogentec
MTT	M5655-1G	Sigma-Aldrich
NaCl	3975.2	Carl Roth

Normal goat serum	5425S	Cell Signaling Technology
PBS	14190-169	Gibco
PBS tablet	18912-014	Gibco
PageRuler™ prestained protein ladder	26617	Thermo Fisher Scientific
Penicillin-Streptomycin	15070-063	Gibco/Invitrogen
Ponceau S	P7170	Sigma-Aldrich
ProTaq® MountFlour	401603099	quartet
Powdered milk	T145.2	Carl Roth
RIPA buffer 10X	9806	Cell Signaling Technology
Skimmed milk powder	-	Campina
SDS-Blotting grade	0183.2	Carl Roth
TEMED	2362.3	Carl Roth
Todd Hewitt broth	T1438	Sigma-Aldrich
TWEEN20	A1379-100ml	Sigma-Aldrich
Tris	4855.2	Carl Roth
Triton-X-100	3051.2	Carl Roth
Trypan blue	15250-061	Gibco
30 % Acrylamide-Bis Solution	1610156	BioRad
4X Laemmli sample buffer	1610747	BioRad

Table 2: Kits

Products	Cat Number	Manufacturer
Cellular ROS Assay Kit	ab113851	Abcam
Clariom™ S Assay	902927	Thermo Fisher Scientific
Maxima First Strand cDNA Synthesis Kit	00408695	Thermo Fisher Scientific
MitoSOX™ Red Mitochondrial Superoxide Indicator	M36008	Thermo Fisher Scientific
Mitoprobe™ JC-1 Assay Kit	M34152	Thermo Fisher Scientific
Mitochondrial Fractionation Kit	40015	Active Motif
Pierce™ BCA Protein Assay Kit	23227	Thermo Fisher Scientific
Pierce™ ECL Plus Western Blotting Substrate	32134	Thermo Fisher Scientific
RealTime-Glo™ MT Cell Viability Assay	G9711	Promega
RNase-free DNase Kit	79254	Qiagen
RNeasy Plus Mini Kit	74034	Qiagen
SuperSignal™ West Femto	34094	Thermo Fisher Scientific

SuperSignal™ West Pico	34577	Thermo Fisher Scientific
------------------------	-------	--------------------------

3.2. Technical devices

Table 3: Technical devices

Products	Model	Manufacturer
Centrifuge	Allegra® X-15R	Beckman Coulter
Centrifuge	Multifuge® 1S-R	Heraeus
Centrifuge	Centrifuge 5417-R	Eppendorf
Clean bench	HERAsafe® KS	Heraeus
CO ₂ incubator	NU-8500E	Integra Bioscience
CO ₂ incubator (Labotect)	C-16	Labotect
Counting chamber	Neabauer	Marienfeld Superior
Fluorescence microscope	Zeiss Axiovert 200m	Carl Zeiss MicroImaging
Flow Cytometer	BD FACS Canto™ II	Thermo Fisher Scientific
Gas washing bottle (100 ml)	5 5100 37	Lenz Laborglas
Homogenizer Dounce (2 ml)	CXC8.1	Carl Roth
Imager (Amersham™)	Imager 600	GE Healthcare
Imager	ChemoCam	INTAS Science Imaging
Laboratory Balance	Pioneer®	Ohaus
Magnetic Stirrer	C-MAG HS7	IKA
Microplate reader	Synergy™ HT	BioTek
Microscope	Eclipse TE200	Nikon Instruments Inc
Microscope (TEM)	Libra 120 Plus	Carl Zeiss MicroImaging
Mini gel electrophoresis	Mini-Protean tetracell	BioRad
Peristaltic pump	BT100-2J	Longer pump
Precision Plus Protein™	161-0373	BioRad
pH measuring instrument	EL20	Mettler Toledo
Roller mixer	SRT9	Stuart
Semi-dry Blotter	Maxi	Carl Roth
Shaker	DOS-10L	Neolab
Shaker	Polymax 1040	Heidolph Instruments
Spectrophotometer	GeneQuant™ pro	Amersham Bioscience
Spectrophotometer	ND-1000	Nanodrop Technologies
Suction pump	Vacusaft	Integra Bioscience
Thermomixer	Thermomixer comfort	Eppendorf
Ultramicrotome	Ultracut UC7	Leica
Vortex	Vortex Genie 2	Scientific Industries

3.3. Antibodies- immunostaining

In the following, all used antibodies for immunostaining are listed. Each antibody was diluted prior to the experiment with the dilution buffer.

Table 4: Antibodies used for immunoblotting.

Antibody	Company	Working concentration	Cat-number	Clone
AMPK- α	Cell Signaling Technology	1:1000	2532	-
p-AMPK α (Thr172)	Cell Signaling Technology	1:1000	2535	40H9
β -actin	Cell Signaling Technology	1:2000-1:5000	4970	13E5
BNIP3	Cell Signaling Technology	1:1000	3769S	-
BNIP3L	Cell Signaling Technology	1:1000	12396	D4R4B
COXIV	Cell Signaling Technology	1:1000	4850	3E11
DRP1	Cell Signaling Technology	1:1000	8570	D7C7
ERR α	Abcam	1:1000	ab76228	EPR46 Y
FUNDC1	Santa Cruz Biotechnology	1:500	sc-133597	H22
GABARAPL1	Proteintech Group	1:1000	11010-1-AP	-
GAPDH	Cell Signaling Technology	1:5000-1:10000	5174	D16H11
Hexokinase II	Cell Signaling Technology	1:1000	2867	C64G5
LC3B	Cell Signaling Technology	1:1000	2775	-
MFN2	Santa Cruz Biotechnology	1:500	sc-515647	F-5
NLRX1	Cell Signaling Technology	1:1000	13829	D4M3Z
NRF1	Abcam	1:1000	ab55744	2F9
OXPPOS subunits	MitoScience LLC	1:1000	MS604	-
PINK	Novus Biologicals	1:2000	BC100-494	-
SQSTM1 (p62)	Cell Signaling Technology	1:1000	5114	-
TOMM20	Abcam	1:1000	ab186734	EPR155 81-39
ULK1	Cell Signaling Technology	1:1000	8054	D8H5
p-ULK1 (Ser555)	Cell Signaling Technology	1:1000	5869	D1H4

VDAC1	Cell Signaling Technology	1:500	4866	-
Polyclonal Goat anti-Mouse IgG HRP	Vector laboratories	1:10000	BA-9200	-
Polyclonal Goat anti-Rabbit IgG HRP	Cell Signaling Technology	1:10000	7074S	-
Polyclonal Swine anti-Rabbit IgG HRP	Dako-Agilent	1:1000-1:10000	P0399	-
Polyclonal Rabbit anti-Mouse IgG HRP	Dako-Agilent	1:1000-1:10000	P0161	-

Table 5: Antibodies used for immunofluorescence.

Antibody	Company	Working concentration	Cat-number	Clone
DRP1	Santa Cruz Biotechnology	1:50	sc-271583	C-5
p-DRP1 (Ser616)	Cell Signaling Technology	1:300	3455	-
TOMM20 (F-10)	Santa Cruz Biotechnology	1:50	sc-17764	-
ZO-1	Cell Signaling Technology	1:400	13663	D6L1E
E-cadherin	Cell Signaling Technology	1:200	3195	24E10
ERR α	Abcam	1:100	EPR46Y	ab76228
Anti-rabbit IgG Fab2 Alexa fluor (R) 488	Cell Signaling Technology	1:1000	4412S	-
Anti-rabbit IgG Fab2 Alexa fluor (R) 647	Cell Signaling Technology	1:1000	4410S	-
Donkey Anti-Rabbit IgG	BioLegend	1:1000	406414	Poly4064

3.4. Buffer and media composition

Table 6: *Sp* culture media

Media	Composition	Solvents
THY medium	3.7 g Todd Hewitt broth 1 g Bacto™ Yeast	100 ml Milli Q

Table 7: MEM complete

Component	Final concentration
MEM with GlutaMAX	500 ml
FCS	10 % (v/v)
Penicillin/Streptomycin	1 % (v/v)

L-Glutamine (200 mM)

2 mM

Table 8: FACS buffer

Component	Final Concentration
PBS, pH 7.4	-
BSA	0.5 % v/v
EDTA	2 mM

Table 9: 1X sample buffer for immunoblotting

Component	Final Concentration
4X Laemmli buffer	-
β -Mercaptoethanol	1 % v/v
MilliQ	-

Table 10: 1X SDS-PAGE running buffer

Component	Final Concentration
Tris	25 mM
Glycine	192 mM
SDS	0.1 %

Table 11: 1X transfer buffer

Component	Final Concentration
Tris	25 mM
Glycine	192 mM
Methanol	15 % v/v

Table 12: TBST buffer (i) for immunoblotting

Component	Final Concentration
Tris-base	200 mM
NaCl	1.4 M
Tween20	0.1 % v/v

Table 13: TBST buffer (ii) for immunoblotting

Component	Final Concentration
Tris-base	20 mM
NaCl	137 mM
Tween20	0.1 % v/v

Table 14: Fixative buffer for TEM

Component	Final Concentration
EM-HEPES buffer	0.1 M
Paraformaldehyde	5 % v/v
Glutaraldehyde	2 % v/v
MgCl ₂	

Table 15: 0.1 M EM-HEPES buffer for TEM

Component	Final Concentration
Sucrose	0.09 M
CaCl ₂	10 mM
MgCl ₂	10 mM

4. Methods

4.1. Cell culture

16HBE-14o SV-40 immortalized airway epithelial cell line was kindly donated by Professor Dieter Gruenert, University of California. The cells were cultivated in T75 flask (Greiner BioOne GmbH) in MEM with earle's salt supplemented with 10 % fetal calf serum, L-Glutamine 2 mM and 1 % penicillin/streptomycin and kept in a humidified incubator at 37 °C with 7.5 % CO₂. Upon 90 % confluency, the cells were detached and harvested with Trypsin/EDTA 0.025 %.

4.2. *Streptococcus pneumoniae* culture

Sp clinical isolate of 19F (BHN100) was obtained from the laboratory of Birgitta Henriques-Normark (Karolinska Institute), and plated on Columbia blood agar and kept at 37 °C with 5 % CO₂ overnight. The single colonies were removed by a sterile cotton swab and transferred to autoclaved pre-warmed THY medium. The initial OD₆₀₀ of the broth was measured and set at ~0.09 using a spectrophotometer. THY without inoculating *Sp* was used as blank. The bacteria were grown until mid-log phase point which measured between 0.2-0.3 in the generated growth curve (**Figure. 19**). The MOI was adjusted based on the repetitive measurement of CFU per ml of mid-log phase *Sp* stock. Before each experiment, the bacterial stock was prepared separately, by washing the bacterial stock three times in cold 1X PBS and centrifuging at 14000 ×g at 4 °C. The bacterial pellets were then resuspended in 1 ml antibiotic-free MEM.

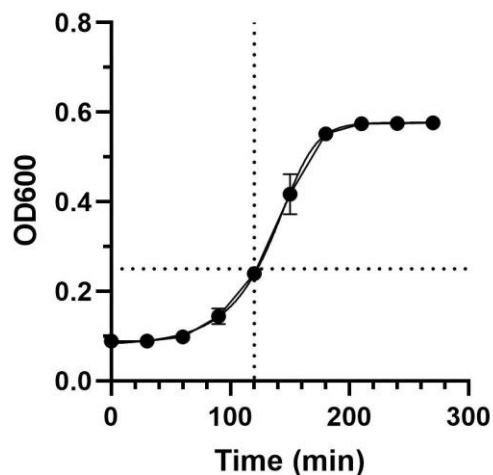


Figure 19: Logarithmic phase of *Sp* growth. The OD₆₀₀ of *Sp* in THY broth was recorded until plateau phase of *Sp* growth. The *Sp* growth curve was plotted against time by non-linear sigmoidal curve fit analysis.

4.3. CSE preparation

In order to prepare CSE, 3RF research cigarettes (University of Kentucky, US) which have standardized contents were purchased and used during the study. After cutting the filter ends with

a scalpel, cigarettes were attached to 1ml pipette tip and inserted to a 100 ml gas washing bottle using a rubber tube. The gas washing bottle was filled with 25 ml serum-free MEM medium. The vacuum head of the gas washing bottle was attached to a peristaltic pump. Following adjusting the speed on 100 rpm (flow rate: 180 ml/min), the cigarette was combusted, and fumes bubbled into the medium in a fume hood with sufficient ventilation. Each puff was set to last three seconds with twenty seconds pause in between. Two cigarettes bubbled through the medium considered as 100 % concentration and further diluted to the desired concentrations (5-20 %) with culture medium upon the experiments. The prepared CSE was immediately filtered through 0.22 μm filter (Merck Millipore) to remove particles and pathogens. The aqueous CSE was prepared freshly upon each experiment respectively, and used not more than 30 min after preparation.

4.4. Proliferation assays (based on metabolic activity)

4.4.1. MTT assay

To determine the optimal concentration of CSE which exerts minimal toxic effects on 16HBE cells, a cytotoxicity test using MTT was performed. MTT was diluted in 1X PBS and filter-sterilized using 0.22 μm filter strip (Merck Millipore). 16HBE cells were seeded into a transparent 96-well at 10^4 density and placed into a humidified with 7.5 % CO_2 incubator until forming a confluent monolayer. Subsequently, the cells were stimulated with different concentrations of CSE (5 %, 10 % and 15 %) for 24 h. After removing the medium, diluted MTT with final concentrations of 0.5 mg/ml was added to the cells in 100 μl phenol-red free medium. Following 4 h incubation in the incubator in dark, the insoluble formazan produced by viable cells turned to soluble solution using 200 μl cell-grade DMSO. After 30 min incubation on a shaker, the absorbance was read in each well at 560 nm wavelength using the microplate reader.

4.4.2. RealTime-Glo MT assay

This method was used to confirm the impact of CSE on the proliferation of metabolically active cells. For this purpose, the cells were initially seeded with different densities (5×10^3 , 10^4 and 2×10^4 cells/well) in a 96-well white-walled with transparent bottom (Greiner BioOne GmbH) to find an optimal cell density in which the read-out signal remains linear throughout the experiment. According to the **Figure 20 B**, this was the case for the cell density of 10^4 cells/well with a linear read-out signal until the end of the experiment. Next the cells were seeded at the 10^4 cell density and incubated with 2X RealTime-Glo reagent (MT substrate + Nanoluc enzyme). The luminescence at assay start (0 h) was then measured with the microplate reader. Following incubation of the cells with the reagents, the cells were stimulated with different concentration of CSE (5-20 %) and incubated at 37 °C with 7.5 % CO_2 . The luminescence was measured every

2 h for a total 30 h in the plate. The luminescence signal was plotted versus cell number using linear curve fit in the GraphPad software.

4.5. Oxidative stress assays

4.5.1. Intracellular ROS levels

Intracellular ROS levels were evaluated based on detection of fluorescent dye H2-DCFDA using microplate reader. The cells were seeded at 10^4 cells/well density into 96-well black-walled plate with transparent bottom (Greiner BioOne GmbH) and incubated for 3 days. Next, the cells were washed once with diluted assay buffer and stained with 25 μ M of H2-DCFDA diluted in assay buffer for 45 min. The cells were then stimulated with different concentrations of CSE and a ROS positive control compound, tBHP diluted in the complete serum-free medium. The initial fluorescence signal was initially measured at 0 h before stimulating the cells. H2-DCFDA dye was excited at 488 nm and emission light was detected at 528 nm (FITC filter set) with PMT gain set to 45. Then the plate kept in the incubator and read every two hours until 27 h. The fluorescence signal was calculated by subtracting unstained background and normalizing the signals from each condition to 0 h.

4.5.2. FACS staining for MitoSOX

The mitochondrial ROS levels was measured by MitoSOX fluorescent-based labelling of the superoxides generated in the mitochondria of 16HBE cells and subsequent by detection of signal with flow cytometry. The cells were seeded into 6-well plate at 3×10^5 cells/well and placed in humidified incubator until 90 % confluency. The antibiotic-supplemented medium was replaced with antibiotic-free medium 24 h before the experiment to rule out the impact of antibiotic on pneumococci growth. Next, the stimulated cells were harvested by trypsin/EDTA and washed once with 1X PBS. The cells were then stained with 5 μ M of diluted MitoSOX dye (5 mM stock in DMSO) in serum- and phenol red-free medium for 15 min. Subsequently, the cells were washed three times with 1X PBS and stained with a live/dead fluorescent dye (Fixable Viability Dye efluor 780) diluted in FACS buffer to gate out dead cells. The fluorescent signal was detected with 8-colors FACS CantoII device (Blue laser and PE channel for MitoSOX, Red laser and APC Cy7 channel). The MitoSOX-positive cell populations were gated using FlowJo software version 10.3.

4.6. Mitochondrial membrane potential analysis

JC-1 dye, which shows potential-dependent localization into the mitochondrial membrane, was used to assess the impacts of CSE and *Sp* on mitochondrial membrane potential. 16HBE cells

were plated at 10^4 cell/ well in black-wall 96-welled plate (Greiner BioOne GmbH). After 3 days, the medium was removed, and the cells were incubated in $2 \mu\text{M}$ JC-1 dye diluted in serum-free MEM for 1 h. After measuring the signal from J-aggregates and monomer at 0 h, the cells were stimulated with CSE, *Sp* MOI 10 and 20, and FCCP $50 \mu\text{M}$ as a mitochondrial complex V uncoupler. The ratio of J-aggregates to green monomers which is considered to be dependent on mitochondrial membrane potential was measured using the microplate reader by exciting the dye at 488 nm and detecting light emission at 529 nm and 590 nm for monomer and J-aggregates, respectively. After subtraction of background, the ratio of red/green fluorescent signal was then normalized to 0 h and plotted versus time. Data were obtained from two independent experiments.

4.7. Gene expression array

4.7.1. RNA isolation

RNA from 16HBE cells was isolated and purified using RNeasy Mini plus kit and was subjected to DNase treatment with the RNase-free DNase kit. Following stimulation, the cells (10^6 per 6 well plate) were washed twice with 1X PBS and lysed with $350 \mu\text{L}$ RLT plus buffer containing 1 % v/v β -Mercaptoethanol for 30 sec and then placed at -80°C overnight. Next, the lysate was thawed and homogenized using 1 ml syringes by repeatedly passing the lysate through 20-gauge needle. The homogenates were then transferred to the gDNA eliminator column and centrifuged for 30 sec at $9000 \times g$ at room temperature. $350 \mu\text{l}$ 70 % ethanol was added and the solution was transferred to the RNeasy plus mini column and centrifuged for 15 sec at $9000 \times g$. The column was then washed with $700 \mu\text{L}$ RW1 buffer once and briefly centrifuged at $9000 \times g$. Following two washing steps with $500 \mu\text{L}$ RPE buffer, RNA was eluted in $50 \mu\text{L}$ RNase-free water. The potential gDNA remnants was digested using RNase-free DNase (Ambion). RNA yield was calculated based on measured absorbance using the Nanodrop spectrophotometer.

4.7.2. DNA removal by DNase

For DNA digestion, the RNase-free DNase was directly added to the mini column during RNA isolation procedure as recommended in manufacturer's protocol RNA. Accordingly, diluted DNase solution was added to the RNeasy column after pre-soaking the membrane in RW1 buffer. and kept for 20-30 min at room temperature. Following the incubation, the column was washed with RW1 buffer again and centrifuged for 15 sec at $9000 \times g$. The procedure was continued with washing with RPE buffer and the elution stage. Finally, RNA concentration was determined with the NanoDrop spectrophotometer.

4.7.3. Microarray analysis

RNAs from 16HBE cells stimulated with CSE and *Sp* were isolated as described above. Samples were amplified, labelled, fragmented and hybridized to human Clariom™ S assay and treated according to manufacturer's instructions by Genome Analytics group at Helmholtz Centre for Infection Research (HZI). Microarray scanning was performed using an GeneChip™ 3000 scanner and GCOSv1.1 software. Data analyses were conducted using Transcriptome Analysis Console 4.0 (Thermo Fisher Scientific). First, data were \log_2 transformed and normalized using SST-RMA algorithm. In order to eliminate lowly expressed transcripts, a percentile filter was applied to the microarray data, which removes transcripts with SIs consistently below the 20th percentile of the average SI distribution in all microarrays. Differential expression between stimulated conditions and untreated medium control was calculated based on ANOVA method with $FDR < 0.05$ and applying a FC cut-off of: $-3 < FC > +3$. Volcano plots were generated in Python using Matplotlib library and the Spyder programming environment. K-means clustering of z-score transformed normalized \log_2 SI of differentially regulated genes was analyzed and plotted using Genesis software version 1.8.1. GSEA was performed with GSEA software 4.1.0 and gene sets of the Molecular Signature Database.

4.8. Sample preparation for immunoblotting

4.8.1. Total cell lysate

2×10^6 cells were seeded into 10 cm culture dishes (Corning) and placed in the humidified incubator until reaching 90 % confluency. The cells were lysed with 1X chilled RIPA buffer containing EDTA-free protease inhibitor cocktail and after centrifugation for 10 min at $14000 \times g$ the supernatants were collected and kept at $-80^\circ C$ until further use.

4.8.2. Mitochondrial fractionation

Mitochondrial fractions were isolated from the cells using a commercial kit (Active Motif) by gradient centrifugation. Accordingly, 2×10^6 cells were seeded into the culture dishes and placed in the humidified incubator until reaching confluency. For each condition, 3 plates were used, and the cell pellets were combined to harvest 3×10^7 cells at the end. Next, the cells were washed and collected by gently scratching the culture surface in cold PBS using cell scraper (Greiner BioOne GmbH). Following lysis of the cells with a 2 ml pestle homogenizer, debris and intact cells were separated using centrifugation at $800 \times g$. Next, the lysates were centrifuged two times at $10000 \times g$ to pellet the mitochondria. Eventually, the isolated mitochondria were lysed in the mitochondrial buffer including protease inhibitor and DTT. The mitochondrial fractions were then aliquoted and transferred to $-80^\circ C$.

4.9. Immunoblotting

16HBE cells were seeded into 10 cm culture dishes (Corning) and placed in the humidified incubator until reaching 90 % confluency. Based on the experimental design, the cells were either stimulated with medium control and CSE for 3 h, 14 h and 24 h or stimulated with CSE for 28 h, *Sp* MOI 10 and MOI 20 for 4 h, CSE for 24 h followed by both MOI of *Sp* for 4 h as well as CSE for 24 h followed by medium for 4 h and FCCP 50 μ M for 4 h.

For immunoblotting of total protein content of cells, the cells were lysed with 1X chilled RIPA buffer containing EDTA-free protease inhibitor cocktail and after centrifugation for 10 min at 14000 \times g the supernatants were collected and kept at -80°C until further use.

For immunoblotting of mitochondrial proteins, mitochondria were isolated from the cells as described in section 4.10.2.

The immunoblotting was performed to compare the expression of selected proteins in both total cell lysates and the cytosolic or mitochondrial fractions. Hence, the protein concentrations in each cell lysate were measured using a BCA kit following the manufacturer's instruction. After calculating and normalizing the protein concentration, the lysates were diluted in 1X sample buffer and boiled at 95°C for 5 min and then transferred to -80°C . Immunoblotting was conducted using two different protocols, respectively *i* and *ii*. The samples (4.25-10 μ g protein) were loaded together with *i*. one protein ladder or *ii*. at least two protein ladders into *i*. manually casted SDS-PAGE gels or *ii*. Criterion XT Precast 4-12 % or 12 % Bis-Tris gels (BioRad). Subsequently, the proteins were separated by electrophoresis at 100-130 V for respectively *i*. 2.5 h or *ii*. 1 h. The proteins on the gels were then transferred to a membrane by electroblotting to *i*. methanol activated PVDF membrane (Merck Millipore, 0.45 μ M) using semi-dry transfer system or *ii*. or *ii*. nitrocellulose transfer membrane (0.45 μ M; BioRad) using a Bio-Rad Criterion Blotter. In case of protocol *ii*, the Nitrocellulose membranes were incubated for 5 min with 0.2 % (w/v) Ponceau S in 1 % (v/v) acetic acid followed by MilliQ water washing and imaging, conducted to quantify total protein content for normalization, using the AmershamTM Imager 600. Subsequently, the membranes were washed, and non-specific binding sites were blocked by 1 h incubation in TBST buffer supplemented with *i*. 5 % skimmed milk in TBST or *ii*. 3 % non-fat dry milk in TBST. Next, the membranes were washed and incubated at 4°C overnight in buffer containing primary target-specific antibodies (**Table 4**). Buffers were either TBST with 3 % BSA or TBST with 5 % non-fat dry milk. Following a washing step, the membranes were incubated 1 h at room temperature in TBST buffers containing horseradish peroxidase-conjugated secondary antibodies (**Table 5**). The membranes were finally washed with TBST

before imaging. The membranes were incubated for 1-3 min with *i.* the chemiluminescent substrate PierceTM ECL and visualized using a CCD imager or *ii.* visualized using the AmershamTM Imager 600.

The abundance of the target proteins was quantified and normalized using *i.* ImageJ software and normalized to loading control proteins GAPDH or β -actin or *ii.* Image Quant software (GE Healthcare) and total protein loading content assessed by Ponceau S staining over the entire size range of proteins (250 kDa - 10 kDa). Selected western blot images of one treatment group are representative of changes for the replicates. Representative western blot images shown in the figures of this manuscript have been equally adjusted for brightness and contrast throughout the picture.

4.10. Immunocytochemistry

The cells were seeded into the FluroDish (WPI) at 15×10^4 cells/dish and stimulated with either CSE 28 h or with 24 h CSE followed by 4 h MitoTEMPO 50 μ M or MOTS-c 25 μ M. The cells were then fixed with pure chilled methanol. After washing, the cells were permeabilized with 5 % goat serum and 0.01 % TritonX-100 in 1X PBS for 1 h. Subsequently, the cells were incubated in primary antibodies (**Table 5**) diluted in 1 % BSA in PBS and kept at 4 °C overnight. Following washing with 5 % goat serum in PBS, the cells were incubated in the secondary antibodies (goat anti rabbit Alexa fluor 647, goat anti mouse Alexa fluor 488) for 1 h. After the final washing, the cells were stained with DAPI to locate the nucleus. The cells were then mounted with a mounting medium and covered with coverslips and placed at 4 °C overnight. Microscopy was performed under a fluorescent microscope Zeiss Axiovert 200m with the appropriate filter sets at 400X magnification. The images were analyzed using the latest version of ImageJ software.

4.11. Mitochondrial ultrastructure analysis

The cells were prepared as mentioned above and fixed in six well plates by adding the fixative solution, a 0.1 M EM-HEPES buffer with 5 % paraformaldehyde and 2 % glutaraldehyde. The fixed samples were washed twice with 0.1 M EM-HEPES buffer and treated with osmium tetroxide (1 % in HEPES buffer) for 1 h at room temperature. After additional washing steps with HEPES buffer, cells were mechanically detached from the surface and centrifuged in a swingout rotor for 4 min at 5000 RPM. The pellet was stabilized in 2 % noble agar before dehydration in a graded series of ethanol (10, 30, 50, 70, and 90 %) on ice, and two steps in 100 % ethanol at room temperature, each step for 30 minutes. Samples were subsequently infiltrated with the LR

White (LRW) resin (LRW: EtOH: 1:1, 2:1, 2x 100 %), each incubating step for approx. 8 h or overnight respectively followed by a polymerization step in small gelatin capsules at 50° C for 48 h. Ultrathin sections of approx. 50-70 nm thickness were prepared with a Ultramicrotome Ultracut UC7 and counterstained with 4 % aqueous uranyl acetate for 3 min and with and without lead citrate for 15 sec. TEM image acquisition at calibrated magnifications was performed with a Libra 120 Plus using an acceleration voltage of 120 kV. For image analysis the software ITEM (Olympus) was used.

4.12. Epithelial antibacterial response test

16HBE cells were cultivated in MEM according to section 4.1. until 90 % confluency. Subsequently, the cells were stimulated with antibiotic-free MEM medium and CSE for 3 h and 24 h in humidified incubator at 37 °C with 7.5 % CO₂. *Sp* were initially plated on Columbia blood agar plates and incubated at 37 °C and with 5 % CO₂ overnight. The single colonies were then washed and inoculated in THY broth for 2 h until reaching the mid-log OD 0.25. Next, the inoculum was washed three times with 1X chilled PBS and diluted in antibiotic-free MEM. The cells were then infected with MOI 10 and MOI 20 of *Sp* for 4 h and incubated in the incubator at 37 °C with 7.5 % CO₂. Following incubation, 100 µL of supernatant was collected from each condition and after serial dilution were cultured on Columbia blood agar plates and placed at 37 °C with 5 % CO₂ overnight. Next day, the grown single colonies were counted, and CFU/ml was calculated.

4.13. Statistical analysis

Statistical analysis was done using GraphPad prism version 9.3.1. All data were analyzed by at least two independent repeated measurements and plotted as mean \pm SEM. Dependent on the experimental condition, the significant differences between the conditions were determined using one-way ANOVA and two-way ANOVA with Dunnett's multiple comparison test or unpaired two-tailed t-test with Welch's post-hoc correction test.

5. Results

In this chapter, the three majors aim of the thesis will be addressed using an *in vitro* experimental model. First, AECs were exposed to CSE to find the impacts of CSE on mitochondrial function. Next, upon determination of CSE concentration, the cells were pre-exposed to CSE followed by *Sp* infection to examine whether pre-exposure to CSE would alter mitochondrial function as well as other cellular responses including innate immune responses to *Sp* infection as well as epithelial barrier function.

5.1. AEC proliferation upon CSE exposure

MTT assay and RealTime Glo MT were performed to find the concentration of CSE that minimally affect viability while suppressing mitochondrial activity. The reduction of MTT dye to formazan is dependent on mitochondrial succinate dehydrogenase activity in the cells, thus representing the presence of mitochondrial metabolically active cells. The results of MTT assay showed that the conversion of MTT to formazan reduced in response to CSE in a concentration-dependent manner, with 20 % showing the highest reduction in formazan levels following 24 h stimulation with CSE (**Figure 20 A**), suggesting exposure of 16HBE cells to 15 % and 20 % of CSE reduced cell proliferation. Furthermore, RealTime Glo MT assay was performed to check the effects of CSE on cell proliferation in a time-course experiment. First, three seeding densities of 16HBE cells (5×10^3 , 10^4 , 2×10^4) were used to find the linearity of luminescent signal versus time. As displayed in **Figure 20 B**, the signal decreased in proportion to cell density for the highest used density (2×10^4), while it remained linear for two lower cell densities (5×10^3 , 10^4). Therefore, 7×10^3 cell/96 well was selected for further experiment. Exposing 16HBE cells to CSE (10-20 %) showed a similar reduction in RealTime-Glo RLU compared to the medium treatment, suggesting a reduction in cell proliferation starting from 1 h (**Figure 20 B**).

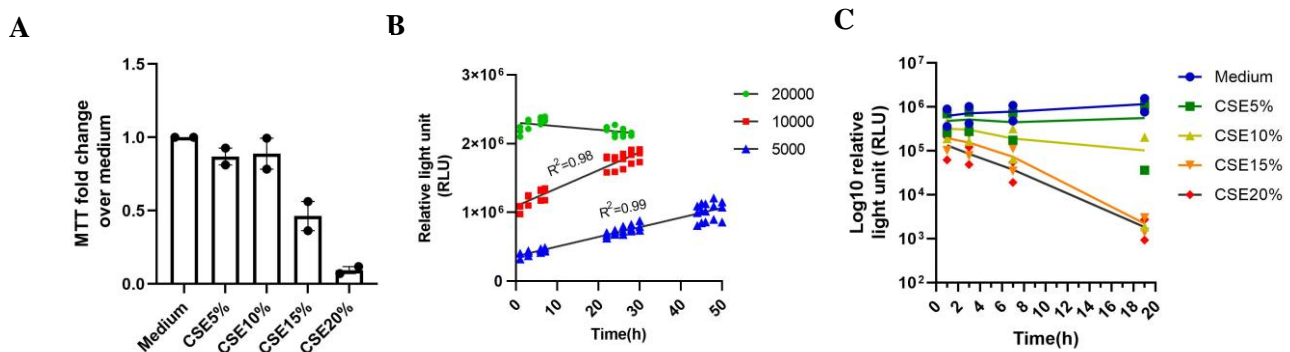


Figure 20: Optimization of CSE-induced epithelial dysfunction model by measurement of cell proliferation in 16HBE cells. A) MTT optical density at 560 nm was measured in 16HBE cells upon stimulation with medium or various concentrations of CSE (5-20 %) for 24 h using MTT test. The preliminary data is representative of mean of

fold change over medium of two independent experiments. **B)** Linear increase in cell proliferation in proportion to the culture cell density as measured by luminescent-based Real-Time Glo MT assay. Three seeding densities of 16HBE cells (5×10^3 , 10^4 and 2×10^4 cells/96 well) were used to find the optimal density that the signal stays linear until 19 h by measuring RLU every two hours using a microplate reader. **C)** 16HBE cells were seeded at 7×10^3 cells/well and stimulated with either medium or CSE 5-20 %. RLU was recorded in a time-point measurement until 19 h. The preliminary data is representative of mean of two independent experiments.

These findings showed that higher concentrations of CSE suppress proliferation of 16HBE cells potentially via affecting mitochondrial OXPHOS.

5.2. Total and mitochondrial oxidative stress upon CSE exposure

Next, ROS levels was measured to find the concentration of CSE that highly increases ROS production. Total intracellular ROS levels was measured by H2-DCFDA fluorescent-based method. As shown in **Figure 21 A**, the ROS levels was increased upon stimulation with CSE in a time- and concentration-dependent manner, with 20 % showing the maximal H2-DCFDA signal compared to the medium control (**Figure 21 A**). Mitochondrial ROS levels which were detected with fluorescent-based method by staining the cells with MitoSox increased in 24 h treatment with various concentrations of CSE, displayed by a shift in the signal as compared to the medium control (**Figure 21 B**).

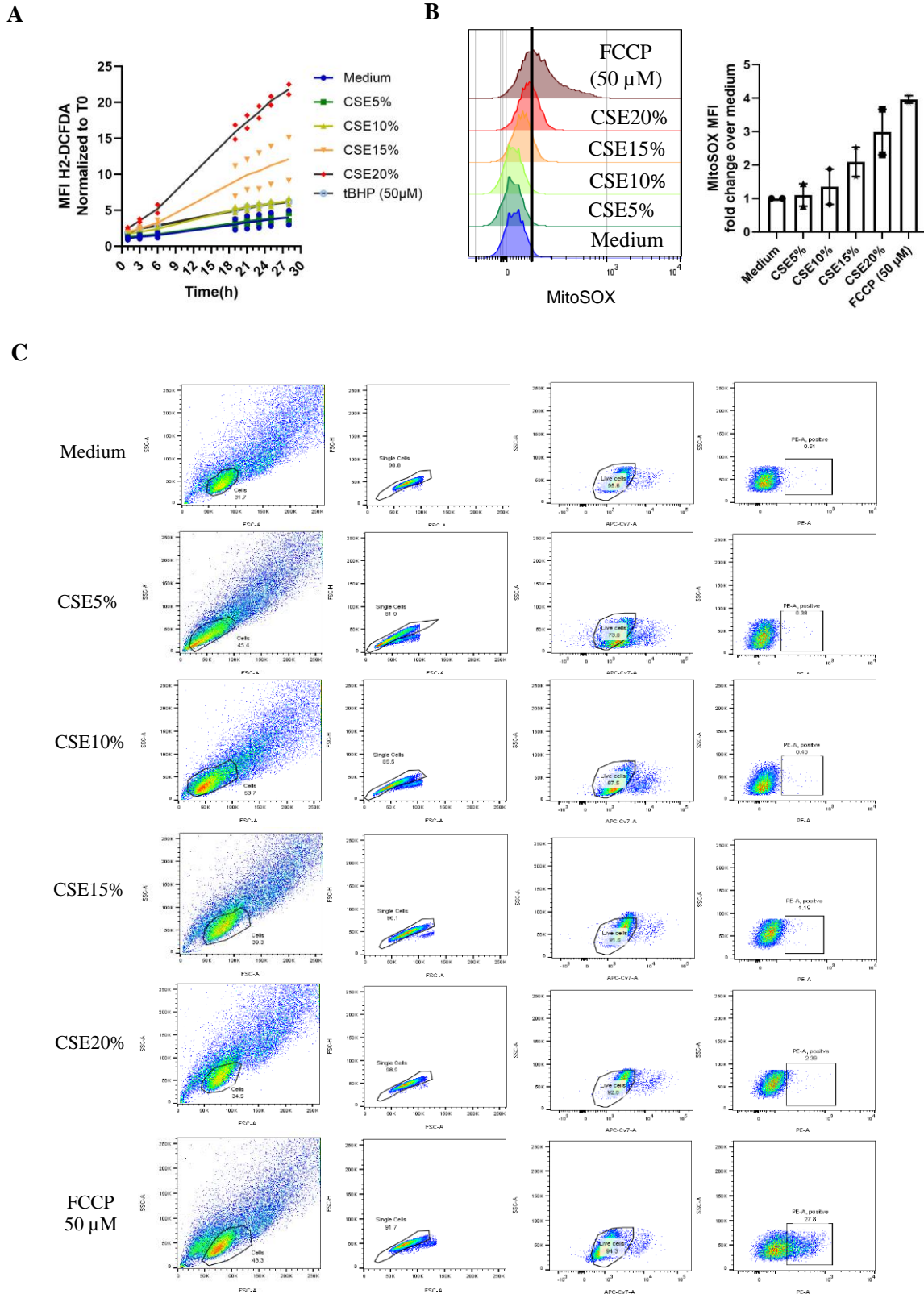


Figure 21: Cellular oxidative stress levels upon stimulation of 16HBE cells with CSE. A) The cells were incubated with either medium or various concentrations of CSE (5-20 %) and tBHP 50 µM for 24 h and the total ROS levels was measured using H2-DCFDA test by measuring fluorescent signal every 2 h until 28 h by a microplate reader (excitation: 488 nm and emission: 520 nm). The preliminary data is representative of mean of two independent experiments. **B)** Half offset histogram showing changes in the curve of MitoSOX-positive cell fluorescent signal (PE channel) upon CSE and FCCP as positive regulator of ROS as measured by FACS and analyzed with FlowJo, indicative of changes in mitochondrial ROS levels (left panel), and fold change of MFI of

MitoSOX-positive cells over medium (right panel). C) A gating strategy for live MitoSOX-positive subsets of 16HBE cells that exposed to various concentrations of CSE as well as FCCP 50 μM are shown in pseudocolored plot.

Preliminary data of ROS production revealed that 15 % and 20 % CSE induces an increase in oxidative stress by enhancing total ROS and mitochondrial ROS in a time and concentration-dependent fashion.

5.3. Mitochondrial membrane potential upon CSE exposure

In order to find the concentration of CSE that induce a loss in mitochondrial membrane potential JC-1 test was performed. JC-1 is a fluorescent-based method that indicate mitochondrial membrane potential by dividing (J-aggregate) red/ (monomer) green ratio in a time course. As displayed in **Figure 22**, normalized mean of red/green ratio was decreased in all CSE-treated concentrations with 20 % showing the highest decrease in ratio. The drop in the mitochondrial membrane potential started as early as 3 h post-CSE and with highest drop at 27 h post-CSE for 10-20 % concentrations. FCCP 50 μM was used as a positive control and induced a clear reduction in mitochondrial membrane potential as compared to the medium control.

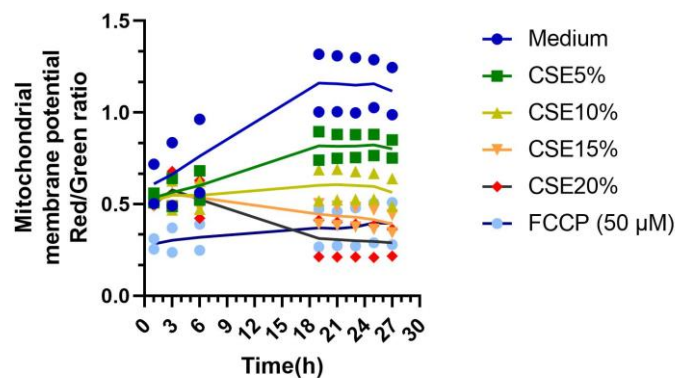


Figure 22: Mitochondrial membrane potential upon stimulation with various concentrations of CSE. 16HBE cells were exposed to either medium or CSE 5-20 % as well as FCCP 50 μM for 27 h. Mitochondrial membrane potential was measured using JC-1 test by dividing J-aggregate (red signal) by monomer (green signal) and was normalized to the ratio in the corresponding condition at assay start (0 h). The preliminary data is representative of mean of red/green ratio of two independent experiments (Aghapour et al., 2022).

These results suggest that CSE exposure diminishes mitochondrial membrane potential in a time- and concentration-dependent manner. As such, 15 % of CSE was selected for subsequent experiments and for the sake of simplicity, we will use the abbreviation CSE without further stating the percentage of 15 % in the following paragraphs.

5.4. Mitochondrial complex protein levels upon CSE exposure

Immunoblotting was performed to check the impact of CSE not only on the expression of different mitochondrial OXPHOS complex proteins, but also to investigate the expression of mitochondrial outer membrane proteins.

Mitochondrial proteins were initially probed in total cell lysates of 16HBE cells stimulated with CSE for 3 h, 14 h and 24 h (**Figure 23 A**). Data of immunoblotting revealed a significant reduction in abundance of total complex IV protein (COXIV) 3 h post CSE, however, it returned to the basal levels after 14 h and stayed unchanged until 24 h (**Figure 23 B**). The levels of subunits of complex V (ATP5A) and complex III (UQCRC2) protein expression remained unchanged at 3 h, 14 h and 24 h after treatment with CSE compared to the medium control (**Figure 23 C** and **Figure 23 D**). Moreover, a significant reduction in abundance of the subunit of complex II protein (SDHB) was observed after 24 h compared to the medium (**Figure 23 F**). A significant decrease in the OMM protein VDAC1 expression was observed in the cells stimulated with CSE for 24 h (**Figure 23 G**). In addition, the mitochondrial proteins were probed in the cytoplasmic and mitochondrial fractions upon stimulation of 16HBE cells with CSE for 24 h (**Figure 23 H**). The abundance of subunits of complex V (ATP5A) and complex III (UQCRC2) slightly increased upon CSE for 24 h in the mitochondrial fractions (**Figure 23 I** and **Figure 23 J**). The levels of SDHB significantly decreased upon stimulation with CSE for 24 h in the mitochondrial fractions (**Figure 23 K**). The abundance of TOMM20 enhanced upon stimulation with CSE compared to the medium control (**Figure 23 L**). Moreover, the expression of mitochondrial proteins was not detected in the cytoplasmic fractions of all stimulated cells, suggesting the purity of the isolated mitochondrial fraction.

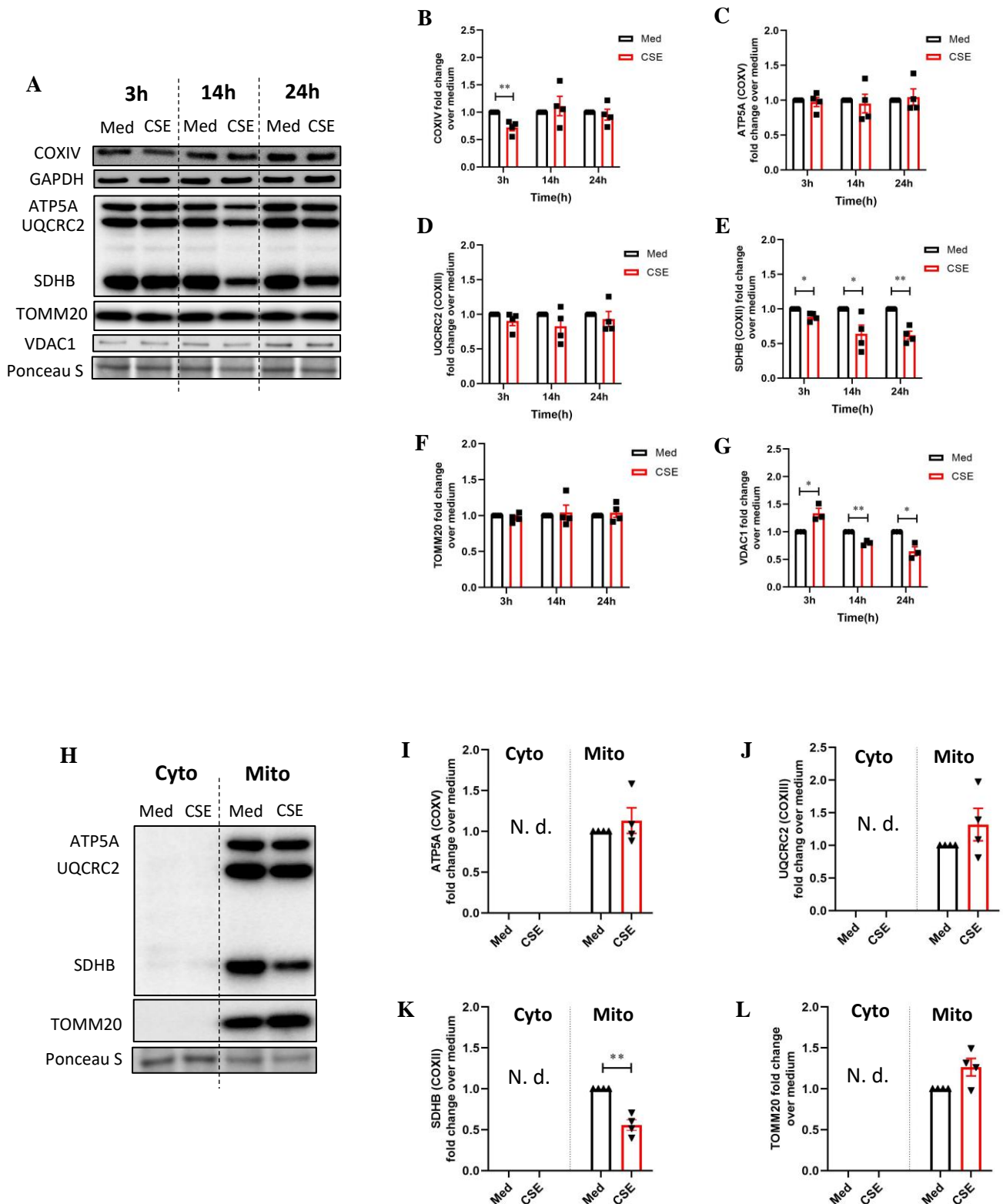


Figure 23: Abundance of mitochondrial complex components as well as constituents of OMM upon CSE15 % stimulation in 16HBE cells. **A)** Immunoblot representing protein expression of subunits of mitochondrial complex proteins including subunits of complex II (SDHB), subunit of complex III (UQCRC2), total complex IV (COXIV), subunit of complex V (ATP5A) and OMM proteins TOMM20 and VDAC1 in the total cell lysates of the cells treated with Med control or CSE for 3 h, 14 h and 24 h. **B)** Fold change of COXIV, **C)** ATP5A, **D)** UQCRC2, **E)** SDHB, **F)** TOMM20 and **G)** VDAC1 in the total cell lysates upon CSE over Med control. The data are represented as mean \pm SEM of four independent experiments (N=4). **H)** Fold change of ATP5A protein expression, **J)** UQCRC2,

K) SDHB as well as **L)** TOMM20 over the medium control. The data are represented as mean \pm SEM of four independent experiments (N=4). Normalization of protein expression was performed by GAPDH or Ponceau S staining. Statistically significant values were calculated with multiple t-test and with Holm-Sidak post-hoc correction test (*p<0.05, **p<0.001) (Aghapour et al., 2022).

Together, these data show that CSE reduces the abundance of subunits of OXPHOS complexes, suppresses OMM protein and increases mitochondrial mass in 16HBE cells.

5.5. Mitochondrial-specific autophagy (mitophagy) upon CSE exposure

Mitochondrial quality control processes, including mitophagy, are crucial for maintaining mitochondrial homeostasis especially upon damage by e.g., exogenous stimuli. In order to assess the influence of CSE on these processes, the proteins involved in mitochondrial-specific autophagy (i.e., mitophagy) were probed in total cell lysates by immunoblotting (**Figure 24 A**). Protein expression of a constituent involved in receptor-mediated mitophagy and autophagosome formation, GABARAPL1, was increased in the total cell lysates after 14 h and 24 h stimulation with CSE (**Figure 24 B**). The levels of another protein involved in receptor-mediated mitophagy and cell death BNIP3 were significantly reduced after 24 h of exposure of the cells to CSE (**Figure 24 C**). However, the abundance of BNIP3L did not alter upon stimulation with CSE (**Figure 24 D**). Moreover, the abundance of autophagy-associated constituents SQSTM1 were increased upon 14 h and 24 h stimulation with CSE compared to the matched medium control (**Figure 24 E**). The protein levels of another constituent of autophagy LC3BI increased 14 h and 24 h post-CSE stimulation (**Figure 24 F**). The protein levels of ubiquitin-mediated mitophagy factor PINK-I were significantly increased in CSE 24 h in the total cell lysates of 16HBE cells stimulated with CSE for 24 h as compared to the medium control (**Figure 24 G**). Furthermore, these mitophagy proteins were probed in the cytoplasmic and mitochondrial fractions upon stimulation with medium or CSE for 24 h (**Figure 24 H**). The levels of GABARAPL1 increased in both cytoplasmic and mitochondrial fractions upon CSE 24 h (**Figure 24 I**). The abundance of SQSTM1 and LC3BII/LC3BI ratio, were significantly increased in the mitochondrial fraction of CSE-stimulated cells for 24 h compared to the medium control (**Figure 24 J** and **Figure 24 K**).

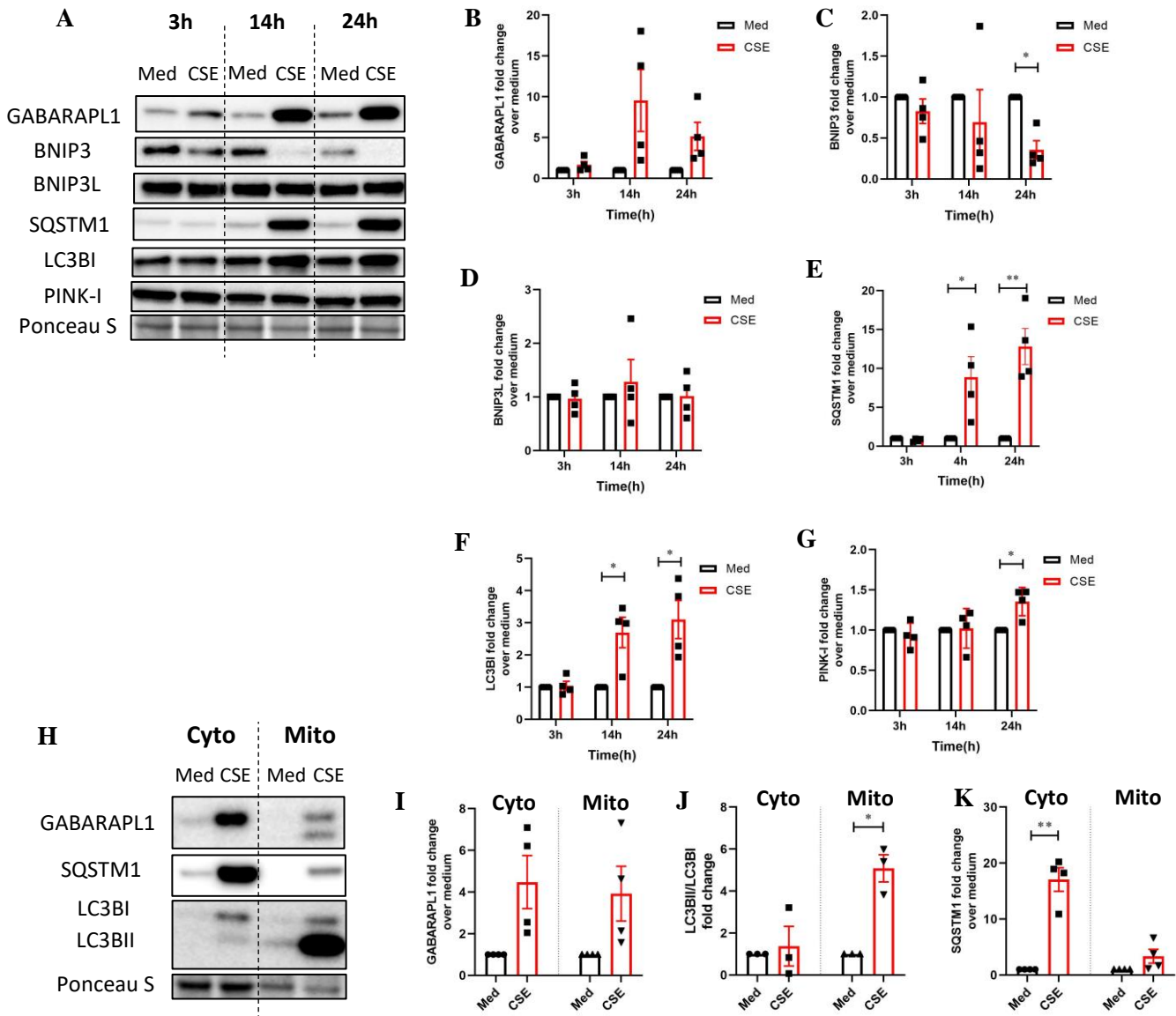


Figure 24: Abundance of key regulators involved in mitophagy in 16HBE cells upon stimulation with CSE15 %. **A)** Immunoblots representing protein expression of receptor-mediated constituents GABARAPL1, BNIP3, BNIP3L and ubiquitin-mediated PINK-I mitophagy factors as well as mitophagy adaptor proteins SQSTM1 and LC3BII/I in 16HBE cells stimulated with CSE for 3 h, 14 h and 24 h in total cell lysates. **B)** Fold change of GABARAPL1, **C)** BNIP3, **D)** BNIP3L, **E)** SQSTM1, **F)** LC3BI, **G)** PINK-I over medium control. **H)** Immunoblots representing the selected mitophagy factors in the Cyto and Mito fractions of the cells incubated with either medium or CSE for 24 h. **I)** Fold change of GABARAPL1, **J)** LC3BII/LC3BI ratio and **K)** SQSTM1 in CSE stimulated group over medium control. Normalization of protein expression was performed by Ponceau S staining. Significant values were calculated by multiple t-test with Holm-Sidak post-hoc correction test (* $p < 0.05$, ** $p < 0.001$) (Aghapour et al., 2022).

Together, these findings indicate that CSE stimulation induced the constituents associated with ubiquitin-mediated mitophagy and autophagy and reduced abundance of a receptor-mediated mitophagy.

5.6. Involvement of AMPK and ULK1 in CSE-induced alterations in mitophagy

To investigate the involvement of potential pathways that regulating autophagy e.g., AMPK α and ULK1 protein levels was assessed by immunoblotting. Furthermore, phosphorylation of AMPK α at threonine 172 and ULK1 at serine 555 was probed using immunoblotting in the total cell lysates of 16HBE cells stimulated with CSE for 14 h and 24 h (**Figure 25 A** and **Figure 25 B**). The findings show that the ratio of phosphorylated ULK1 to total ULK1 increased upon 14 h stimulation with CSE compared to the medium control (**Figure 25 C**). Moreover, the ratio of phosphorylated AMPK α to total AMPK α slightly decreased 14 h post-CSE (**Figure 25 D**). These ratios returned to the basal levels 24 h post-CSE compared to the medium control (**Figure 25 E** and **Figure 25 F**).

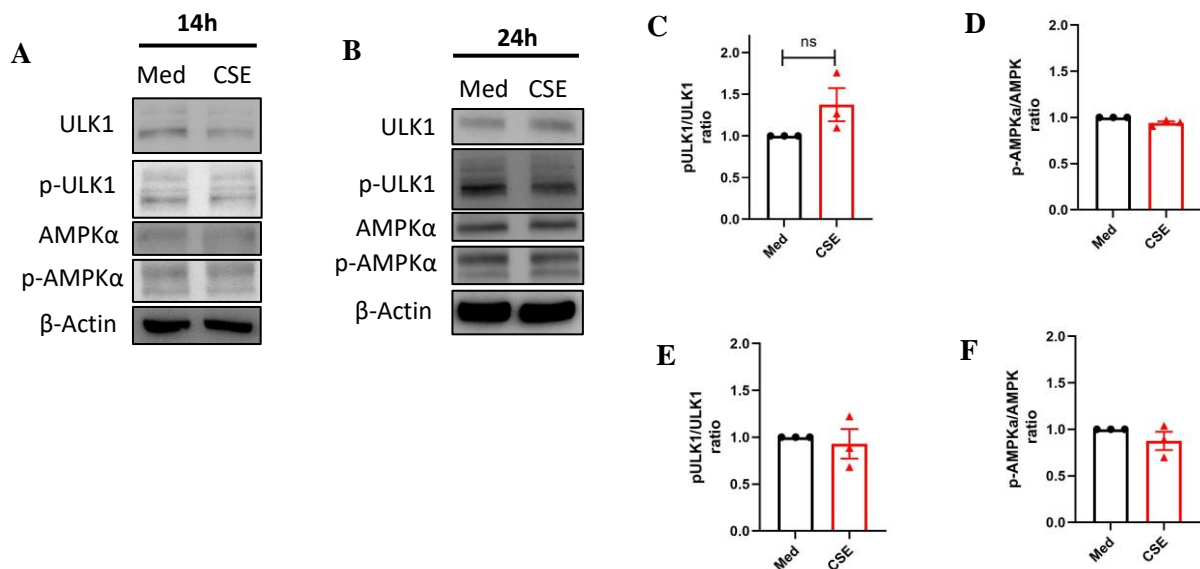


Figure 25: Mitophagy factors regulatory protein levels upon stimulation of 16HBE cells with CSE15 %. 16HBE cells were either incubated with medium and CSE for 14 h or 24 h. **A)** Immunoblots representing ULK1, phospho-ULK1 (Ser555), AMPK α and phospho-AMPK α (Thr172), ULK1 upon 14 h and **B)** 24 h stimulation with CSE. **C)** Fold change of pULK1/ULK1 ratio **D)** p-AMPK/AMPK ratio upon stimulation with CSE for 14 h. **E)** Fold change of p-ULK1/ULK1 ratio and **F)** p-AMPK/AMPK ratio upon incubation with medium or CSE for 24 h. Protein expression for each target protein was normalized to the loading control protein β -actin. The data are represented as mean \pm SEM of three independent experiments (N=3). Significant values were calculated by multiple t-test with Holm-Sidak post-hoc correction test (* $p < 0.05$, ** $p < 0.001$) (Aghapour et al., 2022).

Together, these data show that CSE-induced increase in mitophagy minimally affected by major pathways regulating mitophagy in AECs.

5.7. Mitochondrial fission and fusion levels upon CSE exposure

To elucidate the effects of CSE on the mitochondrial dynamic processes (i.e., mitochondrial fission and fusion), the levels of key regulators of fission and fusion were assessed using immunoblotting (**Figure 26 A**). MFN2, one of the proteins regulating mitochondrial fusion

significantly increased upon 3 h stimulation with CSE, while reduced upon 24 h CSE stimulation compared to the medium control (**Figure 26 B**).

The abundance of a mitochondrial fission regulator DRP1 increased upon 3 h, 14 h and 24 h treatment of 16HBE cells with CSE but failed to reach statistically significant difference compared to the medium control (**Figure 26 C**). Immunostaining was performed to check the levels of phosphorylated DRP1 at Serine 616. The phosphorylated DRP1 at Serine 616 increased in the cells stimulated with FCCP 50 μ M and a slightly in the cells stimulated with CSE compared to the medium control as visually observed by increase in the signal. Treatment with MOTS-c 25 μ M for 4 h increased the signal of total DRP1 and slightly reduced the increase in p-DRP1 signal induced by CSE pre-exposure (**Figure 26 D**).

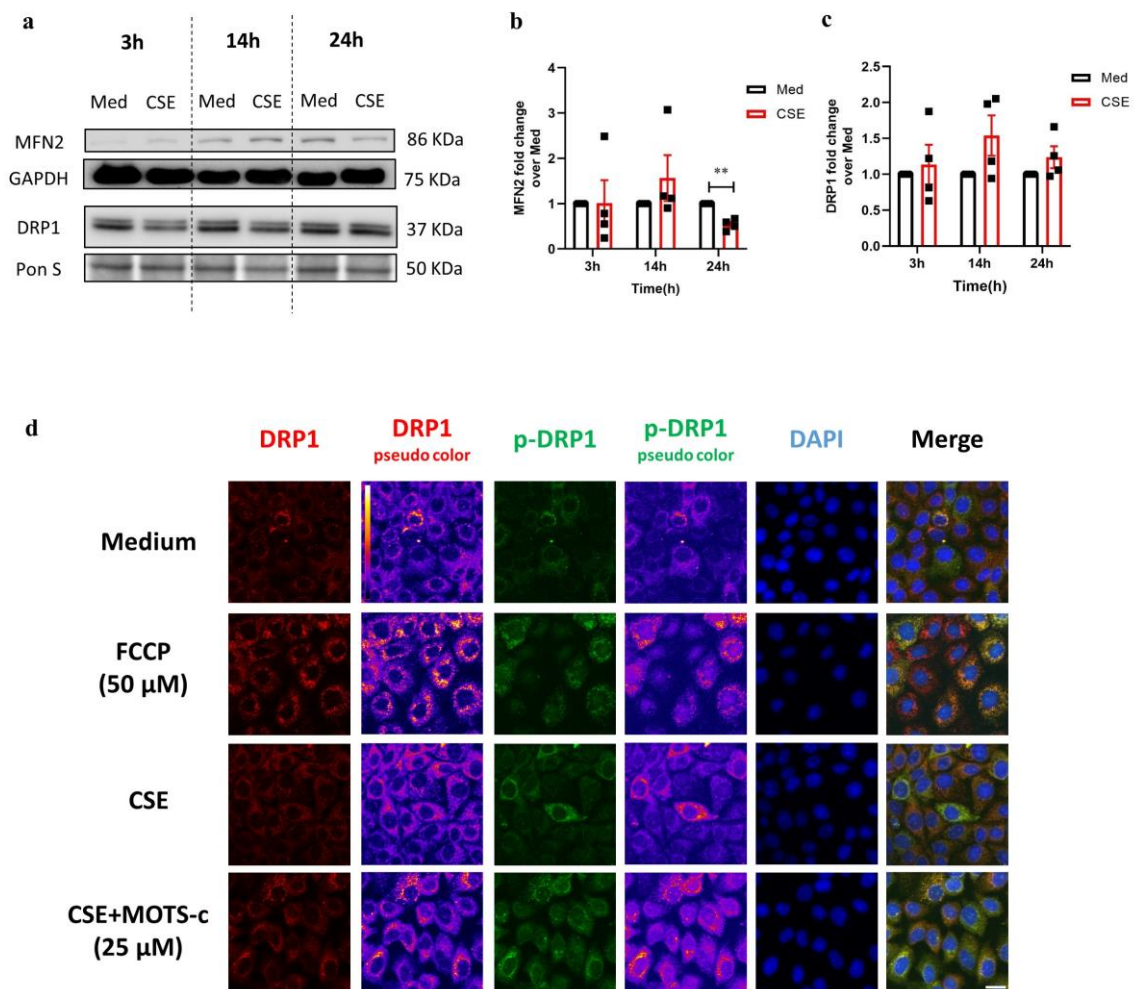


Figure 26: Mitochondrial fission and fusion levels upon stimulation of 16HBE cells with CSE15 %. **A)** Immunoblot representing protein expression of MFN2 and DRP1 in 16HBE cells incubated with either medium or CSE for 3 h, 14 h and 24 h. The data are represented as mean \pm SEM of four independent experiments (N=4). **B)** Immunostaining of DRP1 (red) and phospho-DRP at serine 616 (green) in combination with DAPI (nuclei) (blue). 16HBE cells upon incubation with medium, FCCP, CSE for 28 h or CSE 24 h followed by 4 h treatment with MOTSC-c 25 μ M. False color-coded image columns are shown here to depict differences in staining intensity. Merged images have been gamma-corrected to visualize weak signals without losing the highlights. The scale bar is equivalent to 20 μ m (Aghapour et al., 2022).

In summary, CSE was shown to disturb mitochondrial dynamic processes by reducing a constituent regulating mitochondrial fusion and increasing another constituent regulating mitochondrial fission in 16HBE cells.

5.8. Mitochondrial biogenesis upon CSE exposure

Mitochondrial biogenesis was probed by quantifying the expression of proteins essentially involved in the molecular control of this process including NRF1 and ERR α in the total cell lysates (**Figure 27 A**). The abundance of NRF1 was reduced 14 h post-CSE exposure (although not statistically significant), but increased upon 24 h stimulation compared to the medium control (**Figure 27 B**). ERR α protein levels were reduced after both 14 h and 24 h post-CSE (**Figure 27 C**). Moreover, NRF1 and ERR α were probed in the cytoplasmic and mitochondrial fractions of 16HBE cells exposed to CSE for 24 h (**Figure 27 D**). The levels of NRF1 significantly increased in the cytoplasmic fraction upon CSE for 24 h (**Figure 27 E**), whereas ERR α was reduced in the mitochondrial fraction compared to the medium (**Figure 27 F**). Furthermore, immunostaining with ERR α revealed an increase in pre-nuclear accumulation of the ERR α signal when the cells were stimulated with CSE for 28 h (**Figure 27 G**). The pre-nuclear accumulation of ERR α induced by CSE was not altered by 4 h post-treatment with MOTSC-c 25 μ M, a mitochondrial-derived peptide regulating OXPHOS. Stimulation with FCCP 50 μ M increased spread of fragmented ERR α signal in the cytoplasm.

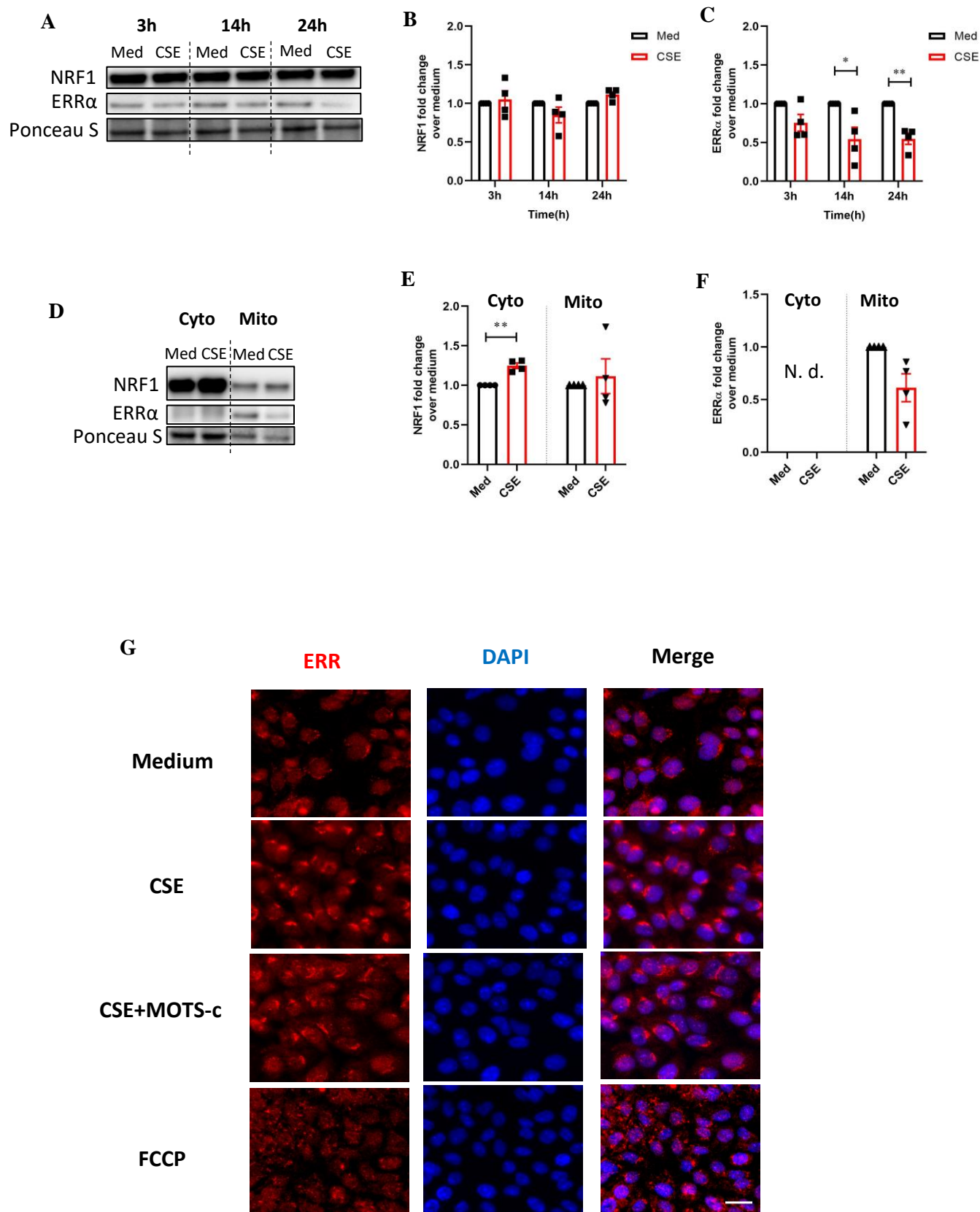


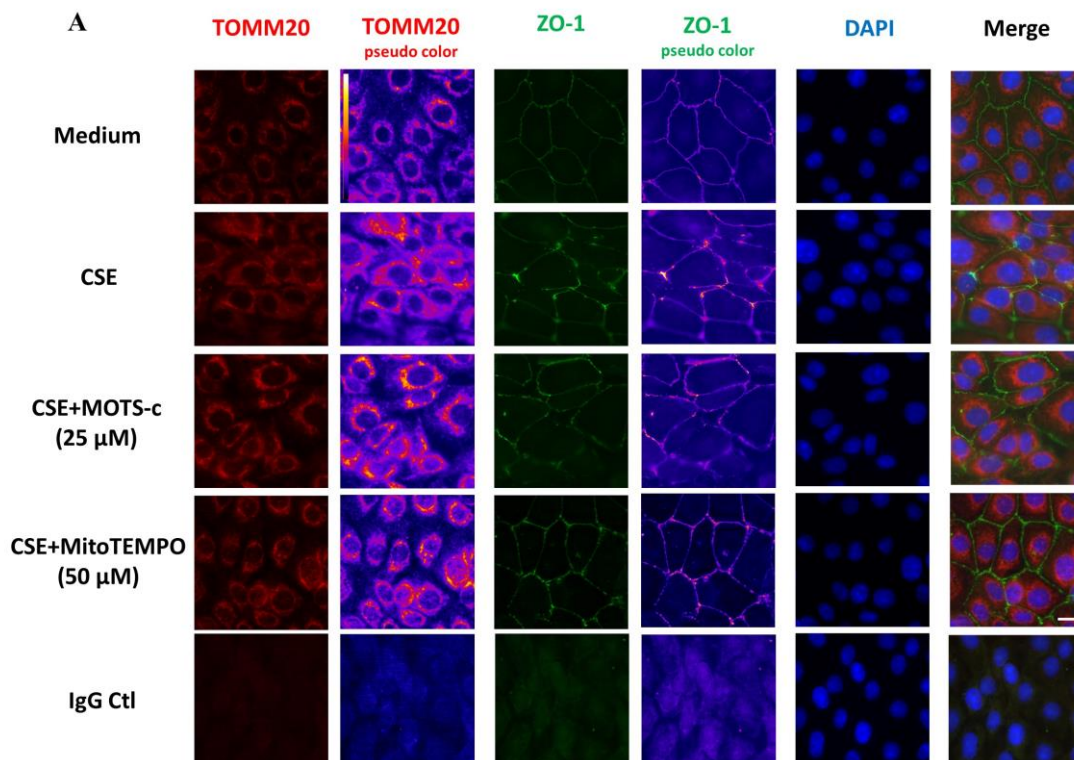
Figure 27: Mitochondrial biogenesis upon stimulation of 16 HBE cells with CSE15 %. **A)** Immunoblots representing the protein expression of the constituents of mitochondrial biogenesis including NRF1 and ERR α in the total cell lysate upon incubation with either medium or CSE for 3 h, 14 h, and 24 h. **B)** Fold change of NRF1 protein expression as well as **C)** ERR α upon CSE compared to the medium control (N=4). **D).** Immunoblot

representing NRF1 and ERR α in the Cyto and Mito fractions upon stimulation with either medium or CSE for 24 h. **E)** Fold change of NRF1 protein expression as well as **F)** ERR α compared to the medium control (N=4). Normalization of protein expression was performed by Ponceau S staining. The data are represented as mean \pm SEM of four independent experiments (N=4). Statistically significant values were calculated with paired two-tailed t-test (*p<0.05, **p<0.001). **G)** Immunostaining for estrogen related receptor α (ERR α). The 16HBE cells were incubated with medium control, CSE for 28 h, CSE 24 h followed by MOTS-c 25 μ M for 4h or with FCCP 50 μ M. Immunofluorescence staining was performed using antibodies for ERR α (red) and DAPI (blue) for nuclei staining. The scale is equivalent to 20 μ m (Aghapour et al., 2022).

These data indicate that CSE affect mitochondrial biogenesis by altering the levels of ERR α protein that is essential for mitochondrial. Moreover, ERR α may be exchanged between the nucleus and mitochondria and the cytoplasmic levels of ERR α could trigger mitochondrial damage.

5.9. CSE-induced epithelial barrier dysfunction rescued with mitochondrial compounds

In order to unravel the links between CSE-induced mitochondrial dysfunction and epithelial cell junction integrity, mitochondrial targeted compounds were used to examine whether improving mitochondrial function affects barrier integrity. The cells were stimulated with CSE 28 h and CSE for 24 h followed by MitoTEMPO (50 μ M) and MOTS-c (25 μ M) for 4 h. We found that CSE reduces ZO-1 and E-cadherin signal, which was partly reversible with MOTS-c treatment (**Figure 28 A** and **Figure 28 B**). However, post-treatment with MitoTEMPO for 4 h only improved E-cadherin signal (**Figure 28 B**).



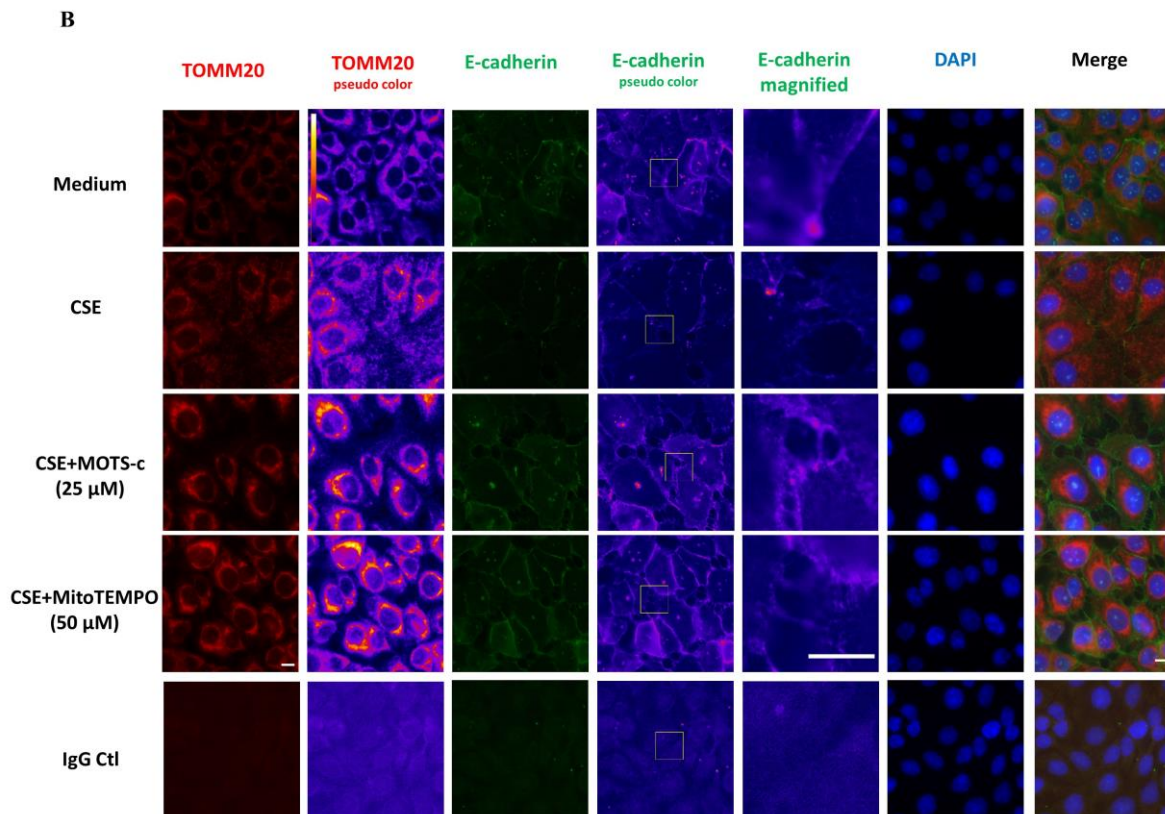


Figure 28: Post-treatment with mitochondrial-targeted compounds reverses CSE-induced airway epithelial barrier disruption. 16HBE cells incubated with medium or CSE15 % for 28 h and CSE15 % for 24 h followed by either MOTS-c 25 μ M or MitoTEMPO 50 μ M for 4 h. **A**) The cells were co-stained with mitochondrial outer membrane protein TOMM20 (red) and tight junction protein ZO-1 (green) antibodies. **B**) 16HBE cells were stained with anti-TOMM20 and anti-E-cadherin antibodies. The nucleus was stained with DAPI (blue). False color-coded image columns shown here to depict differences in intensities. To visualize the barrier disruption, magnified regions of interest are indicated in the fourth column and shown in column five. Merged images have been gamma-corrected to visualize weak signals without losing the highlights. The scale bar is equivalent to 20 μ m (**A**) and 10 μ m (**B**) (Aghapour et al., 2022).

The findings on physical epithelial barrier function shows that, while CSE disrupts the cell-cell junctions, mitochondrial compounds post-treatments repair the disrupted cell junctions induced

5.10. Effect of CSE on *Sp* growth

In order to find the impact of CSE on growth of *Sp*, co-stimulation of CSE and *Sp* was performed. For this purpose, *Sp* was cultured in Columbia blood agar and inoculated in THY medium. Subsequently, various concentrations of CSE (5-20 %) were added to the *Sp* in broth medium and OD₆₀₀ measured every 30 min until the plateau phase of bacterial growth (330 min). As displayed in **Figure 29**, lower concentrations of CSE (5-15 %) slightly elevate the curve at later

time points (starting at 210 min post-stimulation), while high concentrations (20 and 25 %) slightly shift the curve to down at earlier time points (starting at 120 min post-stimulation), meaning that at the same time point lower concentrations showed higher OD than the lower concentrations.

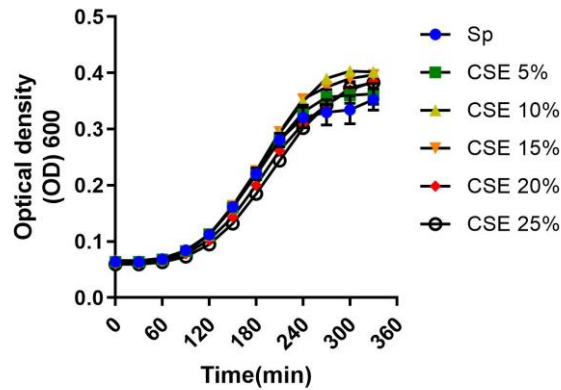


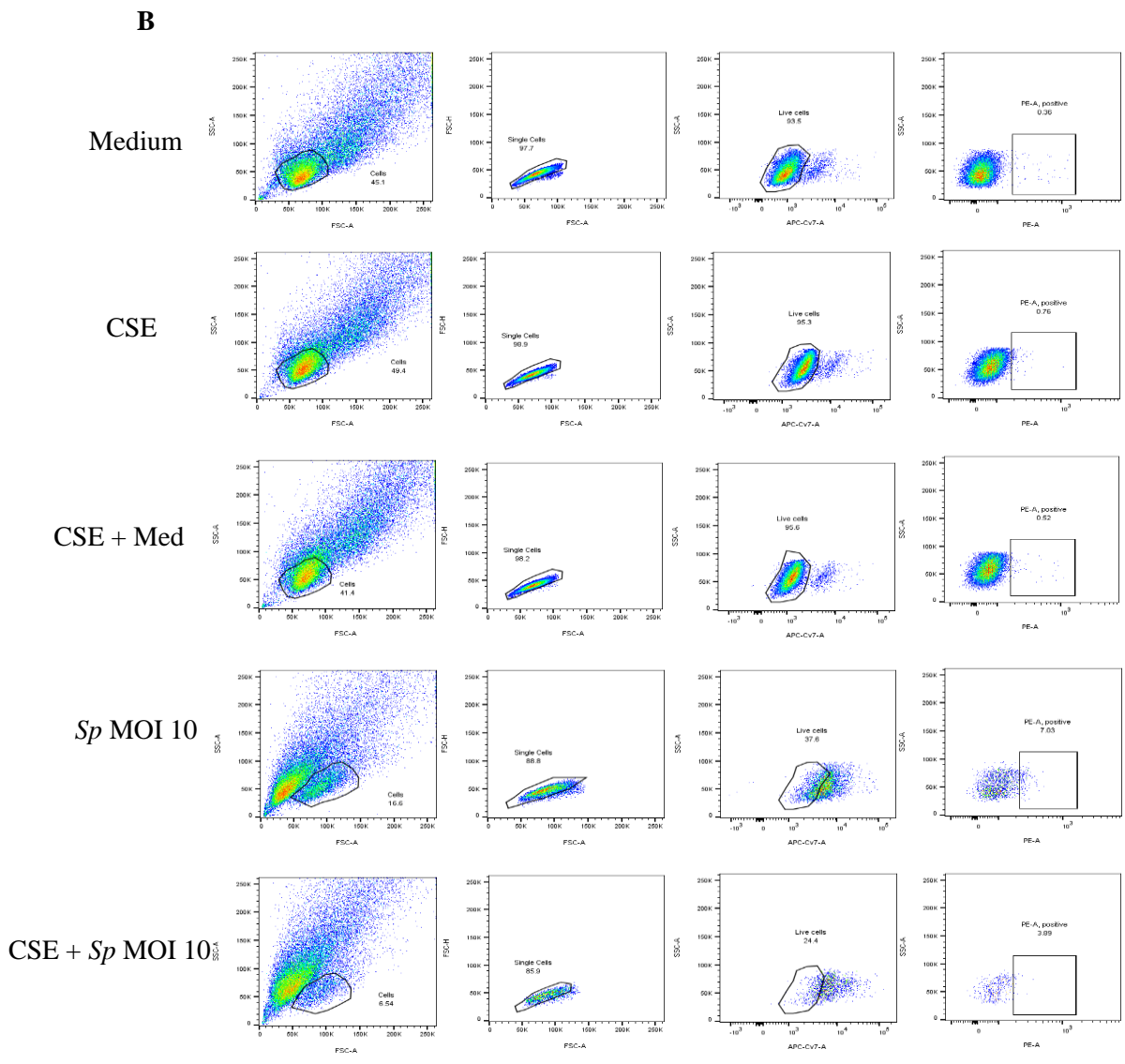
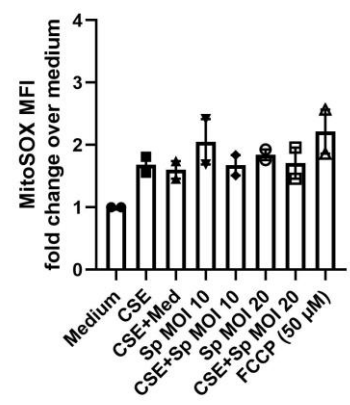
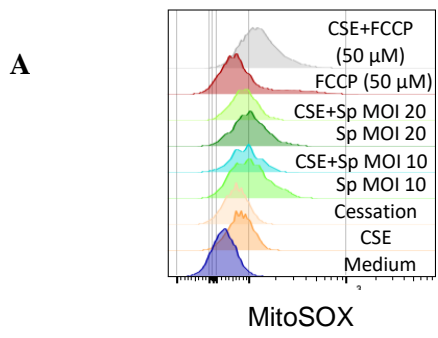
Figure 29: Growth curve of *Sp* upon CSE stimulation. *Sp* growth curve in presence and absence of different concentrations of CSE (5-25 %) as measured by OD₆₀₀ nm for 330 min in 16HBE cells compared to the control medium infected with *Sp*. Data were represented as mean ± SEM.

These results show that lower concentrations of CSE may accelerate *Sp* growth, whereas higher concentrations delayed *Sp* growth.

5.11. Mitochondrial oxidative stress upon CSE and *Sp* co-stimulation

Fluorescent-based MitoSOX assay was performed to investigate the impact of *Sp* infection and pre-exposure to CSE on mitochondrial oxidative stress levels in 16HBE cells. The data show that *Sp* infection induced an eminent shift in the signal as compared to the medium control (**Figure 30 A**). CSE exposure for 28 h induced a weaker shift in MitoSOX signal than *Sp* infection alone and 24 h CSE pre-exposure caused a slight reduction in the shift induced by *Sp* alone (**Figure 30 A**). FCCP 50 μM was used as a positive control for mitochondrial ROS, which induced a shift in the signal curve. Interestingly, combination of 24 h pre-exposure of 16HBE cells to CSE and FCCP 50 μM for 4 h induced the highest shift in the signal which is in contrast with the effects induced by combination of CSE and *Sp*. The gating strategy including the MitoSOX positive population are displayed in pseudocolor plots (**Figure 30 B**).

These findings revealed that *Sp* infection highly induces a mitochondrial oxidative stress, which is distinct from the impact of CSE in 16HBE cells. More importantly, the effect of *Sp* on mtROS production inhibited by pre-exposure to CSE.



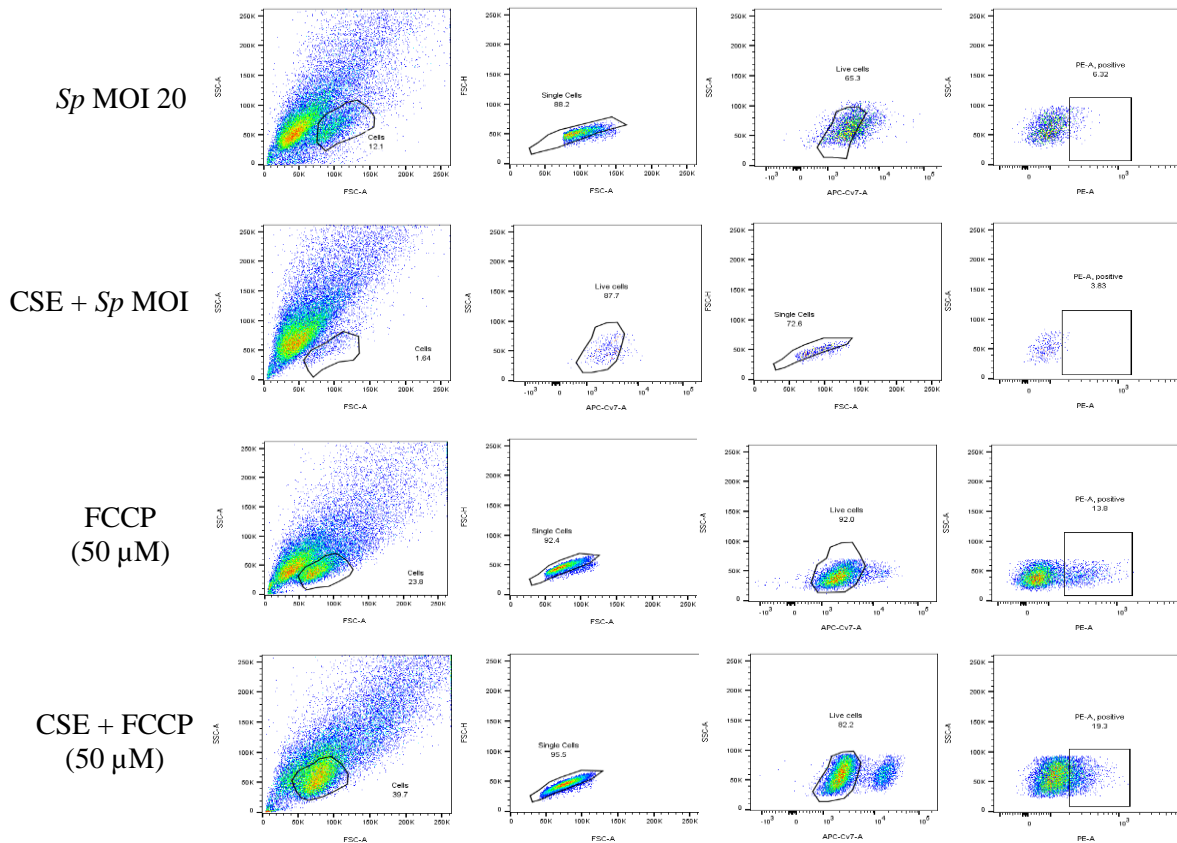


Figure 30: CSE15 % pre-exposure followed by *Sp* infection induced an increase in mitochondrial oxidative stress. MitoSOX was measured using FACS and by MitoSOX staining of 16HBE cells after incubation with either medium for 28 h or CSE15 % for 28 h and infection with MOI 10 and 20 of *Sp* for 4 h as well as pre-exposure with CSE15 % for 24 h followed by *Sp* infection for 4 h and CSE15 % for 24 h followed by medium for 4 h (cessation). FCCP 50 μM for 4 h used a positive control for mtROS production. **A)** Half offset histogram representing a shift in the MitoSOX fluorescent signal as detected by FACS and analyzed by FlowJo (left panel) and MitoSOX MFI fold change compared to the medium (right panel). **B)** A gating strategy for live MitoSOX-positive subsets of 16HBE cells that exposed to various concentrations of CSE as well as FCCP 50 μM are shown in pseudocolored plot.

5.12. Mitochondrial membrane potential upon CSE followed by *Sp* infection

Mitochondrial membrane potential was measured in 16HBE cells to elucidate the impacts of *Sp* infection and pre-exposure with CSE on mitochondrial membrane integrity. *Sp* infection with MOI 20 induced a significant increase in mitochondrial membrane potential after 1 h, however, it significantly dropped 4 h post-infection as compared to the medium control. The changes induced by MOI 10 of *Sp* was similarly affected mitochondrial membrane potential although it did not reach the statistically significant values. Pre-exposure with CSE followed by *Sp* infection induced a decline in mitochondrial membrane potential similar to the effects induced by CSE alone as well as FCCP 50 μM (**Figure 31**).

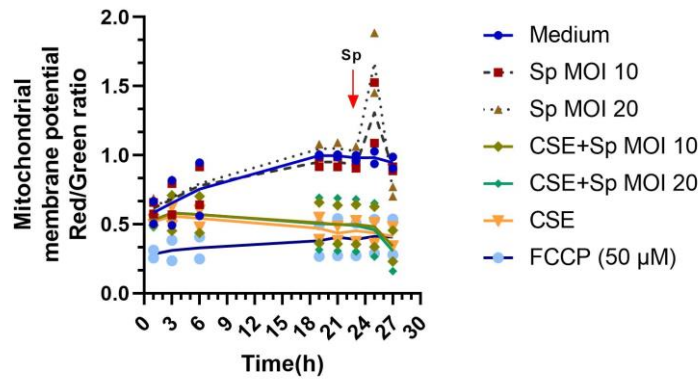


Figure 31: CSE15 % followed by *Sp* infection alters mitochondrial membrane potential. JC-1 fluorescent-based method was performed to measure changes in mitochondrial membrane potential induced by *Sp* in 16HBE cells. The cells were infected with *Sp* MOI 10 and MOI 20 for 4 h and CSE15 % for 24 h followed by *Sp* MOI 10 and 20 for 4 h. The preliminary data is representative of mean of red/green ratio of two independent experiments (Aghapour et al., 2022).

These findings point out that the effect of CSE on mitochondrial membrane potential is dominant to the effects that is induced by *Sp* infection alone.

5.13. Mitochondrial complex protein expression upon CSE followed by *Sp* infection

Immunoblotting was performed to find the impacts of *Sp* infection on the mitochondrial components involved in OXPHOS and glycolysis and how pre-exposure to CSE affect the abundance of these components (**Figure 32 A**). *Sp* infection slightly increased the levels of a subunit of mitochondrial complex V (ATP5A) in 16HBE cells compared to the medium control (**Figure 32 B**), and this increase was significantly different when compared to the CSE cessation group and CSE followed by *Sp*. CSE exposure significantly decreased the abundance of a subunit of mitochondrial complex III (UQCRC2) in 16HBE cells as compared to the medium control and this CSE-induced decrease in UQCRC2 did not alter after removing CSE from the medium for 4 h (**Figure 32 C**). *Sp* infection did not alter the protein levels of UQCRC2 in 16HBE cells (**Figure 32 C**). CSE exposure alone and CSE pre-exposure followed by *Sp* infections significantly reduced abundance of a subunit of complex II protein (SDHB) compared to the medium control (**Figure 32 D**). Moreover, CSE alone decreased the levels of mitochondrial complex IV (COXIV), however, neither *Sp* infections nor CSE followed by *Sp* infections did not alter the levels of COXIV in 16HBE cells (**Figure 32 E**). CSE alone and CSE followed by *Sp* reduced the glycolysis protein levels HKII as compared to the medium control (**Figure 32 F**). Importantly, the effects of CSE on HKII levels was reversible by 4 h removing of CSE from the medium (cessation). Furthermore, although CSE did not change the abundance of VDAC1, *Sp* infection alone and CSE followed by *Sp* increased VDAC1 protein as compared to the control (**Figure 32**

G). CSE exposure reduced the level of TOMM20, while *Sp* infection alone and together with CSE pre-exposure slightly increased TOMM20 as compared to the medium control (**Figure 32**

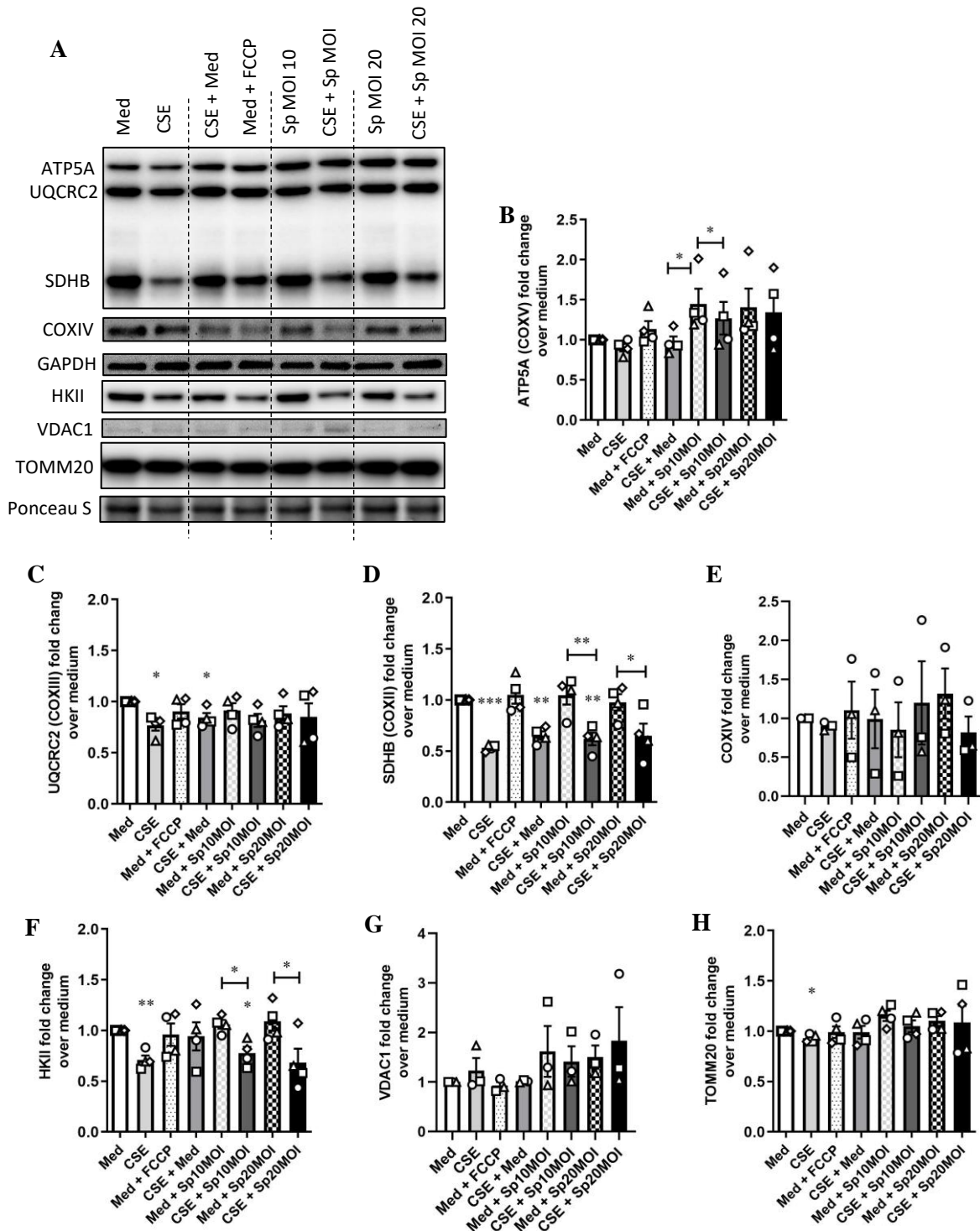


Figure 32: Mitochondrial OXPHOS and OMM protein expression upon stimulation with CSE15 % and *Sp*. A) Immunoblots representing the protein expression of subunits of mitochondrial OXPHOS including ATP5A (complex V), UQCRC2 (complex III), SDHB (complex II) and total COXIV (complex IV) and glycolysis including HKII, VDAC1 and GAPDH in the total cell lysate upon stimulation of 16HBE cells with medium for 28 h and CSE15 % for 28 h or infection with *Sp* MOI 10 and 20 for 4 h as well as CSE15 % 24 h followed by *Sp* MOI 10 and

20 for 4 h. The cells were also stimulated with CSE15 % for 24 h and then deprived of CSE1 % for 4 h (cessation). FCCP 50 μ M was used as a positive control that induces mitochondrial dysfunction. The intensity of the detected bands quantified with ImageJ, and the fold change calculated for following bands over medium control; **B**) ATP5A (COXV), **C**) UQCRC2 (COXIII), **D**) SDHB (COXII), **E**) COXIV, **F**) HKIIL, **G**) VDAC1, **H**) TOMM20. The data are represented as mean \pm SEM of four independent experiments (N=4). Statistically significant differences were calculated with paired two-tailed t-test (* p <0.05, ** p <0.001, *** p <0.0001) (Aghapour et al., 2022).

H). Interestingly, FCCP 50 μ M for 4 h only induced a slight decrease in the abundance of UQCRC2 protein.

Together these data indicate that while CSE alone and CSE pre-exposure decreases the protein levels of subunits of OXPHOS complexes in the beginning of ETC as well as mitochondrial outer membrane, *Sp* infection only increases the protein abundance of the end ETC regulating ATP production.

5.14. Mitochondrial biogenesis levels upon CSE followed by *Sp* infection

Immunoblotting was performed to assess the levels of constituents involved in mitochondrial biogenesis upon *Sp* infection alone and *Sp* infection in CSE pre-stimulated 16HBE cells (**Figure 33 A**). The abundance of NRF1 significantly decreased upon *Sp* infections as well as upon CSE exposure together with *Sp* infection in comparison with medium control (**Figure 33 B**). Moreover, CSE exposure reduced the abundance of ERR α and this reduction was further aggravated by combination of CSE pre-exposure followed by *Sp* infection, which significantly reduced the abundance of ERR α compared to *Sp* infections alone (**Figure 33 C**). Together, these data show that *Sp* infection significantly suppress mitochondrial biogenesis in 16HBE cells, and this suppression exacerbated with CSE pre-exposure.

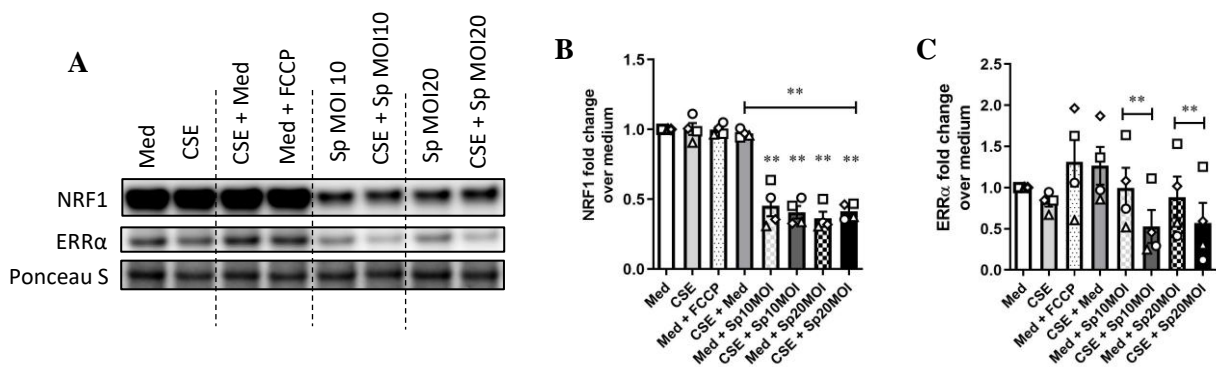


Figure 33: CSE15 % followed by *Sp* infection altered mitochondrial biogenesis in 16HBE cells. 16HBE cells were incubated with medium 28 h, CSE15 % 28 h, CSE15 % 24 h followed by medium 4 h (cessation), *Sp* MOI 10 for 4 h, CSE15 % for 24 h followed by *Sp* MOI 10 for 4 h, *Sp* MOI 20 for 4 h, CSE15 % for 24 h followed by *Sp* MOI 20 for 4 h, FCCP 50 μ M for 4 h and CSE15 % for 24 h followed by FCCP 50 μ M for 4 h. **A**) Immunoblot representing protein expression of oxidative the constituents of mitochondrial biogenesis in the total cell lysates

upon stimulation with medium for 28 h, CSE15 % for 28 h, FCCP 50 μ M for 4 h, cessation, *Sp* MOI 10 for 4 h, CSE15 % for 24 h followed by *Sp* MOI 10 for 4 h, *Sp* MOI 20 for 4 h, CSE15 % for 24 h followed by *Sp* MOI 20 for 4 h. The intensity of the detected bands quantified, and the fold change calculated over medium for **B**) NRF1 as well as **C**) ERR α . The data are represented as mean \pm SEM of four independent experiments (N=4). The significant values calculated with paired two-tailed t-test (**p<0.001) (Aghapour et al., 2022).

5.15. Mitophagy levels upon CSE followed by *Sp* infection

In order to investigate the impact of *Sp* infection and prior CSE exposure on the protein expression of mitophagy factors immunoblotting was performed (**Figure 34 A**). The results show that the abundance of receptor-mediated mitophagy BNIP3 significantly reduced upon CSE stimulation, while CSE pre-exposure followed by *Sp* infection with MOI 10 and MOI 20 significantly increased abundance of BNIP3 protein in comparison with medium control (**Figure 34 B**). CSE removal from medium for 4 h counteracted the suppressive effects of CSE on BNIP3 protein levels (**Figure 34 B**). Moreover, CSE exposure and *Sp* infection slightly increased protein levels of BNIP3L compared to the medium control but not significantly (**Figure 34 C**). Moreover, while CSE reduced the abundance of FUNDC1, *Sp* infection slightly increased FUNDC1 as compared to the medium control (**Figure 34 D**). While CSE and *Sp* infection did not alter the abundance of PINK-I, pre-exposure to CSE followed by *Sp* infection elicited an increase in PINK-I protein levels compared to the medium control (**Figure 34 E**). Moreover, the levels of mitophagy adaptor proteins probed in the total cell lysates by immunoblotting (**Figure 34 F**). The abundance of LC3BI increased upon CSE and CSE followed by *Sp* infection, whereas *Sp* infection did not change the levels of this protein as compared to the medium control (**Figure 34 G**). Furthermore, CSE alone and CSE pre-stimulation followed by *Sp* infections increased the levels of GABARAPL1 compared to the medium control, while *Sp* infection alone did not affect GABARAPL1 protein levels (**Figure 34 H**). CSE exposure alone and together with *Sp* infections also induced an increase in the SQSTM1 protein which was not changed by *Sp* infection as compared to the medium (**Figure 34 I**).

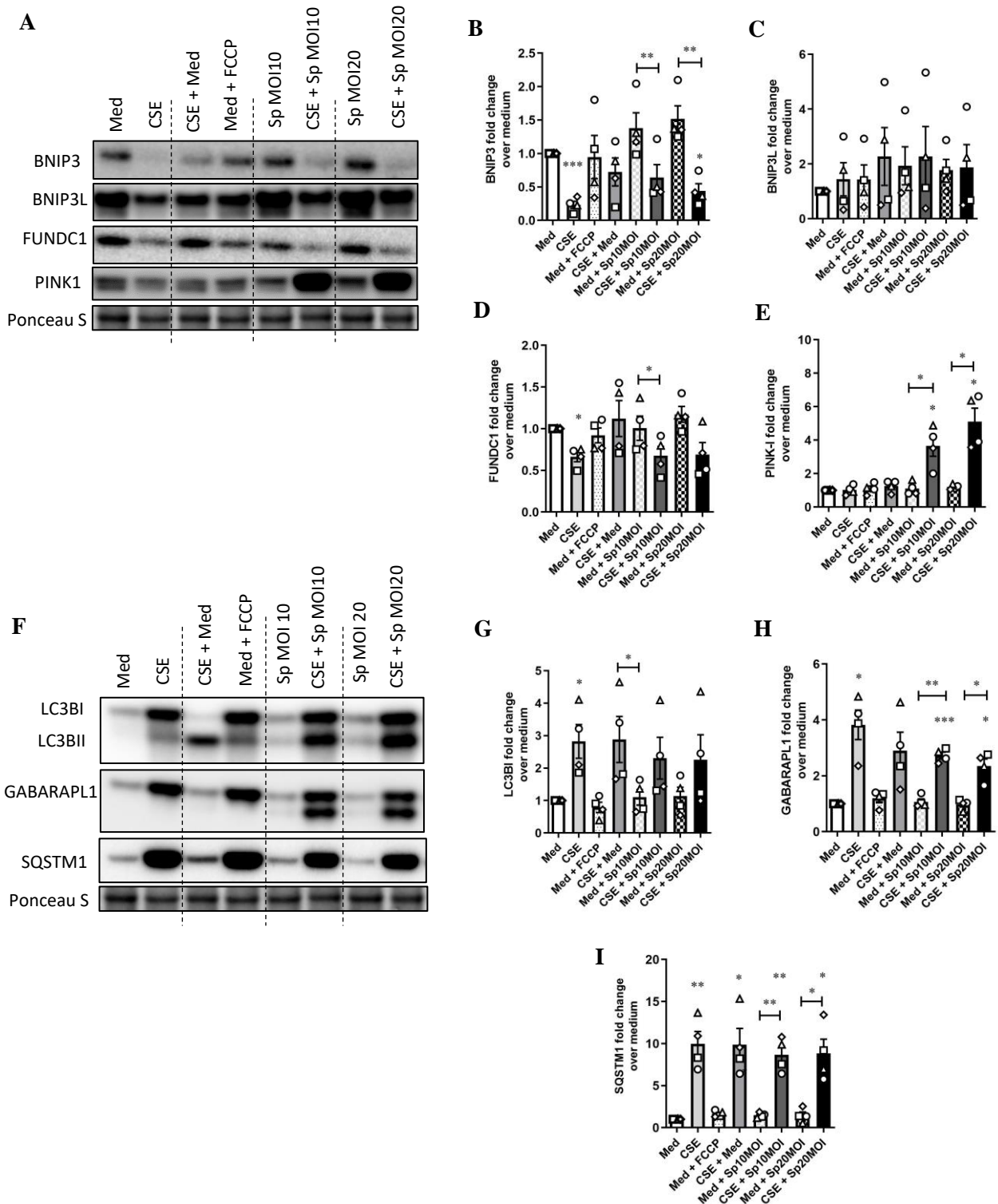


Figure 34: Mitophagy protein expression upon stimulation with CSE15 % and *Sp*. **A**) Immunoblots representing the protein expression of constituents involved in receptor- (BNIP3, BNIP3L and FUNDC1) and ubiquitin-mediated (PINK1) mitophagy in the total cell lysate upon incubation with either medium for 28 h, CSE15 % for 28 h or *Sp* MOI 10 and 20 for 4 h as well as CSE15 % for 24 h followed by infection with *Sp* MOI 10 and 20 for 4 h, FCCP 50 μ M for 4 h, CSE15 % for 24 h followed by 4 h CSE15 % removal from medium. The intensity of the detected bands quantified using ImageJ, and the fold change calculated over medium for **B**) BNIP3, **C**) BNIP3L, **D**) FUNDC1 and **E**) PINK-I. **F**) Moreover, immunoblotting was performed to probe autophagy adaptor proteins including LC3B, GABARAPL1 and SQSTM1 in the total cell lysates from stimulated 16HBE cells. **G**) Fold change of LC3BI, **H**) GABARAPL1 and **I**) SQSTM1 calculated over medium control. The data are represented

as mean \pm SEM of four independent experiments (N=4). The significant differences were calculated with multiple t-test and with Holm-Sidak post-hoc correction test (* p <0.05, ** p <0.001, *** p <0.0001) (Aghapour et al., 2022).

Together, these data indicate that CSE decreased receptor-mediated mitophagy, while promoted the levels of general autophagy adaptor proteins. *Sp* infection enhanced receptor-mediated mitophagy. CSE pre-exposure with *Sp* infections decreased receptor-mediated mitophagy while increased autophagy adaptor protein and disturbed ubiquitin-mediated mitophagy. CSE removal was able to counteract the decrease in receptor-mediated mitophagy.

5.16. Mitochondrial fission and fusion upon CSE followed by *Sp* infection

To investigate the effects of *Sp* infection and prior CSE exposure on mitochondrial dynamic processes, immunoblotting of fission and fusion factors was carried out (**Figure 35 A**). Although the abundance of a constituent involved in fission DRP1 did not alter upon CSE, *Sp* infection alone and with CSE pre-exposure increased the abundance of this protein (**Figure 35 B**). Moreover, the levels of MFN2 slightly increased in 16HBE cells stimulated with CSE 28 h and returned to the basal levels by removal of CSE from the medium. However, *Sp* infection decreased the levels of MFN compared to the medium control (**Figure 35 C**).

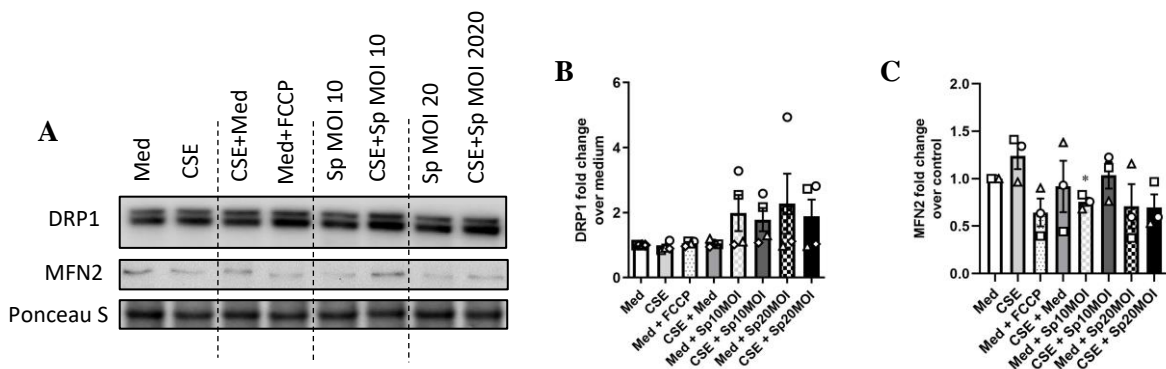


Figure 35: Mitochondrial fission and fusion upon stimulation with *Sp* and CSE15 %. Immunoblots representing the protein expression of DRP1 and MFN2 in the total cell lysate upon incubation with either medium for 28 h, CSE15 % for 28 h or *Sp* MOI 10 and 20 for 4 h as well as CSE15 % for 24 h followed by infection with *Sp* MOI 10 and 20 for 4 h, CSE15 % for 24 h followed by 4 h removal of CSE15 % from medium and FCCP 50 μ M for 4 h. The data are represented as mean \pm SEM of four and three independent experiments, respectively (N=4, N=3). Statistically significant differences were calculated with paired two-tailed t-test (* p <0.05) (Aghapour et al., 2022).

These data demonstrate that *Sp* infection minimally affected fission and fusion processes in 16HBE cells.

5.17. Gene expression analysis upon CSE followed by *Sp* infection

Gene expression microarray was performed to delineate the effects of CSE and *Sp* on gene expression profile with the special emphasis on the contribution of changes in expression of genes regulating innate immune responses to the genes regulating mitochondrial function in 16HBE cells. Different microarray analysis and representation methods was used including GSEA, K-clustering and volcano plots to depict the changes in gene expression that have been described in the following paragraph.

For this purpose, 16HBE cells were stimulated with medium and CSE for 28 h or *Sp* infection alone with MOI 10 and MOI 20, CSE pre-exposure followed by *Sp* infections, FCCP alone and CSE followed by FCCP. These conditions were repeated in two independent experiments with different passage of the cells. Together, transcriptomes of 18 were examined by human Clariom S gene expression microarray. Differentially expressed genes were analyzed by comparing all conditions to the untreated medium, and a fold change cut-off of ± 3 with FDR 0.5 was applied. As depicted in volcano plots in **Figure 36**, 3323 genes were differentially regulated in total. Of these genes, 380 genes were downregulated upon CSE of which *ERP27*, *IFIT1*, *KLK7* were among top 3 downregulated genes based on fold change, and 150 genes were among upregulated including *HSPA6*, *IL-24* and *HMOX1*. Similarly, short removal of CSE from medium resulted in similar pattern in gene expression with 325 genes downregulated and 175 gene upregulated. *Sp* infection with MOI 10 mainly induced upregulation of genes including *TXNIP*, *ARRD4*, *HSPA6* and only 2 genes downregulated. CSE followed by *Sp* MOI 10 induced 624 differential regulated genes with 429 downregulated genes of which top 3 were *GTSE1*, *ERP27* and *IFIT1*, while 195 upregulated including *HSPA6*, *IL-24*, *HMOX1*. *Sp* infection with 20 MOI induced 41 differentially regulated genes including mainly 40 upregulated genes *TXNIP*, *ARRD4*, *HSPA6*. CSE pre-exposure followed by *Sp* 20 MOI induced 700 differentially regulated genes including 514 downregulated genes with top 3 *GTSE1*, *ERP27* and *IFIT1*, and 187 upregulated genes including *HSPA6*, *IL-24*, *HMOX1*. Moreover, 69 genes were upregulated upon FCCP stimulation with 3 top regulated genes *HSPA6*, *ATF3* and *CHAC1*, while only 11 genes downregulated *HIST1H1B*, *IFIT3* and *DNAJC28*. Finally, CSE pre-exposure followed by FCCP induced a highest number of differentially regulated genes with 620 downregulated genes including *ERP27*, *KIF20A* and *IFIT1*, and 168 upregulated genes including *HSPA6*, *IL-24* and *UPP1*.

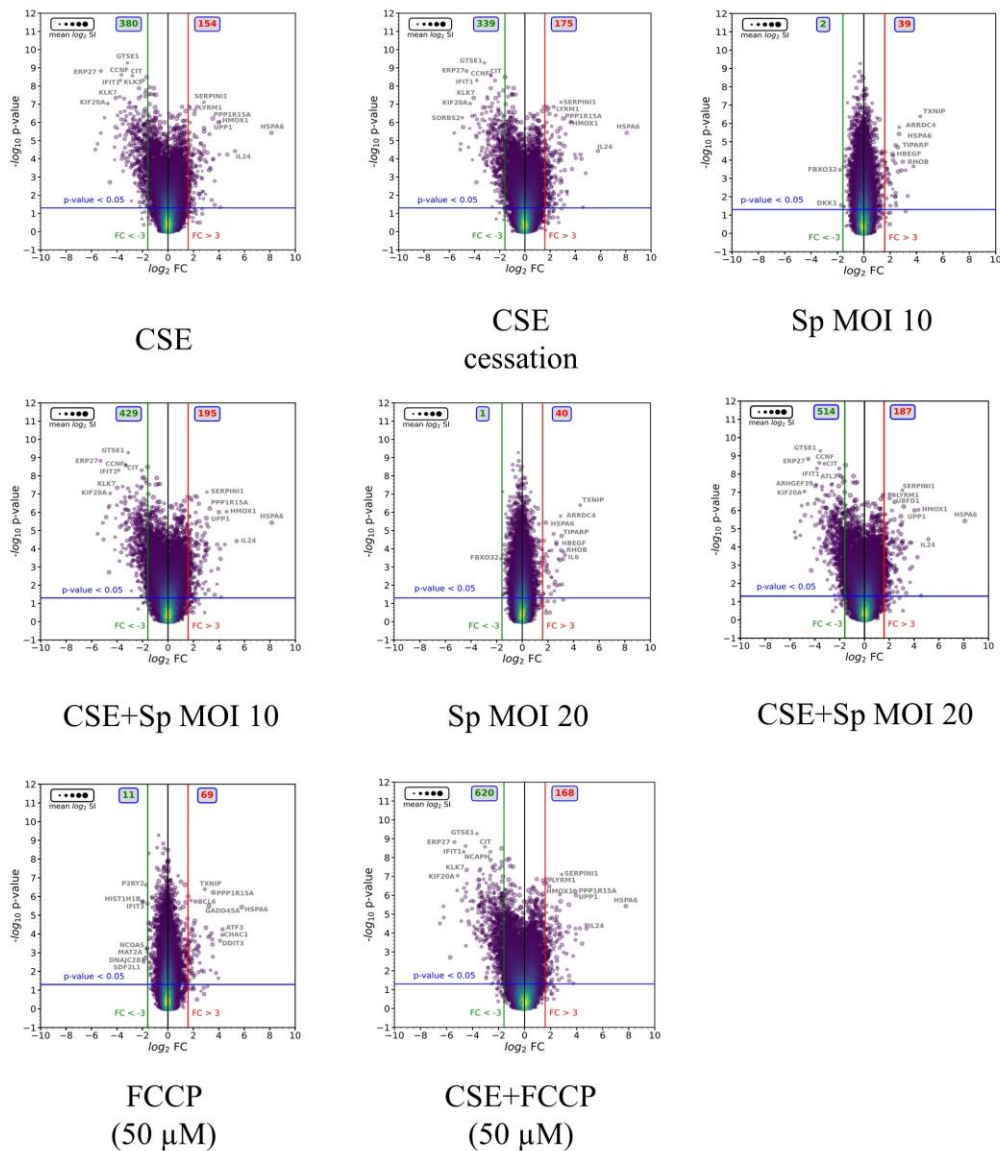


Figure 36: Gene expression plots upon CSE15 % stimulation and *Sp* infection. Volcano plots of validly detected transcripts from indicated microarray comparisons, plotting $-\log_{10}$ FDR vs \log_2 fold change. Point sizes show mean \log_2 SIs of transcripts calculated across all microarrays. Point color code reflects point density. FC (red/green vertical lines) and FDR (blue horizontal lines) criteria for differential gene expression are indicated. Gray boxes show numbers of significantly upregulated (red) and downregulated (green) transcripts. Gene symbols of selected transcripts are shown next to the points.

The findings on volcano plots show that while *Sp* infection alone minimally affect gene expression in 16HBE cells, pre-exposure with CSE followed by *Sp* infection increased the number of differentially regulated genes in particular downregulated genes, suggesting the suppressor effects of CSE on gene expression.

5.17.1. Results of GSEA

GSEA sorts the genes based on their rank in the corresponding functional category in comparison with the medium control regardless of regulation levels. GSEA was used to analyze expression pattern of genes belonging to ROS production, mitochondrial OXPHOS/glycolysis, cell junction integrity as well as pathway regulating cellular autophagy and innate immune responses to *Sp*. The results show that both CSE and CSE pre-exposure with *Sp* infection increased the enrichment of ROS hallmark in 16HBE cells compared to the untreated medium (**Figure 37 A**). Furthermore, data from GSEA analysis showed a decrease in enrichment of genes involved in apical junction hallmarks in CSE stimulated 16HBE cells compared to the untreated medium. *Sp* infection alone and with CSE pre-exposure also induced a similar decrease in enrichment of apical junction gene hallmark. *Sp* infection with MOI 10 as well as FCCP 50 μ M induced an increase in enrichment of EMT hallmark genes in 16HBE cells (**Figure 37 B**). These data indicate that although *Sp* does not affect ROS gene set enrichment, it reduced enrichment of barrier function gene set hallmark, which is similar to the effects induced by CSE alone.

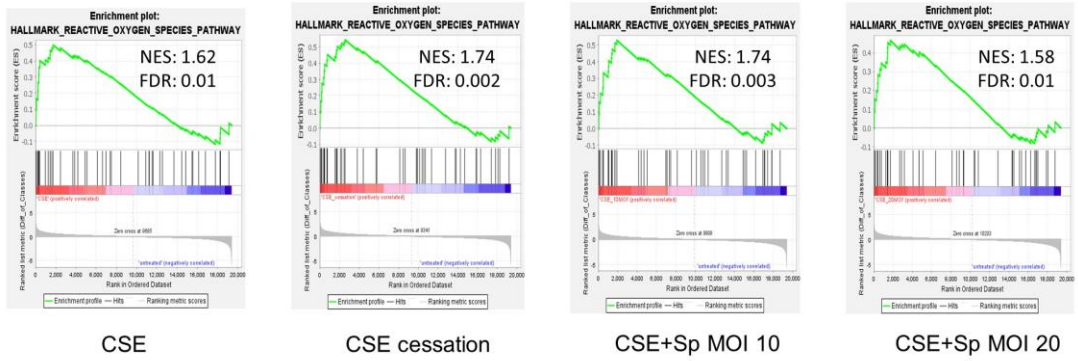
Moreover, CSE stimulation for 28 h decreased enrichment of the genes involved in glycolysis compared to the untreated medium. In contrast, *Sp* infection with MOI 10 increased enrichment of the genes involved in both OXPHOS and glycolysis. CSE pre-exposure followed by infection with MOI 10 of *Sp* increased enrichment of OXPHOS genes while decreased enrichment of genes involved in glycolysis. Stimulation with the mitochondrial uncoupler FCCP 50 μ M for 4 h increased enrichment of the genes involved in glycolysis as compared to the untreated medium (**Figure 38 A**). Data from GSEA analysis with Reactome gene set showed that CSE pre-exposure followed by *Sp* infection MOI 10 increased enrichment of the genes belonging to mitochondrial genes and mitochondrial ribosomal translation machinery compared to the untreated medium. Furthermore, *Sp* infection with MOI alone induced an increase in enrichment of mitochondrial translation and mitochondrial import hallmark genes upon infection with *Sp* MOI 10 compared to the medium control. (**Figure 38 B**). Collectively, these data show that CSE and *Sp* dysregulate hallmark genes of mitochondrial function, although this effect was different in terms of the effect on mitochondrial respiration. Furthermore, CSE followed by *Sp* have stronger effects than CSE alone on mitochondrial gene expression.

CSE increased the enrichment of macroautophagy hallmark genes compared to the untreated medium (**Figure 39 A**). Furthermore, CSE alone and CSE pre-exposure followed by *Sp* infection increased enrichment of genes involved in mTORC1 signalling pathway that regulates autophagy compared to the untreated medium. The enrichment of genes involved in mTORC1 signalling

increased upon *Sp* infection alone compared to the untreated medium. Interestingly, removal of CSE from medium decreased the enrichment of mTORC1 compared to the medium control. (**Figure 39 B**). Furthermore, stimulation with FCCP 50 μ M in CSE pre-exposed cells increased the enrichment of mTORC1 genes compared to the untreated medium. This suggest that CSE may increase autophagy gene expression which could be independent of mTOR pathway as the autophagy inhibitory pathway.

In addition, data from GSEA analysis showed that CSE alone significantly decreases enrichment of the genes involved in MHCII pathway compared to the untreated medium. Comparison of normalized SI shows that genes belonging to MHCII upregulated in CSE-exposed conditions, while these genes were downregulated in only *Sp* infected conditions (**Figure 40 A**). Moreover, CSE alone and CSE pre-exposure followed by *Sp* infection decreased the enrichment of innate immune response genes including interferon α and interferon γ hallmark genes as compared to the untreated medium. In contrast, *Sp* infection increased the enrichment of both interferon hallmark genes compared to the match untreated medium (**Figure 40 B**). Several of these enriched genes were shown to be downregulated upon CSE while upregulated in *Sp* infected conditions. In line, CSE exposure decreased enrichment of complement hallmark genes in 16HBE cells, while *Sp* increased the enrichment of same hallmark genes compared to the untreated medium (**Figure 40 C**). Together, these findings show that CSE downregulates innate immune response genes and in specific interferon responses to *Sp* infection.

A



B

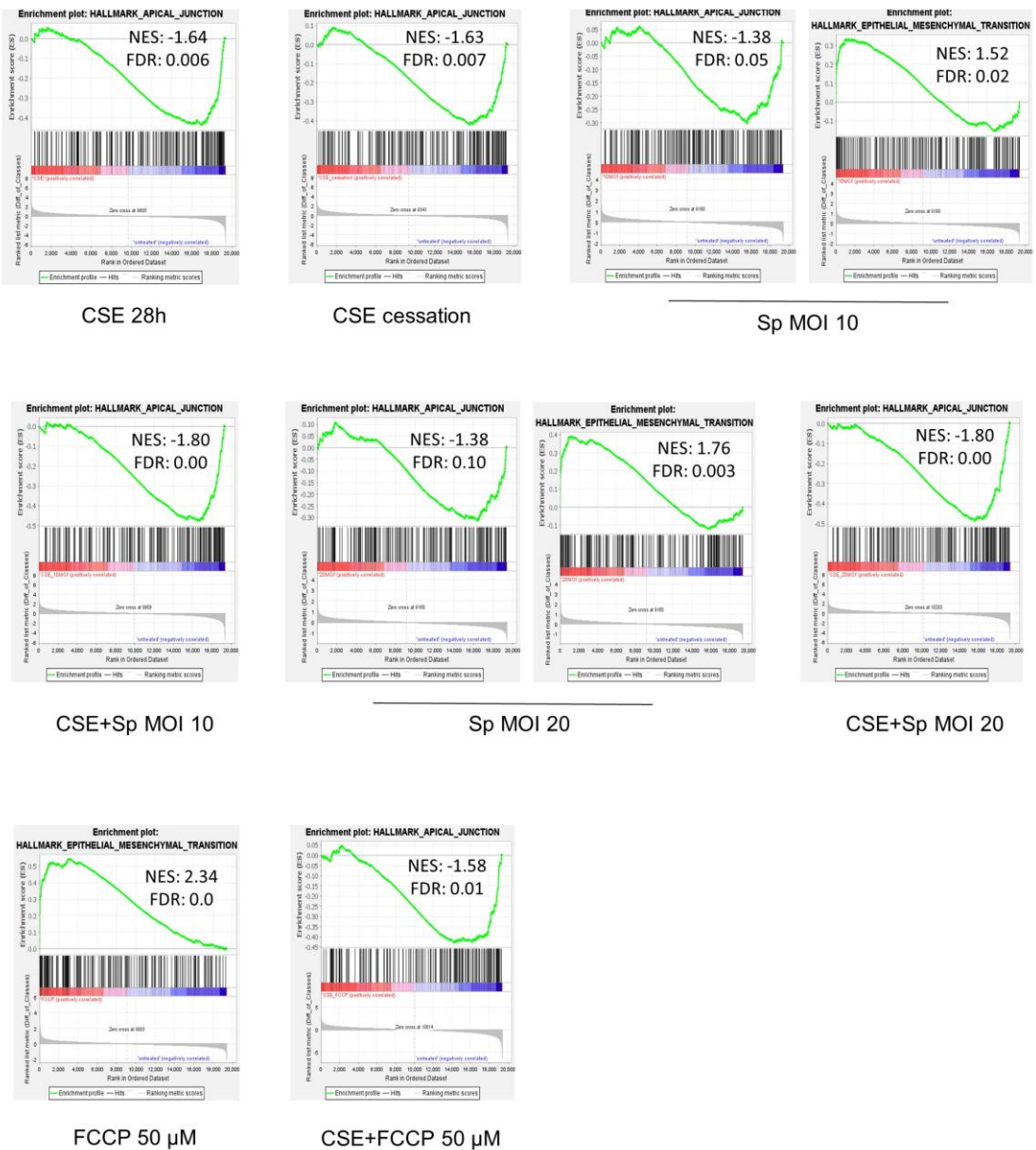
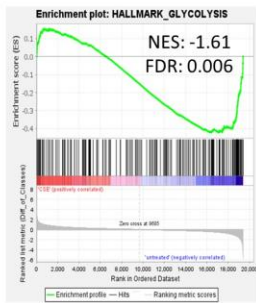
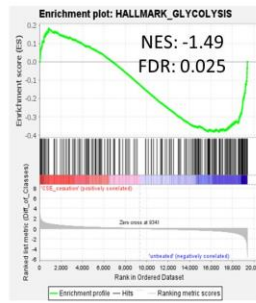


Figure 37: CSE15 % increases ROS hallmark genes and decreases apical junction gene hallmarks in 16HBE cells. The cells were stimulated with either Med or CSE15 % for 28 h, *Sp* MOI 10 for 4 h, *Sp* MOI 20 for 4 h, CSE15 % for 24 h followed by *Sp* MOI 10 for 4 h and CSE15 % for 24 h followed by *Sp* MOI 20 for 4 h. Microarray data for each condition was analyzed by GSEA with untreated Med control as reference (ranked by fold change, FDR < 0.1). GSEA graphs of **A)** ROS hallmark genes as well as **B)** apical junction hallmark genes in the indicated conditions as compared to the untreated Med.

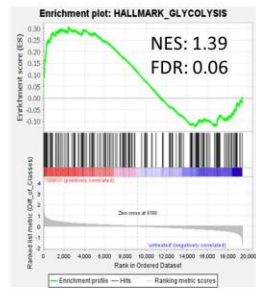
A



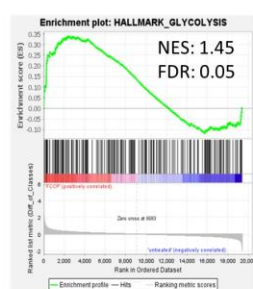
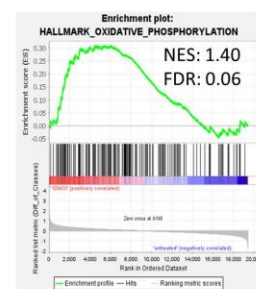
CSE 28h



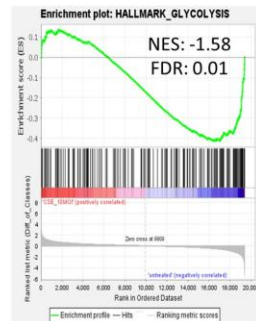
CSE cessation



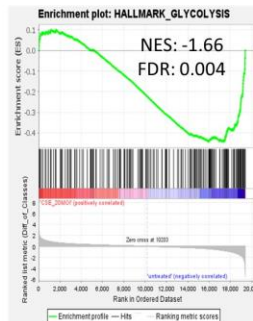
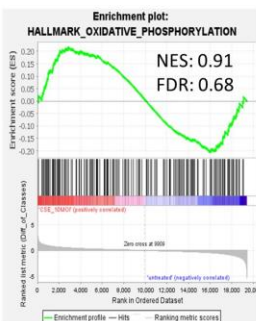
Sp MOI 10



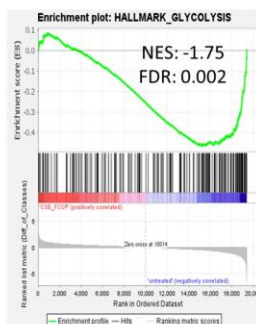
FCCP 50 μ M



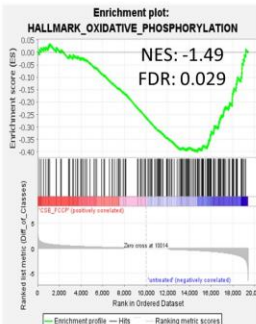
CSE+Sp MOI 10



CSE+Sp MOI 20



CSE+FCCP 50 μ M



B

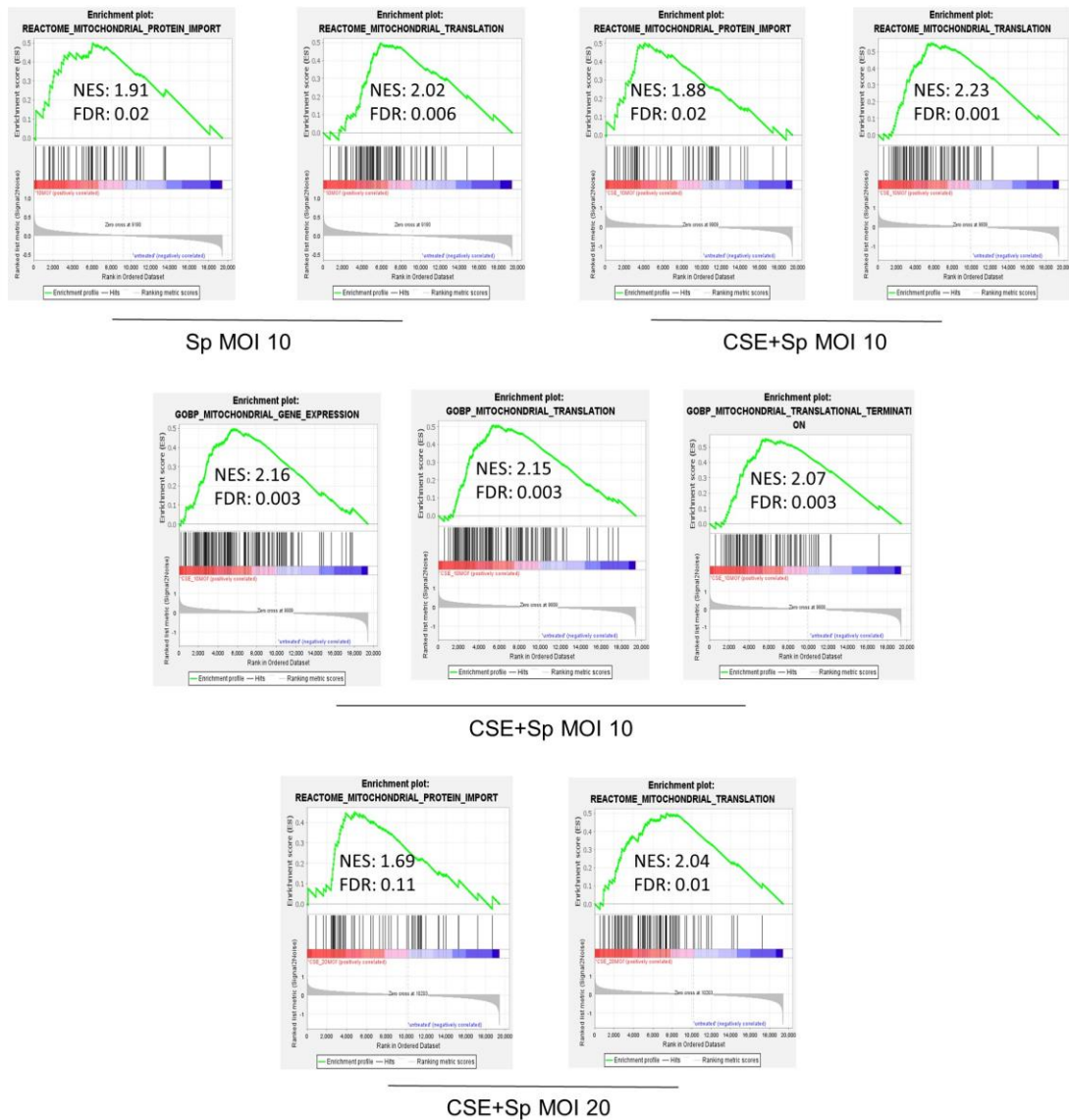
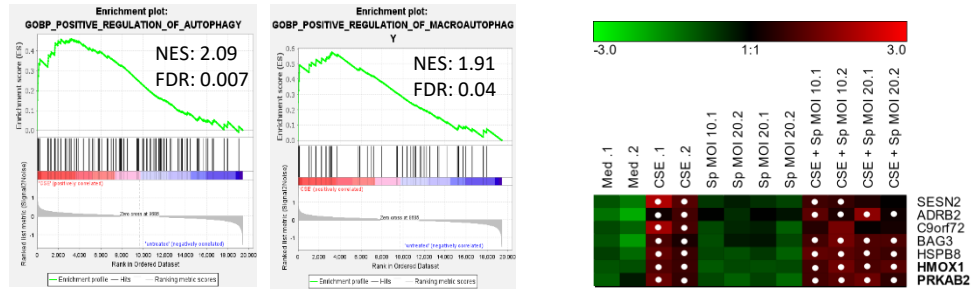


Figure 38: CSE15 % and *Sp* affect enrichment of mitochondrial hallmark genes in 16HBE cells. The cells were incubated with either Med or CSE15 % for 28 h, *Sp* MOI 10 for 4 h, *Sp* MOI 20 for 4 h, CSE15 % for 24 h followed by *Sp* MOI 10 for 4 h and CSE15 % for 24 h followed by *Sp* MOI 20 for 4 h. Microarray data for each condition was analyzed by GSEA with untreated Med control as reference (ranked by fold change, FDR < 0.1). GSEA graphs of **A**) mitochondrial OXPHOS and glycolysis hallmark genes as well as **B**) mitochondrial translation and mitochondrial import in the indicated conditions versus the untreated Med.

A



B

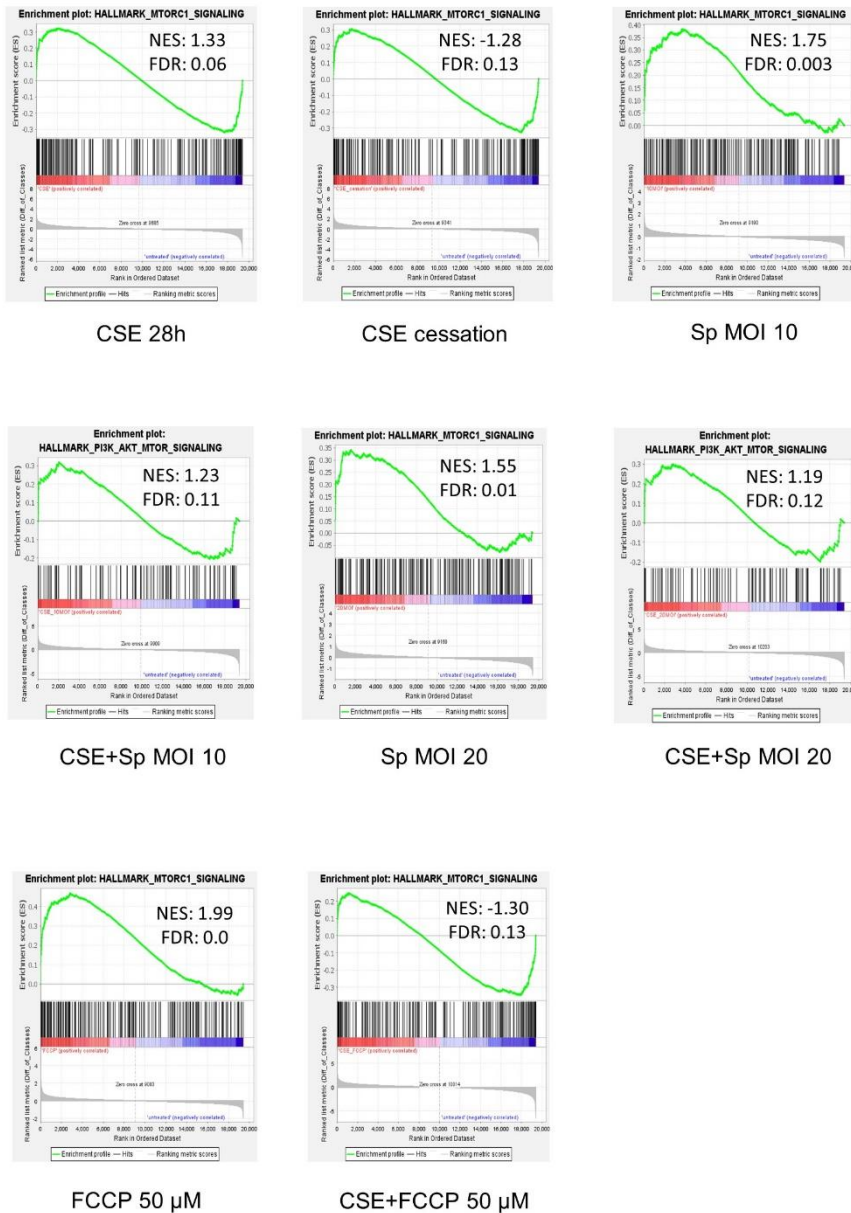


Figure 39: CSE15 % promotes enrichment of autophagy hallmark genes in 16HBE cells. Microarray data for each condition was analyzed by GSEA with untreated Med control as reference (ranked by fold change, FDR < 0.1). Normalized log₂ signal intensities of core-enriched genes were z-score transformed, color-coded and plotted as heatmap (row labels: gene symbols). Details on bold gene symbols are mentioned in the text. Significance of

differential expression with fold change cutoff $|FC| > 3$ in reference Med control was calculated by ANOVA ($p < 0.05$). White points in heatmap plots indicate $|FC| > 3$ with $p < 0.05$. Green/black/red color bars represent z-scores. Only selected significantly over-represented gene sets for **A**) autophagy, with their according heat map of core-enriched genes are shown. The cells were stimulated with either Med or CSE15 % for 28 h, *Sp* MOI 10 for 4 h, *Sp* MOI 20 for 4 h, CSE15 % for 24 h followed by *Sp* MOI 10 for 4 h and CSE15 % for 24 h followed by *Sp* MOI 20 for 4 h.

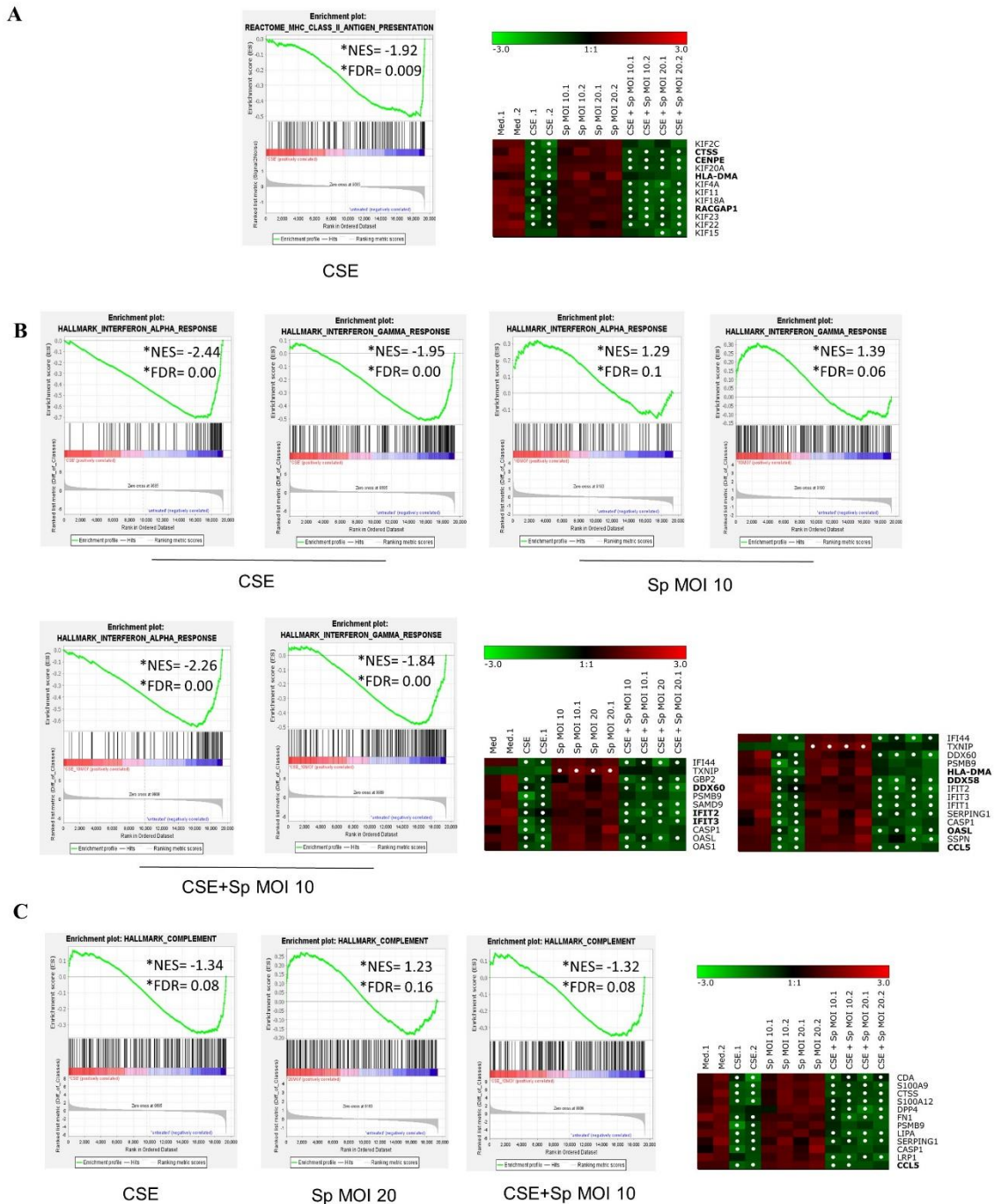


Figure 40: CSE15 % impairs innate immune responses to *Sp* in 16HBE cells. The cells were incubated with either Med or CSE15 % for 28 h, *Sp* MOI 10 for 4 h, *Sp* MOI 20 for 4 h, CSE15 % for 24 h followed by *Sp* MOI 10 for 4 h and CSE15 % for 24 h followed by *Sp* MOI 20 for 4 h. Microarray data for each condition was analyzed by GSEA with untreated Med control as reference (ranked by fold change, $FDR < 0.1$). Normalized \log_2 signal intensities of core-enriched genes were z-score transformed, color-coded and plotted as heatmap (row labels: gene symbols). Details on bold gene symbols are mentioned in the text. Significance of differential expression with fold change cutoff $|FC| > 3$ in reference Med control was calculated by ANOVA ($p < 0.05$). White points in heatmap plots

indicate $|FC| > 3$ with $p < 0.05$. Green/black/red color bars represent z-scores. Only selected significantly over-represented gene sets for **A**) MHC class II, **B**) IFN- γ and IFN- α and **C**) complement with their according heat map of core-enriched genes are shown.

5.17.2. K-mean clustering

In order to delineate the differences in gene expression profile upon CSE, *Sp* and CSE followed by *Sp* vs untreated medium 16HBE cells in broader overview, \log_2 signal intensities of the identified transcripts were z-score transformed and subjected to k-means cluster algorithm (k=9). Cluster numbering was carried out based on average mean expression profiles of each cluster and ascendingly sorted according to the stimulated conditions. Next, gene clusters were assessed by GO enrichment analysis to find statistically overrepresented biological processes in the GO category (FDR < 0.05). The following section will elaborate on the description of clustering and GO-enrichment results for stimulated conditions.

As displayed in **Figure 41 A**, K-clustering resulted in 47 (cluster 1), 12 (cluster 2), 199 (cluster 3), 77 (cluster 4), 559 (cluster 5), 150 (cluster 6), 77 (cluster 7), 21 (cluster 8), 16 (cluster 9) groups of genes, respectively. Cluster 1 represents mostly low z-scores in majority of conditions, except for CSE followed by FCCP condition where a robust gene expression with high z-scores was observed (**Figure 41 B**). Interestingly, transcripts belonging to defensin family of antimicrobial peptides increased strongly upon CSE followed by FCCP. Functional enrichment of genes in cluster 1 attributes to biological processes such as cell positive regulation of cell motility (60 transcripts), telomer organization (28 transcripts), regulation of organelle organization (69 transcripts), cholesterol metabolic process (23 transcripts) and regulation of chromosome organization (20 transcripts) (**Figure 41 C**).

Cluster 2 (12 transcripts) indicates the smallest cluster (**Figure 41 A**). In this cluster, majority of genes have low z-score upon FCCP and CSE followed by FCCP stimulation and partly in untreated medium, while these genes showed medium to high z-score in CSE alone, *Sp* infection alone as well as CSE followed by *Sp* (**Figure 41 B**). Therefore, cluster 2 transcripts vividly were not induced in FCCP stimulated condition. Biological function analysis attributions revealed GO-enriched associated with negative regulation of cell migration (35 transcripts), positive regulation of cell differentiation (94 transcripts) and activation of protein kinase activity (39 transcripts) (**Figure 41 C**).

Cluster 3 represents one of the largest cluster containing transcripts with two distinct phenotypes of low to high z-scores. In detail, untreated medium as well as *Sp* infected condition showed minimal z-scores, whilst all CSE exposed conditions showed medium to high z-score with CSE followed by *Sp* having high and very high z-score. Of note, acute phase genes including *IL-1 β* , *IL-6R*, *IL-24* and *HMOX1* upregulated upon CSE, *Sp* and CSE followed by *Sp*. Further functional attributions

indicated GO-enrichment in many biological processes including microtubule polymerization, negative regulation of cell cycle process, regulation of cytokine production, negative regulation of apoptosis, cell cycle arrest as well as negative regulation of protein metabolic process.

Cluster 4 (77 transcripts) shows a largely different expression profile compared to previously mentioned clusters. In cluster 4, while transcripts of majority of CSE stimulated conditions showed higher z-score, transcripts untreated medium showed very low z-score and medium to high z-score for *Sp* infected conditions only. The functional attributions show robust enrichment of regulation of nuclear division, negative regulation of phosphorylation, regulation of cyclin-dependent protein serine/threonine kinase activity, cell cycle arrest and MAPK activity as well as regulation of cytokine production. Of note, acute phase response cytokines *CXCL8*, *IL-1A* and *IL-23A* are strongly upregulated in 16HBE cells upon CSE and CSE followed by *Sp*.

Cluster 5 (559 transcripts) constitutes the largest cluster and most interesting differentially regulated genes in terms of cell cycle, innate immune response as well as cell junction genes that are mostly downregulated upon CSE as displayed by lowered z-score. Biological GO annotation demonstrates strong attribution of cluster 5 transcripts to DNA damage, cell cycle arrest, fatty acid biosynthesis, regulation of metabolic process, regulation of MAPK cascade, positive regulation of cytokine production and IFN- α and IFN- γ responses (virus receptor activity). Notably, many cluster 5 genes belong to interferon responses including IFN- γ -inducible proteins *IFI44*, *IFI16*, *IFI6* or viral receptors such as *IFIT1*, *IFIT2*, *IFIT3*, *IFT122*, *DDX60*, *TLR3* and *SCARB1* as well as IFN- β and IFN- λ response genes including *IFNL2* and *IFNB1*. These transcripts play a central role in recognition of both bacterial and viral pathogens as well as acute response to these pathogens as a part of innate immunity. Moreover, the certain transcripts related to interferon response also downregulated upon CSE including *IKBKE*, *TRIM29*, *PLK1*, *OASL*, *HLA-DMA*, *CTSS*, *DDX58*, *PYCARD* and *IL27RA* all involved in innate immune response to pathogens. In this cluster, there were transcripts that attribute to antimicrobial clearance of bacteria such as *SLPI*, *HMGB2*, *S100A8*, *S100A9*, *S100A12*, *GBP2* and *KLK5* and *KLK7* all of which were downregulated upon CSE stimulation. In addition, transcripts belonging to cell junctions showed lower z-score in upon CSE in this cluster including *CDH5*, *CLDN9*, *ITGB4*, *ITGB6*, *ITGB8* and *TGFB2*.

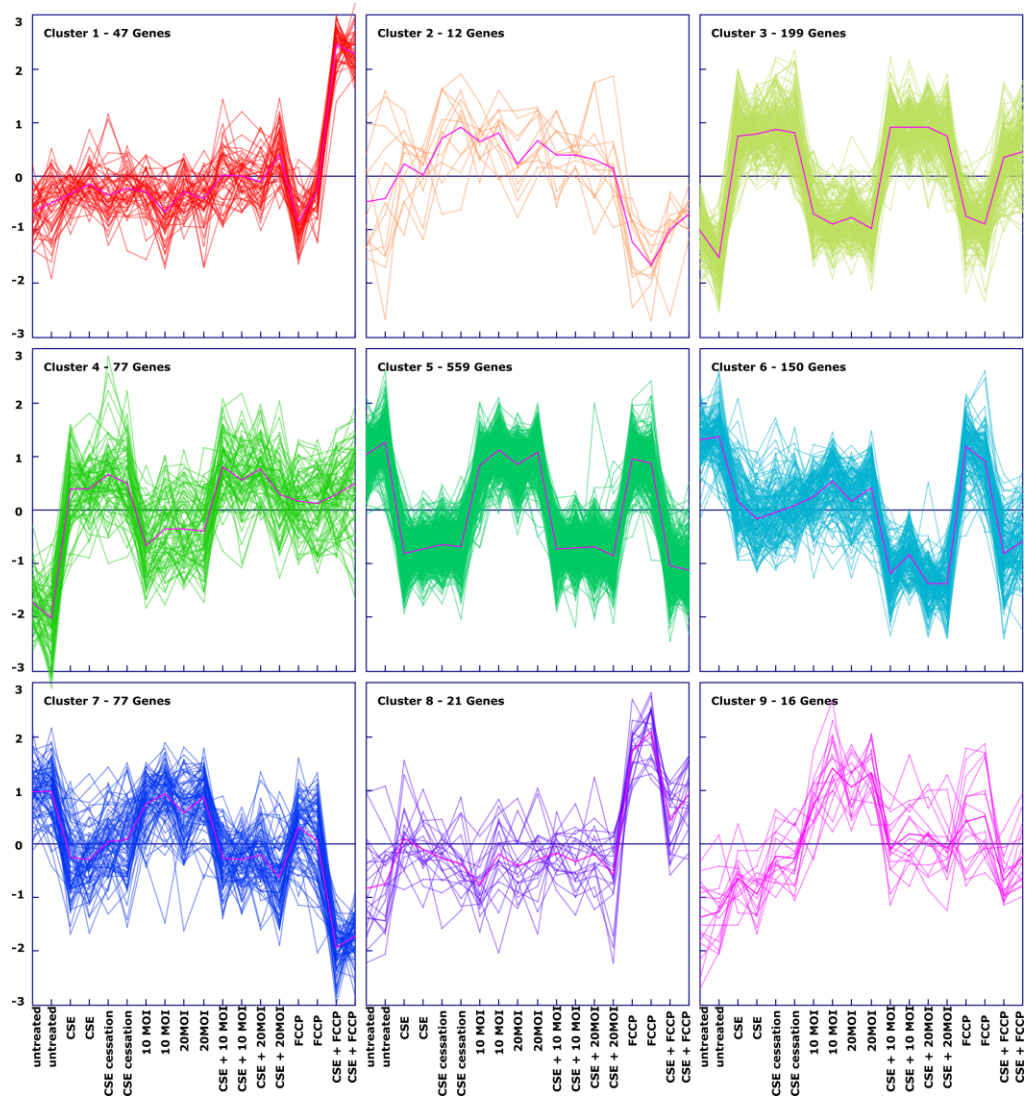
In cluster 6 (150 transcripts) majority of transcripts showed medium z-score which were stimulated with CSE alone and *Sp* alone, whereas CSE followed by *Sp* and CSE followed by FCCP showed low to very low z-score which were in contrast with the untreated medium. GO-enrichment revealed significantly enriched transcripts involved in negative regulation of protein kinase, negative regulation of phosphorylation, virus receptor activity as well as protein serine/threonine kinase activity (**Figure 41 C**). *MARCH8*, *TLR6*, *CXADR* and *PC* are interesting genes in this cluster.

Cluster 7 (77 transcripts) represents high transcript induction upon *Sp* infections, while CSE stimulated conditions and in particular CSE followed by FCCP showed medium to low z-score. Functional GO attributions revealed profound enrichments of epigenetic regulation of gene expression, chromatin assembly and silencing, and intrinsic apoptosis signaling. The most prominent genes in this cluster are *SRC*, *CYTB*, *BAD* and *PCDH1*.

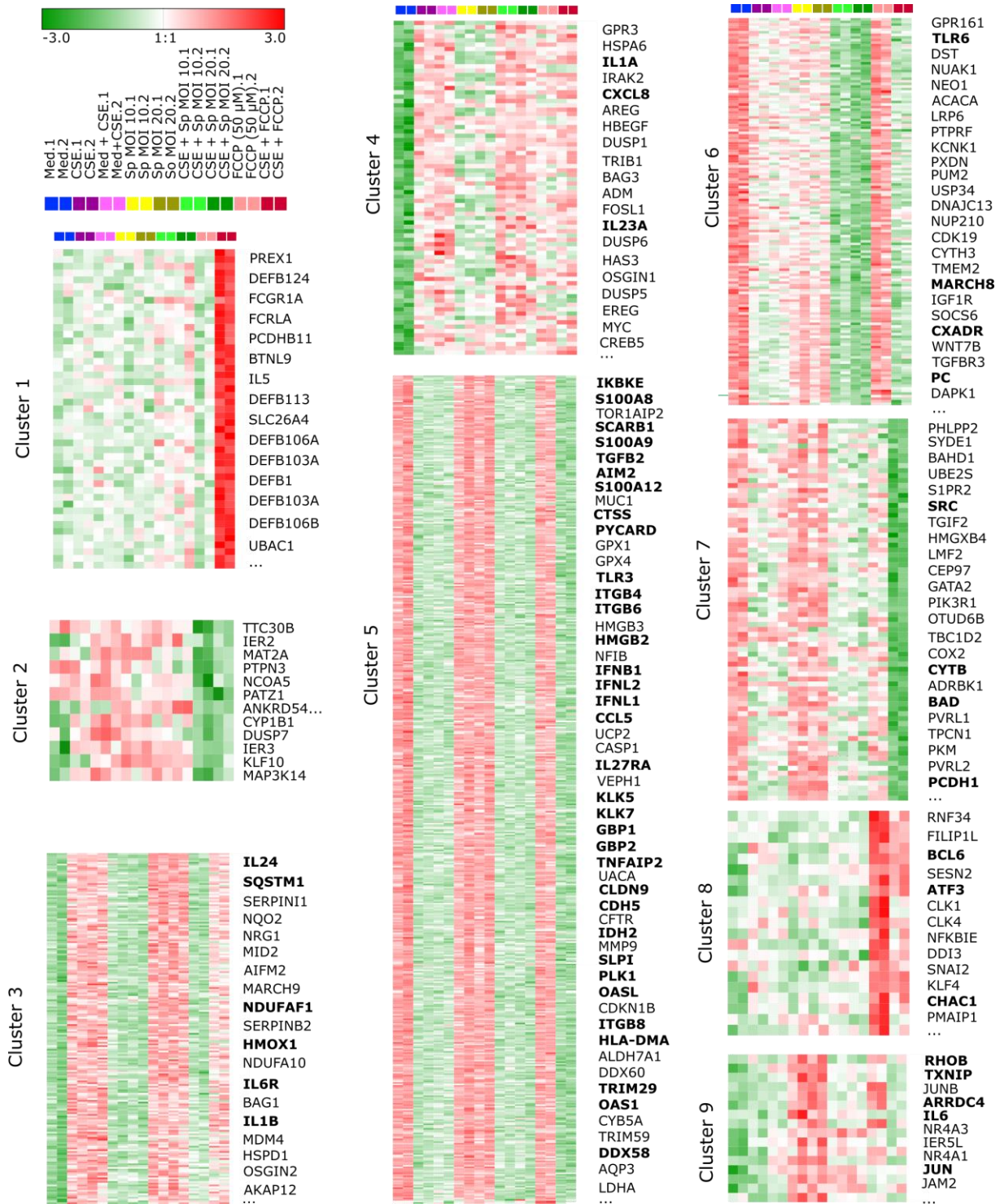
Cluster 8 comprises a small cluster of 21 differentially regulated transcripts which are mostly related to FCCP condition, where all transcripts showed strong induction by high z-score. Other conditions only showed medium to low z-score. GO results revealed attributions of DNA damage response, intrinsic apoptotic signalling pathway and negative regulation of intracellular signal transduction. Of note, *ATF3*, *CHAC1* and *BCL6* are among the most important regulated genes in this cluster.

Cluster 9 is the last small cluster with 16 differentially regulated transcripts which mostly induced upon *Sp* infection. The most interesting transcripts that induced by *Sp* are *DDIT4*, *JUNB*, and *IL6*. Interestingly, CSE pre-exposure inhibited induction of these transcripts. Moreover, CSE alone showed medium to low z-score with exception of certain transcripts which showed high z-score including *ARRDC4*, *JUN*, *TXNIP* and *RHOB* while removal of CSE from the medium counteracted this effect. Other conditions only showed medium to low z-score. Functional GO demonstrated attributions of gene silencing, carbohydrate transport, transmembrane receptor protein kinase activity and positive regulation of cell motility.

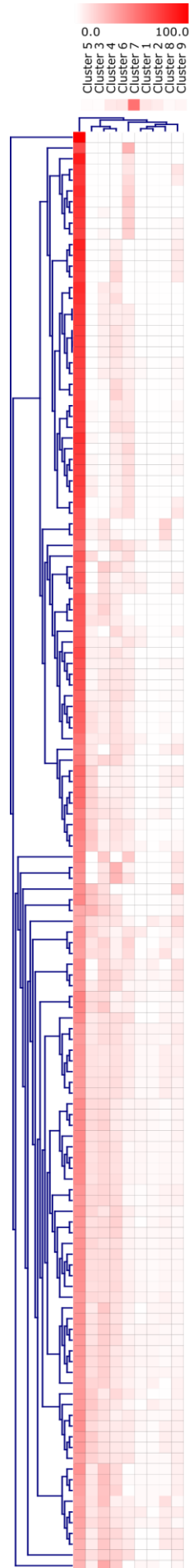
A



B



C



Average of all currently displayed genes

GO:0051255	spindle midzone assembly (6)
GO:0007056	spindle assembly involved in female meiosis (4)
GO:0006335	DNA replication-dependent nucleosome assembly (11)
GO:0000183	rDNA heterochromatin assembly (12)
GO:0045652	regulation of megakaryocyte differentiation (17)
GO:0045814	negative regulation of gene expression, epigenetic (29)
GO:0005342	chromatin silencing (18)
GO:0040029	regulation of gene expression, epigenetic (35)
GO:0097549	chromatin organization involved in negative regulation of transcription (31)
GO:0034401	chromatin organization involved in regulation of transcription (33)
GO:0051310	metaphase plate congression (18)
GO:0007080	mitotic metaphase plate congression (14)
GO:0016126	sterol biosynthetic process (17)
GO:0006695	cholesterol biosynthetic process (15)
GO:2000816	negative regulation of mitotic sister chromatid separation (14)
GO:0030071	regulation of mitotic metaphase/anaphase transition (18)
GO:0030521	androgen receptor signaling pathway (16)
GO:0060765	regulation of androgen receptor signaling pathway (16)
GO:0033045	regulation of sister chromatid segregation (20)
GO:0010965	regulation of mitotic sister chromatid separation (20)
GO:0051306	mitotic sister chromatid separation (20)
GO:1902850	microtubule cytoskeleton organization involved in mitosis (48)
GO:0007051	spindle organization (54)
GO:0000819	sister chromatid segregation (53)
GO:0007076	mitotic chromosome condensation (13)
GO:0006323	DNA packaging (51)
GO:0071103	DNA conformation change (54)
GO:0030261	chromosome condensation (19)
GO:0006334	nucleosome assembly (37)
GO:0034508	centromere complex assembly (15)
GO:0031497	chromatin assembly (40)
GO:0006333	chromatin assembly or disassembly (43)
GO:0030728	nucleosome organization (40)
GO:0065004	protein-DNA complex assembly (46)
GO:0030219	megakaryocyte differentiation (18)
GO:0016458	gene silencing (36)
GO:0030330	DNA damage response, signal transduction by p53 class mediator (21)
GO:0042770	signal transduction in response to DNA damage (24)
GO:0042476	oöntogenesis (21)
GO:0031145	anaphase-promoting complex-dependent catabolic process (17)
GO:0000079	regulation of cyclin-dependent protein serine/threonine kinase activity (18)
GO:0051225	spindle assembly (27)
GO:0090307	mitotic spindle assembly (18)
GO:0007093	mitotic cell cycle checkpoint (25)
GO:0051783	regulation of nuclear division (27)
GO:0000075	cell cycle checkpoint (30)
GO:0008203	cholesterol metabolic process (23)
GO:0033143	regulation of intracellular steroid hormone receptor signaling pathway (21)
GO:2001251	negative regulation of chromosome organization (20)
GO:0033044	regulation of chromosome organization (43)
GO:0140014	mitotic nuclear division (73)
GO:0000280	nuclear division (78)
GO:0006325	chromatin organization (94)
GO:0000226	microtubule cytoskeleton organization (83)
GO:1901987	regulation of cell cycle phase transition (57)
GO:1901990	regulation of mitotic cell cycle phase transition (55)
GO:0032200	telomere organization (28)
GO:0008643	carbohydrate transport (23)
GO:0004693	cyclin-dependent protein serine/threonine kinase activity (22)
GO:0052547	regulation of peptidase activity (53)
GO:0052548	regulation of endopeptidase activity (49)
GO:0010948	negative regulation of cell cycle process (51)
GO:1901988	negative regulation of cell cycle phase transition (39)
GO:0045930	negative regulation of mitotic cell cycle (43)
GO:0004622	cellular protein-containing complex assembly (104)
GO:0010639	negative regulation of organelle organization (49)
GO:0010638	positive regulation of organelle organization (69)
GO:0090224	regulation of spindle organization (11)
GO:0022612	gland morphogenesis (22)
GO:0034644	cellular response to UV (19)
GO:0048661	positive regulation of smooth muscle cell proliferation (18)
GO:0031109	microtubule polymerization or depolymerization (23)
GO:0046785	microtubule polymerization (18)
GO:0043542	endothelial cell migration (30)
GO:2000147	positive regulation of cell motility (60)
GO:0008630	intrinsic apoptotic signaling pathway in response to DNA damage (20)
GO:0097193	intrinsic apoptotic signaling pathway (40)
GO:0045637	regulation of myeloid cell differentiation (37)
GO:0030099	myeloid cell differentiation (57)
GO:0001568	blood vessel development (70)
GO:0019221	cytokine-mediated signaling pathway (79)
GO:0007050	cell cycle arrest (38)
GO:0010629	negative regulation of gene expression (114)
GO:0048534	hematopoietic or lymphoid organ development (94)
GO:0030097	hemopoiesis (91)
GO:0045892	negative regulation of transcription, DNA-templated (131)
GO:0051253	negative regulation of RNA metabolic process (133)
GO:0045934	negative regulation of nucleobase-containing compound metabolic process (141)
GO:0031327	negative regulation of cellular biosynthetic process (149)
GO:2000113	negative regulation of cellular macromolecule biosynthetic process (146)
GO:0001934	positive regulation of protein phosphorylation (84)
GO:0042327	positive regulation of phosphorylation (92)
GO:0045937	positive regulation of phosphate metabolic process (98)
GO:0031401	positive regulation of protein modification process (104)
GO:0001932	regulation of protein phosphorylation (134)
GO:0019220	regulation of phosphate metabolic process (166)
GO:0042325	regulation of phosphorylation (150)
GO:0031399	regulation of protein modification process (164)
GO:0032269	negative regulation of cellular protein metabolic process (99)
GO:0051248	negative regulation of protein metabolic process (106)
GO:0140096	catalytic activity, acting on a protein (290)
GO:0004674	protein serine/threonine kinase activity (97)
GO:0004672	protein kinase activity (142)
GO:0032268	regulation of cellular protein metabolic process (225)
GO:0006468	protein phosphorylation (175)
GO:0051247	positive regulation of protein metabolic process (150)
GO:0032270	positive regulation of cellular protein metabolic process (144)
GO:0016301	kinase activity (155)
GO:1902531	regulation of intracellular signal transduction (175)
GO:0071900	regulation of protein serine/threonine kinase activity (63)
GO:0043408	regulation of MAPK cascade (75)
GO:0045859	regulation of protein kinase activity (96)
GO:0043549	regulation of kinase activity (103)
GO:0033674	positive regulation of kinase activity (69)
GO:0045860	positive regulation of protein kinase activity (63)
GO:0000165	MAPK cascade (91)
GO:0032147	activation of protein kinase activity (45)
GO:0051493	regulation of cytoskeleton organization (66)
GO:0030336	negative regulation of cell migration (35)
GO:0030334	regulation of cell migration (104)
GO:0001817	regulation of cytokine production (81)
GO:0043069	negative regulation of programmed cell death (91)
GO:0043066	negative regulation of apoptotic process (87)
GO:0001819	positive regulation of cytokine production (54)
GO:0045936	negative regulation of phosphate metabolic process (62)
GO:0031400	negative regulation of protein modification process (62)
GO:0042326	negative regulation of phosphorylation (52)
GO:1902532	negative regulation of intracellular signal transduction (55)
GO:0004713	protein tyrosine kinase activity (33)
GO:0009968	negative regulation of signal transduction (134)
GO:0019199	transmembrane receptor protein kinase activity (28)
GO:0004714	transmembrane receptor protein tyrosine kinase activity (25)
GO:0001618	virus receptor activity (17)
GO:0006469	negative regulation of protein kinase activity (32)

Figure 41: Microarray analysis of gene expression upon CSE15 % stimulation and *Sp* infection. For details on data analysis, see material and methods and text. 16HBE cells were incubated with Med or CSE15 % for 28 h, CSE15 % for 24 h and medium for 4 h (CSE cessation), *Sp* MOI 10 and 20 for 4 h, CSE15 % for 24 h followed by *Sp* MOI 10 and 20 for 4 h, FCCP 50 μ M for 4 h and CSE15 % for 24 h followed by FCCP 50 μ M for 4 h. Total RNA was isolated and investigated by using human Clariom S microarray. **A)** Differentially expressed transcripts were determined by comparing each condition with Med control ($|FC| > 3$ -fold, $FDR < 0.05$). **B)** \log_2 SI data of the transcripts were z-score transformed and k-means clustered ($k=9$), and transcripts in resulting clusters were sorted by maximal absolute z-score. Data were represented as color-coded z-scores. **C)** Enrichment analysis for GO category ($FDR < 0.05$, GO-level ≥ 8). GO term groups with highest significance and numbers over over-represented genes for stimulated conditions versus untreated Med. Data are represented hierarchically clustered average of enriched genes (as depicted by color code), that fall into indicated k-means clusters. Numbers in brackets represent number of enriched genes per GO-term. Note: In cooperation with Helmholtz Centre for Infection Research Braunschweig, Research Group Genome Analytics and Dr. Andreas Jeron (Institute for Medical Microbiology and Hospital Hygiene Magdeburg, Research Group Infection Immunology).

5.18. Mitochondrial morphology upon CSE followed by *Sp* infection

In order to find the impacts of CSE and *Sp* on mitochondrial morphology, TEM was performed to visualize mitochondrial structures in the micrographs. The data show that while exposure of 16HBE cells to CSE for 28 h increases mitochondrial area (which is in line with increased mitochondrial mass observed by increased abundance of TOMM20), *Sp* infection alone and in combination with 24 h pre-exposure to CSE decreased this morphometric parameter. The number of diffused mitochondria increased once the cells infected with MOI 10 of *Sp* and in CSE followed by *Sp* infection. Pre-exposure to CSE for 24 h following with *Sp* MOI 10 infection for 4 h induced a visible damage to mitochondria in 16HBE cells as observed by swollen mitochondria with defected crista (**Figure 42**). Moreover, swollen mitochondria with loss of crista were observed in 16HBE cells stimulated with FCCP 50 μ M for 4 h.

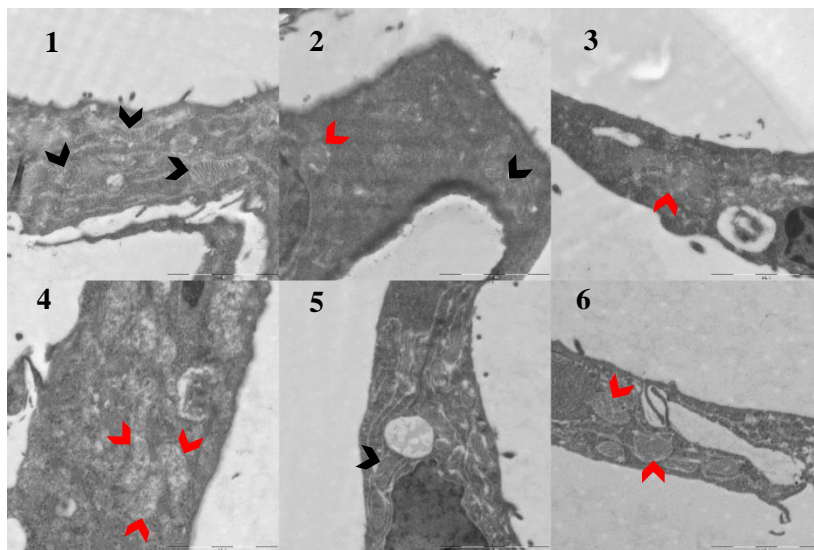


Figure 42: CSE15 % followed by *Sp* infection induced ultrastructural alterations in mitochondria in 16HBE cells. Ultrastructure of 16HBE cells upon *Sp* infection was analyzed under TEM. Dark arrows indicating normal mitochondrial morphology, whereas red arrows showing loss of crista and swollen mitochondria. **1)** medium for 28 h, **2)** CSE15 % for 28 h, **3)** *Sp* MOI 10 for 4 h, **4)** CSE15 % for 24 h followed by *Sp* MOI 10 for 4 h, **5)** CSE15 %

for 24 h followed by medium for 4 h (cessation model) and **6**) FCCP 50 μ M for 4 h. The scale bar is equivalent to 2 μ m. Note: In cooperation with Dr. Mathias M \ddot{u} sken (Central Facility for Microscopy, Helmholtz Centre for Infection Research, Braunschweig).

These data show that CSE pre-exposure exacerbates the effects induced by *Sp* infection on mitochondrial ultrastructure.

5.19. Effect of CSE-induced mitochondrial dysfunction on innate immune responses to *Sp* infection

Data from gene set enrichment analysis show that while *Sp* infection increases enrichment of the genes involved in the complement, interferon α and interferon γ responses, enrichment of the same gene categories reduced in all CSE-stimulated conditions. This is also in line with significant downregulation of *Ifnb1*, *Ifnl1* and *Ifnl2* gene expression in CSE stimulated condition. Antiviral TLR3 also significantly downregulated upon CSE stimulation. The results of ANOVA analysis which displayed in heat map graphs (cluster 5) shows that CSE downregulated *CCL5* and *IL27Ra*, while they stay upregulated in the other conditions. Finally, we observed that CSE while CSE for 14 h increased NLRX1 protein levels in the total cell lysate (**Figure 43 A**), CSE for 24 h significantly did not increase the abundance of mitochondrial-located NLRX1 protein when compared to the medium control (**Figure 43 B**).

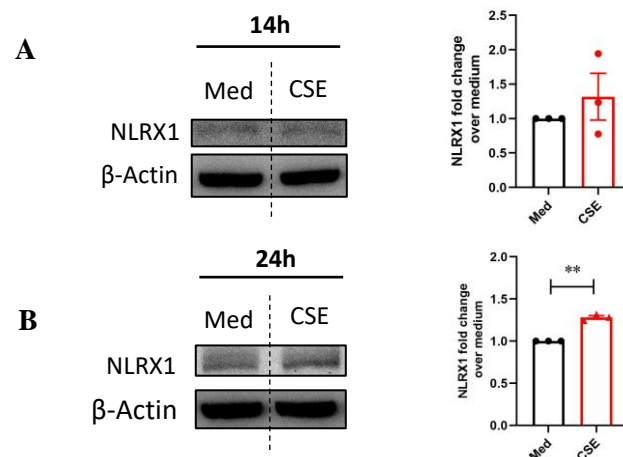


Figure 43: CSE15 %-induced impairment innate immune responses may associate with NLRX1. 16HBE cells were exposed to medium or CSE15 % for 14 h and 24 h and immunoblotting was performed to probe NLRX1. **A**) The abundance of NLRX1 was measured as fold change of band intensities of CSE15 %-stimulated condition for 14 h over medium control (Med). **B**) The levels of NLRX1 were quantified upon stimulation with CSE15 % for 24 h as fold change over Med. The data are represented as mean \pm SEM of three independent experiments (N=3). Significant values were calculated by paired two-tailed t-test compared to Med (**p<0.001) (Aghapour et al., 2022).

These results suggest that CSE-induced downregulated interferon responses may be mediated by increased levels of NLRX1.

5.20. Effects of CSE on epithelial *Sp* colonization/clearance

Bacterial viability assay using the number of colonies in the cell supernatant was performed to find the impacts of CSE on the epithelial antibacterial responses. For this purpose, the cells were pre-exposed to CSE for 24 h and further infected with *Sp* MOI 10 and MOI 20 for 4 h. The number of viable *Sp* (CFU/ml) in the supernatant of 16HBE cells exposed to CSE for 3 h did not change (data were not shown), while CSE exposure for 24 h significantly reduced this number (**Figure 44**). The number of viable cells were significantly lower in the cells pre-exposed to CSE for 24 h and infected with *Sp* MOI 10 for 4 h compared to the medium control.

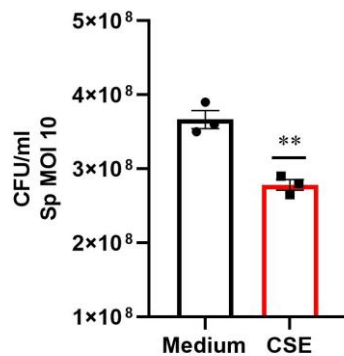


Figure 44: CSE15 % pre-stimulation reduced the number of *Sp* in the supernatant of 16HBE cells. The cells were stimulated with either Med or CSE15 % for 24 h and subsequently infected with *Sp* for 4 h. The supernatants were collected and after serially diluting the diluents were culture on Columbia blood agar. The number of colonies were plotted for each condition. CFU/ml was counted for CSE15 % pre-exposed cells for 24 h and infected with *Sp* MOI 10. The data is representative of mean \pm SEM of three independent experiments. Significant differences were calculated by unpaired two-tailed t-test with Welch's post-hoc correction test compared to Med (* $p < 0.05$).

The above results show that CSE pre-exposure may decrease viability of *Sp* in a time-dependent manner which could be as a result of increase in colonization of *Sp* into mucosal surfaces or induction of acute phase pro-inflammatory responses.

In summary, results of this study indicated that acute CSE exposure induces mitochondrial dysfunction by increasing mitochondrial oxidative stress, mitophagy and autophagy as well as reducing mitochondrial OXPHOS complexes protein levels and altering mitochondrial ultrastructure in AECs. Moreover, CSE suppressed expression of innate immune response genes in AECs. Increased levels of NLRX1 were observed upon CSE exposure in AECs, which may contribute to suppressed interferon responses in AECs. In contrast, *Sp* infection reduced autophagy and mitochondrial biogenesis, and increased interferon gene expression in AECs. *Sp* infection with CSE pre-exposure not only induced similar but more strong mitochondrial alteration as CSE but also more strongly suppressed mitochondrial biogenesis than *Sp* infection. A summary of the findings of this thesis has been illustrated in **Figure 45**.

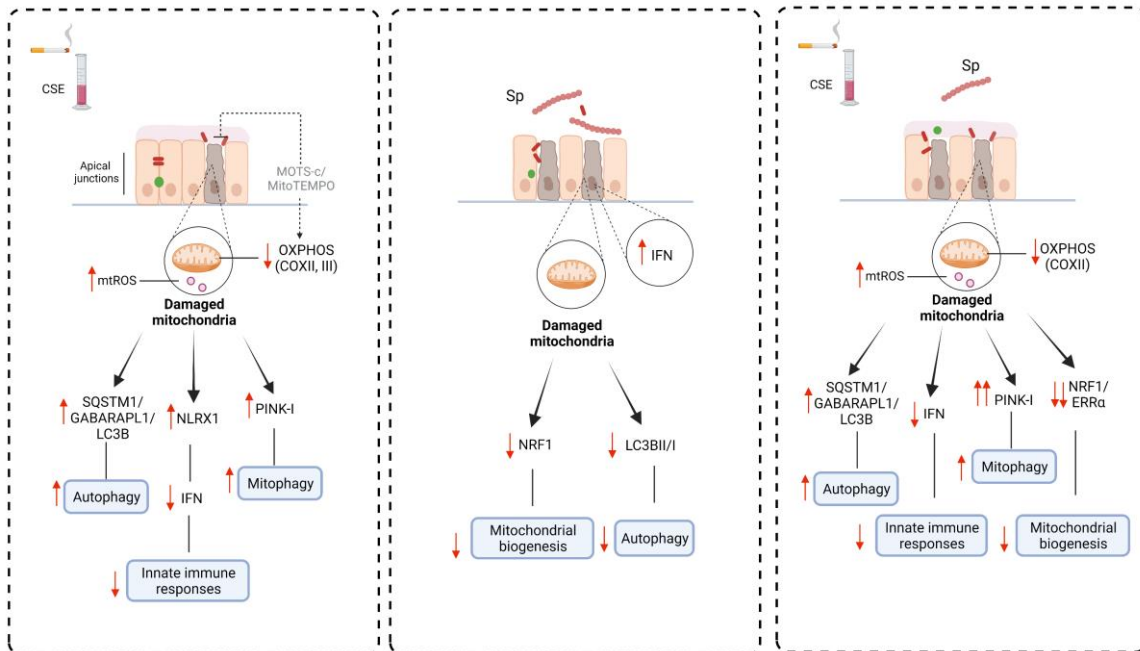


Figure 45: Schematic figure summarizing key findings of the thesis. For full details see results section. The figure was adopted from a cited reference (Aghapour et al., 2022).

6. Discussion

Contribution of mitochondrial dysfunction to metabolic diseases has been widely reported. The findings of the current thesis added to the previous knowledge on the impact of smoking on mitochondrial function and showcased specific epithelial responses that could be altered by mitochondrial dysfunction upon CS. Furthermore, the impact of acute exposure of 16HBE cells to CSE on mitochondrial function in the presence or absence of subsequent infection with *Sp* was investigated. The major aim was to investigate the impact of mitochondrial abnormalities induced by CSE on AEC responses, particularly innate immune responses, and airway epithelial barrier function. Moreover, we sought to determine any mitochondrial changes and innate immune responses in 16HBE cells by CSE and *Sp* alone and in combination.

As shown in the thesis, short-term CSE exposure induced mitochondrial abnormalities in the structure of AECs by enhancing mitochondrial mass and loss of mitochondrial crista (**Figure 42**). Moreover, mitochondrial membranes and in particular OMM which maintains mitochondrial homeostasis by regulating ion and small protein transport is affected by CSE. Of note CSE induced mitochondrial membrane damage as observed by reduced levels of proteins located in the OMM such as VDAC1 and MFN2 (**Figure 23 C** and **Figure 26 B**). VDAC1 is the most abundant protein in the OMM which serves as a channel controlling transport of ATP as well as ions such as calcium together with members of mPTP such as ANT, TSPO and PiC, hence it may play a key role in cellular homeostasis particularly during apoptosis. Reduction or closure of VDAC1 may lead to accumulation of ions and metabolites in the mitochondria, leading to mitochondrial swelling. Indeed, CSE-induced reduction of VDAC1 lead to mitochondrial swelling as observed by an increase in abundance of TOMM20 upon CSE. In addition, VDAC1 interacts with HKII in the OMM which increases the availability of ATP for the phosphorylation of glucose, leading to increased glycolysis process and more cell growth and survival (Camara et al., 2017). Reduced VDAC1 and HKII protein levels may explain the reduced cell growth observed upon CSE in 16HBE cells. Moreover, it was shown that knockdown of isoforms of VDAC including VDAC1 *in vitro* reduces mitochondrial membrane potential which may lead to increased cell death (Maldonado et al., 2013). On the other hand, OMM GTPases regulating mitochondrial fusion promotes cell survival via improving mitochondrial OXPHOS/glycolysis capacity. MFN2 is one of such OMM GTPases mainly controlling mitochondrial fusion. MFN2 was reported to regulate mitochondrial OXPHOS capacity via maintaining the level of coenzyme Q, which is essential for the function of complex I and II of OXPHOS (Mourier et al., 2015). Furthermore, it was shown that increased demand of ATP is compensated by mitochondrial

fusion via improving OXPHOS and that genetic deletion of MFN2 *in vitro* leads to suppressed cell proliferation mainly via decrease in OXPHOS (C.-H. Yao et al., 2019). Despite the negative impacts of loss of MFN2 on mitochondrial biogenesis, it was suggested that excessive reduction in MFN2 may lead to activation of mechanisms involved in mitochondrial biogenesis to prevent further mtDNA damage (Kawalec et al., 2015). It was shown that the effects of MFN2 on bioenergetics is dependent on the localization of MFN2 on ER. MFN2 deficient cells may undergo disturbances in calcium levels both in mitochondria and ER that may affect mitochondrial biogenesis (Casellas-Díaz et al., 2021). More interestingly, it was reported that MFN2 is required for antibacterial innate immune responses against mycobacteria via maintaining glycolysis in mice macrophages (Silwal et al., 2021). MFN2 was shown to interact with MAVS and that both MFN2 deficiency and reduced mitochondrial membrane potential diminishes interferon responses (Koshihara et al., 2011). Apart from OMM, IMM also play a minimal role in transportation of ions and metabolites, and a major role in ETC as proteins regulating OXPHOS residing on IMM. Mitochondrial membrane potential is an electrochemical process generated as a result of pH and proton gradients in ETC (particularly complexes I, III and V) and further passive influx of cations required for OXPHOS such as Fe across IMM to the more negative side of the membrane, and counter efflux of anions to the positive side which eventually leads to ATP production. Interestingly, high level of intracellular ATP supports stability of mitochondrial membrane potential. Depolarization of mitochondrial membrane may lead to increased opening of mitochondrial channels and release of mitochondrial by-products such as mtROS and cytochrome c as well as accumulated ions and metabolites, leading to apoptosis. Prolonged depolarization of IMM may be irreversible and proceed with cell death. On the other hand, although high mitochondrial membrane potential (repolarization) may enhance the total energy levels in IMM it may boost mtROS production and leads to cellular damage (Zorova et al., 2018). In this thesis, it was shown that CSE gradually diminishes mitochondrial membrane potential in a time and concentration-dependent manner (**Figure 22**), which may lead to observed decrease in cell proliferation as well as cell damage. The mitochondrial damages observed in this thesis are in line with previous studies showing similar morphological and functional changes in mitochondria within AECs upon short and long-term exposure to low doses of CSE (Hoffmann et al., 2013; Sundar et al., 2019).

Furthermore, in this thesis peri-nuclear accumulation of mitochondria observed with increased density of TOMM20 upon post-treatment with compounds improving mitochondrial OXPHOS, while CSE increased dissemination of TOMM20 (**Figure 28A** and **28B**). Previous findings reported increased peri-nuclear accumulation of mitochondria in primary AECs (Sundar et al.,

2019). This may suggest increased crosstalk between mitochondria and nucleus, which may affect mitochondrial biogenesis (Eisenberg-Bord & Schuldiner, 2017).

In addition to morphological changes in OMM and IMM and the functional consequences on cell function, CS also affects components of ETC and OXPHOS which may also alter certain cellular functions. In this thesis, CSE diminished the mitochondrial OXPHOS in AECs as observed by suppressed levels of different subunits of mitochondrial OXPHOS (**Figure 23**) and increased mtROS production (**Figure 21 A**). In specific, CSE exposure reduced SDHB (subunit of complex II) (**Figure 23 E and 23 K**), which shuffles succinate into TCA cycle to reduce it to fumarate to transfer electron to ubiquinol in complex III (Vercellino & Sazanov, 2022). SDHB subunit of complex II contains three Fe-S clusters (Bezawork-Geleta et al., 2017). SDH function was associated with inflammatory responses, in a way that inhibition of SDH was shown to suppress pro-inflammatory responses in macrophages (Mills et al., 2016). SDH dysfunction leads to accumulation of succinate, which could be used by certain pathogenic bacteria as a source of energy and hence enhance airway infection (Esposito et al., 2019). Furthermore, compensatory carboxylation mechanism that maintain generation of citrate and other TCA intermediates (Martínez-Reyes & Chandel, 2020), may also be impacted by CSE, as 3-fold downregulation of isocitrate dehydrogenase 2 (*IDH2*), a NADPH-dependent enzyme that converts isocitrate to α -ketoglutarate was observed upon CSE (**Figure 41, cluster 5**), which further leads to accumulation of succinate.

In addition, CSE affected mitochondrial quality control processes by attenuating mitochondrial fusion and altering mitochondrial fission and mitophagy. The abnormal mitophagy was identified through increased mitochondrial protein levels of LC3B/GABARAPL and SQSTM1, abnormal ubiquitin-mediated mitophagy as observed by increased PINK-I levels and decreased receptor-mediated mitophagy through BNIP3 and FUNDC1 in AECs upon CSE exposure (**Figure 24**). Moreover, the expression of *SQSTM1*, *GABARAPL1*, *MAP1LC3B* genes were increased upon CSE. The decreased protein levels of BNIP3 and FUNDC1 upon CSE in the current thesis (**Figure 24 C and 24 E**) could be explained by reduced number of mitochondria or mitochondrial membrane damage, as both proteins reside in the outer mitochondrial membrane and their decrease levels were reported in the skeletal muscles of COPD patients (Leermakers et al., 2018). Phosphorylation of FUNDC1 at Tyr18 (e.g. by Src kinase) which leads to activation of FUNDC1 was reported to be downregulated upon depolarization of mitochondrial membrane, leading to decreased interaction of FUNDC1 and LC3BII (W. Zhang, 2020). Although no changes were observed in the levels of BNIP3L upon CSE, previous study reported an increase in BNIP3L in BEAS-2B cells upon CSE for 24 h, which was associated with mitochondrial damage (M. Zhang

et al., 2019). This discrepancy may occur due to higher CSE concentration used in the other study. Moreover, in line with the observed findings, previous studies showed stabilization of PINK-I upon CSE and in AECs upon airway disease, and genetic suppression of PINK-I was protected cells from CS-induced mitochondrial dysfunction and cell death (Mizumura et al., 2014). PINK-I is a serine-threonine protein kinase that regulate mitochondrial homeostasis (Ito et al., 2015), which upon stabilization as a result of Parkin insufficiency accumulates in mitochondria and may lead to further proteasomal degradation of Parkin and mitochondrial damage (Araya et al., 2019). Other mechanistic explanations that can be suggested for the observed imbalanced abundance of mitophagy-associated constituents upon CSE, respectively include regulation via mTOR signaling, oxidative stress response or AMPK regulation. The LC3B/GABARAPL-SQSTM1-mediated increase in mitophagy seems to be not affected by mTOR signaling, the negative regulator of autophagy, as a subtle upregulation of genes involved in mTORC1 pathway particularly SQSTM1 and CDKN1a was observed upon CSE (**Figure 41, cluster 5**). Interestingly, CSE deprivation from medium was able to counteract the enrichment in mTORC1 gene set, indicating that the activation of mTOR may be transient. The impact of increased oxidative stress in CSE-induced mitophagy was ruled out by using the mtROS inducer FCCP, which did not alter the levels of mitophagy markers. Given the fact that AMPK α phosphorylation positively regulates initiation of autophagy via phosphorylation of ULK1 at serine 555 (J. W. Lee et al., 2010), it was hypothesized that AMPK may regulate GABARAPL1-mediated mitophagy upon CSE stimulation. AMPK α is a metabolic sensor which is dependent on mitochondrial OXPHOS activity, and a decrease in its phosphorylated form has been reported in the lung of patients with airway disease (X.-Y. Cheng et al., 2017). It is postulated that the levels of phosphorylated AMPK α initially increases in response to CSE to resolve the inflammation by increasing antioxidant regulators such as mitochondrial SOD2 and NRF2 (X.-Y. Cheng et al., 2017; Morsch et al., 2019; Y. Wang et al., 2018). However, it is not fully understood whether this pattern of AMPK α phosphorylation is associated with the severity of the airway damages. In contrast, several *in vitro* studies reported that CSE exposure resulted in decreased AMPK α phosphorylation in AECs in a time-dependent manner both *in vitro* and *in vivo* (Cui et al., 2018; J. S. Lee et al., 2015). In the present study, it was observed that stimulation of 16HBE cells with CSE slightly reduced phosphorylation of AMPK α at Thr172 (**Figure 25**), while it upregulated AMPK β 2 (*PRKAB2*) gene expression (**Figure 39 A**), suggesting potential involvement of other subunits of AMPK in CSE-induced increase in mitophagy. Phosphorylation of ULK1 by AMPK leads to its translocation to the mitochondria and increased mitophagy (Tian et al., 2015b). Immunoblotting for phospho-ULK1 at Ser555 only showed a slight increase upon

stimulation with CSE for 14h (**Figure 25 C**), suggesting that the increased mitophagy induced by CSE was minimally affected by AMPK α /ULK1 pathway and mainly triggered by other mitophagy regulators. For examples, increased enrichment of hallmark of UPR that have been observed in this thesis upon CSE, was reported to trigger autophagy via ER stress response. Furthermore, expression of IRE1 gene (*ERN1*) increased 6-fold upon CSE compared to the medium, which was reported to trigger autolysosome formation through activation of JNK pathway.

Besides the finding on CSE-induced impairment in mitochondrial function and disrupted regulation of mitochondrial quality control processes in AEC, existing literature have shown that CS exposure dysregulates innate immune responses to pathogens resulting in secondary bacterial infection with e.g. *Sp* serotypes which may induce exacerbation of airway complications (Gaschler et al., 2009; Kulkarni et al., 2010; Voss et al., 2015). *Sp* serotypes are composed of non-invasive common nasal colonizer serotypes such as serotype 15A, 19A, 19F and 23B were frequently isolated from patients with exacerbations (Pérez-Trallero et al., 2011). 19F is one of the increasingly isolated serotypes that does not respond to routine antimicrobial treatments (H. A. T. Nguyen et al., 2019). It was reported that *Sp* infection increases oxidative burden and reduces MMP in the lung of aged mice (Plataki et al., 2019). Furthermore, stimulation with virulence factors of *Sp* pneumolysin and hydrogen peroxide were shown to induce mitochondrial membrane permeability in alveolar epithelial cells leading to mitochondrial DNA release and a pro-inflammatory response (Y. Gao et al., 2019; Nerlich et al., 2018). In this thesis, it was shown that while infecting 16HBE with *Sp* considerably increased mtROS levels (**Figure 30 A**), *Sp* infection did not alter protein levels of subunits of mitochondrial OXPHOS (**Figure 32**), suggesting potential direct ROS-generating capacity of *Sp* that does not require mitochondrial OXPHOS components. Furthermore, *Sp* infection enhanced the abundance of mitochondrial fission protein DRP1 (**Figure 35**), showing that increased mitochondrial fragmentation may proceed with cell death in *Sp* infection, which is also in line with the observed decrease in mitochondrial biogenesis. Morphological analysis also confirmed this, as loss of crista and mitochondrial swelling were observed together with damaged mitochondria (**Figure 42**). Moreover, increased receptor-mediated mitophagy levels (**Figure 34**) and increased levels of HKII (**Figure 32 F**) and enhanced enrichment of genes involved in glycolysis (**Figure 38 A**) were observed upon *Sp* infection, which are in contrast to CSE-stimulated conditions. These alterations may be caused by increased hypoxia upon *Sp* infection which enhances both hypoxia-mediated mitophagy and glycolysis. *Sp* infection with CSE pre-exposure induced similar but stronger changes on the levels of subunits of mitochondrial OXPHOS in 16HBE cells, in

particular SDHB (**Figure 32 D**), which may in turn disturb TCA cycle and lead to aggravated infection. Furthermore, significant increase in the levels of PINK-I was observed upon *Sp* infection with CSE pre-exposure (**Figure 34 E**), suggesting major changes in proteasomal regulation of mitophagy regulators in the *Sp* exacerbation model. Together, infection with non-invasive *Sp* alone elicited different mitochondrial abnormalities than those induced by CSE alone and in combination with *Sp* in 16HBE cells.

Inhaled pathogens and noxious gases first encounter physical and chemical barriers in AECs as the gatekeeper of innate immune responses (Hiemstra et al., 2015). Mitochondrial function may regulate the innate immune response during infection and inflammation (Aghapour et al., 2020). Although early pro-inflammatory responses to the pathogens may resolve the infection and mitigate the damage, chronic infection with persistent inflammation may break this barrier (Thoo et al., 2019). It was shown that CSE increases pro-inflammatory responses by increasing acute phase response gene expression of cytokines for example neutrophil attractants such as *CXCL8* and *IL-23A*, and *IL1 β* (**Figure 41 B**). This early protective inflammatory response was confirmed in our model by the observation that pre-incubation of 16HBE cells with CSE reduces bacterial viability. Contrary, CS is known to suppress certain antimicrobial responses of airway epithelium to the pathogens such as epithelial β -defensins (Amatngalim et al., 2017). It was observed that while *Sp* infection increased type I and II interferon responses as well as complement activity at mRNA levels, CSE dampened these responses in AECs (**Figure 40**). Of the analyzed interferon responses, *IL27Ra* gene expression, which was observed in lung epithelial cells and was dependent on IFN responses via activation of STAT1 (Cao et al., 2014), was downregulated upon CSE and upregulated post-*Sp* infection in 16HBE cells. Importantly *IL27Ra*-deficient mice showed increased disease severity upon respiratory viral infection and co-infection with *S. aureus* (Muallem et al., 2017). Interestingly these mice were resistant to post-influenza *Sp* infection, possibly by increased IL-17 responses (Cao et al., 2014), further explaining an early increased *Sp* clearance in CSE-stimulated cells. Moreover, IL-27, the ligand for IL27Ra was reported to exert barrier protective and antibacterial responses in intestinal epithelial cells model of colitis (Diegelmann et al., 2012). Treatment with exogenous IL-27 protected the lung from injuries induced by influenza and post-influenza *Sp* infection by reducing the recruitment of inflammatory cells to the lung, particularly neutrophils (Cao et al., 2014; F. D. M. Liu et al., 2014), which play a major role in the pathogenesis of COPD (Hoenderdos & Condliffe, 2013). In line, several studies reported that CS exposure suppresses innate immune responses in AECs by negatively regulating IFN responses (Duffney et al., 2018; Modestou et al., 2010; W. Wu et al., 2016). The CSE-induced impaired IFN responses and consequent dampened IL-27

expression may be triggered through NLRP12-mediated downregulation of RIG-I, MDA-5 and TLR3 via IKBE-mediated regulation of IRFs transcription factors as observed by downregulation of RIG-I, MDA-5 and TLR3 genes upon CSE stimulation (**Figure 41 B**). Additionally, CSE-induced attenuation of interferon responses may be triggered by increased levels of MAVS inhibitors such as E3 ligases Trim29, Smurf1/2, March5 that degrade MAVS or by NLRX1-mediated MAVS inhibition (Hanada et al., 2020). This NLRX-mediated inhibition of MAVS and downregulation in interferon response is reported to be regulated via TUFM (Lei et al., 2012). The observed CSE-induced increase in NLRX1 (**Figure 43 B**) may in turn inhibit MAVS that may subsequently suppress interferon responses via both TBK1 and TNFAIP2, leading to more susceptibility to pathogens such as *Sp*. In addition to the effects on interferon responses, mitochondrially localized NLRX1 is reported to affect mitophagy via TUFM (Lei et al., 2012) or via direct interaction with LC3B (Y. Zhang et al., 2019). As such, increased NLRX1 protein levels upon CSE (**Figure 43 B**), may subsequently inhibit MAVS and likely contributes to the increased mitophagy. Therefore, CSE-induced mitochondrial dysfunction may regulate interferon responses and mitophagy in AECs especially at the earlier phase of infection.

Next, mitochondrial-targeted compounds were used to untangle the impacts of improving mitochondrial function on restoring airway epithelial physical barrier function that was disrupted by CSE. As shown in this thesis, both mitochondrial-derived peptide MOTS-c as well as mitochondrial antioxidant MitoTEMPO restore disrupted tight and adherens junction induced by CSE (**Figure 28**). MOTS-c is a mitochondrial short open reading frame peptide with a potential metabolic activity by activating AMPK and increasing glucose uptake (C. Lee et al., 2016). Furthermore, MOTS-c improves SIRT1 through increasing NAD⁺ levels and thus enhances glycolysis (C. Lee et al., 2016). To our knowledge, this is a first report showing an epithelial barrier protective effect for MOTS-c. The barrier protective effects of both mitochondrial compounds may be triggered via improvement of mitochondrial biogenesis via increased glycolysis as already reported for MitoTEMPO in AECs upon rhinovirus infection (Michi et al., 2021).

Finally, in the current thesis it was demonstrated that CSE exposure decreases ERR α protein levels in 16HBE cells (**Figure 27 C**). Importantly, ERR α which is mainly a nuclear receptor and known for its role in mitochondrial biogenesis, was contributed to metabolic reprogramming and inflammatory responses. ERR α was reported to have protective effects in bacterial infection and its deficiency exacerbates systemic inflammatory responses via TLR4-mediated activation of NF κ B in mice. It was shown ERR α expression is regulated with TLR4-mediated activation of AMPK and is dependent on PGC1 α transcript induction. On the other hand, ERR α deficient

murine macrophages showed decreased oxidative phosphorylation and increased glycolysis. $ERR\alpha$ may suppress inflammatory responses via NAD^+ -dependent activation of SIRT1, leading to deacetylation of $NF\kappa B$ p65 and inhibition of pro-inflammatory responses. Alternatively, $ERR\alpha$ inhibits nuclear translocation of p65 via TNFAIP3-mediated suppression of TRAF6, leading to attenuated inflammatory responses (Yuk et al., 2015). Indeed, $ERR\alpha$ deficient mice showed increased intestinal epithelial inflammation and disturbed microbiota in a colitis model. Moreover, deletion of $ERR\alpha$ lead to downregulation of innate immune responses, in particular PIGR in intestinal epithelial cells (Tran et al., 2021). Interestingly, as displayed in this thesis, $ERR\alpha$ could translocate into the cytoplasm and localized to mitochondria upon CSE, and that this decrease was not reversible by pharmacological improvement of OXPHOS. This further confirmed by aggregated $ERR\alpha$ in the cytoplasm upon FCCP treatment (**Figure 27 G**). Therefore, translocation of $ERR\alpha$ to cytoplasm may occur due to nuclear damage or for controlling mitochondrial damage and inflammatory responses. In addition, it was demonstrated that $ERR\alpha$ also triggers mitophagy process against bacterial infection by promoting autophagosome formation (S. Y. Kim et al., 2018). These observations indicate the multifaceted role of $ERR\alpha$ during acute and chronic inflammation and linking mitochondria to inflammatory responses.

Together, CSE-induced mitochondrial dysfunction may contribute to weakened immunological and physical epithelial barrier function in AECs (**Figure 46**). Current study was however limited by several technical issues. First, this study was carried out only with monolayer of undifferentiated and immortalized airway epithelial cells. In physiological condition, AECs function in interaction with other airway structural cells as well as resident and circulated immune cells. Moreover, CSE that has been used in this study mainly contains soluble gas phase contents, excluding the particle phase. In addition, short-term exposure to certain concentration of CSE may only mimic acute model and cannot completely recapitulate more chronic conditions. Although *Sp* used in this study is one of the most frequently isolated bacteria during exacerbations, there are other pathogenic bacteria that are overrepresented in the airways that may compete to colonize the airway epithelium and affect epithelial cell responses. In this thesis, it was shown that colonizing serotype of *Sp* induced certain mitochondrial abnormalities in AECs, however, it is not clear which whether other more invasive serotypes of *Sp* exert similar effects and what specific virulence factor is responsible for these effects. Finally, mitochondrial function such as respiration or acidification could be assessed by more functional assays.

Future studies will further illuminate the impacts of mitochondrial dysfunction induced by exposing animals or differentiated AECs to whole CS on the epithelial responses by considering

the interaction with resident and circulating immune cells. Moreover, the role of mitochondrial ETC complex II and in specific succinate during *Sp*-induced exacerbation warrants further studies. Furthermore, mitochondrial constituents that have been reported in previous studies to regulate interferon responses needs to be mechanistically investigated via functional studies e.g., by investigating interferon pathway proteins in MFN2 deficient or NLRX1 overexpressed AECs. The role of mitochondria in airway epithelial barrier function needs to be similarly investigated by mechanistically finding the mitochondrial OXPHOS/glycolysis components e.g., those regulating AMPK/SIRT1 pathway that may affect barrier function. Further functional experiments may also clarify the role of mitophagy during post-CS bacterial infection, as there are different types of mitophagy seem to be dominant upon smoke exposure or *Sp* infection and whether CS-induced mitophagy could be protective in terms of controlling *Sp* infection by directly limiting bacterial internalization for invasive serotypes is unclear. Moreover, due to interesting roles of $ERR\alpha$ in both mitochondrial bioenergetic and inflammatory responses and the observed decrease upon CSE in AECs in this thesis, it would be intriguing to scrutinize the role of $ERR\alpha$ in CS-induced airway diseases by potentially using $ERR\alpha$ deficient *in vitro* or *in vivo* models.

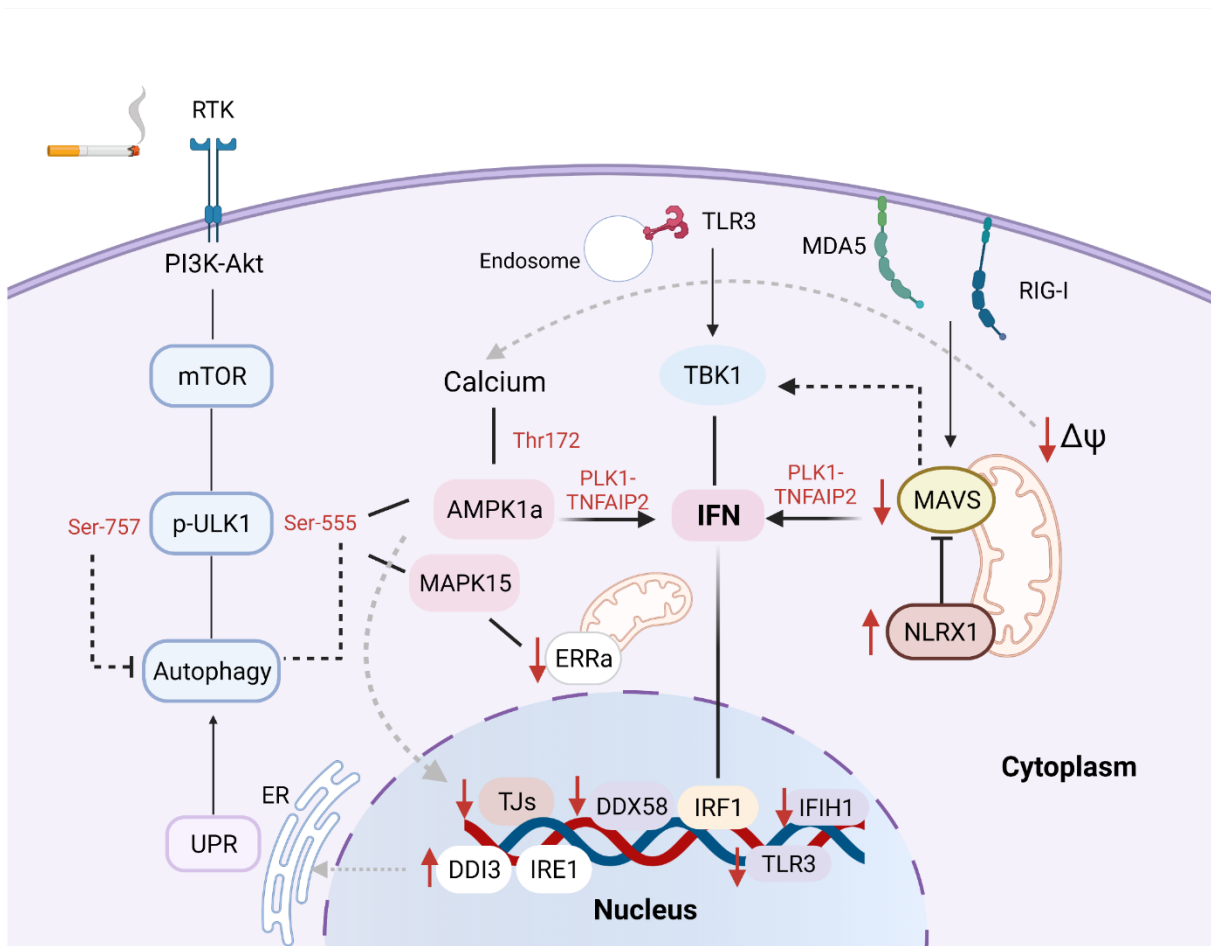


Figure 46: Summary of proposed mechanisms linking CS-induced mitochondrial alterations to airway epithelial responses. For full details, see the text in the discussion.

7. Summary

In this thesis, we established an *in vitro* model of airway epithelial mitochondrial dysfunction by exposing 16HBE AECs to CSE followed by infection with *Sp*. To confirm induction of mitochondrial dysfunction, the levels of mitochondrial stress-response proteins as well as mitochondrial membrane potential were quantified. Furthermore, mtROS and intracellular ROS levels, which are representative of oxidative stress status in the cells, were measured. In order to characterize the role of mitochondrial dysfunction in innate immune responses of airway epithelial cells, restoration of mitochondrial oxidative phosphorylation by mitochondrial-targeted compounds was addressed. The impact of mitochondrial dysfunction on airway epithelial innate immune responses was examined by quantifying the expression of neutrophil chemoattractant genes, the levels of cytokines and proteins involved in inflammatory pathways and host defense, as well as antibacterial activity of AECs.

We found that acute CSE exposure substantially induced mitochondrial dysfunction in airway epithelial cells by suppressing mitochondrial complex protein levels, reducing mitochondrial membrane potential, increasing mitochondrial stress, and disturbing proteasomal-mediated mitophagy. The observed increase in mitophagy was correlated with significant increase in mitophagy adaptor proteins p62, GABARAPL1 and LC3B, while it was independent of the phosphorylation of AMPK α (Thr172) and ULK1 (Ser555). Moreover, CSE pre-exposed 16HBE cells showed downregulated mitochondrial complex protein expression upon *Sp* infection, which was in contrast to *Sp* only infection where the protein levels of mitochondrial complex proteins were slightly elevated. CSE-induced mitochondrial dysfunction correlated with reduced enrichment of genes involved in apical junctions and innate immune responses to *Sp*, particularly type I interferon responses. Improving mitochondrial respiration with mitochondrial-targeted compounds restored airway epithelial junctional disruption induced by CSE. Together, our results demonstrated that CSE-induced mitochondrial dysfunction may contribute to impaired innate immune responses to *Sp*. Therefore, we propose that mitochondrial-targeted therapies may be beneficial in prevention of pneumococcal-induced airway epithelial dysfunction upon CSE exposure.

Zusammenfassung

In dieser Dissertation etablierten wir ein in-vitro-Modell der epithelialen mitochondrialen Dysfunktion der Atemwege, indem wir 16HBE-AECs CSE aussetzten, gefolgt von einer Infektion mit *Sp*. Um die Induktion einer mitochondrialen Dysfunktion zu bestätigen, wurden die Niveaus der mitochondrialen Stressreaktionsproteine sowie das mitochondriale Membranpotential quantifiziert. Darüber hinaus wurden mtROS- und intrazelluläre ROS-Spiegel gemessen, die repräsentativ für den oxidativen Stresstatus in den Zellen sind. Um die Rolle der mitochondrialen Dysfunktion bei der angeborenen Immunantwort von Atemwegsepithelzellen zu charakterisieren, wurde die Wiederherstellung der mitochondrialen oxidativen Phosphorylierung durch auf die Mitochondrien gerichtete Verbindungen untersucht. Der Einfluss der mitochondrialen Dysfunktion auf die angeborene Immunantwort des Atemwegsepithels wurde untersucht, indem die Expression von neutrophilen chemoattraktiven Genen, die Konzentrationen von Zytokinen und Proteinen, die an Entzündungswegen und der Wirtsabwehr beteiligt sind, sowie die antibakterielle Aktivität von AECs quantifiziert wurden.

Wir fanden heraus, dass eine akute CSE-Exposition im Wesentlichen eine mitochondriale Dysfunktion in Epithelzellen der Atemwege induzierte, indem sie den mitochondrialen Komplexproteinspiegel unterdrückte, das mitochondriale Membranpotential reduzierte, den mitochondrialen Stress erhöhte und die proteasomal vermittelte Mitophagie störte. Die beobachtete Zunahme der Mitophagie korrelierte mit einer signifikanten Zunahme der Mitophagie-Adapterproteine p62, GABARAPL1 und LC3B, während sie unabhängig von der Phosphorylierung von AMPK α (Thr172) und ULK1 (Ser555) war. Darüber hinaus zeigten CSE-vorexponierte 16HBE-Zellen eine herunterregulierte mitochondriale Komplexproteinexpression bei einer *Sp*-Infektion, was im Gegensatz zu einer *Sp*-only-Infektion stand, bei der die Proteinspiegel von mitochondrialen Komplexproteinen leicht erhöht waren. CSE-induzierte mitochondriale Dysfunktion korrelierte mit reduzierter Anreicherung von Genen, die an apikalen Verbindungen und angeborenen Immunantworten auf *Sp* beteiligt sind, insbesondere Typ-I-Interferon-Antworten. Die Verbesserung der mitochondrialen Atmung mit auf die Mitochondrien ausgerichteten Verbindungen stellte die durch CSE induzierte Störung der Atemwegsepithelverbindung wieder her. Zusammengefasst zeigten unsere Ergebnisse, dass eine CSE-induzierte mitochondriale Dysfunktion zu einer Beeinträchtigung der angeborenen Immunantwort auf *Sp* beitragen kann. Basierend auf diesen Daten gehen wir davon aus, dass auf Mitochondrien ausgerichtete Therapien bei der Prävention von Pneumokokken-induzierter Dysfunktion des Atemwegsepithels nach CSE-Exposition von Vorteil sein können.

8. References

1. Aaron, S. D., Angel, J. B., Lunau, M., Wright, K., Fex, C., Le Saux, N., & Dales, R. E. (2001). Granulocyte inflammatory markers and airway infection during acute exacerbation of chronic obstructive pulmonary disease. *Am J Respir Crit Care Med*, *163*(2), 349–355. <https://doi.org/10.1164/ajrccm.163.2.2003122>.
2. Agarwal, A. R., Yin, F., & Cadenas, E. (2014). Short-term cigarette smoke exposure leads to metabolic alterations in lung alveolar cells. *Am J Respir Cell Mol Biol*, *51*(2), 284–293. <https://doi.org/10.1165/rcmb.2013-0523OC>.
3. Agarwal, A. R., Zhao, L., Sancheti, H., Sundar, I. K., Rahman, I., & Cadenas, E. (2012). Short-term cigarette smoke exposure induces reversible changes in energy metabolism and cellular redox status independent of inflammatory responses in mouse lungs. *Am J Physiol. Lung Cell Mol Physiol*, *303*(10), L889–898. <https://doi.org/10.1152/ajplung.00219.2012>.
4. Aghapour, M., Raei, P., Moghaddam, S. J., Hiemstra, P. S., & Heijink, I. H. (2018). Airway epithelial barrier dysfunction in chronic obstructive pulmonary disease: Role of cigarette smoke exposure. *Am J Respir Cell Mol Biol*, *58*(2), 157–169. <https://doi.org/10.1165/rcmb.2017-0200TR>.
5. Aghapour, M., Remels, A. H. V., Pouwels, S. D., Bruder, D., Hiemstra, P. S., Cloonan, S. M., & Heijink, I. H. (2020). Mitochondria: At the crossroads of regulating lung epithelial cell function in chronic obstructive pulmonary disease. *Am J Physiol. Lung Cell Mol Physiol*, *318*(1), L149–L164. <https://doi.org/10.1152/ajplung.00329.2019>.
6. Aguilera-Aguirre, L., Bacsi, A., Saavedra-Molina, A., Kurosky, A., Sur, S., & Boldogh, I. (2009). Mitochondrial dysfunction increases allergic airway inflammation. *J Immunol*, *183*(8), 5379–5387. <https://doi.org/10.4049/jimmunol.0900228>.
7. Ahmad, T., Sundar, I. K., Lerner, C. A., Gerloff, J., Tormos, A. M., Yao, H., & Rahman, I. (2015). Impaired mitophagy leads to cigarette smoke stress-induced cellular senescence: Implications for chronic obstructive pulmonary disease. *FASEB J*, *29*(7), 2912–2929. <https://doi.org/10.1096/fj.14-268276>.
8. Alevy, Y. G., Patel, A. C., Romero, A. G., Patel, D. A., Tucker, J., Roswit, W. T., Miller, C. A., Heier, R. F., Byers, D. E., Brett, T. J., & Holtzman, M. J. (2012). IL-13-induced airway mucus production is attenuated by MAPK13 inhibition. *J Clin Invest*, *122*(12), 4555–4568. <https://doi.org/10.1172/JCI64896>.
9. Alysandratos, K.-D., Herriges, M. J., & Kotton, D. N. (2021). Epithelial stem and progenitor cells in lung repair and regeneration. *Annu Rev Physiol*, *83*, 529–550. <https://doi.org/10.1146/annurev-physiol-041520-092904>.
10. Amatngalim, G. D., Schrupf, J. A., Henic, A., Dronkers, E., Verhoosel, R. M., Ordonez, S. R., Haagsman, H. P., Fuentes, M. E., Sridhar, S., Aarbiou, J., Janssen, R. A. J., Lekkerkerker, A. N., & Hiemstra, P. S. (2017). Antibacterial defense of human airway epithelial cells from chronic obstructive pulmonary disease patients induced by acute exposure to nontypeable *Haemophilus influenzae*: Modulation by cigarette smoke. *J Innate Immun*, *9*(4), 359–374. <https://doi.org/10.1159/000455193>.
11. Amatngalim, G. D., van Wijck, Y., de Mooij-Eijk, Y., Verhoosel, R. M., Harder, J., Lekkerkerker, A. N., Janssen, R. A. J., & Hiemstra, P. S. (2015). Basal cells contribute to innate immunity of the airway epithelium through production of the antimicrobial protein RNase 7. *J Immunol*, *194*(7), 3340–3350. <https://doi.org/10.4049/jimmunol.1402169>.

12. Anderson, J. M. (2001). Molecular structure of tight junctions and their role in epithelial transport. *News in Physiol Sci*, *16*, 126–130. <https://doi.org/10.1152/physiologyonline.2001.16.3.126>.
13. Antico Arciuch, V. G., Elguero, M. E., Poderoso, J. J., & Carreras, M. C. (2012). Mitochondrial regulation of cell cycle and proliferation. *Antioxid Redox Signal*, *16*(10), 1150–1180. <https://doi.org/10.1089/ars.2011.4085>.
14. Aravamudan, B., Kiel, A., Freeman, M., Delmotte, P., Thompson, M., Vassallo, R., Sieck, G. C., Pabelick, C. M., & Prakash, Y. S. (2014). Cigarette smoke-induced mitochondrial fragmentation and dysfunction in human airway smooth muscle. *Am J Physiol. Lung Cell Mol Physiol*, *306*(9), L840-854. <https://doi.org/10.1152/ajplung.00155.2013>.
15. Araya, J., Tsubouchi, K., Sato, N., Ito, S., Minagawa, S., Hara, H., Hosaka, Y., Ichikawa, A., Saito, N., Kadota, T., Yoshida, M., Fujita, Y., Utsumi, H., Kobayashi, K., Yanagisawa, H., Hashimoto, M., Wakui, H., Ishikawa, T., Numata, T., ... Kuwano, K. (2019). PRKN-regulated mitophagy and cellular senescence during COPD pathogenesis. *Autophagy*, *15*(3), 510–526. <https://doi.org/10.1080/15548627.2018.1532259>.
16. Bailey, K. L., Kharbanda, K. K., Katafiasz, D. M., Sisson, J. H., & Wyatt, T. A. (2018). Oxidative stress associated with aging activates protein kinase C ϵ , leading to cilia slowing. *Am J Physiol Lung Cell Mol Physiol*, *315*(5), L882–L890. <https://doi.org/10.1152/ajplung.00033.2018>.
17. Ballweg, K., Mutze, K., Königshoff, M., Eickelberg, O., & Meiners, S. (2014). Cigarette smoke extract affects mitochondrial function in alveolar epithelial cells. *Am J Physiol Lung Cell Mol Physiol*, *307*(11), L895-907. <https://doi.org/10.1152/ajplung.00180.2014>.
18. Bals, R., & Hiemstra, P. S. (2004). Innate immunity in the lung: How epithelial cells fight against respiratory pathogens. *Eur Respir J*, *23*(2), 327–333. <https://doi.org/10.1183/09031936.03.00098803>.
19. Banoth, B., & Cassel, S. L. (2018). Mitochondria in innate immune signaling. *Transl Res*, *202*, 52–68. <https://doi.org/10.1016/j.trsl.2018.07.014>.
20. Barceló, B., Pons, J., Fuster, A., Sauleda, J., Noguera, A., Ferrer, J. M., & Agustí, A. G. N. (2006). Intracellular cytokine profile of T lymphocytes in patients with chronic obstructive pulmonary disease. *Clin Exp Immunol*, *145*(3), 474–479. <https://doi.org/10.1111/j.1365-2249.2006.03167.x>.
21. Barnes, P. J. (2020). Oxidative stress-based therapeutics in COPD. *Redox Biol*, *33*, 101544. <https://doi.org/10.1016/j.redox.2020.101544>.
22. Bezawork-Geleta, A., Rohlena, J., Dong, L., Pacak, K., & Neuzil, J. (2017). Mitochondrial complex II: At the crossroads. *Trends Biochem Sci*, *42*(4), 312–325. <https://doi.org/10.1016/j.tibs.2017.01.003>.
23. Bezerra, F. S., Valença, S. S., Pires, K. M. P., Lanzetti, M., Pimenta, W. A., Schmidt, A. C., Porto, L. C., & Zin, W. A. (2011). Long-term exposure to cigarette smoke impairs lung function and increases HMGB-1 expression in mice. *Respir Physiol Neurobiol*, *177*(2), 120–126. <https://doi.org/10.1016/j.resp.2011.03.023>.
24. Bhattacharyya, A., Chattopadhyay, R., Mitra, S., & Crowe, S. E. (2014). Oxidative stress: An essential factor in the pathogenesis of gastrointestinal mucosal diseases. *Physiol Rev*, *94*(2), 329–354. <https://doi.org/10.1152/physrev.00040.2012>.
25. Bradshaw, J. L., Rafiqullah, I. M., Robinson, D. A., & McDaniel, L. S. (2020). Transformation of nonencapsulated *Streptococcus pneumoniae* during systemic infection. *Sci Rep*, *10*(1), 18932. <https://doi.org/10.1038/s41598-020-75988-5>.

26. Brooks, L. R. K., & Mias, G. I. (2018). Streptococcus pneumoniae's virulence and host immunity: Aging, diagnostics, and prevention. *Front Immunol*, 9, 1366. <https://www.frontiersin.org/article/10.3389/fimmu.2018.01366>.
27. Bueno, M., Lai, Y.-C., Romero, Y., Brands, J., St Croix, C. M., Kamga, C., Corey, C., Herazo-Maya, J. D., Sembrat, J., Lee, J. S., Duncan, S. R., Rojas, M., Shiva, S., Chu, C. T., & Mora, A. L. (2015). PINK1 deficiency impairs mitochondrial homeostasis and promotes lung fibrosis. *J Clin Invest*, 125(2), 521–538. <https://doi.org/10.1172/JCI74942>.
28. Bustamante-Marin, X. M., & Ostrowski, L. E. (2017). Cilia and Mucociliary Clearance. *Cold Spring Harb Perspec Biol*, 9(4), a028241. <https://doi.org/10.1101/cshperspect.a028241>.
29. Byfield, F. J., Kowalski, M., Cruz, K., Leszczyńska, K., Namiot, A., Savage, P. B., Bucki, R., & Janmey, P. A. (2011). Cathelicidin LL-37 increases lung epithelial cell stiffness, decreases transepithelial permeability, and prevents epithelial invasion by Pseudomonas aeruginosa. *J Immunol*, 187(12), 6402–6409. <https://doi.org/10.4049/jimmunol.1102185>.
30. Camara, A. K. S., Zhou, Y., Wen, P.-C., Tajkhorshid, E., & Kwok, W.-M. (2017). Mitochondrial VDAC1: A key gatekeeper as potential therapeutic target. *Front Physiol* 8, 460. <https://www.frontiersin.org/article/10.3389/fphys.2017.00460>.
31. Canfield, P. E., Geerdes, A. M., & Molitoris, B. A. (1991). Effect of reversible ATP depletion on tight junction integrity in LLC-PK1 cells. *Am J Physiol*, 261, F1038-1045. <https://doi.org/10.1152/ajprenal.1991.261.6.F1038>.
32. Cantin, A. M. (2010). Cellular response to cigarette smoke and oxidants. *Proc Am Thorac Soc*, 7(6), 368–375. <https://doi.org/10.1513/pats.201001-014AW>.
33. Cao, J., Wang, D., Xu, F., Gong, Y., Wang, H., Song, Z., Li, D., Zhang, H., Li, D., Zhang, L., Xia, Y., Xu, H., Lai, X., Lin, S., Zhang, X., Ren, G., Dai, Y., & Yin, Y. (2014). Activation of IL-27 signalling promotes development of postinfluenza pneumococcal pneumonia. *EMBO Mol Med*, 6(1), 120–140. <https://doi.org/10.1002/emmm.201302890>.
34. Casellas-Díaz, S., Larramona-Arcas, R., Riqué-Pujol, G., Tena-Morraja, P., Müller-Sánchez, C., Segarra-Mondejar, M., Gavalda-Navarro, A., Villarroya, F., Reina, M., Martínez-Estrada, O. M., & Soriano, F. X. (2021). Mfn2 localization in the ER is necessary for its bioenergetic function and neuritic development. *EMBO Rep*, 22(9), e51954. <https://doi.org/10.15252/embr.202051954>.
35. Centers for Disease Control and Prevention (US), National Center for Chronic Disease Prevention and Health Promotion (US), & Office on Smoking and Health (US). (2010). *How Tobacco Smoke Causes Disease: The Biology and Behavioral Basis for Smoking-Attributable Disease: A Report of the Surgeon General*. Centers for Disease Control and Prevention (US). <http://www.ncbi.nlm.nih.gov/books/NBK53017/>.
36. Cereijido, M., Valdés, J., Shoshani, L., & Contreras, R. G. (1998). Role of tight junctions in establishing and maintaining cell polarity. *Annu Rev Physiol*, 60, 161–177. <https://doi.org/10.1146/annurev.physiol.60.1.161>.
37. Cheng, S. L., Yu, C. J., Chen, C. J., & Yang, P. C. (2004). Genetic polymorphism of epoxide hydrolase and glutathione S-transferase in COPD. *Eur Respir J*, 23(6), 818–824. <https://doi.org/10.1183/09031936.04.00104904>.

38. Cheng, X.-Y., Li, Y.-Y., Huang, C., Li, J., & Yao, H.-W. (2017). AMP-activated protein kinase reduces inflammatory responses and cellular senescence in pulmonary emphysema. *Oncotarget*, 8(14), 22513–22523. <https://doi.org/10.18632/oncotarget.15116>.
39. Chiu, Y.-H., Lin, S.-C. A., Kuo, C.-H., & Li, C.-J. (2021). Molecular machinery and pathophysiology of mitochondrial dynamics. *Front Cell Develop Biol*, 9, 743892. <https://www.frontiersin.org/article/10.3389/fcell.2021.743892>.
40. Cloonan, S. M., & Choi, A. M. K. (2016). Mitochondria in lung disease. *J Clin Invest*, 126(3), 809–820. <https://doi.org/10.1172/JCI81113>.
41. Coyne, C. B., Vanhook, M. K., Gambling, T. M., Carson, J. L., Boucher, R. C., & Johnson, L. G. (2002). Regulation of airway tight junctions by proinflammatory cytokines. *Mol Biol Cell*, 13(9), 3218–3234. <https://doi.org/10.1091/mbc.e02-03-0134>.
42. Crakes, K. R., Santos Rocha, C., Grishina, I., Hirao, L. A., Napoli, E., Gaulke, C. A., Fenton, A., Datta, S., Arredondo, J., Marco, M. L., Sankaran-Walters, S., Cortopassi, G., Giulivi, C., & Dandekar, S. (2019). PPAR α -targeted mitochondrial bioenergetics mediate repair of intestinal barriers at the host–microbe intersection during SIV infection. *Proc Natl Acad Sci U S A*, 116(49), 24819–24829. <https://doi.org/10.1073/pnas.1908977116>.
43. Cui, W., Zhang, Z., Zhang, P., Qu, J., Zheng, C., Mo, X., Zhou, W., Xu, L., Yao, H., & Gao, J. (2018). Nrf2 attenuates inflammatory response in COPD/emphysema: Crosstalk with Wnt3a/ β -catenin and AMPK pathways. *J Cell Mol Med*, 22(7), 3514–3525. <https://doi.org/10.1111/jcmm.13628>.
44. Dahl, M., Bowler, R. P., Juul, K., Crapo, J. D., Levy, S., & Nordestgaard, B. G. (2008). Superoxide dismutase 3 polymorphism associated with reduced lung function in two large populations. *Am J Respir Crit Care Med*, 178(9), 906–912. <https://doi.org/10.1164/rccm.200804-549OC>.
45. Damera, G., Pham, T.-H., Zhang, J., Ward, C. K., Newbold, P., Ranade, K., & Sethi, S. (2016). A sputum proteomic signature that associates with increased IL-1 β levels and bacterial exacerbations of COPD. *Lung*, 194(3), 363–369. <https://doi.org/10.1007/s00408-016-9877-0>.
46. Das, G., Shrivage, B. V., & Baehrecke, E. H. (2012). Regulation and Function of Autophagy during Cell Survival and Cell Death. *Cold Spring Harb Perspect Biol*, 4(6), a008813. <https://doi.org/10.1101/cshperspect.a008813>.
47. De Proost, I., Pintelon, I., Brouns, I., Kroese, A. B. A., Riccardi, D., Kemp, P. J., Timmermans, J.-P., & Adriaensen, D. (2008). Functional live cell imaging of the pulmonary neuroepithelial body microenvironment. *Am J Respir Cell Mol Biol*, 39(2), 180–189. <https://doi.org/10.1165/rcmb.2008-0011OC>.
48. de Vos, A. F., Dessing, M. C., Lammers, A. J. J., de Porto, A. P. N. A., Florquin, S., de Boer, O. J., de Beer, R., Terpstra, S., Bootsma, H. J., Hermans, P. W., van 't Veer, C., & van der Poll, T. (2015). The polysaccharide capsule of *Streptococcus pneumoniae* partially impedes MyD88-mediated immunity during pneumonia in mice. *PLoS One*, 10(2), e0118181. <https://doi.org/10.1371/journal.pone.0118181>.
49. Dentener, M. A., Vernooy, J. H. J., Hendriks, S., & Wouters, E. F. M. (2005). Enhanced levels of hyaluronan in lungs of patients with COPD: Relationship with lung function and local inflammation. *Thorax*, 60(2), 114–119. <https://doi.org/10.1136/thx.2003.020842>.
50. Di Stefano, A., Caramori, G., Gnemmi, I., Contoli, M., Vicari, C., Capelli, A., Magno, F., D'Anna, S. E., Zanini, A., Brun, P., Casolari, P., Chung, K. F., Barnes, P. J., Papi, A., Adcock, I., & Balbi, B. (2009). T

- helper type 17-related cytokine expression is increased in the bronchial mucosa of stable chronic obstructive pulmonary disease patients. *Clin Exp Immunol*, 157(2), 316–324. <https://doi.org/10.1111/j.1365-2249.2009.03965.x>.
51. Diegelmann, J., Olszak, T., Göke, B., Blumberg, R. S., & Brand, S. (2012). A novel role for interleukin-27 (IL-27) as mediator of intestinal epithelial barrier protection mediated via differential signal transducer and activator of transcription (STAT) protein signaling and induction of antibacterial and anti-inflammatory proteins. *J Biol Chem*, 287(1), 286–298. <https://doi.org/10.1074/jbc.M111.294355>.
 52. Doe, C., Bafadhel, M., Siddiqui, S., Desai, D., Mistry, V., Rugman, P., McCormick, M., Woods, J., May, R., Sleeman, M. A., Anderson, I. K., & Brightling, C. E. (2010). Expression of the T helper 17-associated cytokines IL-17A and IL-17F in asthma and COPD. *Chest*, 138(5), 1140–1147. <https://doi.org/10.1378/chest.09-3058>.
 53. Domej, W., Oettl, K., & Renner, W. (2014). Oxidative stress and free radicals in COPD – implications and relevance for treatment. *Int J Chron Obstruct Pulm Dis*, 9, 1207–1224. <https://doi.org/10.2147/COPD.S51226>.
 54. Domenech, A., Ardanuy, C., Pallares, R., Grau, I., Santos, S., Campa, A. G. D. la, & Liñares, J. (2013). Some pneumococcal serotypes are more frequently associated with relapses of acute exacerbations in COPD patients. *PLoS One*, 8(3), e59027. <https://doi.org/10.1371/journal.pone.0059027>.
 55. Ducommun, S., Deak, M., Sumpton, D., Ford, R. J., Núñez Galindo, A., Kussmann, M., Viollet, B., Steinberg, G. R., Foretz, M., Dayon, L., Morrice, N. A., & Sakamoto, K. (2015). Motif affinity and mass spectrometry proteomic approach for the discovery of cellular AMPK targets: Identification of mitochondrial fission factor as a new AMPK substrate. *Cell Signal*, 27(5), 978–988. <https://doi.org/10.1016/j.cellsig.2015.02.008>.
 56. Duffney, P. F., McCarthy, C. E., Nogales, A., Thatcher, T. H., Martinez-Sobrido, L., Phipps, R. P., & Sime, P. J. (2018). Cigarette smoke dampens antiviral signaling in small airway epithelial cells by disrupting TLR3 cleavage. *Am J Physiol Lung Cell Mol Physiol*, 314(3), L505–L513. <https://doi.org/10.1152/ajplung.00406.2017>.
 57. Dufour, S., Mège, R.-M., & Thiery, J. P. (2013). α -catenin, vinculin, and F-actin in strengthening E-cadherin cell-cell adhesions and mechanosensing. *Cell Adh Migrat*, 7(4), 345–350. <https://doi.org/10.4161/cam.25139>.
 58. Ebnet, K., Suzuki, A., Ohno, S., & Vestweber, D. (2004). Junctional adhesion molecules (JAMs): More molecules with dual functions? *J Cell Sci*, 117(Pt 1), 19–29. <https://doi.org/10.1242/jcs.00930>.
 59. Eddleston, J., Lee, R. U., Doerner, A. M., Herschbach, J., & Zuraw, B. L. (2011). Cigarette smoke decreases innate responses of epithelial cells to rhinovirus infection. *Am J Respir Cell Mol Biol*, 44(1), 118–126. <https://doi.org/10.1165/rcmb.2009-0266OC>.
 60. Eisenberg-Bord, M., & Schuldiner, M. (2017). Ground control to major TOM: Mitochondria-nucleus communication. *FEBS J*, 284(2), 196–210. <https://doi.org/10.1111/febs.13778>.
 61. Elliott, E. I., Miller, A. N., Banoth, B., Iyer, S. S., Stotland, A., Weiss, J. P., Gottlieb, R. A., Sutterwala, F. S., & Cassel, S. L. (2018). Cutting Edge: Mitochondrial Assembly of the NLRP3 Inflammasome Complex Is Initiated at Priming. *J Immunol*, 200(9), 3047–3052. <https://doi.org/10.4049/jimmunol.1701723>.

62. Esposito, S., Vilella, V. R., Rossin, F., Tosco, A., Raia, V., & Luciani, A. (2019). Succinate links mitochondria to deadly bacteria in cystic fibrosis. *Ann Transl Med*, 7(Suppl 8), S263. <https://doi.org/10.21037/atm.2019.12.49>.
63. Faiz, A., Heijink, I. H., Vermeulen, C. J., Guryev, V., van den Berge, M., Nawijn, M. C., & Pouwels, S. D. (2018). Cigarette smoke exposure decreases CFLAR expression in the bronchial epithelium, augmenting susceptibility for lung epithelial cell death and DAMP release. *Sci Rep*, 8(1), 12426. <https://doi.org/10.1038/s41598-018-30602-7>.
64. Faner, R., Sobradillo, P., Noguera, A., Gomez, C., Cruz, T., López-Giraldo, A., Ballester, E., Soler, N., Arostegui, J. I., Pelegrín, P., Rodriguez-Roisin, R., Yagüe, J., Cosio, B. G., Juan, M., & Agustí, A. (2016). The inflammasome pathway in stable COPD and acute exacerbations. *ERJ Open Res*, 2(3), 00002–02016. <https://doi.org/10.1183/23120541.00002-2016>.
65. Feng, H., Lenarcic, E. M., Yamane, D., Wauthier, E., Mo, J., Guo, H., McGivern, D. R., González-López, O., Misumi, I., Reid, L. M., Whitmire, J. K., Ting, J. P.-Y., Duncan, J. A., Moorman, N. J., & Lemon, S. M. (2017). NLRX1 promotes immediate IRF1-directed antiviral responses by limiting dsRNA-activated translational inhibition mediated by PKR. *Nat Immunol*, 18(12), 1299–1309. <https://doi.org/10.1038/ni.3853>.
66. Finigan, J. H., Faress, J. A., Wilkinson, E., Mishra, R. S., Nethery, D. E., Wyler, D., Shatat, M., Ware, L. B., Matthay, M. A., Mason, R., Silver, R. F., & Kern, J. A. (2011). Neuregulin-1-human epidermal receptor-2 signaling is a central regulator of pulmonary epithelial permeability and acute lung injury. *J Biol Chem*, 286(12), 10660–10670. <https://doi.org/10.1074/jbc.M110.208041>.
67. Foronjy, R. F., Mirochnitchenko, O., Propokenko, O., Lemaitre, V., Jia, Y., Inouye, M., Okada, Y., & D'Armiento, J. M. (2006). Superoxide dismutase expression attenuates cigarette smoke- or elastase-generated emphysema in mice. *Am J Respir Crit Care Med*, 173(6), 623–631. <https://doi.org/10.1164/rccm.200506-850OC>.
68. Forteza, R. M., Casalino-Matsuda, S. M., Falcon, N. S., Valencia Gattas, M., & Monzon, M. E. (2012). Hyaluronan and layilin mediate loss of airway epithelial barrier function induced by cigarette smoke by decreasing E-cadherin. *J Biol Chem*, 287(50), 42288–42298. <https://doi.org/10.1074/jbc.M112.387795>.
69. Ganesan, S., Comstock, A. T., & Sajjan, U. S. (2013). Barrier function of airway tract epithelium. *Tissue Barriers*, 1(4), e24997. <https://doi.org/10.4161/tisb.24997>.
70. Gao, F., Koenitzer, J. R., Tobolewski, J. M., Jiang, D., Liang, J., Noble, P. W., & Oury, T. D. (2008). Extracellular superoxide dismutase inhibits inflammation by preventing oxidative fragmentation of hyaluronan. *J Biol Chem*, 283(10), 6058–6066. <https://doi.org/10.1074/jbc.M709273200>.
71. Gao, Y., Xu, W., Dou, X., Wang, H., Zhang, X., Yang, S., Liao, H., Hu, X., & Wang, H. (2019). Mitochondrial DNA Leakage Caused by Streptococcus pneumoniae Hydrogen Peroxide Promotes Type I IFN Expression in Lung Cells. *Front Microbiol*, 10, 630. <https://doi.org/10.3389/fmicb.2019.00630>.
72. Garmendia, J., Morey, P., & Bengoechea, J. A. (2012). Impact of cigarette smoke exposure on host–bacterial pathogen interactions. *Eur Respir J*, 39(2), 467–477. <https://doi.org/10.1183/09031936.00061911>.
73. Gaschler, G. J., Skrtic, M., Zavitz, C. C. J., Lindahl, M., Onnervik, P.-O., Murphy, T. F., Sethi, S., & Stämpfli, M. R. (2009). Bacteria challenge in smoke-exposed mice exacerbates inflammation and skews

- the inflammatory profile. *Am J Respir Crit Care Med*, 179(8), 666–675. <https://doi.org/10.1164/rccm.200808-1306OC>.
74. Gindele, J. A., Kiechle, T., Benediktus, K., Birk, G., Brendel, M., Heinemann, F., Wohnhaas, C. T., LeBlanc, M., Zhang, H., Strulovici-Barel, Y., Crystal, R. G., Thomas, M. J., Stierstorfer, B., Quast, K., & Schymeinsky, J. (2020). Intermittent exposure to whole cigarette smoke alters the differentiation of primary small airway epithelial cells in the air-liquid interface culture. *Sci Rep*, 10(1), 6257. <https://doi.org/10.1038/s41598-020-63345-5>.
 75. Gkikas, I., Palikaras, K., & Tavernarakis, N. (2018). The role of mitophagy in innate immunity. *Front Immunol*, 9, 1283. <https://www.frontiersin.org/article/10.3389/fimmu.2018.01283>.
 76. González-Mariscal, L., Tapia, R., & Chamorro, D. (2008). Crosstalk of tight junction components with signaling pathways. *Biochim Biophys Acta*, 1778(3), 729–756. <https://doi.org/10.1016/j.bbamem.2007.08.018>.
 77. Gou, X., Zhang, Q., More, S., Bamunuarachchi, G., Liang, Y., Haider Khan, F., Maranville, R., Zuniga, E., Wang, C., & Liu, L. (2019). Repeated exposure to *Streptococcus pneumoniae* exacerbates chronic obstructive pulmonary disease. *Am J Pathol*, 189(9), 1711–1720. <https://doi.org/10.1016/j.ajpath.2019.05.012>.
 78. Hackett, T.-L., Singhera, G. K., Shaheen, F., Hayden, P., Jackson, G. R., Hegele, R. G., Van Eeden, S., Bai, T. R., Dorscheid, D. R., & Knight, D. A. (2011). Intrinsic phenotypic differences of asthmatic epithelium and its inflammatory responses to respiratory syncytial virus and air pollution. *Am J Respir Cell Mol Biol*, 45(5), 1090–1100. <https://doi.org/10.1165/rcmb.2011-0031OC>.
 79. Hanada, Y., Ishihara, N., Wang, L., Otera, H., Ishihara, T., Koshiba, T., Mihara, K., Ogawa, Y., & Nomura, M. (2020). MAVS is energized by Mff which senses mitochondrial metabolism via AMPK for acute antiviral immunity. *Nat Commun*, 11(1), 5711. <https://doi.org/10.1038/s41467-020-19287-7>.
 80. Hara, H., Araya, J., Ito, S., Kobayashi, K., Takasaka, N., Yoshii, Y., Wakui, H., Kojima, J., Shimizu, K., Numata, T., Kawaiishi, M., Kamiya, N., Odaka, M., Morikawa, T., Kaneko, Y., Nakayama, K., & Kuwano, K. (2013). Mitochondrial fragmentation in cigarette smoke-induced bronchial epithelial cell senescence. *Am J Physiol Lung Cell Mol Physiol*, 305(10), L737-746. <https://doi.org/10.1152/ajplung.00146.2013>.
 81. Hara, H., Kuwano, K., & Araya, J. (2018). Mitochondrial quality control in COPD and IPF. *Cells*, 7(8), E86. <https://doi.org/10.3390/cells7080086>.
 82. Hardyman, M. A., Wilkinson, E., Martin, E., Jayasekera, N. P., Blume, C., Swindle, E. J., Gozzard, N., Holgate, S. T., Howarth, P. H., Davies, D. E., & Collins, J. E. (2013). TNF- α -mediated bronchial barrier disruption and regulation by src-family kinase activation. *J Allergy Clin Immunol*, 132(3), 665-675.e8. <https://doi.org/10.1016/j.jaci.2013.03.005>.
 83. Hartsock, A., & Nelson, W. J. (2008). Adherens and tight junctions: Structure, function and connections to the actin cytoskeleton. *Biochim Biophys Acta*, 1778(3), 660–669. <https://doi.org/10.1016/j.bbamem.2007.07.012>.
 84. Hawkins, G. A., & Mora, A. L. (2017). FAM13A, A fatty acid oxidation switch in mitochondria. Friend or foe in chronic obstructive pulmonary disease pathogenesis? *Am J Respir Cell Mol Biol*, 56(6), 689–691. <https://doi.org/10.1165/rcmb.2017-0080ED>.

85. Heijink, I. H., Brandenburg, S. M., Noordhoek, J. A., Postma, D. S., Slebos, D.-J., & van Oosterhout, A. J. M. (2010). Characterisation of cell adhesion in airway epithelial cell types using electric cell-substrate impedance sensing. *Eur Respir J*, *35*(4), 894–903. <https://doi.org/10.1183/09031936.00065809>.
86. Heijink, I. H., Brandenburg, S. M., Postma, D. S., & van Oosterhout, A. J. M. (2012). Cigarette smoke impairs airway epithelial barrier function and cell-cell contact recovery. *Eur Respir J*, *39*(2), 419–428. <https://doi.org/10.1183/09031936.00193810>.
87. Heijink, I. H., Kies, P. M., Kauffman, H. F., Postma, D. S., van Oosterhout, A. J. M., & Vellenga, E. (2007). Down-regulation of E-cadherin in human bronchial epithelial cells leads to epidermal growth factor receptor-dependent Th2 cell-promoting activity. *J Immunol*, *178*(12), 7678–7685. <https://doi.org/10.4049/jimmunol.178.12.7678>.
88. Heijink, I. H., Noordhoek, J. A., Timens, W., van Oosterhout, A. J. M., & Postma, D. S. (2014). Abnormalities in airway epithelial junction formation in chronic obstructive pulmonary disease. *Am J Respir Crit Care Med*, *189*(11), 1439–1442. <https://doi.org/10.1164/rccm.201311-1982LE>.
89. Heijink, I. H., van Oosterhout, A., & Kapus, A. (2010). Epidermal growth factor receptor signalling contributes to house dust mite-induced epithelial barrier dysfunction. *Eur Respir J*, *36*(5), 1016–1026. <https://doi.org/10.1183/09031936.00125809>.
90. Henriques-Normark, B., & Tuomanen, E. I. (2013). The pneumococcus: Epidemiology, microbiology, and pathogenesis. *Cold Spring Harb Perspect Med*, *3*(7), a010215. <https://doi.org/10.1101/cshperspect.a010215>.
91. Herzig, S., & Shaw, R. J. (2018). AMPK: Guardian of metabolism and mitochondrial homeostasis. *Nat Rev Mol Cell Biol*, *19*(2), 121–135. <https://doi.org/10.1038/nrm.2017.95>.
92. Hewitt, R. J., & Lloyd, C. M. (2021). Regulation of immune responses by the airway epithelial cell landscape. *Nat Rev Immunol*, *21*(6), 347–362. <https://doi.org/10.1038/s41577-020-00477-9>.
93. Hiemstra, P. S., & Bourdin, A. (2014). Club cells, CC10 and self-control at the epithelial surface. *Eur Respir J*, *44*(4), 831–832. <https://doi.org/10.1183/09031936.00089214>.
94. Hiemstra, P. S., McCray, P. B. J., & Bals, R. (2015). The innate immune function of airway epithelial cells in inflammatory lung disease. *Eur Respir J*, *45*(4), 1150–1162. <https://doi.org/10.1183/09031936.00141514>.
95. Hirota, Y., Yamashita, S., Kurihara, Y., Jin, X., Aihara, M., Saigusa, T., Kang, D., & Kanki, T. (2015). Mitophagy is primarily due to alternative autophagy and requires the MAPK1 and MAPK14 signaling pathways. *Autophagy*, *11*(2), 332–343. <https://doi.org/10.1080/15548627.2015.1023047>.
96. Hodge, G., Nairn, J., Holmes, M., Reynolds, P. N., & Hodge, S. (2007). Increased intracellular T helper 1 proinflammatory cytokine production in peripheral blood, bronchoalveolar lavage and intraepithelial T cells of COPD subjects. *Clin Exp Immunol*, *150*(1), 22–29. <https://doi.org/10.1111/j.1365-2249.2007.03451.x>.
97. Hoenderdos, K., & Condliffe, A. (2013). The neutrophil in chronic obstructive pulmonary disease. *Am J Respir Cell Mol Biol*, *48*(5), 531–539. <https://doi.org/10.1165/rcmb.2012-0492TR>.
98. Hoffmann, R. F., Zarrintan, S., Brandenburg, S. M., Kol, A., de Bruin, H. G., Jafari, S., Dijk, F., Kalicharan, D., Kelders, M., Gosker, H. R., Ten Hacken, N. H., van der Want, J. J., van Oosterhout, A. J., & Heijink,

- I. H. (2013). Prolonged cigarette smoke exposure alters mitochondrial structure and function in airway epithelial cells. *Respir Res*, *14*(1), 97. <https://doi.org/10.1186/1465-9921-14-97>.
99. Hogg, J. C. (1982). Bronchial mucosal permeability and its relationship to airways hyperreactivity. *Eur J Respir Dis. Supplement*, *122*, 17–22.
100. Hommes, T. J., Lieshout, M. H. van, Veer, C. van 't, Florquin, S., Bootsma, H. J., Hermans, P. W., Vos, A. F. de, & Poll, T. van der. (2015). Role of nucleotide-binding oligomerization domain-containing (NOD) 2 in host defense during pneumococcal pneumonia. *PLoS One*, *10*(12), e0145138. <https://doi.org/10.1371/journal.pone.0145138>.
101. Hoschuetzky, H., Aberle, H., & Kemler, R. (1994). Beta-catenin mediates the interaction of the cadherin-catenin complex with epidermal growth factor receptor. *J Cell Biol*, *127*(5), 1375–1380. <https://doi.org/10.1083/jcb.127.5.1375>.
102. Hu, Q., Ren, H., Ren, J., Liu, Q., Wu, J., Wu, X., Li, G., Wang, G., Gu, G., Guo, K., Hong, Z., Liu, S., & Li, J. (2018). Released mitochondrial DNA following intestinal ischemia reperfusion induces the inflammatory response and gut barrier dysfunction. *Sci Rep*, *8*(1), 7350. <https://doi.org/10.1038/s41598-018-25387-8>.
103. Hu, Q., Ren, J., Li, G., Wu, J., Wu, X., Wang, G., Gu, G., Ren, H., Hong, Z., & Li, J. (2018). The mitochondrially targeted antioxidant MitoQ protects the intestinal barrier by ameliorating mitochondrial DNA damage via the Nrf2/ARE signaling pathway. *Cell Death Dis*, *9*(3), 403. <https://doi.org/10.1038/s41419-018-0436-x>.
104. Hyams, C., Camberlein, E., Cohen, J. M., Bax, K., & Brown, J. S. (2010). The Streptococcus pneumoniae capsule inhibits complement activity and neutrophil phagocytosis by multiple mechanisms. *Infect Immun*, *78*(2), 704–715. <https://doi.org/10.1128/IAI.00881-09>.
105. Ilizarov, A. M., Koo, H. C., Kazzaz, J. A., Mantell, L. L., Li, Y., Bhatpat, R., Pollack, S., Horowitz, S., & Davis, J. M. (2001). Overexpression of manganese superoxide dismutase protects lung epithelial cells against oxidant injury. *Am J Respir Cell Mol Biol*, *24*(4), 436–441. <https://doi.org/10.1165/ajrcmb.24.4.4240>.
106. Ito, S., Araya, J., Kurita, Y., Kobayashi, K., Takasaka, N., Yoshida, M., Hara, H., Minagawa, S., Wakui, H., Fujii, S., Kojima, J., Shimizu, K., Numata, T., Kawaiishi, M., Odaka, M., Morikawa, T., Harada, T., Nishimura, S. L., Kaneko, Y., ... Kuwano, K. (2015). PARK2-mediated mitophagy is involved in regulation of HBEC senescence in COPD pathogenesis. *Autophagy*, *11*(3), 547–559. <https://doi.org/10.1080/15548627.2015.1017190>.
107. Iyer, S. S., He, Q., Janczy, J. R., Elliott, E. I., Zhong, Z., Olivier, A. K., Sadler, J. J., Knepper-Adrian, V., Han, R., Qiao, L., Eisenbarth, S. C., Nauseef, W. M., Cassel, S. L., & Sutterwala, F. S. (2013). Mitochondrial cardiolipin is required for Nlrp3 inflammasome activation. *Immunity*, *39*(2), 311–323. <https://doi.org/10.1016/j.immuni.2013.08.001>.
108. Janoff, E. N., Rubins, J. B., Fasching, C., Charboneau, D., Rahkola, J. T., Plaut, A. G., & Weiser, J. N. (2014). Pneumococcal IgA1 protease subverts specific protection by human IgA1. *Mucosal Immunol*, *7*(2), 249–256. <https://doi.org/10.1038/mi.2013.41>.
109. Jiang, Z., Lao, T., Qiu, W., Polverino, F., Gupta, K., Guo, F., Mancini, J. D., Naing, Z. Z. C., Cho, M. H., Castaldi, P. J., Sun, Y., Yu, J., Laucho-Contreras, M. E., Kobzik, L., Raby, B. A., Choi, A. M. K., Perrella,

- M. A., Owen, C. A., Silverman, E. K., & Zhou, X. (2016). A chronic obstructive pulmonary disease susceptibility gene, FAM13A, regulates protein stability of β -Catenin. *Am J Respir Crit Care Med*, *194*(2), 185–197. <https://doi.org/10.1164/rccm.201505-0999OC>.
110. Kadioglu, A., Weiser, J. N., Paton, J. C., & Andrew, P. W. (2008). The role of *Streptococcus pneumoniae* virulence factors in host respiratory colonization and disease. *Nat Rev Microbiol*, *6*(4), 288–301. <https://doi.org/10.1038/nrmicro1871>.
111. Kang, M.-J., Yoon, C. M., Kim, B. H., Lee, C.-M., Zhou, Y., Sauler, M., Homer, R., Dhamija, A., Boffa, D., West, A. P., Shadel, G. S., Ting, J. P., Tedrow, J. R., Kaminski, N., Kim, W. J., Lee, C. G., Oh, Y.-M., & Elias, J. A. (2015). Suppression of NLRX1 in chronic obstructive pulmonary disease. *J Clin Invest*, *125*(6), 2458–2462. <https://doi.org/10.1172/JCI171747>.
112. Kanneganti, T.-D. (2015). The inflammasome: Firing up innate immunity. *Immunol Rev*, *265*(1), 1–5. <https://doi.org/10.1111/imr.12297>.
113. Kashatus, J. A., Nascimento, A., Myers, L. J., Sher, A., Byrne, F. L., Hoehn, K. L., Counter, C. M., & Kashatus, D. F. (2015). Erk2 phosphorylation of Drp1 promotes mitochondrial fission and MAPK-driven tumor growth. *Mol Cell*, *57*(3), 537–551. <https://doi.org/10.1016/j.molcel.2015.01.002>.
114. Kawalec, M., Boratyńska-Jasińska, A., Beręsewicz, M., Dymkowska, D., Zabłocki, K., & Zabłocka, B. (2015). Mitofusin 2 deficiency affects energy metabolism and mitochondrial biogenesis in MEF cells. *PLoS One*, *10*(7), e0134162. <https://doi.org/10.1371/journal.pone.0134162>.
115. Khan, E. M., Lanir, R., Danielson, A. R., & Goldkorn, T. (2008). Epidermal growth factor receptor exposed to cigarette smoke is aberrantly activated and undergoes perinuclear trafficking. *FASEB J*, *22*(3), 910–917. <https://doi.org/10.1096/fj.06-7729>.
116. Kim, J., Kundu, M., Viollet, B., & Guan, K.-L. (2011). AMPK and mTOR regulate autophagy through direct phosphorylation of Ulk1. *Nat Cell Biol*, *13*(2), 132–141. <https://doi.org/10.1038/ncb2152>.
117. Kim, J.-H., Choi, T. G., Park, S., Yun, H. R., Nguyen, N. N. Y., Jo, Y. H., Jang, M., Kim, J., Kim, J., Kang, I., Ha, J., Murphy, M. P., Tang, D. G., & Kim, S. S. (2018). Mitochondrial ROS-derived PTEN oxidation activates PI3K pathway for mTOR-induced myogenic autophagy. *Cell Death Diff*, *25*(11), 1921–1937. <https://doi.org/10.1038/s41418-018-0165-9>.
118. Kim, S. Y., Yang, C.-S., Lee, H.-M., Kim, J. K., Kim, Y.-S., Kim, Y.-R., Kim, J.-S., Kim, T. S., Yuk, J.-M., Dufour, C. R., Lee, S.-H., Kim, J.-M., Choi, H.-S., Giguère, V., & Jo, E.-K. (2018). ESRRA (estrogen-related receptor α) is a key coordinator of transcriptional and post-translational activation of autophagy to promote innate host defense. *Autophagy*, *14*(1), 152–168. <https://doi.org/10.1080/15548627.2017.1339001>
119. Kim, S.-J., Ahn, D.-G., Syed, G. H., & Siddiqui, A. (2018). The essential role of mitochondrial dynamics in antiviral immunity. *Mitochondrion*, *41*, 21–27. <https://doi.org/10.1016/j.mito.2017.11.007>.
120. Kirkham, P. A., Caramori, G., Casolari, P., Papi, A. A., Edwards, M., Shamji, B., Triantaphyllopoulos, K., Hussain, F., Pinart, M., Khan, Y., Heinemann, L., Stevens, L., Yeadon, M., Barnes, P. J., Chung, K. F., & Adcock, I. M. (2011). Oxidative stress-induced antibodies to carbonyl-modified protein correlate with severity of chronic obstructive pulmonary disease. *Am J Respir Crit Care Med*, *184*(7), 796–802. <https://doi.org/10.1164/rccm.201010-1605OC>.
121. Koppe, U., Suttorp, N., & Opitz, B. (2012). Recognition of *Streptococcus pneumoniae* by the innate immune system. *Cell Microbiol*, *14*(4), 460–466. <https://doi.org/10.1111/j.1462-5822.2011.01746.x>.

122. Korfei, M., MacKenzie, B., & Meiners, S. (2020). The ageing lung under stress. *Eur Respir Rev*, 29(156). <https://doi.org/10.1183/16000617.0126-2020>.
123. Koshiba, T., Yasukawa, K., Yanagi, Y., & Kawabata, S. (2011). Mitochondrial membrane potential is required for MAVS-mediated antiviral signaling. *Sci Signal*, 4(158), ra7. <https://doi.org/10.1126/scisignal.2001147>.
124. Kosmider, B., Lin, C.-R., Karim, L., Tomar, D., Vlasenko, L., Marchetti, N., Bolla, S., Madesh, M., Criner, G. J., & Bahmed, K. (2019). Mitochondrial dysfunction in human primary alveolar type II cells in emphysema. *EBioMedicine*, 46, 305–316. <https://doi.org/10.1016/j.ebiom.2019.07.063>.
125. Krause, G., Winkler, L., Mueller, S. L., Haseloff, R. F., Piontek, J., & Blasig, I. E. (2008). Structure and function of claudins. *Biochim Biophys Acta*, 1778(3), 631–645. <https://doi.org/10.1016/j.bbamem.2007.10.018>.
126. Kulkarni, R., Rampersaud, R., Aguilar, J. L., Randis, T. M., Kreindler, J. L., & Ratner, A. J. (2010). Cigarette smoke inhibits airway epithelial cell innate immune responses to bacteria. *Infect Immun*, 78(5), 2146–2152. <https://doi.org/10.1128/IAI.01410-09>.
127. Kuroda, A., Hegab, A. E., Jingtao, G., Yamashita, S., Hizawa, N., Sakamoto, T., Yamada, H., Suzuki, S., Ishii, M., Namkoong, H., Asakura, T., Ozaki, M., Yasuda, H., Hamamoto, J., Kagawa, S., Soejima, K., & Betsuyaku, T. (2017). Effects of the common polymorphism in the human aldehyde dehydrogenase 2 (ALDH2) gene on the lung. *Respir Res*, 18(1), 69. <https://doi.org/10.1186/s12931-017-0554-5>.
128. Lacho-Contreras, M. E., Polverino, F., Gupta, K., Taylor, K. L., Kelly, E., Pinto-Plata, V., Divo, M., Ashfaq, N., Petersen, H., Stripp, B., Pilon, A. L., Tesfaigzi, Y., Celli, B. R., & Owen, C. A. (2015). Protective role for club cell secretory protein-16 (CC16) in the development of COPD. *Eur Respir J*, 45(6), 1544–1556. <https://doi.org/10.1183/09031936.00134214>.
129. Lee, C., Kim, K. H., & Cohen, P. (2016). MOTS-c: A novel mitochondrial-derived peptide regulating muscle and fat metabolism. *Free Radic Biol Med*, 100, 182–187. <https://doi.org/10.1016/j.freeradbiomed.2016.05.015>.
130. Lee, J. S., Park, S. J., Cho, Y. S., Huh, J. W., Oh, Y.-M., & Lee, S.-D. (2015). Role of AMP-activated protein kinase (AMPK) in smoking-induced lung inflammation and emphysema. *Tuberc Respir Dis*, 78(1), 8–17. <https://doi.org/10.4046/trd.2015.78.1.8>.
131. Lee, J. W., Park, S., Takahashi, Y., & Wang, H.-G. (2010). The association of AMPK with ULK1 regulates autophagy. *PLoS One*, 5(11), e15394. <https://doi.org/10.1371/journal.pone.0015394>.
132. Leermakers, P. A., Schols, A. M. W. J., Kneppers, A. E. M., Kelders, M. C. J. M., de Theije, C. C., Lainscak, M., & Gosker, H. R. (2018). Molecular signalling towards mitochondrial breakdown is enhanced in skeletal muscle of patients with chronic obstructive pulmonary disease (COPD). *Sci Rep*, 8(1), 15007. <https://doi.org/10.1038/s41598-018-33471-2>.
133. Lei, Y., Wen, H., Yu, Y., Taxman, D. J., Zhang, L., Widman, D. G., Swanson, K. V., Wen, K.-W., Damania, B., Moore, C. B., Giguère, P. M., Siderovski, D. P., Hiscott, J., Razani, B., Semenkovich, C. F., Chen, X., & Ting, J. P.-Y. (2012). The mitochondrial proteins NLRX1 and TUFM form a complex that regulates type I interferon and autophagy. *Immunity*, 36(6), 933–946. <https://doi.org/10.1016/j.immuni.2012.03.025>.

134. Li, J., Dai, A., Hu, R., Zhu, L., & Tan, S. (2010). Positive correlation between PPARgamma/PGC-1alpha and gamma-GCS in lungs of rats and patients with chronic obstructive pulmonary disease. *Acta Biochim Biophys Sinica*, *42*(9), 603–614. <https://doi.org/10.1093/abbs/gmq071>.
135. Liu, F. D. M., Kenngott, E. E., Schröter, M. F., Köhl, A., Jennrich, S., Watzlawick, R., Hoffmann, U., Wolff, T., Norley, S., Scheffold, A., Stumhofer, J. S., Saris, C. J. M., Schwab, J. M., Hunter, C. A., Debes, G. F., & Hamann, A. (2014). Timed action of IL-27 protects from immunopathology while preserving defense in influenza. *PLoS Pathogens*, *10*(5), e1004110. <https://doi.org/10.1371/journal.ppat.1004110>.
136. Liu, X., & Chen, Z. (2017). The pathophysiological role of mitochondrial oxidative stress in lung diseases. *J Transl Med*, *15*(1), 207. <https://doi.org/10.1186/s12967-017-1306-5>.
137. Lupfer, C., Thomas, P. G., Anand, P. K., Vogel, P., Milasta, S., Martinez, J., Huang, G., Green, M., Kundu, M., Chi, H., Xavier, R. J., Green, D. R., Lamkanfi, M., Dinarello, C. A., Doherty, P. C., & Kanneganti, T.-D. (2013). Receptor interacting protein kinase 2-mediated mitophagy regulates inflammasome activation during virus infection. *Nat Immunol*, *14*(5), 480–488. <https://doi.org/10.1038/ni.2563>.
138. Ma, K., Chen, G., Li, W., Kepp, O., Zhu, Y., & Chen, Q. (2020). Mitophagy, mitochondrial homeostasis, and cell fate. *Front Cell Develop Biol*, *8*, 467. <https://doi.org/10.3389/fcell.2020.00467>.
139. Maier, B. B., Hladik, A., Lakovits, K., Korosec, A., Martins, R., Kral, J. B., Mesteri, I., Strobl, B., Müller, M., Kalinke, U., Merad, M., & Knapp, S. (2016). Type I interferon promotes alveolar epithelial type II cell survival during pulmonary *Streptococcus pneumoniae* infection and sterile lung injury in mice. *Eur J Immunol*, *46*(9), 2175–2186. <https://doi.org/10.1002/eji.201546201>.
140. Mailloux, R. J., & Harper, M.-E. (2011). Uncoupling proteins and the control of mitochondrial reactive oxygen species production. *Free Radic Biol Med*, *51*(6), 1106–1115. <https://doi.org/10.1016/j.freeradbiomed.2011.06.022>.
141. Makris, S., Paulsen, M., & Johansson, C. (2017). Type I interferons as regulators of lung inflammation. *Front Immunol*, *8*, 259. <https://www.frontiersin.org/article/10.3389/fimmu.2017.00259>.
142. Maldonado, E. N., Sheldon, K. L., DeHart, D. N., Patnaik, J., Manevich, Y., Townsend, D. M., Bezrukov, S. M., Rostovtseva, T. K., & Lemasters, J. J. (2013). Voltage-dependent anion channels modulate mitochondrial metabolism in cancer cells. *J Biol Chem*, *288*(17), 11920–11929. <https://doi.org/10.1074/jbc.M112.433847>.
143. Malinska, D., Szymański, J., Patalas-Krawczyk, P., Michalska, B., Wojtala, A., Prill, M., Partyka, M., Drabik, K., Walczak, J., Sewer, A., John, S., Luettich, K., Peitsch, M. C., Hoeng, J., Duszyński, J., Szczepanowska, J., van der Toorn, M., & Wieckowski, M. R. (2018). Assessment of mitochondrial function following short- and long-term exposure of human bronchial epithelial cells to total particulate matter from a candidate modified-risk tobacco product and reference cigarettes. *Food Chem Toxicol*, *115*, 1–12. <https://doi.org/10.1016/j.fct.2018.02.013>.
144. Mantero, M., Aliberti, S., Azzari, C., Moriondo, M., Nieddu, F., Blasi, F., & Di Pasquale, M. (2017). Role of *Streptococcus pneumoniae* infection in chronic obstructive pulmonary disease patients in Italy. *Thorax*, *72*(10), 403–407. <https://doi.org/10.1177/1753465817728479>.
145. Martínez-Reyes, I., & Chandel, N. S. (2020). Mitochondrial TCA cycle metabolites control physiology and disease. *Nat Commun*, *11*(1), 102. <https://doi.org/10.1038/s41467-019-13668-3>.

146. Maurice, N. M., Bedi, B., Yuan, Z., Goldberg, J. B., Koval, M., Hart, C. M., & Sadikot, R. T. (2019). *Pseudomonas aeruginosa* induced host epithelial cell mitochondrial dysfunction. *Sci Rep*, 9(1), 11929. <https://doi.org/10.1038/s41598-019-47457-1>.
147. McCarthy, K. M., Skare, I. B., Stankewich, M. C., Furuse, M., Tsukita, S., Rogers, R. A., Lynch, R. D., & Schneeberger, E. E. (1996). Occludin is a functional component of the tight junction. *J Cell Sci*, 109, 2287–2298. <https://doi.org/10.1242/jcs.109.9.2287>.
148. Michi, A. N., Yipp, B. G., Dufour, A., Lopes, F., & Proud, D. (2021). PGC-1 α mediates a metabolic host defense response in human airway epithelium during rhinovirus infections. *Nat Commun*, 12(1), 3669. <https://doi.org/10.1038/s41467-021-23925-z>.
149. Milara, J., Peiró, T., Serrano, A., & Cortijo, J. (2013). Epithelial to mesenchymal transition is increased in patients with COPD and induced by cigarette smoke. *Thorax*, 68(5), 410–420. <https://doi.org/10.1136/thoraxjnl-2012-201761>.
150. Mills, E. L., Kelly, B., Logan, A., Costa, A. S. H., Varma, M., Bryant, C. E., Tourlomousis, P., Däbritz, J. H. M., Gottlieb, E., Latorre, I., Corr, S. C., McManus, G., Ryan, D., Jacobs, H. T., Szibor, M., Xavier, R. J., Braun, T., Frezza, C., Murphy, M. P., & O'Neill, L. A. (2016). Succinate dehydrogenase supports metabolic repurposing of mitochondria to drive inflammatory macrophages. *Cell*, 167(2), 457–470.e13. <https://doi.org/10.1016/j.cell.2016.08.064>.
151. Mishra, P., & Chan, D. C. (2014). Mitochondrial dynamics and inheritance during cell division, development and disease. *Nat Rev Mol Cell Biol*, 15(10), 634–646. <https://doi.org/10.1038/nrm3877>.
152. Mishra, R., Foster, D., Vasu, V. T., Thaikoottathil, J. V., Kosmider, B., Chu, H. W., Bowler, R. P., & Finigan, J. H. (2016). Cigarette smoke induces human epidermal receptor 2-dependent changes in epithelial permeability. *Am J Respir Cell Mol Biol*, 54(6), 853–864. <https://doi.org/10.1165/rcmb.2014-0437OC>.
153. Mitchell, A. M., & Mitchell, T. J. (2010). *Streptococcus pneumoniae*: Virulence factors and variation. *Clin Microbiol Infect*, 16(5), 411–418. <https://doi.org/10.1111/j.1469-0691.2010.03183.x>.
154. Mizumura, K., Cloonan, S. M., Nakahira, K., Bhashyam, A. R., Cervo, M., Kitada, T., Glass, K., Owen, C. A., Mahmood, A., Washko, G. R., Hashimoto, S., Ryter, S. W., & Choi, A. M. K. (2014). Mitophagy-dependent necroptosis contributes to the pathogenesis of COPD. *J Clin Invest*, 124(9), 3987–4003. <https://doi.org/10.1172/JCI74985>.
155. Modestou, M. A., Manzel, L. J., El-Mahdy, S., & Look, D. C. (2010). Inhibition of IFN-gamma-dependent antiviral airway epithelial defense by cigarette smoke. *Respir Res*, 11(1), 64. <https://doi.org/10.1186/1465-9921-11-64>.
156. Moermans, C., Heinen, V., Nguyen, M., Henket, M., Sele, J., Manise, M., Corhay, J. L., & Louis, R. (2011). Local and systemic cellular inflammation and cytokine release in chronic obstructive pulmonary disease. *Cytokine*, 56(2), 298–304. <https://doi.org/10.1016/j.cyto.2011.07.010>.
157. Moore, C. B., Bergstralh, D. T., Duncan, J. A., Lei, Y., Morrison, T. E., Zimmermann, A. G., Accavitti-Loper, M. A., Madden, V. J., Sun, L., Ye, Z., Lich, J. D., Heise, M. T., Chen, Z., & Ting, J. P.-Y. (2008a). NLRX1 is a regulator of mitochondrial antiviral immunity. *Nature*, 451(7178), 573–577. <https://doi.org/10.1038/nature06501>.

158. Mora, A. L., Bueno, M., & Rojas, M. (2017). Mitochondria in the spotlight of aging and idiopathic pulmonary fibrosis. *J Clin Invest*, *127*(2), 405–414. <https://doi.org/10.1172/JCI87440>.
159. Morrow, J. D., Zhou, X., Lao, T., Jiang, Z., DeMeo, D. L., Cho, M. H., Qiu, W., Cloonan, S., Pinto-Plata, V., Celli, B., Marchetti, N., Criner, G. J., Bueno, R., Washko, G. R., Glass, K., Quackenbush, J., Choi, A. M. K., Silverman, E. K., & Hersh, C. P. (2017). Functional interactors of three genome-wide association study genes are differentially expressed in severe chronic obstructive pulmonary disease lung tissue. *Sci Rep*, *7*, 44232. <https://doi.org/10.1038/srep44232>.
160. Morsch, A. L. B. C., Wisniewski, E., Luciano, T. F., Comin, V. H., Silveira, G. de B., Marques, S. de O., Thirupathi, A., Silveira Lock, P. C., & De Souza, C. T. (2019). Cigarette smoke exposure induces ROS-mediated autophagy by regulating sestrin, AMPK, and mTOR level in mice. *Redox Rep*, *24*(1), 27–33. <https://doi.org/10.1080/13510002.2019.1601448>.
161. Mourier, A., Motori, E., Brandt, T., Lagouge, M., Atanassov, I., Galinier, A., Rappl, G., Brodesser, S., Hultenby, K., Dieterich, C., & Larsson, N.-G. (2015). Mitofusin 2 is required to maintain mitochondrial coenzyme Q levels. *J Cell Biol*, *208*(4), 429–442. <https://doi.org/10.1083/jcb.201411100>.
162. Muallem, G., Wagage, S., Sun, Y., DeLong, J. H., Valenzuela, A., Christian, D. A., Harms Pritchard, G., Fang, Q., Buza, E. L., Jain, D., Elloso, M. M., López, C. B., & Hunter, C. A. (2017). IL-27 limits type 2 immunopathology following parainfluenza virus infection. *PLoS Pathog*, *13*(1), e1006173. <https://doi.org/10.1371/journal.ppat.1006173>.
163. Murakami, T., Ockinger, J., Yu, J., Byles, V., McColl, A., Hofer, A. M., & Horng, T. (2012a). Critical role for calcium mobilization in activation of the NLRP3 inflammasome. *Proc Natl Acad Sci U S A*, *109*(28), 11282–11287. <https://doi.org/10.1073/pnas.1117765109>.
164. Nagata, K., Iwasaki, Y., Yamada, T., Yuba, T., Kono, K., Hosogi, S., Ohsugi, S., Kuwahara, H., & Marunaka, Y. (2007). Overexpression of manganese superoxide dismutase by N-acetylcysteine in hyperoxic lung injury. *Respir Med*, *101*(4), 800–807. <https://doi.org/10.1016/j.rmed.2006.07.017>.
165. Negre-Salvayre, A., Coatrieux, C., Ingueneau, C., & Salvayre, R. (2008). Advanced lipid peroxidation end products in oxidative damage to proteins. Potential role in diseases and therapeutic prospects for the inhibitors. *Br J Pharmacol*, *153*(1), 6–20. <https://doi.org/10.1038/sj.bjp.0707395>
166. Nerlich, A., Mieth, M., Letsiou, E., Fatykhova, D., Zscheppang, K., Imai-Matsushima, A., Meyer, T. F., Paasch, L., Mitchell, T. J., Tönnies, M., Bauer, T. T., Schneider, P., Neudecker, J., Rückert, J. C., Eggeling, S., Schimek, M., Witzernath, M., Suttorp, N., Hippenstiel, S., & Hocke, A. C. (2018). Pneumolysin induced mitochondrial dysfunction leads to release of mitochondrial DNA. *Scientific Reports*, *8*(1), 182. <https://doi.org/10.1038/s41598-017-18468-7>.
167. Nguyen, C. T., Kim, E.-H., Luong, T. T., Pyo, S., & Rhee, D.-K. (2015). TLR4 mediates pneumolysin-induced ATF3 expression through the JNK/p38 Pathway in Streptococcus pneumoniae-infected RAW 264.7 cells. *Mol Cells*, *38*(1), 58–64. <https://doi.org/10.14348/molcells.2015.2231>.
168. Nguyen, H. A. T., Fujii, H., Vu, H. T. T., Parry, C. M., Dang, A. D., Ariyoshi, K., & Yoshida, L.-M. (2019). An alarmingly high nasal carriage rate of Streptococcus pneumoniae serotype 19F non-susceptible to multiple beta-lactam antimicrobials among Vietnamese children. *BMC Infect Dis*, *19*(1), 241. <https://doi.org/10.1186/s12879-019-3861-2>.

169. Nguyen, T. N., Padman, B. S., & Lazarou, M. (2016). Deciphering the molecular signals of PINK1/Parkin mitophagy. *Trends Cell Biol*, 26(10), 733–744. <https://doi.org/10.1016/j.tcb.2016.05.008>.
170. Ni, H.-M., Williams, J. A., & Ding, W.-X. (2015). Mitochondrial dynamics and mitochondrial quality control. *Redox Biol*, 4, 6–13. <https://doi.org/10.1016/j.redox.2014.11.006>.
171. Niessen, C. M., & Gottardi, C. J. (2008). Molecular components of the adherens junction. *Biochim Biophys Acta*, 1778(3), 562–571. <https://doi.org/10.1016/j.bbamem.2007.12.015>.
172. Nishimoto, A. T., Rosch, J. W., & Tuomanen, E. I. (2020). Pneumolysin: Pathogenesis and therapeutic target. *Front Microbiol*, 11, 1543. <https://doi.org/10.3389/fmicb.2020.01543>.
173. Oldenburger, A., Poppinga, W. J., Kos, F., de Bruin, H. G., Rijks, W. F., Heijink, I. H., Timens, W., Meurs, H., Maarsingh, H., & Schmidt, M. (2014). A-kinase anchoring proteins contribute to loss of E-cadherin and bronchial epithelial barrier by cigarette smoke. *Am J Physiol Cell Physiol*, 306(6), C585–597. <https://doi.org/10.1152/ajpcell.00183.2013>.
174. Olivera, D., Knall, C., Boggs, S., & Seagrave, J. (2010). Cytoskeletal modulation and tyrosine phosphorylation of tight junction proteins are associated with mainstream cigarette smoke-induced permeability of airway epithelium. *Exp Toxicol Pathol*, 62(2), 133–143. <https://doi.org/10.1016/j.etp.2009.03.002>.
175. Onishi, M., Yamano, K., Sato, M., Matsuda, N., & Okamoto, K. (2021). Molecular mechanisms and physiological functions of mitophagy. *EMBO J*, 40(3), e104705. <https://doi.org/10.15252/emj.2020104705>.
176. Park, J. H., Ko, J., Park, Y. S., Park, J., Hwang, J., & Koh, H. C. (2017). Clearance of damaged mitochondria through PINK1 stabilization by JNK and ERK MAPK signaling in chlorpyrifos-treated neuroblastoma cells. *Mol Neurobiol*, 54(3), 1844–1857. <https://doi.org/10.1007/s12035-016-9753-1>.
177. Parker, D., Martin, F. J., Soong, G., Harfenist, B. S., Aguilar, J. L., Ratner, A. J., Fitzgerald, K. A., Schindler, C., & Prince, A. (2011). Streptococcus pneumoniae DNA initiates type I interferon signaling in the respiratory tract. *MBio*, 2(3), e00016-11. <https://doi.org/10.1128/mBio.00016-11>.
178. Parzych, K. R., & Klionsky, D. J. (2014). An overview of autophagy: Morphology, mechanism, and regulation. *Antioxid Redox Signal*, 20(3), 460–473. <https://doi.org/10.1089/ars.2013.5371>.
179. Pauwels, N. S., Bracke, K. R., Dupont, L. L., Van Pottelberge, G. R., Provoost, S., Vanden Berghe, T., Vandenabeele, P., Lambrecht, B. N., Joos, G. F., & Brusselle, G. G. (2011). Role of IL-1 α and the Nlrp3/caspase-1/IL-1 β axis in cigarette smoke-induced pulmonary inflammation and COPD. *Eur Respir J*, 38(5), 1019–1028. <https://doi.org/10.1183/09031936.00158110>.
180. Pérez-Trallero, E., Marimón, J. M., Larruskain, J., Alonso, M., & Ercibengoa, M. (2011). Antimicrobial susceptibilities and serotypes of Streptococcus pneumoniae isolates from elderly patients with pneumonia and acute exacerbation of chronic obstructive pulmonary disease. *Antimicrob Agents Chemother*, 55(6), 2729–2734. <https://doi.org/10.1128/AAC.01546-10>.
181. Perotin, J.-M., Adam, D., Vella-Boucaud, J., Delepine, G., Sandu, S., Jonvel, A.-C., Prevost, A., Berthiot, G., Pison, C., Lebargy, F., Birembaut, P., Coraux, C., & Deslee, G. (2014). Delay of airway epithelial wound repair in COPD is associated with airflow obstruction severity. *Respir Res*, 15, 151. <https://doi.org/10.1186/s12931-014-0151-9>.

182. Petecchia, L., Sabatini, F., Usai, C., Caci, E., Varesio, L., & Rossi, G. A. (2012). Cytokines induce tight junction disassembly in airway cells via an EGFR-dependent MAPK/ERK1/2-pathway. *Lab Invest*, *92*(8), 1140–1148. <https://doi.org/10.1038/labinvest.2012.67>.
183. Petecchia, L., Sabatini, F., Varesio, L., Camoirano, A., Usai, C., Pezzolo, A., & Rossi, G. A. (2009). Bronchial airway epithelial cell damage following exposure to cigarette smoke includes disassembly of tight junction components mediated by the extracellular signal-regulated kinase 1/2 pathway. *Chest*, *135*(6), 1502–1512. <https://doi.org/10.1378/chest.08-1780>.
184. Petrache, I., Medler, T. R., Richter, A. T., Kamocki, K., Chukwueke, U., Zhen, L., Gu, Y., Adamowicz, J., Schweitzer, K. S., Hubbard, W. C., Berdyshev, E. V., Lungarella, G., & Tuder, R. M. (2008). Superoxide dismutase protects against apoptosis and alveolar enlargement induced by ceramide. *Am J Physiol Lung Cell Mol Physiol*, *295*(1), L44–L53. <https://doi.org/10.1152/ajplung.00448.2007>.
185. Pinegin, B., Vorobjeva, N., Pashenkov, M., & Chernyak, B. (2018). The role of mitochondrial ROS in antibacterial immunity. *J Cell Physiol*, *233*(5), 3745–3754. <https://doi.org/10.1002/jcp.26117>.
186. Plataki, M., Cho, S. J., Harris, R. M., Huang, H.-R., Yun, H. S., Schiffer, K. T., & Stout-Delgado, H. W. (2019). Mitochondrial dysfunction in aged macrophages and lung during primary *Streptococcus pneumoniae* infection is improved with Pirfenidone. *Sci Rep*, *9*(1), 971. <https://doi.org/10.1038/s41598-018-37438-1>.
187. Ploumi, C., Daskalaki, I., & Tavernarakis, N. (2017). Mitochondrial biogenesis and clearance: A balancing act. *FEBS J*, *284*(2), 183–195. <https://doi.org/10.1111/febs.13820>.
188. Poole, L. P., Bock-Hughes, A., Berardi, D. E., & Macleod, K. F. (2021). ULK1 promotes mitophagy via phosphorylation and stabilization of BNIP3. *Sci Rep*, *11*(1), 20526. <https://doi.org/10.1038/s41598-021-00170-4>.
189. Pourcelot, M., & Arnoult, D. (2014). Mitochondrial dynamics and the innate antiviral immune response. *FEBS J*, *281*(17), 3791–3802. <https://doi.org/10.1111/febs.12940>.
190. Proud, D., Hudy, M. H., Wiehler, S., Zaheer, R. S., Amin, M. A., Pelikan, J. B., Tacon, C. E., Tonsaker, T. O., Walker, B. L., Kooi, C., Traves, S. L., & Leigh, R. (2012). Cigarette smoke modulates expression of human rhinovirus-induced airway epithelial host defense genes. *PLoS One*, *7*(7), e40762. <https://doi.org/10.1371/journal.pone.0040762>.
191. Rahman, I., & Adcock, I. M. (2006). Oxidative stress and redox regulation of lung inflammation in COPD. *Eur Respir J*, *28*(1), 219–242. <https://doi.org/10.1183/09031936.06.00053805>
192. Rai, P., He, F., Kwang, J., Engelward, B. P., & Chow, V. T. K. (2016). Pneumococcal pneumolysin induces DNA damage and cell cycle arrest. *Sci Rep*, *6*(1), 22972. <https://doi.org/10.1038/srep22972>.
193. Rai, P., Parrish, M., Tay, I. J. J., Li, N., Ackerman, S., He, F., Kwang, J., Chow, V. T., & Engelward, B. P. (2015). *Streptococcus pneumoniae* secretes hydrogen peroxide leading to DNA damage and apoptosis in lung cells. *Proc Natl Acad Sci U S A*, *112*(26), E3421–E3430. <https://doi.org/10.1073/pnas.1424144112>.
194. Ramezanpour, M., Moraitis, S., Smith, J. L. P., Wormald, P. J., & Vreugde, S. (2016). Th17 cytokines disrupt the airway mucosal barrier in chronic rhinosinusitis. *Mediators Inflamm*, *2016*, 9798206. <https://doi.org/10.1155/2016/9798206>.

195. Ren, L., Chen, X., Chen, X., Li, J., Cheng, B., & Xia, J. (2020). Mitochondrial dynamics: Fission and fusion in fate determination of mesenchymal stem cells. *Front Cell Develop Biol*, 8, 580070. <https://www.frontiersin.org/article/10.3389/fcell.2020.580070>.
196. Rincon, M., & Irvin, C. G. (2012). Role of IL-6 in asthma and other inflammatory pulmonary diseases. *Int J Biol Sci*, 8(9), 1281–1290. <https://doi.org/10.7150/ijbs.4874>.
197. Rokicki, W., Rokicki, M., Wojtacha, J., & Dżeljić, A. (2016). The role and importance of club cells (Clara cells) in the pathogenesis of some respiratory diseases. *Kardiochir I Torakochirurgia Pol*, 13(1), 26–30. <https://doi.org/10.5114/kitp.2016.58961>.
198. Roos, A. B., Sandén, C., Mori, M., Bjermer, L., Stampfli, M. R., & Erjefält, J. S. (2015). IL-17A is elevated in end-stage chronic obstructive pulmonary disease and contributes to cigarette smoke-induced lymphoid neogenesis. *Am J Respir Crit Care Med*, 191(11), 1232–1241. <https://doi.org/10.1164/rccm.201410-1861OC>.
199. Rowart, P., Wu, J., Caplan, M. J., & Jouret, F. (2018). Implications of AMPK in the formation of epithelial tight junctions. *Int J Mol Sci*, 19(7), E2040. <https://doi.org/10.3390/ijms19072040>.
200. Rusznak, C., Mills, P. R., Devalia, J. L., Sapsford, R. J., Davies, R. J., & Lozewicz, S. (2000). Effect of cigarette smoke on the permeability and IL-1beta and sICAM-1 release from cultured human bronchial epithelial cells of never-smokers, smokers, and patients with chronic obstructive pulmonary disease. *Am J Respir Cell Mol Biol*, 23(4), 530–536. <https://doi.org/10.1165/ajrcmb.23.4.3959>.
201. Ryter, S. W., & Choi, A. M. K. (2010). Autophagy in the lung. *Proc Am Thorac Soc*, 7(1), 13–21. <https://doi.org/10.1513/pats.200909-101JS>.
202. Saatian, B., Rezaee, F., Desando, S., Emo, J., Chapman, T., Knowlden, S., & Georas, S. N. (2013). Interleukin-4 and interleukin-13 cause barrier dysfunction in human airway epithelial cells. *Tissue Barriers*, 1(2), e24333. <https://doi.org/10.4161/tisb.24333>.
203. Saito, T., Ichikawa, T., Numakura, T., Yamada, M., Koarai, A., Fujino, N., Murakami, K., Yamanaka, S., Sasaki, Y., Kyogoku, Y., Itakura, K., Sano, H., Takita, K., Tanaka, R., Tamada, T., Ichinose, M., & Sugiura, H. (2021). PGC-1 α regulates airway epithelial barrier dysfunction induced by house dust mite. *Respir Res*, 22(1), 63. <https://doi.org/10.1186/s12931-021-01663-6>.
204. Saxena, A., Lopes, F., Poon, K. K. H., & McKay, D. M. (2017). Absence of the NOD2 protein renders epithelia more susceptible to barrier dysfunction due to mitochondrial dysfunction. *Am J Physiol. Gastrointest Liver Physiol*, 313(1), G26–G38. <https://doi.org/10.1152/ajpgi.00070.2017>.
205. Schamberger, A. C., Mise, N., Jia, J., Genoyer, E., Yildirim, A. Ö., Meiners, S., & Eickelberg, O. (2014). Cigarette smoke-induced disruption of bronchial epithelial tight junctions is prevented by transforming growth factor- β . *Am J Respir Cell Mol Biol*, 50(6), 1040–1052. <https://doi.org/10.1165/rcmb.2013-0090OC>.
206. Schulzke, J.-D., & Fromm, M. (2009). Tight junctions: Molecular structure meets function. *Ann N Y Acad Sci*, 1165, 1–6. <https://doi.org/10.1111/j.1749-6632.2009.04925.x>.
207. Sebag, S. C., Koval, O. M., Paschke, J. D., Winters, C. J., Comellas, A. P., & Grumbach, I. M. (2018). Inhibition of the mitochondrial calcium uniporter prevents IL-13 and allergen-mediated airway epithelial apoptosis and loss of barrier function. *Exp Cell Res*, 362(2), 400–411. <https://doi.org/10.1016/j.yexcr.2017.12.003>.

208. Sethi, S., & Murphy, T. F. (2008). Infection in the pathogenesis and course of chronic obstructive pulmonary disease. *N Engl J Med*, *359*(22), 2355–2365. <https://doi.org/10.1056/NEJMra0800353>.
209. Shaykhiiev, R., Otaki, F., Bonsu, P., Dang, D. T., Teater, M., Strulovici-Barel, Y., Salit, J., Harvey, B.-G., & Crystal, R. G. (2011). Cigarette smoking reprograms apical junctional complex molecular architecture in the human airway epithelium in vivo. *Cell Mol Life Sci*, *68*(5), 877–892. <https://doi.org/10.1007/s00018-010-0500-x>.
210. Shaykhiiev, R., Zuo, W.-L., Chao, I., Fukui, T., Witover, B., Brekman, A., & Crystal, R. G. (2013). EGF shifts human airway basal cell fate toward a smoking-associated airway epithelial phenotype. *Proc Natl Acad Sci U S A*, *110*(29), 12102–12107. <https://doi.org/10.1073/pnas.1303058110>.
211. Shen, N., Wang, J., Zhao, M., Pei, F., & He, B. (2011). Anti-interleukin-17 antibodies attenuate airway inflammation in tobacco-smoke-exposed mice. *Inhal Toxicol*, *23*(4), 212–218. <https://doi.org/10.3109/08958378.2011.559603>.
212. Shimada, K., Crother, T. R., Karlin, J., Dagvadorj, J., Chiba, N., Chen, S., Ramanujan, V. K., Wolf, A. J., Vergnes, L., Ojcius, D. M., Rentsendorj, A., Vargas, M., Guerrero, C., Wang, Y., Fitzgerald, K. A., Underhill, D. M., Town, T., & Arditi, M. (2012). Oxidized mitochondrial DNA activates the NLRP3 inflammasome during apoptosis. *Immunity*, *36*(3), 401–414. <https://doi.org/10.1016/j.immuni.2012.01.009>.
213. Siedlinski, M., van Diemen, C. C., Postma, D. S., Vonk, J. M., & Boezen, H. M. (2009). Superoxide dismutases, lung function and bronchial responsiveness in a general population. *Eur Respir J*, *33*(5), 986–992. <https://doi.org/10.1183/09031936.00171507>.
214. Silwal, P., Kim, J. K., Jeon, S. M., Lee, J.-Y., Kim, Y. J., Kim, Y. S., Seo, Y., Kim, J., Kim, S. Y., Lee, M. J., Heo, J. Y., Jung, M.-J., Kim, H. S., Hyun, D.-W., Han, J. E., Whang, J., Huh, Y. H., Lee, S.-H., Heo, W. D., ... Jo, E.-K. (2021). Mitofusin-2 boosts innate immunity through the maintenance of aerobic glycolysis and activation of xenophagy in mice. *Commun Biol*, *4*(1), 548. <https://doi.org/10.1038/s42003-021-02073-6>.
215. Singanayagam, A., Loo, S.-L., Calderazzo, M., Finney, L. J., Trujillo Torralbo, M.-B., Bakhsoliani, E., Girkin, J., Veerati, P., Pathinayake, P. S., Nichol, K. S., Reid, A., Footitt, J., Wark, P. A. B., Grainge, C. L., Johnston, S. L., Bartlett, N. W., & Mallia, P. (2019). Antiviral immunity is impaired in COPD patients with frequent exacerbations. *Am J Physiol Lung Cell Mol Physiol*, *317*(6), L893–L903. <https://doi.org/10.1152/ajplung.00253.2019>.
216. Sørheim, I. C., DeMeo, D. L., Washko, G., Litonjua, A., Sparrow, D., Bowler, R., Bakke, P., Pillai, S. G., Coxson, H. O., Lomas, D. A., Silverman, E. K., Hersh, C. P., & International COPD Genetics Network Investigators. (2010). Polymorphisms in the superoxide dismutase-3 gene are associated with emphysema in COPD. *COPD*, *7*(4), 262–268. <https://doi.org/10.3109/15412555.2010.49682>.
217. Soyka, M. B., Wawrzyniak, P., Eiwegger, T., Holzmann, D., Treis, A., Wanke, K., Kast, J. I., & Akdis, C. A. (2012). Defective epithelial barrier in chronic rhinosinuitis: The regulation of tight junctions by IFN- γ and IL-4. *J Allergy Clin Immunol*, *130*(5), 1087-1096.e10. <https://doi.org/10.1016/j.jaci.2012.05.052>.
218. Stokman, G., Kors, L., Bakker, P. J., Rampanelli, E., Claessen, N., Teske, G. J. D., Butter, L., van Andel, H., van den Bergh Weerman, M. A., Larsen, P. W. B., Dessing, M. C., Zuurbier,

- C. J., Girardin, S. E., Florquin, S., & Leemans, J. C. (2017). NLRX1 dampens oxidative stress and apoptosis in tissue injury via control of mitochondrial activity. *J Exp Med*, *214*(8), 2405–2420. <https://doi.org/10.1084/jem.20161031>.
219. Subramanian, N., Natarajan, K., Clatworthy, M. R., Wang, Z., & Germain, R. N. (2013). The adaptor MAVS promotes NLRP3 mitochondrial localization and inflammasome activation. *Cell*, *153*(2), 348–361. <https://doi.org/10.1016/j.cell.2013.02.054>.
220. Sundar, I. K., Maremanda, K. P., & Rahman, I. (2019). Mitochondrial dysfunction is associated with Miro1 reduction in lung epithelial cells by cigarette smoke. *Toxicol Lett*, *317*, 92–101. <https://doi.org/10.1016/j.toxlet.2019.09.022>.
221. Surabhi, S., Jachmann, L. H., Shumba, P., Burchhardt, G., Hammerschmidt, S., & Siemens, N. (2021). Hydrogen peroxide is crucial for NLRP3 inflammasome-mediated IL-1 β production and cell death in pneumococcal infections of bronchial epithelial cells. *J Innate Immun*, 1–15. <https://doi.org/10.1159/000517855>.
222. Taguchi, N., Ishihara, N., Jofuku, A., Oka, T., & Mihara, K. (2007). Mitotic phosphorylation of dynamin-related GTPase Drp1 participates in mitochondrial fission. *J Biol Chem*, *282*(15), 11521–11529. <https://doi.org/10.1074/jbc.M607279200>.
223. Tatsuta, M., Kan-o, K., Ishii, Y., Yamamoto, N., Ogawa, T., Fukuyama, S., Ogawa, A., Fujita, A., Nakanishi, Y., & Matsumoto, K. (2019). Effects of cigarette smoke on barrier function and tight junction proteins in the bronchial epithelium: Protective role of cathelicidin LL-37. *Respir Res*, *20*, 251. <https://doi.org/10.1186/s12931-019-1226-4>.
224. Tattoli, I., Carneiro, L. A., Jéhanno, M., Magalhaes, J. G., Shu, Y., Philpott, D. J., Arnoult, D., & Girardin, S. E. (2008). NLRX1 is a mitochondrial NOD-like receptor that amplifies NF-kappaB and JNK pathways by inducing reactive oxygen species production. *EMBO Rep*, *9*(3), 293–300. <https://doi.org/10.1038/sj.embor.7401161>.
225. Thimmulappa, R. K., Chattopadhyay, I., & Rajasekaran, S. (2019). Oxidative stress mechanisms in the pathogenesis of environmental lung diseases. *Oxidative Stress in Lung Diseases*, 103–137. https://doi.org/10.1007/978-981-32-9366-3_5.
226. Thoo, L., Noti, M., & Krebs, P. (2019). Keep calm: The intestinal barrier at the interface of peace and war. *Cell Death Dis*, *10*(11), 849. <https://doi.org/10.1038/s41419-019-2086-z>.
227. Tian, W., Li, W., Chen, Y., Yan, Z., Huang, X., Zhuang, H., Zhong, W., Chen, Y., Wu, W., Lin, C., Chen, H., Hou, X., Zhang, L., Sui, S., Zhao, B., Hu, Z., Li, L., & Feng, D. (2015a). Phosphorylation of ULK1 by AMPK regulates translocation of ULK1 to mitochondria and mitophagy. *FEBS Lett*, *589*(15), 1847–1854. <https://doi.org/10.1016/j.febslet.2015.05.020>.
228. Tilley, A. E., Walters, M. S., Shaykhiiev, R., & Crystal, R. G. (2015). Cilia dysfunction in lung disease. *Annu Rev Physiol*, *77*, 379–406. <https://doi.org/10.1146/annurev-physiol-021014-071931>.
229. Tran, A., Scholtes, C., Songane, M., Champagne, C., Galarneau, L., Levasseur, M.-P., Fodil, N., Dufour, C. R., Giguère, V., & Saleh, M. (2021). Estrogen-related receptor alpha (ERR α) is a key regulator of intestinal homeostasis and protects against colitis. *Sci Rep*, *11*(1), 15073. <https://doi.org/10.1038/s41598-021-94499-5>.

230. Tunggal, J. A., Helfrich, I., Schmitz, A., Schwarz, H., Günzel, D., Fromm, M., Kemler, R., Krieg, T., & Niessen, C. M. (2005). E-cadherin is essential for in vivo epidermal barrier function by regulating tight junctions. *EMBO J*, *24*(6), 1146–1156. <https://doi.org/10.1038/sj.emboj.7600605>.
231. Unger, B. L., Ganesan, S., Comstock, A. T., Faris, A. N., Hershenson, M. B., & Sajjan, U. S. (2014). Nod-like receptor X-1 is required for rhinovirus-induced barrier dysfunction in airway epithelial cells. *J Virol*, *88*(7), 3705–3718. <https://doi.org/10.1128/JVI.03039-13>.
232. Valdivieso, Á. G., Dugour, A. V., Sotomayor, V., Clauzure, M., Figueroa, J. M., & Santa-Coloma, T. A. (2018). N-acetyl cysteine reverts the proinflammatory state induced by cigarette smoke extract in lung Calu-3 cells. *Redox Biol*, *16*, 294–302. <https://doi.org/10.1016/j.redox.2018.03.006>.
233. van der Poll, T., & Opal, S. M. (2009). Pathogenesis, treatment, and prevention of pneumococcal pneumonia. *Lancet*, *374*(9700), 1543–1556. [https://doi.org/10.1016/S0140-6736\(09\)61114-4](https://doi.org/10.1016/S0140-6736(09)61114-4).
234. van der Toorn, M., Rezayat, D., Kauffman, H. F., Bakker, S. J. L., Gans, R. O. B., Koëter, G. H., Choi, A. M. K., van Oosterhout, A. J. M., & Slebos, D.-J. (2009). Lipid-soluble components in cigarette smoke induce mitochondrial production of reactive oxygen species in lung epithelial cells. *Am J Physiol Lung Cell Mol Physiol*, *297*(1), L109–114. <https://doi.org/10.1152/ajplung.90461.2008>.
235. Van Eeden, S. F., & Sin, D. D. (2013). Oxidative stress in chronic obstructive pulmonary disease: A lung and systemic process. *Can Respir J*, *20*(1), 27–29.
236. Vanella, L., Li Volti, G., Distefano, A., Raffaele, M., Zingales, V., Avola, R., Tibullo, D., & Barbagallo, I. (2017). A new antioxidant formulation reduces the apoptotic and damaging effect of cigarette smoke extract on human bronchial epithelial cells. *Eur Rev Med Pharmacol Sci*, *21*(23), 5478–5484. https://doi.org/10.26355/eurrev_201712_13938.
237. Vargas-Rojas, M. I., Ramírez-Venegas, A., Limón-Camacho, L., Ochoa, L., Hernández-Zenteno, R., & Sansores, R. H. (2011). Increase of Th17 cells in peripheral blood of patients with chronic obstructive pulmonary disease. *Respir Med*, *105*(11), 1648–1654. <https://doi.org/10.1016/j.rmed.2011.05.017>.
238. Vercellino, I., & Sazanov, L. A. (2022). The assembly, regulation and function of the mitochondrial respiratory chain. *Nature Reviews. Mol Cell Biol*, *23*(2), 141–161. <https://doi.org/10.1038/s41580-021-00415-0>.
239. Vollmer, W., Massidda, O., & Tomasz, A. (2019). The cell wall of *Streptococcus pneumoniae*. *Microbiol Spectr*, *7*(3), 7.3.19. <https://doi.org/10.1128/microbiolspec.GPP3-0018-2018>.
240. Voss, M., Wonnenberg, B., Honecker, A., Kamyschnikow, A., Herr, C., Bischoff, M., Tschernig, T., Bals, R., & Beisswenger, C. (2015). Cigarette smoke-promoted acquisition of bacterial pathogens in the upper respiratory tract leads to enhanced inflammation in mice. *Respir Res*, *16*(1), 41. <https://doi.org/10.1186/s12931-015-0204-8>.
241. Wang, A., Keita, Å. V., Phan, V., McKay, C. M., Schoultz, I., Lee, J., Murphy, M. P., Fernando, M., Ronaghan, N., Balce, D., Yates, R., Dickey, M., Beck, P. L., MacNaughton, W. K., Söderholm, J. D., & McKay, D. M. (2014). Targeting mitochondria-derived reactive oxygen species to reduce epithelial barrier dysfunction and colitis. *Am J Pathol*, *184*(9), 2516–2527. <https://doi.org/10.1016/j.ajpath.2014.05.019>.

242. Wang, S., Deng, Z., Ma, Y., Jin, J., Qi, F., Li, S., Liu, C., Lyu, F.-J., & Zheng, Q. (2020). The role of autophagy and mitophagy in bone metabolic disorders. *Int J Biol Sci*, *16*(14), 2675–2691. <https://doi.org/10.7150/ijbs.46627>.
243. Wang, X.-L., Li, T., Li, J.-H., Miao, S.-Y., & Xiao, X.-Z. (2017). The effects of resveratrol on inflammation and oxidative stress in a rat model of chronic obstructive pulmonary disease. *Molecules*, *22*(9), E1529. <https://doi.org/10.3390/molecules22091529>.
244. Wang, Y., Liu, J., Zhou, J.-S., Huang, H.-Q., Li, Z.-Y., Xu, X.-C., Lai, T.-W., Hu, Y., Zhou, H.-B., Chen, H.-P., Ying, S.-M., Li, W., Shen, H.-H., & Chen, Z.-H. (2018). mTOR suppresses cigarette smoke-induced epithelial cell death and airway inflammation in chronic obstructive pulmonary disease. *J Immunol*, *200*(8), 2571–2580. <https://doi.org/10.4049/jimmunol.1701681>.
245. Weiser, J. N., Ferreira, D. M., & Paton, J. C. (2018). Streptococcus pneumoniae: Transmission, colonization and invasion. *Nat Rev Microbiol*, *16*(6), 355–367. <https://doi.org/10.1038/s41579-018-0001-8>.
246. West, A. P., Shadel, G. S., & Ghosh, S. (2011). Mitochondria in innate immune responses. *Nat Rev Immunol*, *11*(6), 389–402. <https://doi.org/10.1038/nri2975>
247. Wiese, K. M., Coates, B. M., & Ridge, K. M. (2017). The role of nucleotide-binding oligomerization domain-like receptors in pulmonary infection. *Am J Respir Cell Mol Biol*, *57*(2), 151–161. <https://doi.org/10.1165/rcmb.2016-0375TR>.
248. Wilson, R., Cohen, J. M., Jose, R. J., de Vogel, C., Baxendale, H., & Brown, J. S. (2015). Protection against Streptococcus pneumoniae lung infection after nasopharyngeal colonization requires both humoral and cellular immune responses. *Mucosal Immunol*, *8*(3), 627–639. <https://doi.org/10.1038/mi.2014.95>.
249. Wooten, J. B., Chouchane, S., & McGrath, T. E. (2006). Tobacco smoke constituents affecting oxidative stress. In B. B. Halliwell & H. E. Poulsen (Eds.), *Cigarette Smoke and Oxidative Stress* (pp. 5–46). Springer. https://doi.org/10.1007/3-540-32232-9_2.
250. Wu, W., Zhang, W., Booth, J. L., Hutchings, D. C., Wang, X., White, V. L., Youness, H., Cross, C. D., Zou, M.-H., Burian, D., & Metcalf, J. P. (2016). Human primary airway epithelial cells isolated from active smokers have epigenetically impaired antiviral responses. *Respir Res*, *17*(1), 111. <https://doi.org/10.1186/s12931-016-0428-2>.
251. Wu, Y.-H., Kuo, W.-C., Wu, Y.-J., Yang, K.-T., Chen, S.-T., Jiang, S.-T., Gordy, C., He, Y.-W., & Lai, M.-Z. (2014). Participation of c-FLIP in NLRP3 and AIM2 inflammasome activation. *Cell Death Differ*, *21*(3), 451–461. <https://doi.org/10.1038/cdd.2013.165>.
252. Xu, W., Janocha, A. J., Leahy, R. A., Klatte, R., Dudzinski, D., Mavrakis, L. A., Comhair, S. A. A., Lauer, M. E., Cotton, C. U., & Erzurum, S. C. (2014). A novel method for pulmonary research: Assessment of bioenergetic function at the air-liquid interface. *Redox Biol*, *2*, 513–519. <https://doi.org/10.1016/j.redox.2014.01.004>.
253. Yang, L., Na, C.-L., Luo, S., Wu, D., Hogan, S., Huang, T., & Weaver, T. E. (2017). The phosphatidylcholine transfer protein Stard7 is required for mitochondrial and epithelial cell homeostasis. *Sci Rep*, *7*, 46416. <https://doi.org/10.1038/srep46416>.

254. Yao, C.-H., Wang, R., Wang, Y., Kung, C.-P., Weber, J. D., & Patti, G. J. (2019). Mitochondrial fusion supports increased oxidative phosphorylation during cell proliferation. *ELife*, *8*, e41351. <https://doi.org/10.7554/eLife.41351>.
255. Yao, H., Arunachalam, G., Hwang, J., Chung, S., Sundar, I. K., Kinnula, V. L., Crapo, J. D., & Rahman, I. (2010). Extracellular superoxide dismutase protects against pulmonary emphysema by attenuating oxidative fragmentation of ECM. *Proc Natl Acad Sci U S A*, *107*(35), 15571–15576. <https://doi.org/10.1073/pnas.1007625107>.
256. Yoo, I.-H., Shin, H.-S., Kim, Y.-J., Kim, H.-B., Jin, S., & Ha, U.-H. (2010). Role of pneumococcal pneumolysin in the induction of an inflammatory response in human epithelial cells. *FEMS Immunol Med Microbiol*, *60*(1), 28–35. <https://doi.org/10.1111/j.1574-695X.2010.00699.x>.
257. M., & Jung, Y.-K. (2018). A molecular approach to mitophagy and mitochondrial dynamics. *Mol Cells*, *41*(1), 18–26. <https://doi.org/10.14348/molcells.2018.2277>.
258. Youle, R. J., & Narendra, D. P. (2011). Mechanisms of mitophagy. *Nat Rev Molr Cell Biol*, *12*(1), 9–14. <https://doi.org/10.1038/nrm3028>.
259. M., Kim, T. S., Kim, S. Y., Lee, H.-M., Han, J., Dufour, C. R., Kim, J. K., Jin, H. S., Yang, C.-S., Park, K.-S., Lee, C.-H., Kim, J.-M., Kweon, G. R., Choi, H.-S., Vanacker, J.-M., Moore, D. D., Giguère, V., & Jo, E.-K. (2015). Orphan nuclear receptor ERR α controls macrophage metabolic signaling and A20 expression to negatively regulate TLR-induced inflammation. *Immunity*, *43*(1), 80–91. <https://doi.org/10.1016/j.immuni.2015.07.003>.
260. Zhang, J., Chu, S., Zhong, X., Lao, Q., He, Z., & Liang, Y. (2013). Increased expression of CD4+IL-17+ cells in the lung tissue of patients with stable chronic obstructive pulmonary disease (COPD) and smokers. *Int Immunopharmacol*, *15*(1), 58–66. <https://doi.org/10.1016/j.intimp.2012.10.018>.
261. Zhang, L., Gallup, M., Zlock, L., Finkbeiner, W. E., & McNamara, N. A. (2013). Rac1 and Cdc42 differentially modulate cigarette smoke-induced airway cell migration through p120-catenin-dependent and -independent pathways. *Am J Pathol*, *182*(6), 1986–1995. <https://doi.org/10.1016/j.ajpath.2013.02.008>.
262. Zhang, L., Gallup, M., Zlock, L., Finkbeiner, W., & McNamara, N. A. (2012). P120-catenin modulates airway epithelial cell migration induced by cigarette smoke. *Biochem Biophys Res Commun*, *417*(1), 49–55. <https://doi.org/10.1016/j.bbrc.2011.11.048>.
263. Zhang, M., Shi, R., Zhang, Y., Shan, H., Zhang, Q., Yang, X., Li, Y., & Zhang, J. (2019). Nix/BNIP3L-dependent mitophagy accounts for airway epithelial cell injury induced by cigarette smoke. *J Cell Physiol*, *234*(8), 14210–14220. <https://doi.org/10.1002/jcp.28117>.
264. Zhang, W. (2020). The mitophagy receptor FUN14 domain-containing 1 (FUNDC1): A promising biomarker and potential therapeutic target of human diseases. *Genes Dis*, *8*(5), 640–654. <https://doi.org/10.1016/j.gendis.2020.08.011>.
265. Zhang, Y., Yao, Y., Qiu, X., Wang, G., Hu, Z., Chen, S., Wu, Z., Yuan, N., Gao, H., Wang, J., Song, H., Girardin, S. E., & Qian, Y. (2019). Listeria hijacks host mitophagy through a novel mitophagy receptor to evade killing. *Nat Immunol*, *20*(4), 433–446. <https://doi.org/10.1038/s41590-019-0324-2>.
266. Zhou, J.-S., Zhao, Y., Zhou, H.-B., Wang, Y., Wu, Y.-F., Li, Z.-Y., Xuan, N.-X., Zhang, C., Hua, W., Ying, S.-M., Li, W., Shen, H.-H., & Chen, Z.-H. (2016). Autophagy plays an essential role in cigarette

- smoke-induced expression of MUC5AC in airway epithelium. *Am J Physiol Lung Cell Mol Physiol*, 310(11), L1042-1052. <https://doi.org/10.1152/ajplung.00418.2015>.
267. Zhou, R., Yazdi, A. S., Menu, P., & Tschopp, J. (2011). A role for mitochondria in NLRP3 inflammasome activation. *Nature*, 469(7329), 221–225. <https://doi.org/10.1038/nature09663>.
268. Zhu, L., Di, P. Y. P., Wu, R., Pinkerton, K. E., & Chen, Y. (2015). Repression of CC16 by cigarette smoke (CS) exposure. *PLoS One*, 10(1), e0116159. <https://doi.org/10.1371/journal.pone.0116159>.
269. Zimorski, V., Ku, C., Martin, W. F., & Gould, S. B. (2014). Endosymbiotic theory for organelle origins. *Current Opinion in Microbiology*, 22, 38–48. <https://doi.org/10.1016/j.mib.2014.09.008>.
270. Zorova, L. D., Popkov, V. A., Plotnikov, E. Y., Silachev, D. N., Pevzner, I. B., Jankauskas, S. S., Babenko, V. A., Zorov, S. D., Balakireva, A. V., Juhaszova, M., Sollott, S. J., & Zorov, D. B. (2018). Mitochondrial membrane potential. *Anal Biochem*, 552, 50–59. <https://doi.org/10.1016/j.ab.2017.07.009>.
271. Zuo, W.-L., Shenoy, S. A., Li, S., O’Beirne, S. L., Strulovici-Barel, Y., Leopold, P. L., Wang, G., Staudt, M. R., Walters, M. S., Mason, C., Kaner, R. J., Mezey, J. G., & Crystal, R. G. (2018). Ontogeny and biology of human small airway epithelial club cells. *Am J Respir Crit Care Med*, 198(11), 1375–1388. <https://doi.org/10.1164/rccm.201710-2107OC>.
272. Zuo, W.-L., Yang, J., Gomi, K., Chao, I., Crystal, R. G., & Shaykhiev, R. (2017). EGF-Amphiregulin interplay in airway stem/progenitor cells links the pathogenesis of smoking-induced lesions in the human airway epithelium. *Stem Cells*, 35(3), 824–837. <https://doi.org/10.1002/stem.2512>.

9. Acknowledgment

I would like to thank my supervisor Prof. Dr. Dunja Bruder for her consistent support and guidance during the running of this project. Furthermore, I would like to thank Dr. Alexander H. Remels and Ms. Chrity Tulen and the rest of the research team at Department of Pharmacology and Toxicology of Maastricht University Medical Center for their great collaborative efforts during data collection and analysis.

I am also thankful to Dr. Andreas Jeron for all his technical efforts and inspirational thoughtfulness which considerably helped me to shape this study.

Enormous thanks also go to Prof. Rüdiger Braun-Dullaeus for the generous support and his research team members, Dr. Sönke Weinert and Mr. Mohsen Abdi Sarabi at the Clinic for Cardiology for valuable experimental assistance.

I would also like to acknowledge the Commission on Funding for Junior Scientists and researchers, Medical Faculty of Otto von Guericke University Magdeburg and German research Foundation (361210922/RTG 2408) for providing financial support for this study.

Last but not least, I would like to thank my dearest family members Maryam, Shahriar, Maziyar, Maral Aghapour and my eternal love Azin Kazemi for all their everlasting supports and encouragements during compilation of this dissertation without which I could not fulfill this upward step in my life.

10. Appendix

10.1. Ehrenerklärung

Ich erkläre, dass ich die der Medizinischen Fakultät der Otto-von-Guericke-Universität zur Promotion eingereichte Dissertation mit dem Titel:

“Insights into the mechanisms of alterations in mitochondria-regulated airway epithelial cell responses upon cigarette smoke extract exposure and pneumococcal infection”

im Institut für Medizinische Mikrobiologie und Krankenhaushygiene
mit Unterstützung durch
Prof. Dr. Dunja Bruder

ohne sonstige Hilfe durchgeführt und bei der Abfassung der Dissertation keine anderen als die dort aufgeführten Hilfsmittel benutzt habe.

Bei der Abfassung der Dissertation sind Rechte Dritter nicht verletzt worden.

Ich habe diese Dissertation bisher an keiner in- oder ausländischen Hochschule zur Promotion eingereicht. Ich übertrage der Medizinischen Fakultät das Recht, weitere Kopien meiner Dissertation herzustellen und zu vertreiben.

Magdeburg, den 19.06.2022

Mahyar Aghapour Ask

10.2. Curriculum vitae

Persönliche Daten

Name: Mahyar Aghapour Ask

Geburtsdatum: 07.03.1991

Geburtsort: Amol

Familienstand: Verheiratet

Nationalität: Iranisch

Bildungsweg

2009 **Abitur**, Sepehr Marefat Gymnasium Amol

2009 - 2016 **Doctor of Veterinary Medicine**

University of Tabriz, Iran

Thema DVM: The effect of killed *Tsukamurella inchonensis* on inhibition of nitric oxide production in murine LPS-activated peritoneal macrophages

Betreuerin: Frau Dr. Katayoon Nofouzi

Durchgeführt am: Department of Pathobiology, Faculty of Veterinary Medicine, University of Tabriz

2018 - 2022 **Promotion**

Thema: Insights into the mechanisms of mitochondria-regulated airway epithelial cell dysfunction upon cigarette smoke extract exposure and pneumococcal infection

Betreuerin: Frau Prof. Dr. Dunja Bruder

Durchgeführt: Otto-von-Guericke Universität Magdeburg, Medizinische Fakultät, Institut für Medizinische Mikrobiologie und Krankenhaushygiene in der Arbeitsgruppe Infektionsimmunologie

Sonstiges

2016 - 2017 Wissenschaftliche Hilfskraft am Immunology Research Center, Tabriz University of Medical Sciences

Seit 2016 Mitglied der European Respiratory Society (ERS) und American Thoracic Society (ATS)

2020 Reisestipendium, 18th ERS Lung Science Conference, Estoril, Portugal